

**Thermochemical screening of lignocellulosic
enzymes for second generation bioethanol
production.**



Leigh Murphy,

PhD Thesis

Department of Science, Systems, and Models (NSM),

Biomaterials,

Roskilde University,

DK-4000 Roskilde, Denmark.

June 2011.

Summary

Oil reserves are depleting while the demand for more transport fuel is on the rise. Bioethanol provides a carbon neutral alternative to fossil fuels, not directly adding to the levels of increasing greenhouse gases. First generation bioethanol relies on the breakdown of starch rich plant matter as a substrate but this has generated controversy with respect to rising food prices, particularly in the third world. This has led to increased efforts in the development of second generation bioethanol. Second generation bioethanol is derived from crop residues, making this a lucrative substrate, but one which is far more difficult to hydrolyze.

These crop residues are comprised of plant matter or biomass which is called lignocellulose. This is mainly lignin, hemicellulose and cellulose. It is the latter that is currently of interest in industry as cellulose may be broken down to glucose which is further fermented by yeast to ethanol. The hydrolysis is a very complex process involving a class of enzymes called cellulases, and it is the study of these enzymes which form the focus of this report. Cellulases have been studied for over 60 years in this context, since the first *T. reesei* fungus degraded a cotton tent in the Pacific Island conflicts of WWII.

From an industrial point of view, it is difficult to screen cellulases as the substrate, cellulose, is an insoluble solid. Other systems involving small soluble oligomers have been used to this end; but have also been shown not to accurately reflect the action of the enzyme class on the real substrate. The current investigation presents a method, using Isothermal titration calorimetry (ITC), which may be used to directly monitor the action of cellulases on insoluble cellulose substrates. The ITC measures rates, providing an extra mechanistic insight in to the action of cellulases, as well as providing a platform for screening variants or wild type enzymes. The use of this method is demonstrated on complex, opaque (lignocellulosic) substrates and using mixtures of cellulases and β -glucosidases.

The action of cellobiohydrolases has been the subject of study for many years with focus on the fast initial rate followed by a far slower hydrolysis process. Here, a coupled enzyme amplification system has been developed to provide an increased thermal signal for the study of these notoriously slow enzymes, which degrade cellulose at a maximal rate in the order of 1-5 catalytic events per second. A study of the action of the two main cellobiohydrolases from *T. reesei*, *TrCel7A* and *TrCel6A* on amorphous (disordered) cellulose, crystalline (highly ordered) cellulose and lignocellulose is presented. Kinetic parameters for the degradation of insoluble cellulose are derived, based on a simple double exponential decay analysis, V_{\max} (cat) which may be equated with the catalytic turnover number of the enzyme and k_4 , the rate constant of inactivation.

The inactivation of cellulases is investigated, using the ITC data, and the differences in extrinsic and intrinsic inactivation are outlined. Extrinsic inactivation is external to the enzyme and is explained here as a primarily a function of the substrate. Intrinsic inactivation is a function of the enzyme itself, where the enzyme becomes inactivated on the cellulose chain, or denatured in a way which removes the enzyme from the population capable of performing catalysis, herein included is product inhibition. A mechanistic interpretation for inactivation is presented. The interaction of the cellulase with cellulose includes binding and catalysis, and this involves two opposing forces, one binding interaction, and the other progressive movement. Through this investigation, we record that both cellobiohydrolases are equally prone to intrinsic inactivation, and thus may perform the same average number of catalytic events per enzyme as a result of this.

The carbohydrate binding module (CBM) binds the enzyme to the cellulose surface and the role of the CBM is investigated using protein engineering variants. Here we have looked at a CBM-free variant which is called the Core, and four point mutation variants, positioned on two different faces of the CBM wedge-like structure. The importance of the back side of the wedge is presented, and the role of histidine (H4) in the interaction between the cellulase and cellulose is highlighted as playing a pivotal role. This is investigated using ITC and a model for the interaction between the CBM and the insoluble surface is presented.

Wild type variants of the enzyme class D-glucono- δ -lactone hydrolase have been screened for, and the use of ITC to determine the kinetics of a less complex soluble enzyme substrate system is demonstrated.

The inactivation of cellulases is not limited to cellobiohydrolases, and this is studied by investigating the three main *endoglucanases* of *T. reesei*. This is a more fundamental investigation into the slowdown of hydrolysis, and this is followed up by investigating the inhibition of cellobiose and glucose on this enzyme class. Here it is demonstrated the endoglucanases are not very prone to typical fermentation product (i.e. glucose and cellobiose) inhibition as a source of inactivation, but rather that the enzymes become trapped in the cellulose complex itself, despite not being processive as the cellobiohydrolases are.

Throughout the report we demonstrate the uses of ITC in the monitoring of cellulolytic enzymatic action, showing the potential uses in screening, as well as the generation of mechanistically important data to further understanding in this area.

Resumé

Oliereserverne bliver mindre, mens efterspørgslen efter transportbrændstof er stigende. Bioethanol giver et carbon neutralt alternativ til fossile brændstoffer, uden direkte at føje til de stigende drivhusgasser. Førstegenerations bioethanol er baseret på nedbrydelse af stivelsesholdige plantedele, men det har skabt kontrovers pga de stigende fødevarerpriser især i den tredje verden. Dette har ført til en øget indsats i udviklingen af andengenerations bioethanol. Andengenerations bioethanol er udvundet af afgrøderester, hvilket gør det til et bærdygtigt substrat, men et som er langt sværere at hydrolysere.

Afgrøderesterne består af plantemateriale, også kendt som biomasse, som kaldes lignocellulose. Lignocellulose består hovedsageligt af lignin, hemicellulose og cellulose. Det er sidstnævnte, der i øjeblikket er interesse for i industrien. Cellulose kan nedbrydes til glukose, som igen, fermenteret af gær, nedbrydes til ethanol. Hydrolysen er en meget kompleks proces, der involverer en klasse af enzymer kaldet cellulaser, og det er studiet af disse enzymer, der danner fokus i denne rapport. Cellulaser er blevet undersøgt i mere end 60 år i denne sammenhæng, siden den første *T. reesei* svamp nedbrød et bomuldstelt på en Stillehavsø under andenverdenskrig.

Fra et industrielt synspunkt, er det vanskeligt at screene cellulaser, fordi substratet cellulose, er en uopløselig masse. Andre metoder, der involverer små opløselige oligomerer har været anvendt til formålet, men har vist sig ikke at præcist afspejle aktiviteten af enzymet på den virkelige substrat. Den nuværende undersøgelse præsenterer en metode, ved hjælp af Isotermisk titrering kalorimetri (ITC), som kan bruges til direkte at overvåge virkningen af cellulaser på uopløselige cellulose substrater. ITC målinger tilføjer en ekstra mekanistisk indsigt i virkningen af cellulaser, samt skaber en platform for screening af varianter eller wild-type enzymer. Brugen af denne metode er demonstreret på komplekse og uigennemsigtige (lignocellulose) substrater og anvendelse af blandinger af cellulases og β -glucosidaser.

Virkningen af cellobiohydrolaser har været genstand for undersøgelse i mange år med fokus på den hurtige initiale hastighed efterfulgt af den meget langsommere hydrolyse proces. Her er et enzym koblet assay blevet udviklet til at øge det termiske signal, som kan undersøge disse notorisk langsomme enzymer, der nedbryder cellulose på en maksimal hastighed i størrelsesordenen af 1-5 katalytisk hændelser per sekund. En undersøgelse af virkningen af de to vigtigste cellobiohydrolaser fra *T. reesei*, *TrCel7A* og *TrCel6A* på amorfe (uordnede) celluloser og krystallinske (meget ordnede) celluloser og lignocellulose er præsenteret. Kinetiske parametre for nedbrydning af uopløselige cellulose er udledt, baseret på en simpel

dobbelt eksponentiel henfaldsanalyse, V_{\max} (cat), som kan sidestilles med katalytisk omsætning antallet af enzymet og k_4 , hastighedskonstanten for inaktivering.

Inaktivering af cellulaser er undersøgt ved hjælp af ITC data, og forskellen i ekstrinsiske og intrinsiske inaktivering er skitseret. Extrinsisk inaktivering er ekstern til enzymet, og er forklaret her som en primær funktion af substratet. Intrinsisk inaktivering er en funktion af enzymet selv, hvor enzymet bliver inaktiveret på cellulosekæden, eller denatureret på en måde, der fjerner enzymet fra populationen, som er i stand til at udføre katalyse, heri er inkluderet produkt-inhibering. En mekanistisk fortolkning for inaktivering præsenteres. Samspillet mellem cellulase og cellulose indeholder bindning og katalyse, og dette indebærer modsatrettede kræfter, en bindende interaktion, og den anden progressive bevægelse. Gennem denne undersøgelse registrerer vi, at begge cellobiohydrolaser er lige følsom over for inaktivering og kan derfor udføre det samme gennemsnitlige antal af katalytiske events pr enzym.

Det kulhydrat bindende modul (CBM) binder enzymet til cellulose overflade og CBM's rolle er undersøgt ved hjælp af protein engineering varianter. Her har vi set på en CBM-fri variant, som kaldes Core, og fire punktmutationsvarianter placeret på to forskellige stader af CBM's kile-lignende struktur. Betydningen af bagsiden af kilen præsenteres og dennes rolle, histidin (H4) i samspillet mellem cellulase og cellulose fremhæves som spillende en afgørende rolle. Dette er undersøgt ved ITC og en model for samspillet mellem CBM og uopløselige overfladen er præsenteret.

Der er blevet screenet for wild type varianter af enzymeklassen D-glucono- δ -lacton hydrolase, og brugt ITC til at bestemme kinetikken af dette mindre komplekse opløseligt enzymsubstrat system.

Inaktivering af cellulaser er ikke begrænset til cellobiohydrolaser. Dette er studeret ved at undersøge de tre vigtigste endoglucanases af *T. reesei*. Dette er en mere grundlæggende undersøgelse af nedsættelsen af hydrolysen, og er fulgt op ved at undersøge produkt-inhiberingen af cellobiose og glucose i denne enzymklasse. Her er det vist, at endoglucanaser ikke er særlig følsom over for typiske gæringsprodukter inhibering (dvs. glukose og cellobiose) som årsag til inaktivering. Vi forslår snarere, at enzymmerne bliver fanget i cellulosekomplekset selv, på trods af at de ikke er processive, som cellobiohydrolases er.

Gennem hele denne rapport demonstrerer vi hvordan man kan bruge ITC til overvågningen af cellulolytic enzymatisk aktivitet, som viser den potentielle anvendelse i screening, samt generering af mekanisk vigtige data til yderligere forståelse på dette område.

Table of Contents

Summary.....	I
Resumé	III
Table of figures	IX
Table of tables	X
Table of equations.....	X
List of Abbreviations.....	XI
Outline of the thesis	XII
Chapter 1.	XII
Chapter 2.	XII
Chapter 3.	XIII
Chapter 4.	XIII
Article 1. A calorimetric assay for enzymatic saccharification of biomass.....	XIII
Article 2. An enzymatic signal amplification system for calorimetric studies of cellobiohydrolases.....	XIV
Article 3. Burst kinetics of <i>T. reesei</i> endoglucanases on insoluble cellulose. (Submitted Manuscript).	XIV
Article 4: Product inhibition of <i>T. reesei</i> endoglucanases. (In preparation).....	XV
Chapter 1. Introduction	1
1.1 Background.....	1
1.2 Lignocellulose	2
1.2.1 Lignin	2
1.2.2 Hemicellulose	3
1.2.3 Cellulose	4
1.3 (Ligno)Cellulose hydrolysis	5
1.4 Cellulases – an introduction	6
1.4.1 Inverting cellulases	8
1.4.2 Retaining cellulases	8
1.5 Measurement of cellulose hydrolysis.....	10
1.6 Measurement of hydrolysis using ITC	12
1.7 Substrates used in the report.....	14
1.7.1 Avicel (Fluka: PH-101) and Sigmacell (Sigma: Type 20).....	14
1.7.2 Phosphoric acid swollen celluloses (PASC), or regenerated amorphous celluloses (RAC).....	14
1.7.3 Bacterial cellulose, (BC)	15

1.7.4 Pretreated corn stover, (PCS)	15
1.8 Some of the factors affecting hydrolysis	15
1.8.1 Degree of polymerization, DP	16
1.8.2 Two areas for hydrolysis?	16
1.8.3 Crystallinity Index, I_{cr}	17
1.8.4 Product Inhibition in hydrolysis	18
1.8.5 Enzyme adsorption to cellulose and cellulose accessible surface area	19
1.9 Thermochemical screening	23
Chapter 2. Thermochemical analysis of cellobiohydrolases; <i>TrCel6A</i> and <i>TrCel7A</i>	25
2.1 Background	25
2.1.1 <i>TrCel7A</i> , CBH I	25
2.1.2 <i>TrCel6A</i> , CBH II	25
2.2 Comparing <i>TrCel7A</i> and <i>TrCel6A</i>	26
2.2.1 Hydrolysis results on RAC	27
2.2.1 Hydrolysis results on BC	29
2.3 Kinetics of cellulases	29
2.3.1 Burst phase kinetics, processivity model	30
2.3.2 Modeling ITC data to the sum of two exponentials	35
2.4 Data analysis for <i>TrCel6A</i> and <i>TrCel7A</i>	36
2.4.1 Direct conversion to rates	36
2.4.2 The rate constant of inactivation: k_4	40
2.5 PCS analysis	41
2.6 Summary and conclusions	43
Chapter 3. Thermochemical screening of <i>TrCel7A</i> CBM I variants	48
3.1 Background	48
3.1.1 Structure	48
3.1.2 Function	49
3.2 <i>TrCel7A</i> point mutations analyzed in this study	50
3.2.1 Purification of protein engineering variants	51
3.2.2 Soluble substrate assays	52
3.3 Results and discussion	52
3.3.1 Normalization	52
3.3.2 Data analysis and ITC results	53

3.3.3 CBM variants action on RAC	55
3.3.4 CBM variants action on PCS.....	56
3.3.5 CBM variants action on PCS (HPLC) hydrolysis results.	56
3.3.6 Overall substrate and temperature trends	57
3.4 Discussion	58
3.4.1 CBM functions solely to increase the overall enzyme concentration	59
3.4.2 CBM functions to decrease intermolecular hydrogen bonding	60
3.4.3 CBM aids in targeting sites for productive binding	61
3.4.4 A mechanistic interpretation.....	62
3.5 Summary and conclusions	63
3.6 Supplemental Information	64
Chapter 4. Thermochemical screening of D-glucono- δ -lactone hydrolases.....	65
4.1 Background.....	65
4.2 Results and discussion	67
4.2.1 Determination of ΔH	67
4.2.2 Determination of kinetic parameters.....	68
4.2.3 Calculating the potential error to amplified signals from the ITC.....	69
4.2.4 Inhibition removal	70
4.2.5 GDLH inhibition.....	71
4.3 Conclusions.....	72
4.3.1 The general kinetics of GDLH	72
4.3.2 Potential for improving the amplification monitoring time.....	72
4.3.3 Future perspectives	73
4.4 Supplemental information	73
4.4.1 Substrate concentrations	73
4.4.2 Enzymatic rates.....	73
Concluding Remarks and Future Perspectives.	74
Acknowledgements	77
Article 1: A calorimetric assay for enzymatic saccharification of biomass.....	78
Article 2: An enzymatic signal amplification system for calorimetric studies of cellobiohydrolases.....	79
Article 3: Burst kinetics of <i>T. reesei</i> endoglucanases on insoluble cellulose.....	80
Article 4: Product inhibition of <i>T. reesei</i> endoglucanases.	81
Contribution to Article 5: A kinetic model for the burst phase of processive cellulases.....	82

<i>Contribution to Article 6: Advantages of isothermal titration calorimetry for xylanase kinetics in comparison to chemical-reducing-end assays.</i>	83
Appendix 1: Quenching and reducing ends assays for the EG work.	84
Ap 1.1 Enzyme quenching	85
Ap 1.2 Efficiency test on TrEG's.....	86
Ap 1.3 Conclusion, quenching.	87
Ap 1.4 Reducing ends assays.....	87
Appendix 2: Congo red ASA materials and methods.....	90
Ap 2.1 Material and Methods	90
References.....	92

Table of figures

Figure 1. An overview of a typical industrial bioethanol process.	2
Figure 2. A representation of the structure of lignocellulose (16).....	3
Figure 3. The repeating unit of cellulose, β -1,4- anhydrocellobiose (25).....	4
Figure 4. The hydrogen bonding pattern in cellulose.	5
Figure 5. A simplified overview of the hydrolysis of cellulose. (23,24,27).....	5
Figure 6. A cellobiohydrolase enzyme, <i>TrCel7A</i> (38).	7
Figure 7. Inverting or retaining mechanism of catalysis for cellulases.	7
Figure 8. The structures of the 4 main enzymes investigated in the current report.	9
Figure 9. The NanoITC 2G from T.A. Instruments.	13
Figure 10. An example of the solid state NMR (CP/MAS) spectra of crystalline and amorphous cellulose types.	18
Figure 11. Adsorption study of Cellulcast 1.5 L and three substrates. T = 25 °C, pH = 5	20
Figure 12. Langmuir isotherms for Avicel and PASC binding Congo red.	21
Figure 13. \circ = The converted rate of hydrolysis of PASC vs. time. The line represents the fit explained below.	22
Figure 14. A direct comparison of the rates of hydrolysis for <i>TrCel7A</i> and <i>TrCel6A</i> on insoluble amorphous cellulose.	28
Figure 15. A direct comparison of the rates of hydrolysis for <i>TrCel7A</i> and <i>TrCel6A</i> on insoluble crystalline cellulose.	29
Figure 16. Possible hindrances affecting the procession of CBHs (165).	33
Figure 17. A model for processive cellulases. (162).....	33
Figure 18. An illustration of the effect of the time constant for the ITC.	34
Figure 19. An example of the sum of two exponential decays model.	36
Figure 20. <i>TrCel7A</i> and <i>TrCel6A</i> action on RAC, 50 °C, pH 5, 50 nM enzyme.....	38
Figure 21. <i>TrCel7A</i> and <i>TrCel6A</i> action on BC, 50 °C, pH 5, 50 nM enzyme.	38
Figure 22. (L) ITC measured burst phase kinetics of cellulases (103). (R) A stylized adaptation of a typical ITC Michaelis-Menten kinetic curve (101).	39
Figure 23. <i>TrCel7A</i> and <i>TrCel6A</i> action on PCS, 50 °C, pH 5, 50 nM enzyme.	42
Figure 24. A, C, D and F show subsites of the <i>TrCel6A</i> active site where there are stacking interactions with glucose.....	46
Figure 25. The CBM of <i>TrCel7A</i>	49
Figure 26. Hydrophobicity of <i>TrCel7A</i> CBM.	49
Figure 27. pNPG (L) and pNPL (R).	52
Figure 28. pNPL activity on the <i>TrCel7A</i> CBM I variants.	53
Figure 29. The raw data from the ITC <i>TrCel7A</i> CBM reactions converted to a k_{cat}	53
Figure 30. The reproducibility of the CBM variant analyses.	54
Figure 31. ITC 50 °C, 30 min amplified reactions on PCS compared to HPLC, 24 h hydrolysis reaction with the same dose of BG.....	57
Figure 32. Integral of the RAC thermograms at 25 °C, compared to PCS integrals at 50 °C.	58
Figure 33. Proposed routes for cellulose association by the CBM. (141,175,203)	62
Figure 34. The coupled amplification system (111).	65
Figure 35. The hydrolysis of D-glucono- δ -lactone to D-gluconic acid.....	66
Figure 36. A depletion experiment for measuring autohydrolysis of D-glucono- δ -lactone in the syringe.	67
Figure 37. Michaelis-Menten (MM) fits for GDLH kinetics, $R^2 > 0.99$ in both cases.	69
Figure 38. D-glucono- δ -lactone hydrolase Wild Type 2, inhibition studies.....	71
Figure 39. Just for fun.	97

Table of tables

Table 1. An overview of the main characteristics of the <i>T. reesei</i> cellulases.	8
Table 2. The sum of two exponentials from Figure 13 parameter values.	22
Table 3. A summary of the hydrolysis rates of <i>TrCel6A</i> and <i>TrCel7A</i> on RAC and BC at 50 °C.	37
Table 4. The double exponential decay fits for <i>TrCel6A</i> and <i>TrCel7A</i> hydrolysis of RAC and BC.	40
Table 5. The number of hydrolytic events <i>TrCel7A</i> and <i>TrCel6A</i> may perform on RAC and BC based on $V_{\max}(\text{cat})/k_4$ at 50 °C.	40
Table 6. The double exponential decay fits and $V_{\max}(\text{cat})$ data for <i>TrCel6A</i> and <i>TrCel7A</i> hydrolysis of PCS.	42
Table 7. List of the mutations carried out on the CBM I of <i>TrCel7A</i> used in this study.	50
Table 8. The $V_{\max}(\text{cat})$ and k_4 , inactivation rate constant for the RAC and PCS ITC fits.	54
Table 9. Kinetic Parameters for the two tested D-glucono- δ -lactone hydrolases.	68
Table 10. The GDLH and BG kinetic data for the comparison of rates.	70
Table 11. Inhibition kinetic parameters for the two tested D-glucono- δ -lactone hydrolases.	71

Table of equations

Equation 1. Converting the heat signal to hydrolysis reaction rates.	14
Equation 2. Using Congo red to estimate the amount of bound protein.	21
Equation 3. Heat associated with the adsorption of 50 nM CBH to cellulose.	27
Equation 4. The Michaelis Menten equation.	30
Equation 5. The uni-bi ordered reaction equation.	31
Equation 6. A model for processive enzymes. (162).....	32
Equation 7. The sum of two exponentials used to model ITC data.	35
Equation 8. Calculation for the conversion of g/L cellulose to μM reducing end equivalents.	39
Equation 9. The rate of inactivation.	41
Equation 10. Calculating the Q_{10} temperature coefficient.	55
Equation 11. Calculating the error associated with autohydrolysis of the D-glucono- δ -lactone.	69
Equation 12. Calculation of the rates for β -glucosidase and D-glucono- δ -lactone hydrolase in the ITC cell.	70
Equation 13. The Michaelis-Menten competitive inhibition model.	71

List of Abbreviations

EHF	Enzymatic hydrolysis and fermentation
SSF	Simultaneous saccharification and Fermentation
CBP	Consolidated Bio-processing
DP	Degree of polymerization
EG	Endoglucanase
CBH	Cellobiohydrolase
I_{cr}	Crystallinity index
GH	Glycoside hydrolases
BG	β-glucosidase
CBM	Carbohydrate binding module
CD, Core	Catalytic domain
ABTS	2,2'-azino-bis(3-ethylbenzthiazoline-6-sulphonic acid)
COS	Cello-oligosaccharides
DNS	3,5-Dinitrosalicylic acid
FPU	Filter paper unit
BCA	2,2'-bicinchoninic acid
CMC	Carboxymethyl cellulose
HEC	Hydroxyethyl cellulose
pNPL	4-Nitrophenyl β-D-lactopyranoside
pNPG	4-Nitrophenyl β-D-glucopyranoside
ITC	Isothermal titration calorimetry
PASC	Phosphoric acid swollen cellulose
RAC	Regenerated amorphous cellulose
BC	Bacterial cellulose
PCS	Pretreated corn stover
NREL	National Renewable Energy Laboratories
DOE	Department of energy
S:E, E:S,	Substrate to enzyme or enzyme to substrate ratio
ES	Enzyme substrate complex
EI	Enzyme inhibitor complex
ASA	Accessible surface area
Suc-AAPF pNA	N-Succinyl-Ala-Ala-Pro-Phe-p-nitroanilide
V_{app}	Apparent rate of hydrolysis
V_{max} (cat)	Turnover based on the maximal measured rate
k₄	Rate constant of inactivation
GOD	Glucose-1-oxidase
SDS PAGE	Sodium dodecyl sulfate polyacrylamide gel electrophoresis
AFM	Atomic force microscopy
XRD	X-ray diffraction
FTIR	Fourier transformed infra red
SEM	Scanning electron microscopy
GDLH	D-glucono-δ-lactone hydrolase
G1OX	Oxidized glucose
G2	Cellobiose

Outline of the thesis

The thesis is divided into four main chapters followed by four main articles and two other articles where the author has contributed to the scientific content, which also serve to increase the readers understanding of the thesis as a whole.

Chapter 1.

The purpose of this chapter is to introduce the reader to the concepts of cellulose hydrolysis and cellulases. The introduction serves to familiarize the reader with typical analysis methods, substrate characteristics and enzyme properties. This is written in the style of a condensed mini review where we have highlighted aspects of the breakdown of biomass using enzymes to further understanding of the rest of the thesis. The reader is presented to the traditional methods of monitoring hydrolysis and cellulase action, including the various advantages and disadvantages of said methods. The reader is also introduced to ITC, Isothermal titration calorimetry, which has been the core of this thesis, and the inspiration for introducing this technique as a method (initially) for monitoring insoluble cellulose breakdown. ITC has the marked advantage of directly measuring the rate of hydrolysis and we discuss the potential for this from a fundamental and screening perspective. We introduce the reader to some of the theories as to why cellulose hydrolysis slows down so drastically and never achieves steady state, in contrast to other enzymatic reactions, as well as some experimental insights into some of the aspects which have been attributed to this rapid degradation in rate. This naturally leads to reader to Article 1, where the ITC method is validated and some of the potential applications are discussed.

Chapter 2.

In chapter 2, we present unpublished results of *TrCel6A* and *TrCel7A* hydrolysis action on amorphous cellulose, crystalline cellulose and lignocellulosic substrates. Here we take time to illustrate the development of the data analysis methods and outline the kinetics of the cellobiohydrolases in a more indepth manner than is possible in a scientific article. To this end we use the coupled enzymatic amplification system developed specifically for monitoring this enzyme class, which is described in detail in Article 2. Here we present the real screening possibilities of ITC; a method not only to determine which enzyme functions better under certain conditions, but the ability to use the same data to elucidate some of the fundamental characteristics of this enzyme class. We introduce the rate constant of decay, a measure for how quickly the enzyme becomes inactivated based on both intrinsic (enzyme) and extrinsic (substrate) properties, and offer mechanistic insights into the mode of action of both cellobiohydrolases.

Chapter 3.

In chapter 3 we continue the investigation into cellobiohydrolases, looking specifically at carbohydrate binding module (CBM) protein engineering variants. Here we investigate the effects of varying four amino acids in the CBM of cellobiohydrolase I (*TrCel7A*), and demonstrate the application of screening on amorphous cellulose and lignocellulosic substrates. With the ITC data we can see a marked difference in the rate constant of inactivation of the tested variants, and we offer mechanistic interpretations for these differences as well as a direct comparison between ITC data and a real hydrolysis situation over 24 h. We demonstrate that a histidine on the back side of the CBM wedge appears to be a critical site for point mutation focus in the future, and offer an explanation for the role this residue plays in the cellulose:cellulase interaction.

Chapter 4.

Chapter 4 represents a relatively independent investigation into the kinetics of an elusive enzyme class, D-glucono- δ -lactone hydrolase. In the coupled enzyme assay, there is a buildup of the product D-glucono- δ -lactone which is a known inhibitor of the enzyme β -glucosidase, mimicking the high energy transition state of the cellobiose to glucose hydrolysis. In an effort to determine if the inhibition could be alleviated through the addition of D-glucono- δ -lactone hydrolase, we use ITC to determine the kinetic parameters of this class of enzyme. While not directly associated with the enzymatic breakdown of biomass, this enzyme class has been difficult to investigate using traditional methods as the product and substrate are quite similar. We demonstrate the use of ITC to determine the kinetics of this enzyme under conditions relevant to the coupled enzymatic assay, and investigate the effects of product inhibition on D-glucono- δ -lactone hydrolases.

Article 1. A calorimetric assay for enzymatic saccharification of biomass

Leigh Murphy, Kim Borch, K.C. McFarland, Christina Bohlina, Peter Westh. (2010) *Enzyme. Microb. Technol.* **46**, 141-146

A limited selection of assay and screening methodologies for cellulolytic enzymes has been stated as a restriction in biomass research. In this report we test the potential of isothermal calorimetry for this purpose. The primary observable in this technique (the heat flow in Watts), scales with the rate of hydrolysis, and unlike other approaches, it provides a continuous picture of the hydrolytic rate. It was found that the activity of a standard enzyme cocktail against purified cellulose substrates and dilute acid pretreated corn stover (PCS) was readily detected in calorimeters of different types, and that the calorimetric signal scaled with the enzyme activity measured by established analytical techniques. Hence, it was concluded that the heat flow provided a valid measure of the hydrolytic rate also in a complex biomass. The hydrolysis process was consistently found to be exothermic, but the amount of heat released per mole of soluble sugar produced varied for different types of substrates. This variation probably reflects heat

contributions from processes which are coupled to the hydrolysis of the glycosidic bond (e.g. dissolution of crystalline substrate or physical transitions in the solid matrix). Calorimetric determinations of absolute reaction rates therefore require initial calibration against another method for each new substrate. However, the main potential of the method lies in real-time measurements of relative changes in hydrolysis rates. This approach may be used both for different starting conditions and the titration of enzyme, substrate, promoters or inhibitors to reacting samples in different stages of the hydrolysis. These experiments are technically straight forward, do not require separate calibrations against other techniques and appear to be useful for studies of the regulation and functional mechanism of cellulases.

Article 2. An enzymatic signal amplification system for calorimetric studies of cellobiohydrolases

Leigh Murphy, Martin J. Baumann, Kim Borch, Matt Sweeney, Peter Westh. (2010) *Anal. Biochem.* **404**, 140-148

The study of cellulolytic enzymes has traditionally been carried out using endpoint measurements by quantitation of reaction products using high-performance liquid chromatography (HPLC) or overall determination of produced reducing ends. To measure catalytic activity, model substrates such as solubilized cellulose derivatives, soluble chromogenic, and fluorogenic oligomeric substrates are often employed even though they do not reflect the natural insoluble substrate hydrolysis. Thermochemical methods using, for example, isothermal titration calorimetry (ITC) yield data where the primary observable is heat production. This can be converted to the rate of reaction and allows direct and continuous monitoring of the hydrolysis of complex substrates. To overcome the low molar enthalpy of the hydrolysis of the glycosidic bond, which is typically in the order of -2.5 kJ mol^{-1} , an enzymatic signal amplification method has been developed to measure even slow hydrolytically active enzymes such as cellobiohydrolases. This method is explained in detail for the amplification of the heat signal by more than 130 times by using glucose oxidase and catalase. The kinetics of this complex coupled reaction system is thoroughly investigated, and the potential use to generate kinetic models of enzymatic hydrolysis of unmodified cellulosic substrates is demonstrated.

Article 3. Burst kinetics of *T. reesei* endoglucanases on insoluble cellulose. (Submitted Manuscript).

Leigh Murphy, Nicolaj Cruys-Bagger, Martin J. Baumann, Søren Nymand Olsen, Kim Borch, Matt Sweeney, Hirosuke Tatsumi Peter Westh.

The kinetics of cellulose hydrolysis have long been described by an initial fast hydrolysis rate, tapering rapidly off, leading to a process that takes days rather than hours to complete. This behavior has been mainly attributed to the action of cellobiohydrolases, and often linked to the processive mechanism of this *exo*-acting group of enzymes. The initial kinetics of *endo*-glucanases (EGs) is far less investigated, partly due to a limited availability of quantitative assay technologies. We have used isothermal calorimetry to monitor the early time course of the hydrolysis of insoluble cellulose by the three main EGs from *Trichoderma reesei* (*Tr*); *TrCel7B* (formerly EG I), *TrCel5A* (EG II), and *TrCel12A* (EG III). These *endo*-glucanases show a distinctive initial burst with a maximal rate which is about 5-fold higher than the rate after 5 min of hydrolysis. The burst is particularly conspicuous for *TrCel7B*, which reaches a maximal turnover of about 20 s^{-1} at $30 \text{ }^\circ\text{C}$, and conducts about 1200 catalytic cycles per enzyme molecule in the initial fast phase. For *TrCel5A* and *TrCel12A* the extent of the burst is 2-300 cycles per enzyme molecule. The availability of continuous data

on EG activity allows an analysis of the mechanisms underlying the initial kinetics, and it is suggested that the slowdown is linked to transient inactivation of enzyme on the cellulose surface. The frequency of structures on the substrate surface that cause inactivation determines the extent of the burst phase.

Article 4: Product inhibition of *T. reesei* endoglucanases. (In preparation).

Leigh Murphy, Kim Borch, Peter Westh.

Product inhibition has long been deemed one of the most critical factors in the slowdown of biomass hydrolysis. Many investigations have been conducted into elucidating this rate retardation, empirically, or using complex kinetic models. These studies have been conducted primarily using crude preparations or commercial mixed cellulase products, and many investigated on lignocellulosic substrates. While this is of interest to Industry, to model a mixture of enzymes and their action on a complex insoluble biomass substrate cannot pinpoint the weak links in cellulose hydrolysis. We propose the necessity of investigating the individual enzymes on a fundamental level first, in order to assess the level of inhibition displayed by each component of the cellulase complex. Only when this has been accomplished will it then be possible to identify which of the cellulase components are limited by product build-up on an industrial scale. Here we report a new method to monitor the inhibition of *T. reesei* endoglucanases, *TrCel7B* (EG I), *TrCel5A* (EG II) and *TrCel12A* (EG III). Through the use of an amorphous insoluble cellulose substrate, and industrially relevant concentrations of glucose and cellobiose, we present new insights into EG sensitivity to product inhibition. All three EG's are largely unaffected by glucose, while cellobiose is determined to be a more potent inhibitor. The concentration of product at which the hydrolysis rate is halved ($V_{0.5}$) is 113 ± 6 mM cellobiose and 2.67 ± 0.21 M glucose for *TrCel5A*, 118 ± 22 mM cellobiose and < 200 mM glucose for *TrCel12A*, whereas *TrCel7B* displays a non-uniform inhibition pattern, initially inhibited but lessening over time.

Chapter 1. Introduction

1.1 Background

The global oil reserves are rapidly depleting and the emission of CO₂ to the atmosphere is increasing at an alarming rate (1). The cost of oil first broke a record \$100/barrel in 2007 and is steadily rising again (2). The use of biorenewable resources for the production of bioethanol as one of the alternative fuel sources to fossil fuels can potentially provide a CO₂-neutral economic solution (3).

From a European legislation viewpoint, directive **2001/77/EC** on the promotion of electricity produced from renewable energy sources and directive **2003/30/EC** on the promotion of the use of biofuels or other renewable fuels for transport, dictate targets for all EU member states (4). The reference % value for biofuels is 5.75 % in all transport to be instigated by December 2010, to be increased to 10 % by 2020. In addition to this, the EU has set ambitious greenhouse gas reduction targets with a reduction of 20 % to be achieved by 2020 (5). In 2006, the bioethanol produced amounted to 18.5 % of the European biofuels production, but altogether this represented less than 1 % of the entire EU petrol and diesel consumption (6). The current situation is thus; in a report issued on the 31st of January 2011, the European Renewable Energy Council (EREC) states “The share of renewables in transport is forecast to reach 11.27 % of diesel and petrol consumption in 2020” (7). It should be noted, however, this is mainly first generation bioethanol, and biodiesel.

This presents an unrelenting demand for the production of second generation bioethanol which is produced from agricultural waste, and thereby an inherently growing market. The 30-fold drop in enzyme cost due to Novozymes and Genencor International has significantly improved the position of bioethanol on the world market (8). Further reduction in processing costs, especially pretreatment will lead to a very competitive product (9). One of the largest contributors to cost is pretreatment, followed by the unit cost of enzymes (3), and therefore the complete utilization of the biomass in a finely tuned enzymatic and microbial system could aid significantly in the reduction of final product costing.

As bioethanol is a high bulk, low value product, one of the efficient ways in which to improve profitability is to increase the productivity by maximizing the utilization of the biomass substrate. Improved enzymatic degradation could potentially increase sugar yields as well as reduce the treatment time, thereby lowering the overall process costs. The industrial process typically takes 4 d at 50 °C to hydrolyze biomass; this incurs significant costs, and further and better understanding of the enzymatic process can alleviate this. Figure 1 shows a typical bioethanol process.

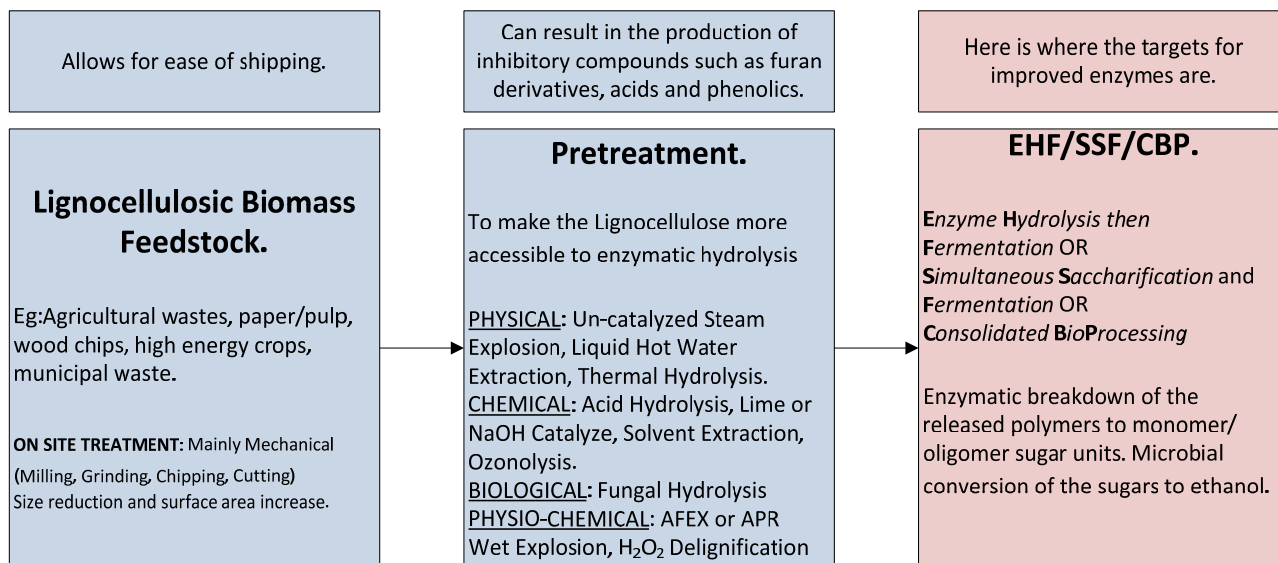


Figure 1. An overview of a typical industrial bioethanol process.

Adapted from (10-12). The focus of this report is the enzymatic hydrolysis (red).

1.2 Lignocellulose

Biomass in the context of this report is mainly agricultural residues. Lignocellulosic biomass is the term used to refer to plant matter composed of lignin, cellulose and hemicelluloses, although the plant cell wall also contains pectin and protein. In brief, lignocellulose is a complex structure containing cellulose (ca. 45 % dry weight), hemicellulose (ca. 30 % dry weight) and lignin (ca. 25 % dry weight), although these values vary from source to source (13). See Figure 2.

1.2.1 Lignin

Lignin (discovered 1838 by Payen in France, from the Latin *Lignum*, "Wood") is an amorphous macromolecule mainly composed of three phenylpropane subunits, which contain aromatic, aliphatic, phenolic, hydroxyl and methoxyl groups (14). During formation of lignin, a peroxidase enzyme removes the hydrogen from the phenolic hydroxyl group which releases a freed electron that traverses the molecule leading to the creation of several highly reactive positions. These radicals condense to form the lignin macromolecule (14). The concentration of each of the phenylpropane units varies according to the source, and the most common bond formed in lignin is the β -O-4 bond with the least stable being the C α -C β bond (15).

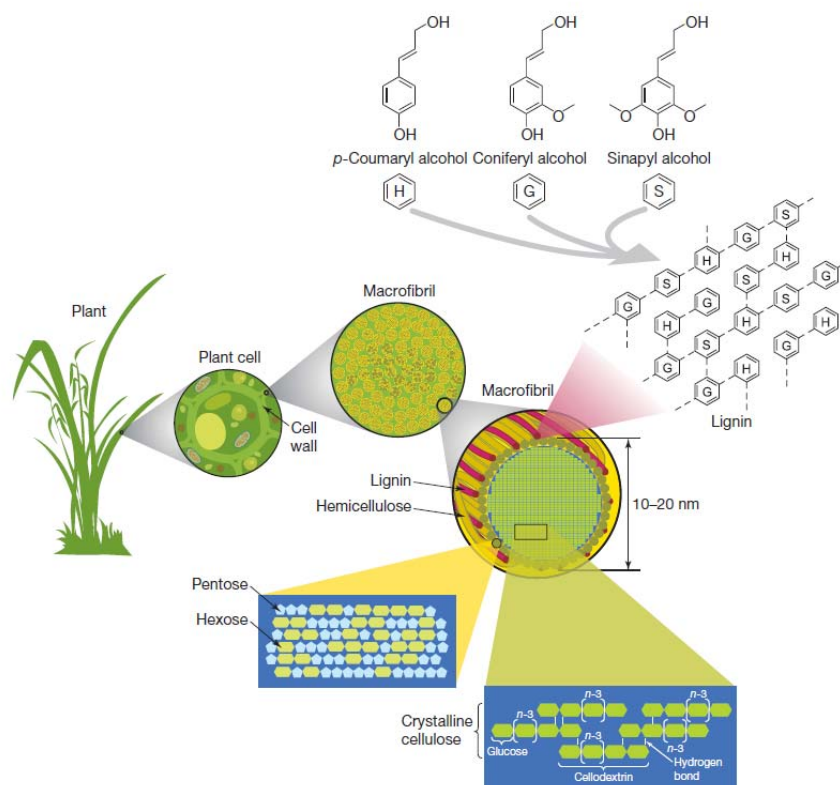


Figure 2. A representation of the structure of lignocellulose (16).

1.2.2 Hemicellulose

Polymeric carbohydrates, which are not cellulose, are collected under the name ‘hemicellulose’. Hemi is a Greek prefix with the meaning ‘not quite’. Naturally such a definition is slightly obtuse, and in current plant science, hemicelluloses are for instance xyloglucan, mannan, galactan, arabinan, mixed linked (1→4), (1→3)-glucans. (17,18). In biomass relevant raw materials, xylan is the dominant hemicellulose, which as part of the secondary cell wall is located between the lignin outer layer and the cellulose homopolymer core of plant cell walls, where it provides cohesion and structural stability through covalent and non-covalent bonding (18,19). Broadly speaking there are three types of xylan; those found in hardwood are highly acetylated, allowing ease of solubility in water; those found in softwoods contain α -L-arabinofuranose units linked by $\alpha(1\rightarrow3)$ -glycosidic bonds at the C-3 position of the xylose, which is a factor in less branching of the polymer; and finally, homoxylan, which contains only xylosyl residues, but is rare in nature (17).

It should be mentioned that although the hardwood acetylated xylan is the most soluble in water, pretreatment effects often release this as acetic acid, and this can lead to a significant reduction in xylan yield from the biomass product (11). Although the xylan substrate is a heteropolymer, the $\beta(1\rightarrow4)$ xylan

backbone is a homopolymeric chain of $\beta(1\rightarrow4)$ -linked β -D-xylopyranose units (19). Due to the complexity of this substrate, there are a number of enzymes involved in the breakdown of xylan. Briefly these include endo-1,4- β -D-xylanases (EC 3.2.1.8), which randomly cleave the backbone, β -D-xylosidases (EC 3.2.1.37) cleave xylose monomers from the non reducing end of the polymer, and side chain enzymes: α -L-arabinofuranosidases (EC 3.2.1.55), α -D-glucuronidases (EC 3.2.1.139), acetylxylan esterases (EC 3.1.1.72), *para*-coumaric acid esterases (EC 3.1.1.-), and ferulic acid esterases (EC 3.1.1.73), to name some (18).

1.2.3 Cellulose

Cellulose is the most abundant polymer in biomass, accounting for 35 – 50 % of a plant's dry weight, depending on the source (20). As opposed to hemicellulose, cellulose is composed of a single type of monomer sugar, glucose (21). However, due to the complex nature of the packing of this polymer, it is quite recalcitrant to degradation (22). Cellulose fibres are composed of micro fibrils, which are composed of proto fibrils, which are approximately 30 cellulose molecules in a tightly packed formation (23). Cellulose is both a crystalline and amorphous structure built up of these fibrils consisting of D-anhydroglucanopyranose joined by β -1,4-glycosidic bonds with a degree of polymerization (DP) varying from 100 to 20,000 (24). The repeating unit is actually anhydrocellobiose, as the adjacent D-anhydroglucanopyranose molecules are rotated 180° with respect to their neighbours (see Figure 3)(25).

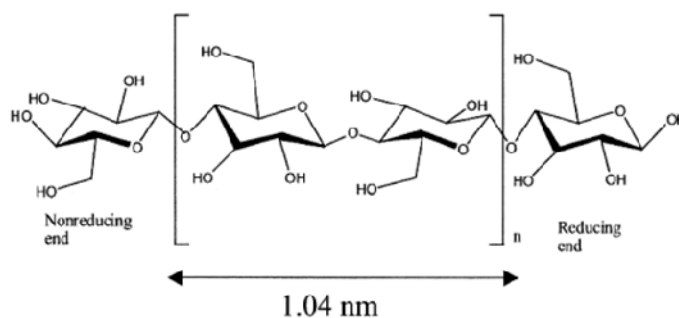


Figure 3. The repeating unit of cellulose, β -1,4- anhydrocellobiose (25).

This rotation allows for a high degree of hydrogen bonding, both inter and intramolecular, see Figure 4, which has a significant (yet controversial) role in the hydrolysis of cellulose, and is further investigated in Chapter 2, using two insoluble cellulose substrates of different crystallinity and comparing the two main cellobiohydrolases from *T. reesei*, *TrCel7A* and *TrCel6A*.

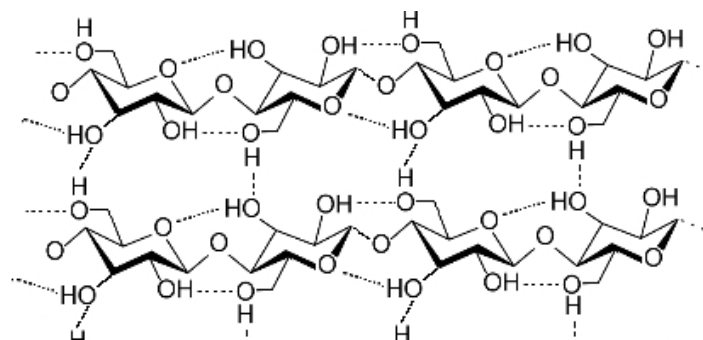


Figure 4. The hydrogen bonding pattern in cellulose.

Bonding Intrachain: endocyclic O5 to O3 and O6 to O2 Interchain: and O3 to O6 and O2 to O3.

A full listing of many of the known enzymes known to degrade, modify, or create glycosidic bonds may be found at carbohydrate active enzymes <http://www.cazy.org/> (26). Here the glycoside hydrolases (GHs) are classified by sequence structurally-relating the catalytic domains of enzymes that degrade, modify, or create glycosidic bonds, rather than the older, now obsolete EC method of substrate specificity.

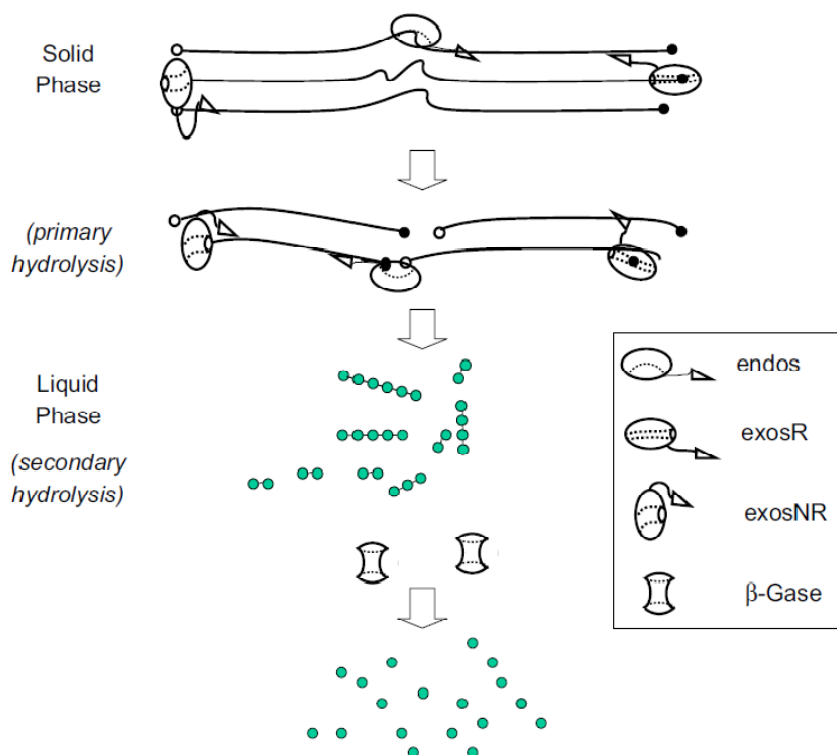


Figure 5. A simplified overview of the hydrolysis of cellulose. (23,24,27)

1.3 (Ligno)Cellulose hydrolysis

The hydrolysis of cellulose is a complex process involving the synergistic action of a combination of glycoside hydrolases (28) collectively called cellulases (20,23). Although not completely understood or

elucidated, the following is the most accepted theory. Traditionally, cellulases are defined or classified into the following groups. Endo-1,4- β -D-glucan-4-glucanohydrolases (EG) (EC 3.2.1.4) randomly cleave the cellulose polymer backbone in the amorphous areas (20,25). In addition to this, there are normally two exo-enzymes, exo-1,4- β -D-glucan-cellobiohydrolase (*TrCel7A* and *TrCel6A*, formerly CBH I and II, respectively) (EC 3.2.1.91) which cleave cellobiose from the reducing and non-reducing ends (29) of the cellulose chain, and degrade the crystalline areas of cellulose most efficiently (23,30). Finally, β -D-glucoside glucohydrolase (BG, *cellobiase*) (EC 3.2.1.21) hydrolyzes the cellobiose (and other soluble cello-oligosaccharides) into glucose monomers (30). The individual enzymes will be further discussed in detail later, although there is primary focus on the *endo*- and *exo*-cellulases over the β -glucosidase.

1.4 Cellulases – an introduction

Cellulases are produced by a wide variety of bacteria and fungi, mesophiles and thermophiles (31). Of the noncomplexed cellulases, it is those from aerobic fungi that have been most studied, with *Hypocrea jecorina* (historically called after the anamorph form: *Trichoderma reesei*) being the primary industrial producer (10). Similar to xylanases, they are produced and exported from the cell as extracellular enzymes, where they break down cellulose to monomer sugar units (23). Most extracellular cellulases are not very efficient at degrading crystalline cellulose, and so another tactic employed by nature is the assembly of the synergistic enzymes into a multi-enzyme complex called a cellulosome (32). The cellulosome was first discovered in *Clostridium thermocellum* in 1983, and is a complex with interlinking domains called “Cohesin” “dockerin” and “scaffoldin” whereby the enzymes are assembled into a single large supra-molecular cellulose binding and degrading units (32).

It is, however, non-complexed cellulases which are used in the biomass industry and these are the focus of the current report. *Trichoderma reesei*'s discovery dates back to the Second World War, where the fungus was responsible for the deterioration of cotton fatigues and tents in the South Pacific. It was determined there was a variety of few enzymes that were responsible for this cotton decay, and since then the cellulases and hemicellulases of this fungus have been cultivated (33). Cellulases from *T. reesei* have been studied for over 60 years (34-37) and remain the most fully understood to date.

Most cellulases have two distinct domains joined by a heavily *O*-glycosylated linker peptide rich in serine and threonine residues; a catalytic domain (CD or Core) and a carbohydrate binding module (CBM), see Figure 6 (23). The role of the CBM and a more extensive description of this domain are presented in Chapter 3.

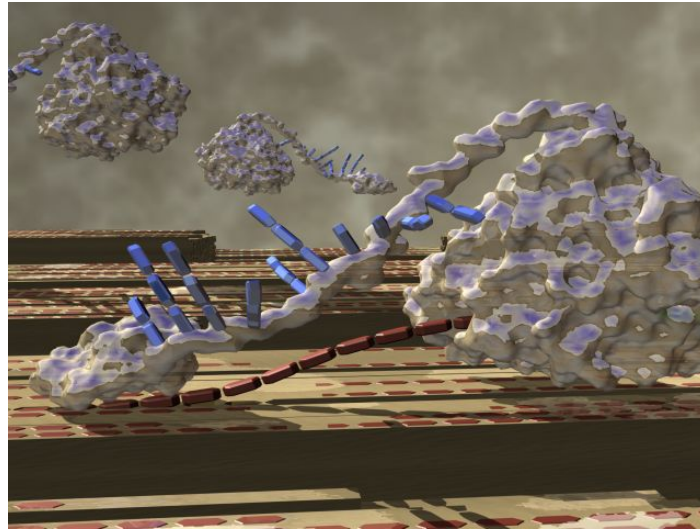


Figure 6. A cellobiohydrolase enzyme, *TrCel7A* (38).

Shown are the two distinct domains and the glycosylated linker region (blue sugar residues). Here the chain of the cellulose may be seen feeding into the catalytic domain (right).

The hydrolytic mode of action is based on the spatial arrangement in the catalytic site, especially of the two catalytic carboxyl groups relative to the bound substrate. The catalytic residues are either glutamic (e.g. *TrCel7A* (39)) or aspartic acids (e.g. *TrCel6A*(40)). Hydrolysis results in either the overall retention or inversion of the anomeric carbon (32).

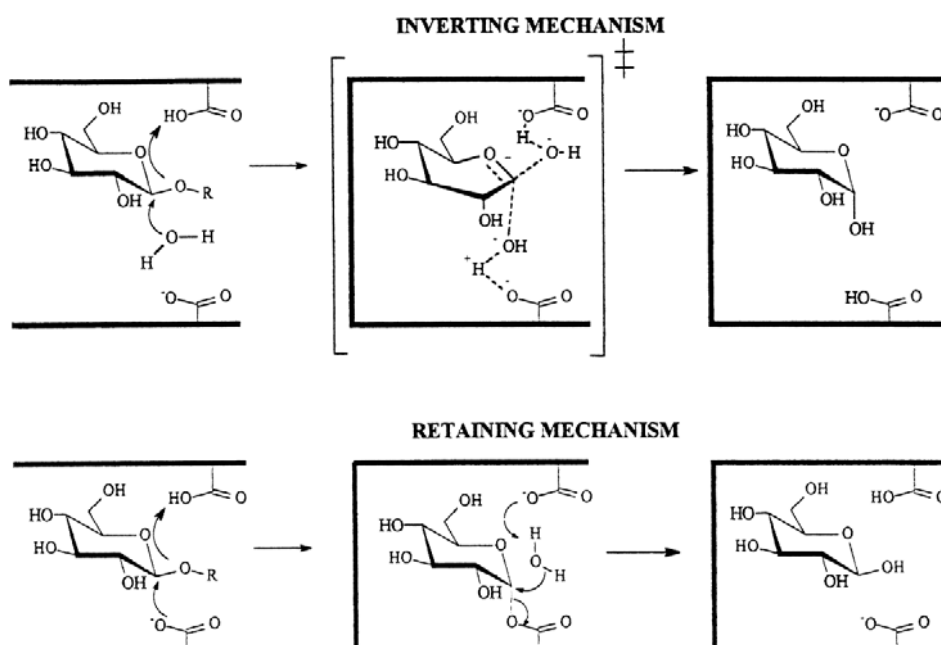


Figure 7. Inverting or retaining mechanism of catalysis for cellulases.

The carboxylic acids involved in inverting are typically 11 Å apart, for retaining cellulases this is 5 Å. (41)

1.4.1 Inverting cellulases

For inverting cellulases, one carboxylic acid acts as a general acid and the other a general base. There is no covalent intermediate formed. The general base activates the water by abstracting a proton enabling the oxygen to perform a nucleophilic attack on the anomeric carbon. The leaving group is activated by general acid catalysis through donation of a proton to the departing oxygen.

1.4.2 Retaining cellulases

With the retaining mechanism, there are two transition states. Firstly a deprotonated carboxylic acid acts as a nucleophile and attacks the C1 anomeric carbon forming a glucosyl-enzyme intermediate. Now the carboxylic acid on the other side of the cleft acts as a general acid and protonates the leaving group. Secondly the same carboxylic acid deprotonates the water, which then attacks the covalent intermediate and breaks it down. This is a double displacement mechanism (41,42).

Figure 8 shows the main structural features of the four major cellulases investigated in the current report, and Table 1 summarizes some of their properties. The reader should note *TrCel5A* EG II was formerly known as EG III, and *TrCel12A* EG III as a *small molecular weight* EG. The modern nomenclature is adapted from this point on where *Tr* is *T. reesei*, *Cel* is cellulase and the number and letter are derived from the genes, although abbreviations for classes such as EG for endoglucanases and CBH for cellobiohydrolases are also used in non-specific cases.

Table 1. An overview of the main characteristics of the *T. reesei* cellulases.

Enzyme	Formerly	Abundance† (25)	Mode of Catalysis(32)	CBM	Attack Point
<i>TrCel7A</i>	CBH I(39)	50 %	Retention	C-terminal CBM I(43)	<i>Reducing End</i> *(29)
<i>TrCel6A</i>	CBH II(40)	20 %	Inversion	N-terminal CBM I(44)	<i>Non reducing</i> (29) <i>end</i> *
<i>TrCel7B</i>	EG I(45)	15 %	Retention	C-terminal CBM I(46)	Amorphous regions(23)
<i>TrCel5A</i>	EG II(47)	10 %	Retention	N-terminal CBM I(46)	Amorphous regions(23)
<i>TrCel12A</i>	EG III(48)	1 %	Retention	None(48)	Amorphous regions(23)
<i>Others</i>	<i>EG IV, EG V.</i> <i>others</i>	4 %	-	-	-

†Represents the relative abundance of the enzymes in a typical *T. reesei* system.

*For the purpose of introducing the reader to cellulases only. Newer data indicates both *TrCel7A* and *6A* can initiate catalysis in an endoglucanase fashion, i.e. from a random attack point not an end. (49-52).

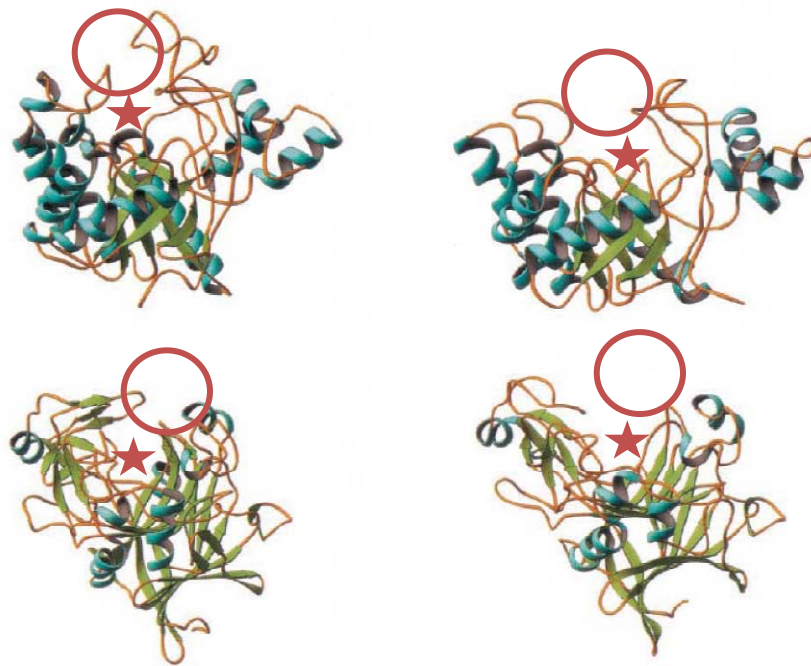


Figure 8. The structures of the 4 main enzymes investigated in the current report.

Top right: *TrCel5A* Clan GH-A, ($\beta\alpha$)₈, Top Left: *TrCel6A* $\alpha\beta$ barrel folds, Bottom right: *TrCel7B*, Bottom left: *TrCel7A* both β jelly rolls of Clan GH-B.(53) Star = catalytic cleft, Ringed = looped areas. *These are approximate locations for illustrative purposes.*

The classical mode of action is such that CBHs bind to a free end of a cellulose chain, using the CBM to increase the proximity of the catalytic domain to the substrate and cleave mainly cellobiose units off the chain end; this is regarded as *exo*-activity. The CBH then progresses along the chain in a processive manner, cleaving off a new glucose-dimer with each successive catalytic event. EG's on the other hand, bind to an amorphous region and cleave internally (*endo*-activity) in the cellulose chain (20,23,25,54-56). This causes an increase in new ends and thus new attack points for CBHs and a rapid decrease in the degree of polymerization (DP), which may be followed in a viscometer (57). From Figure 8, it may be seen there are loops enclosing the catalytic domains (the cleft regions) of the two CBHs, *TrCel7A* having four loops forming a 50 Å long tunnel (58) and *TrCel6A* two, forming a shorter 20 Å tunnel (59). The closed structure has been linked to processivity and it may be seen *TrCel5A* and *TrCel7B* have missing or shorter loops. In addition to this, the amount of binding sites for glucosyl moieties differs from *TrCel7A* with ten (58), *TrCel6A* with four (40), *TrCel7B* with four (60) *TrCel5A* with five (61), and *TrCel12A* with five (48).

The role of endoglucanases is investigated in Article 3 and expanded upon in Article 4, while the processivity of CBHs and the role of the CBM are investigated in Chapters 2 and 3, using *TrCel7A*, *TrCel6A* and *TrCel7A*-CBM protein engineering variants action on an insoluble cellulose substrate.

1.5 Measurement of cellulose hydrolysis

There are a number of reviews and articles on the basic measurement techniques for cellulose hydrolysis (24,62-65), including the guidelines issued by IUPAC in 1987 (66).

Measurement of total cellulose hydrolysis is typically based on the determination of soluble products, total reducing ends produced, or the depletion of the substrate. Depletion of the substrate may be determined gravimetrically or chemically. Gravimetric analysis is very dependent on the sample start weight (24), while the chemical analyses such as total sugar analysis (67) are deemed labor intensive. Soluble products such as predominantly cellobiose and glucose may be determined using HPLC and lower levels of cellobiose have been determined using β -glucosidase, glucose oxidase, peroxidase and ABTS¹ (68) as outlined in (69). This allows for the determination of lower concentrations of cellobiose, but many β -glucosidases (BG) are also active on other soluble cello-oligosaccharides (COS) (70), which could lead to an overestimation of activity if there is any BG present initially. Other methods to determine glucose include various kits available commercially, such as the hexokinase and glucose-6-phosphate dehydrogenase kit (24).

Total reducing ends are typically determined spectrophotometrically using a reagent which is in turn oxidized to produce a colored product (71-77). Determination of reducing ends on a mixture of soluble (COS, DP < 7) and insoluble products have proven difficult (78), and these assays often do not correlate well (62). The length of the cello-oligosaccharides also has been known to affect results, with certain reagents not reacting in a stoichiometric fashion precluding the determination of a representative overall activity when based on a glucose standard curve (79-82). The popular DNS² assay (63,66,71) underestimates cellobiose by 18 % when standardized using glucose (own observations unpublished, (83)). Both the Nelson-Somogyi (75) and DNS reagents (71) contain potassium sodium tartrate which interferes with the reduction reaction (64). The BCA (2,2'-bicinchoninic acid) assay, however, appears to be the most effective method to date (own observations unpublished, see Appendix 1, (84)), and although it is subject to interference from interaction with the proteins (24), this is easily corrected for by using an enzyme blank control (52).

¹ABTS: 2,2'-azino-bis(3-ethylbenzthiazoline-6-sulphonic acid) is normally used in conjunction with the production of hydrogen peroxide and a peroxidase enzyme. The formation of a green soluble end product through the oxidation of ABTS is monitored spectrophotometrically at 400-420 nm.

² DNS: 3,5-Dinitrosalicylic acid is reduced to 3-amino-5-nitrosalicylic acid in the presence of reducing sugars and may be quantified at 540 nm .

Total cellulase activity is measured by the filter paper unit assay (66,71,85). This assay is known for operator to operator variation and poor reproducibility (80), with FPU³ values on the same commercial preparation (Celluclast® 1.5 L⁴) being reported from 40 (86) to 120 (87) FPU/mL. Viscometry has also been used to determine cellulase activity, primarily on substituted substrates such as carboxymethyl cellulose (CMC) or hydroxyethyl cellulose (HEC) (57,62,88-90). The transition from the concentrated phase where the viscosity is initially governed both by polymer-polymer and polymer-solvent interactions, to the dilute phase where the interactions are primarily polymer-solvent makes modeling the decay in viscosity mathematically challenging (62), and the assay is linear only up to 12 % of CMC conversion (63). CMC, being an ionic substituted substrate, is also subject to changes in viscosity dependent on ionic strength, pH and polyvalent cations (91). Azurine-crosslinked polysaccharide substrates are also used quantitatively, releasing a blue color into the soluble phase as a function of hydrolysis (92).

Individual enzyme activities are generally measured using different substrates. Filter paper or Avicel is used to determine cellobiohydrolase (*exo*,CBH) (Avicelase) activity (25,55), whereas the substituted CMC (CMCase) or HEC is favored for endoglucanases (*endo*, EG) as the processive nature of CBH's is retarded by the substituents (62,64,66,89). Substituted small soluble oligosaccharides have also been used to study the kinetics of cellulases; such as 4-methylumbelliferyl- β -D-lactoside for *TrCel7A* (93), *p*-nitrophenyl- β -D-cellobioside which measures only *TrCel7A* activity and not *TrCel6A* (24), and *p*-nitrophenyl- β -D-lactoside which measures both *TrCel7A* and *TrCel6A* activity (94). Interference from β -glucosidase (BG) may be removed using the inhibitor D-glucono- δ -lactone (95), as well as tested for using *p*-nitrophenyl- β -D-glucopyranoside (96,97). However, action on small soluble substrates does not reflect action on complex biomass or insoluble substrates (24). Another drawback is the relatively high pK_a (6.6 (98)) of the *p*-nitrophenol group which is released. This means no direct monitoring of the CBH is possible at lower pH's (optimum pH \approx 5.0), and that all reactions are therefore quenched with base (typically NaOH) to produce the colored phenol salts. This may be overcome by using a CNP (chloro-pNP, reduces pK_a to approximately 5.2) derivative (61) but it is also not possible to study processive kinetics using soluble substrates (49).

Modification of the substrate or enzyme has also been carried out to monitor enzyme activity. Examples include cellulose ³H or ¹⁴C labeling (69,99) *TrCel6A* ¹²⁵I labeling (100), cellulose fluorescence labeling (49,52), 4-methylumbelliferyl labeling of COS (47,93), and reduction of the reducing end to successfully investigate

³ FPU: Filter paper unit. A complex unit loosely defined by the conversion of 4 % of 50 mg of filter paper to glucose by 0.5 mL of enzyme at 50 °C, over 60 min. The assay is non-linear.

⁴ Celluclast 1.5 L is a commercial cellulase mixture of both *endo*- and *exo*-activities, supplied by Novozymes A/S,

cellulase kinetics on complex substrates, although these methods rely on determining the end products as described above.

There exists a clear and present need for cellulase assays and a deeper understanding of the enzyme substrate interaction and this forms the core of the current work. The current assay technologies quite often provide little or no *mechanistic* information about cellulose hydrolysis. The initial focus of the current work has been to introduce calorimetry as a viable method for determining direct rates of hydrolysis. Calorimetry is a differential method and so measures the rate of reaction directly (101,102), providing excellent time resolution during the hydrolysis of complex opaque substrates. In the Article 1 (103), the calorimetric methods are outlined and benchmarked against the more traditional methods of monitoring cellulose hydrolysis. The potential for using a double exponential decay to describe the hydrolysis process is also introduced.

1.6 Measurement of hydrolysis using ITC

Given this thesis is primarily based on observations derived from the use of Isothermal Titration Calorimetry (ITC) see Figure 9, the following serves to introduce readers unfamiliar with this method to the principles employed in the course of this investigation. ITC is typically used for measuring ligand interaction, binding affinity, or other association reactions or specificities (104,105). ITC has, however, also been established as a method to determine reaction rates on soluble substrates, even for cellulases (101,102,106-110). In Article 2 (111) a typical stepwise experiment is employed to determine the kinetic parameters of a β -glucosidase, and in Chapter 4, the use of ITC to investigate the kinetics and product inhibition of D-glucono- δ -lactone hydrolases is demonstrated.

Here, to the best of our knowledge, for the first time, we introduce ITC as a technique for monitoring hydrolysis of insoluble substrates in Article 1 (103). This provides the advantages of no substrate modification, little sample preparation, and being non-destructive, further sample analysis is also possible. The basis for thermochemical changes during hydrolysis is that there is a physical (substrate) and chemical (bond) change in the system. The solute:solute, solvent:solvent, and solute:solvent interactions are altered, in our case through enzymatic hydrolysis and this leads to a change in the Gibbs free energy of the system (112). In the specific case of cellulose hydrolysis, the hydrogen bonds/van der Waals forces/hydrophobic interactions linking the cellulose to cellulose must be broken, the hydrogen bonds in the solute (water) broken, the covalent β ,1-4 bond hydrolyzed and finally the new cellulose polymers or COS are released into solution, generating new solvent:solute (solvation) interactions. These contribute to an overall enthalpy (H)

which may be measured as heat (Q) at constant pressure directly. The change in enthalpy, ΔH , is the overall sum of these endothermic and exothermic interactions according to Hess' Law.

The enthalpy for the release of energy by breaking the β ,1-4 glycosidic bond is an absolute value, typically reported under 5 kJ/mol (106,113-115), with slight variation as a result of the measurement technique. However, the *measured* enthalpy is dependent on both the substrate type and the enzyme product profile. This is seen in the case of substrates in Article 1 (103), where the measured enthalpy ranges from -2.65 ± 0.29 kJ/mol (PASC, an amorphous form of cellulose) up to -6.7 ± 0.2 kJ/mol (lignocellulose), and again in Article 3, where the hydrolysis of the same substrate (RAC, an amorphous form of cellulose) produces different enthalpies depending on the enzyme used varying from -1.7 kJ/mol (*TrCel7B*) to -5.4 kJ/mol (*TrCel12A*). This is a relatively low value, so in order to be able to investigate the individual cellobiohydrolase catalysis it is necessary to amplify the thermal signal. This is described in detail in Article 2 (111) where an enzymatic amplification system has been developed. This is a coupled assay where the product of the previous enzyme is then the substrate for the next in a chain of reactions. Briefly, the cellobiose is cleaved to individual glucose monomers using a β -glucosidase, the glucose is then oxidized by glucose-1-oxidase and the hydrogen peroxide product of the oxidation is removed by catalase. The overall enthalpy is in this way increased from -2.6 kJ/mol to almost -360 kJ/mol. This allows the monitoring of μg of cellobiohydrolase enzymes, which provides a powerful tool for thermochemical screening. The uses of this amplification system are expanded upon in Chapters 2 and 3.

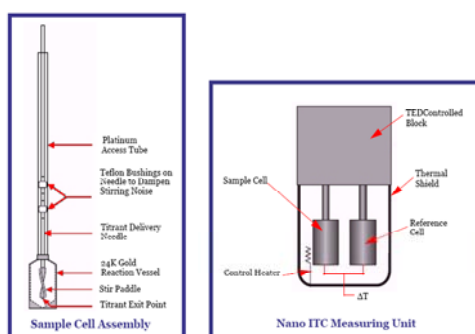


Figure 9. The NanoITC 2G from T.A. Instruments.

The two cellobiohydrolases (unlike EGs) have a well defined product, cellobiose, and a similar mode of action as described earlier. This means the molar enthalpy measured during the hydrolysis of insoluble cellulose which is then amplified is not affected by different substrates. This has been tested by calibrating the system in the presence of the three substrates used in investigating CBHs. This was achieved as outlined in Article 2 (111), and shown in Fig. 3 of that article. There, a known concentration cellobiose is titrated to the cell containing the amplification enzymes at a constant rate. Knowing the rate of addition in

$\mu\text{mol/s}$, the heat signal may be read upon reaching equilibrium (constant heat signal) in $\mu\text{J/s}$, and thus the molar enthalpy may be directly measured in J/mol . This was repeated by loading the cell with the amplification mixture in the presence of bacterial cellulose, BC, regenerated amorphous cellulose, RAC or pretreated corn stover, PCS and repeating this procedure. There was no significant deviation from the earlier reported $\Delta_{\text{app}}H$ of -360 kJ/mol in buffer alone.

The power compensated ITC has a reference cell maintained at a set ΔT from the sample cell and the amount of power needed to maintain this temperature difference during a reaction is measured as the applied heat Q , over time, dQ/dt . Conversion of the heat signal to the rate of reaction is achieved thus (101-103,110,111,116):

$$\text{Power} = \frac{dQ}{dt}$$

$$Q = n \cdot \Delta_{\text{app}}H = [P]_{\text{total}} \cdot V_r \cdot \Delta_{\text{app}}H$$

$$\frac{dQ}{dt} = \frac{d[P]}{dt} \cdot V_r \cdot \Delta_{\text{app}}H$$

$$\frac{d[P]}{dt} = \frac{dQ}{dt} \cdot \frac{1}{V_r \cdot \Delta_{\text{app}}H}$$

Equation 1. Converting the heat signal to hydrolysis reaction rates.

Where Q = heat, P = product, n = moles, $\Delta_{\text{app}}H$ = molar enthalpy, and V_r = reaction volume.

Hence, once the $\Delta_{\text{app}}H$ has been determined, the rate of reaction for the system may be monitored directly.

Typical calibrations are explained in Article 1 (103).

1.7 Substrates used in the report

1.7.1 Avicel (Fluka: PH-101) and Sigmacell (Sigma: Type 20)

Both are commercial preparations of treated α -cellulose⁵; the main difference is in the starting particle size, Avicel at $50 \mu\text{m}$, and Sigmacell at $20 \mu\text{m}$. For the optimal use in ITC, when preparing these substrates they are first suspended in the standard assay buffer, 50 mM sodium acetate, 2 mM CaCl_2 and 0.01 % Triton X-100, and then subjected to homogenization using a Ultra Turrax T8 homogenizer for a maximum of 5 – 10 min on ice. Both Avicel and Sigmacell have a crystallinity index⁶ (I_{cr}) of approximately 0.6. Given values reported for the accessible surface area of Avicel (25), and the study we present later in this introduction;

⁵“Given a cellulose-containing material, the carbohydrate portion that does not dissolve in a 17.5% solution of sodium hydroxide at $20 \text{ }^\circ\text{C}$ is α -cellulose. “

⁶ I_{cr} is a measure of how crystalline or ordered the substrate is. On a scale from 0 to 1, 1.0 is 100 % crystalline.

we propose the Turrax increases the available area of these commercial substrates. No effect on the I_{cr} has been recorded here; the 0.57 value measured after Turrax treatment by solid state NMR is in good agreement with product specifications of 0.60.

1.7.2 Phosphoric acid swollen celluloses (PASC), or regenerated amorphous celluloses (RAC)

These are prepared from commercially available substrates. Here, PASC is prepared from Avicel and RAC from Sigmacell. In the current study PASC was used in Article 1 (103) and prepared according to (117), and afterwards RAC (118) was used as it has been described as an easier hydrolysable, more homogenous substrate. During the preparation of the amorphous substrates, the crystallinity is reduced significantly by dissolving the cellulose in 85 % phosphoric acid, see Figure 10 (under Crystallinity Index section). This leads to a decrease in order of the parallel hydrogen bonding system seen in (118,119) Figure 4, and thus a decrease in the crystallinity index to approximately 0.

1.7.3 Bacterial cellulose, (BC)

BC is very pure highly crystalline bacterial cellulose prepared from a commercial product, Nato de Coco⁷, as described in Article 2 (111). The crystallinity index is in the order of 0.9.

1.7.4 Pretreated corn stover, (PCS)

PCS is an agricultural residue treated with dilute sulfuric acid prepared according to the National Renewable Energy Laboratories (NREL) specifications (103), and is the lignocellulose substrate used in this study. The dilute sulfuric acid, heat and pressure treatment serve to separate the lignin, hemicellulose and cellulose fractions from each other (11). The hemicellulose is largely removed (7 % w/w is left after treatment and washing), whereas the lignin and cellulose fractions remain largely unaffected, with 57 % cellulose and 27 % lignin present in the PCS substrate used in this study (103). Neither crystallinity nor the degree of polymerization is reported here for PCS. The lignin fraction interferes with both the NMR and spectrophotometric methods.

1.8 Some of the factors affecting hydrolysis

We have now introduced the enzymes and substrates as well as some of the more basic background for this project. The purpose of this section is to introduce the reader to the next level of cellulase:cellulose interactions, some of which will be dealt with in more detail in the following chapters and articles. We

⁷ Apparently a Filipino dessert, haven't tasted it. ☺

introduce the burst phase (fast initial rate) and slowdown of hydrolysis and some potential substrate characteristics which have been attributed to this.

There are many substrate related factors which play a role in the enzymatic degradation of cellulose. The ratio of crystalline to amorphous areas, I_{cr} , the degree of polymerization, DP_N , the accessible surface area, ASA, the ratio of substrate to enzyme S:E, the degree of conversion, product inhibition, and enzyme inactivation to name a few (20,21,23,25,32). It is beyond the scope of the current project to address all of the above factors but we have endeavored to limit some of them in order to study the effects of others.

1.8.1 Degree of polymerization, DP

The degree of polymerization (as reported here) is measured using a spectrophotometric method where the number of reducing ends are determined by the BCA assay (as described earlier, and outlined in Article 2 (111)) and the total sugars are measured by dissolving the cellulose completely to glucose monomers, which are then quantified by the phenol-sulfuric acid method (67,79). The DP_N is then the ratio of total sugars to free reducing ends. This is an important parameter for the processive CBH's which typically are represented as attacking from the chain ends, and may be equated with a substrate concentration for this enzyme class. The length of the cellulose chain is also of interest in CBH kinetics, as this represents the theoretical maximum number of catalytic events before the CBH must release and find another chain end to begin a new round of hydrolysis.

The DP_N is also used to follow EG activity over time as described earlier as a result of their internal attack on the cellulose chain, rapidly decreasing the DP_N (23,25,50). We see this in Article 1 (103) where PASC hydrolysis by a mixture of cellulase enzymes is followed over time, and the decrease in DP_N is directly proportional to a decrease in heat signal. The degree of polymerization of cellulose remains relatively constant for each substrate in the study, approximately 200 glucose units per cellulose chain is the number averaged DP_N , measured on Avicel, Sigmacell, PASC, RAC and BC. This is in good agreement with reported values although BC is low (reported approximately 1000 (25)). We attribute this to the further processing of BC after extraction, in that the substrate is blended to homogeneity, and mechanical action may affect the DP_N . No DP_N is reported for PCS, due to the opaque nature of the substrate, precluding spectrophotometric quantification.

1.8.2 Two areas for hydrolysis?

One theory is that there are two areas or portions of cellulose available to the enzyme for hydrolysis, one is preferred, and is hydrolyzed first accounting for the rapid initial rate, followed by a slower rate as all these

“good” sites are removed. This would lead to a fast initial rate of hydrolysis followed by a slower rate as these areas disappeared.

A convincing study by Yang and co-workers was carried out using so-called restart experiments (120). Here, the hydrolysis was allowed to continue for a certain amount of time, stopped, and all enzyme removed. If the easily accessible regions were depleted, addition of fresh enzyme to the same substrate would result in a hydrolysis rate similar to the rate just prior to stopping. However, upon removal of the enzyme, a complete burst phase was re-established when new enzyme was introduced to the partially digested substrate. This is a very good indication the fast initial rate is not solely due to different regions of substrate.

We support this conclusion through a type of restart experiment unique to ITC where we add fresh enzyme to partially hydrolyzed substrate in Article 1 (103). We do not remove the enzyme but can re-establish up to 85 % of the original burst phase with a similar kinetic profile. The remaining 15 % may be a result of the remaining enzyme still on the cellulose surface.

1.8.3 Crystallinity Index, I_{cr}

As mentioned in the substrate section, the crystallinity index is a measure of how crystalline the substrate is. In this report the I_{cr} is measured using solid state NMR, based on the ratio of the C-4 peaks by integrating the areas, calculated as $X/(X+Y)$ as shown in Figure 10 on the left (121-123). The role of crystallinity is complex and there are conflicting reports about the importance of this substrate characteristic (124-130).

The role of crystallinity is connected to the previous theory in observations where it has been postulated the two areas are represented by the amorphous and crystalline regions; in that the amorphous areas should be easier to degrade than the crystalline cellulose, thus representing the easy and hard areas, respectively. In other words, the cellulases degrade the amorphous regions first, and this is followed by the harder to degrade crystalline regions. If this were the case, it follows there would be an increase in the relative crystallinity index of the substrate as the hydrolysis continued and the amorphous regions are decreased. Indeed, some researchers have reported this (124-126), and Lee (127) reported an increase in I_{cr} from 0.78 to 0.84 over the course of a 96 h hydrolysis. This could reflect a preferential decay pattern in that if the amorphous regions are degraded first, the overall crystallinity index will increase as described here.

This has been contested by reports that there is no effective change in the I_{cr} over hydrolysis periods, and rather that other structural features play a more prominent role such as surface area and the degree of polymerization (128,129). Indeed, a recent study by Hall and co-workers (130) suggests the hydrolysis rate

may be dictated by the crystallinity, but that all regions are depleted simultaneously, measuring up to 90 % conversion of Avicel with no I_{cr} change.

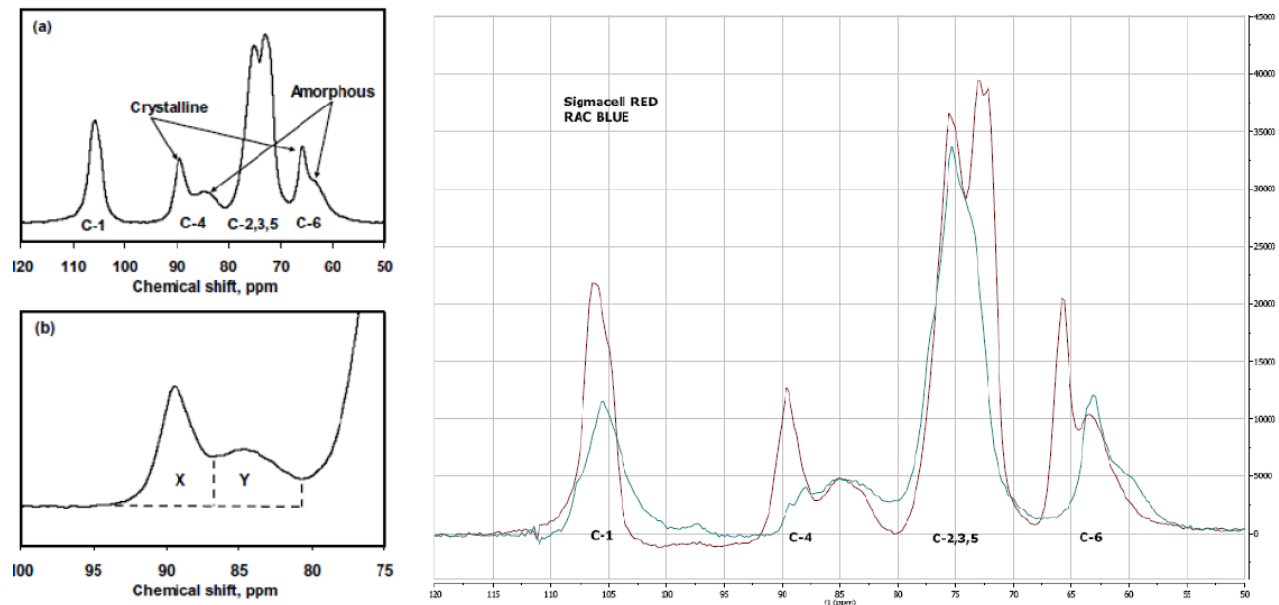


Figure 10. An example of the solid state NMR (CP/MAS⁸) spectra of crystalline and amorphous cellulose types.

(L) An example of the calculation is performed for determining the crystallinity index (121). (R) The Sigmacell is the untreated commercial product with a crystallinity index, I_{cr} of 0.57. The RAC is prepared from the Sigmacell and is presented here as the blue spectrum. We have chosen to define the complete disappearance of the crystalline top as completely amorphous for the purpose of this investigation. The samples are freeze dried and solid state NMR performed as outlined in Article 1 (103)

Hall and co-workers generated a series of the same Avicel substrate with different crystallinity indexes through varying the concentration of the phosphoric acid, and thus the amount of conversion to an amorphous substrate. A higher crystallinity index was directly associated with a slower initial rate, but measuring the I_{cr} throughout the hydrolysis of Avicel (untreated) showed that the amorphous regions were not degraded first. They propose therefore it is other physical changes that account for the slowdown of cellulases.

In the Chapter 2 we return to this introduction and investigate further the effects of crystallinity on hydrolysis.

1.8.4 Product Inhibition in hydrolysis

Rather than a specific substrate factor, the slowdown of cellulose hydrolysis has also been attributed to certain enzymatic factors, including inhibition. This includes cellulase inhibition by glucose and cellobiose, the main products in an industrial setting. Product inhibition has become more of a focus in recent times

⁸ Cross polarized, magic angle spinning.

due to the higher concentrations present in high solids (> 10 % dry weight) hydrolysis reactions (131). This decreases the overall cost of the process but leads to higher concentrations of products in the reaction vessels. Both glucose and cellobiose have been shown to inhibit in particular CBHs and β -glucosidase, although many studies have been focused on cellulase mixtures and complex (lignocellulosic) substrates (69,87,95,132-135). We propose in order to truly understand the inhibition effect, studying the individual enzymes on a less complex substrate is first necessary in order to pin point where the weak links in a cellulase mixture are.

In Article 3 the activity of EG on RAC is monitored directly, without any added enzyme amplification. The enzyme doses are by necessity higher than those of the amplified CBHs in order to attain a significant thermogram, but here we compare the three main EGs produce by *T. reesei* and observe even with an EG and an ideal amorphous cellulose substrate do not lead to a steady state kinetic behavior. We build upon the investigation of EGs by adding cellobiose and glucose to determine the effects of product inhibition, as outlined in Article 4.

It is not possible to study CBH product inhibition using the amplification system (described in Article 2 (111)) as added cellobiose or glucose would contribute greatly to the heat signal. Product inhibition of the cellobiohydrolases is removed in the amplification system through the excess dosing of BG, converting the cellobiose rapidly to glucose.

1.8.5 Enzyme adsorption to cellulose and cellulose accessible surface area

In this section we present some experimental data. Here we have performed an adsorption study simultaneously with a hydrolysis reaction for a number of substrates. The purpose of this is to relate the amount of enzyme bound to the substrate, with the rate of hydrolysis.

Two of the three substrates were measured for their available surface area prior to this and the correlation between the amount of enzyme adsorbed and the accessible surface area is also presented here. The same amount of enzyme was added to the three substrates and aliquots taken over timed intervals to determine the concentration of hydrolysis products and the amount of enzyme still present in the supernatant.

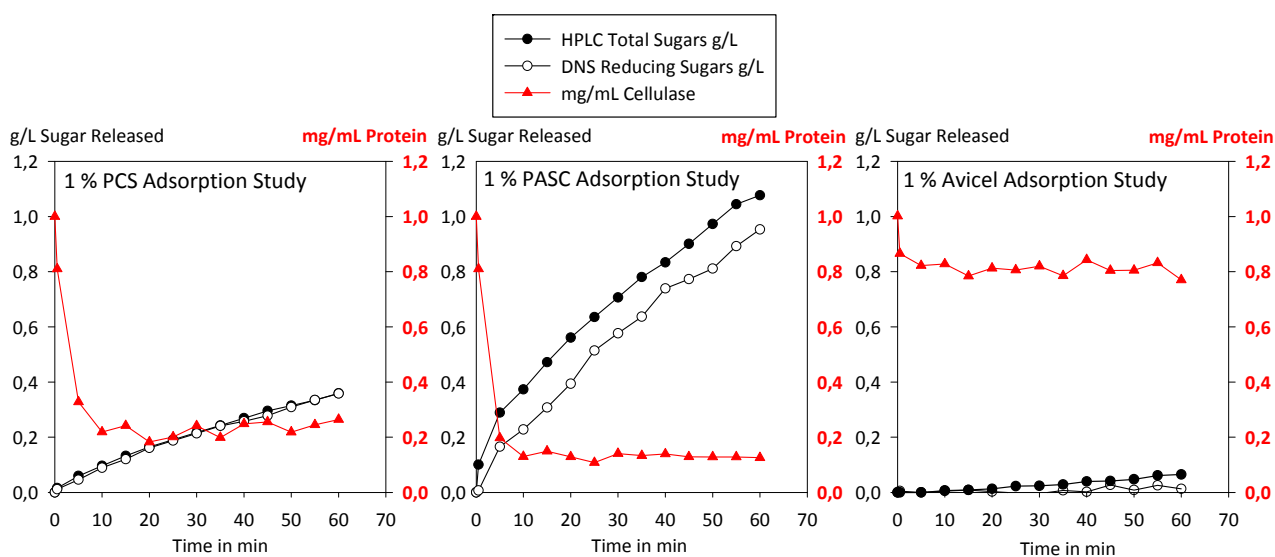


Figure 11. Adsorption study of Cellulcast 1.5 L and three substrates. T = 25 °C, pH = 5

Samples were taken at timed intervals and quenched using 20 % H₂SO₄ (50 µL/mL). HPLC and DNS were measured as outlined in Article 1 (103). Protein concentration based on the Bradford assay (136), and all Cellulcast 1.5 L standard curves were produced in the filtered supernatants of the selected substrates to minimize background error. The buffer control registered no decrease in enzyme concentration over the monitoring period (data not shown).

Shown above are three different substrates, lignocellulose PCS, amorphous PASC and crystalline Avicel. To each has been added 1 mg/mL total protein from a commercial mixture of cellulases, Cellulcast 1.5 L. The very first sample for sugar and protein concentration was taken as soon as a homogenous mixture had been attained (ca. 30 s). Here we see there is an immediate adsorption of at least 0.2 mg/mL which is the equivalent of 4 µM total protein. It is interesting to note that even though the amount of protein adsorbed to PASC is only approximately three times that adsorbed to Avicel; the difference in sugar production rates is almost double this value with PASC producing 1.1 g/L after 1 h compared to Avicel with 0.07 g/L. So we may state that even for the same amount of enzyme bound to the surface, the rate of hydrolysis is not the same. This may already be an indication of the crystallinity playing a role⁹, and is further investigated using CBH's in Chapter 2. Almost the same amount of enzyme is adsorbed to PCS as to PASC but it is uncertain how much of this is active and how much is bound to lignin; and this may explain the slower rate of hydrolysis.

To further investigate and see the effect of available surface area, a dye binding experiment using Congo red as outlined by (137,138) was carried out (See Appendix 2 for materials, methods and set up). This is based on the binding of Congo red which binds as a dimer to the accessible surface area of the cellulose. While this is an indication of the amount of relative area available, it should be remembered the size of

⁹I_{cr} PASC = ca. 0, Avicel = 0.57

Congo red is far smaller than that of a cellulase molecule (area = ca. 2 nm² compared to cellulase of ca. 30 nm²). However, this dye experiment does allow for direct comparison of two substrates. Congo red is thought to bind to cellulose in a manner similar to a CBM i.e. through stacking interactions¹⁰.

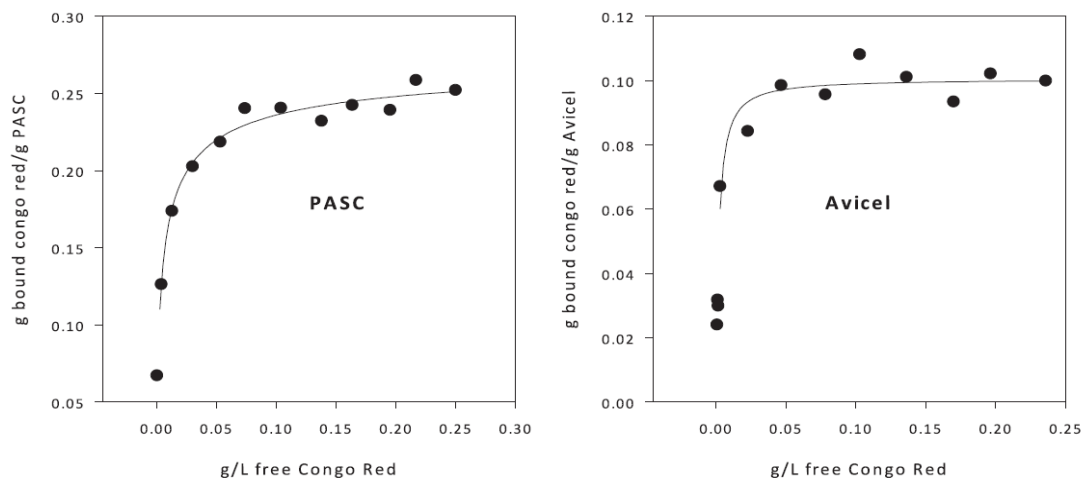


Figure 12. Langmuir isotherms for Avicel and PASC binding Congo red.

Modeling the data to the Langmuir adsorption isotherm (Appendix 2), the values of a , the maximum adsorption are PASC 0.27 g/g and Avicel 0.1 g/g. So there is approximately a factor three in the difference. This could have been higher initially, but the Avicel has been treated using a Turrax for ITC experiments to homogenize the particulate suspension, and this mechanical action may have increased the relative accessible surface area (other methods report a difference of up to 20:1 in ASA of these two substrates (25)). To try and directly compare the maximum adsorption levels of Congo red to bound protein, the following may be shown.

$$\frac{0.27 \text{ g Congo red}}{\text{g PASC}} \times \frac{10 \text{ g}}{\text{L}} \text{ PASC} \times \frac{2 \text{ nm}^2 (\text{congo red}) \times 2 (\text{dimer})}{30 \text{ nm}^2 (\text{avg. cellulase})} = 0.36 \text{ g/L Max. bound cellulase}$$

Equation 2. Using Congo red to estimate the amount of bound protein.

For PASC we measure 0.78 g/L bound enzyme using the Bradford assay. Taking into account that we measure total protein in the supernatant, and use an averaged molar weight for all cellulases, this is an acceptable correlation. The ratio of PASC-bound enzyme to Avicel-bound enzyme is 0.78 mg/mL to 0.23 mg/mL or 3.4:1. Given the ratio of accessible surface areas using this technique is essentially identical at 2.7:1, this is a very good indication that the surface area plays a very important role in determining how much enzyme initially binds to the substrate.

¹⁰ The aromatic residues on the cellulose binding module interact with the glucosyl units on the cellulose surface.

We now investigate the rate of hydrolysis, taking the PASC HPLC data as an example. We convert to g/L/s and plot this rate as a function of time. Here we also include a later measurement performed after 2 h of hydrolysis. This serves to introduce the reader to ITC data where we will be directly measuring a rate rather than converting single points of concentrations to rates. Neither the PCS nor Avicel data could be analyzed in this way as the concentrations were too low.

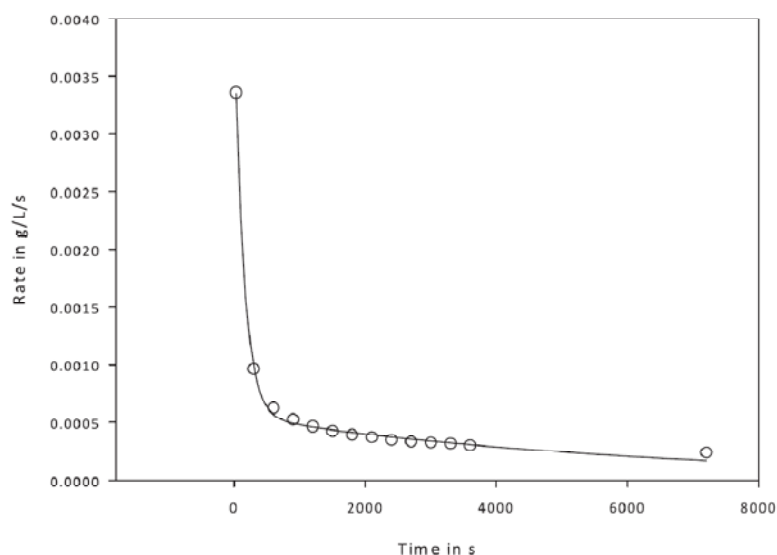


Figure 13. ○ = The converted rate of hydrolysis of PASC vs. time. The line represents the fit explained below.

In brief, the rate data is fitted to the following function using Origin Pro V 8.0,

$$y = A1.e^{(-at)} + A2.e^{(-bt)},$$

where y is the heat flow, t is time, $A1$, $A2$, are amplitude constants and a and b are decay constants. For now these values are treated empirically, and the purpose of this example is to illustrate the decay in rate. The use and application of this sum of two exponentials fit will be expanded upon in the Chapter 2. Table 2 summarizes the parameters found. $R^2 = 0.99$

Table 2. The sum of two exponentials from Figure 13 parameter values.

Parameter	Value
A1	0.0034 g/L/s
a	0.0068 s ⁻¹
A2	0.0006 g/L/s
b	0.00017 s ⁻¹

Despite the fact there is the same amount of enzyme still bound to the surface after 30 min; the rate of hydrolysis is severely decreased. We can see there is also a need for better time resolution in the case of PCS and Avicel, which can be provided by direct rate measurements using ITC. In addition to simply being

able to see the difference in two enzymes, we also provide mechanistic information from the ITC Data in the following chapters. Investigating why this rate decreases so drastically is of paramount interest and we demonstrate the uses of ITC to this end.

In the following studies, we investigate singular purified enzymes, at far lower doses than here. A typical dose is 50 nM which is approximately 2.5 mg/L, and therefore the surface area of the cellulose should not play a significant role there.

1.9 Thermochemical screening

Screening *per se* is the general name given to the method by which candidates are selected for further testing and application development in Industry. The method of screening must reflect the best candidate for the application, rather than the best candidate for the screening method. This is coined in the age old adage “You always get what you screen for”.

This of course also refers to the concept that enzyme discovery is precluded due to the intractable nature of screening techniques. This is a fundamental issue with modern screening, in that the best candidate screened may not reflect the best candidate for the application. This is not limited to cellulases, as the following example explains. Screening for protease activity for a detergent application using a soluble substrate Suc-AAPF pNA¹¹ on Carlsberg Subtilase had a k_{cat}/K_M eight times higher than BPN' Subtilisin. k_{cat}/K_M is often explained as the enzymatic efficiency, combining the maximum rate of hydrolysis with the apparent affinity of the enzyme for that substrate. However, wash tests showed BPN' Subtilisin had far better stability and performance (139). The same may be said for cellulases, and the comparison between soluble substrate assays and insoluble hydrolysis results often do not correlate (24). This is due to a variety of factors as illustrated above. The action of a cellulase on a soluble substrate cannot reasonably be equated with its activity towards an insoluble two dimensional cellulose surface. However, these soluble substrates are a good tool in some cases. For example, in Chapter 3 we demonstrate the use of such a substrate to measure the relative activities of protein engineering variants of TrCel7A. As the variants have been altered in their carbohydrate binding module, and this has no effect on activity to soluble substrates (140,141), we use this activity to measure the amount of *active* protein present, a critical factor in screening.

At this point the reader is directed to read Article 1 (103). This will provide an introduction to hydrolysis reactions and measurements using ITC. Here we present hydrolysis by cellulase mixtures of three typical

¹¹ N-Succinyl-Ala-Ala-Pro-Phe-p-nitroanilide is a polypeptide used for protease activity measurements.

substrates used in academia and industry. We demonstrate how calorimetry may be used to directly measure the rates of hydrolysis, regardless of the physical attributes of the tested substrates. This will provide a better understanding for the coming investigations where this technology will be applied to both screening and mechanistic interpretation of ITC data.

Chapter 2. Thermochemical analysis of cellobiohydrolases; *TrCel6A* and *TrCel7A*

2.1 Background

2.1.1 *TrCel7A*, CBH I

TrCel7A, formerly CBH I of *T. reesei* is the most abundant cellulase produced by the fungus, and is consequently the most studied (39,55,142-144). As briefly described in Chapter 1, the cellulase has two distinct domains, the catalytic domain (CD, Core) and a carbohydrate binding module (CBM) found at the C-terminal end of the protein (43,44). The role and function of the CBM is dealt with in more in detail in Chapter 3, where we investigate protein engineering variants of *TrCel7A*-CBM I. The structure of *TrCel7A* has been elucidated (39,144). The catalytic domain is a 50 Å long tunnel, enclosed by 4 loops partially stabilized by disulfide bridges with 10 glucosyl binding residues numbered -7 to +3 (with -1/+1 assigned the hydrolysis center) (55,58,143,144). *TrCel7A* is traditionally represented as progressing along the cellulose chain from the reducing end (29), releasing cellobiose as the main product (25). The interaction with the cellulose chain in the tunnel involves hydrogen bonding and stacking interactions with four essential tryptophan residues which serve to rotate the chain up to 140 ° in order to orientate the β , (1-4) bond in the appropriate alignment for hydrolysis (58). Hydrolysis is carried out by the two glutamic acid residues E212 and E217 by a double displacement retention mechanism (42,143). *TrCel7A* is widely believed to act in an *exo*-fashion in that it attacks from the free reducing ends of the cellulose chain and not in an *endo*-fashion attacking randomly at the cellulose surface (23). This theory is supported by the concept that the twisting action in the active site tunnel which would not be optimal if the tunnel opened to attack the cellulose chain (142). There is also a lack of activity on CMC¹² with highly purified *TrCel7A* preparations (145) which indicates the enzyme is blocked by the chemical substitutions, as would be expected for a processive enzyme. There have also been labeled reducing end studies (49), following the hydrolysis of *TrCel7A* based on the release of a labeled reducing end, this would not be the case if *endo*-attacks were initiated. This is however, challenged by recent results comparing *exo*- and *endo*-attack products indicating that *TrCel7A* can indeed open the catalytic tunnel to attack the cellulose chain in an *endo*-fashion (52).

2.1.2 *TrCel6A*, CBH II

TrCel6A, formerly CBH II is the second most abundant cellulase produced by *T. reesei*. It too has the distinct two domain structure although the CBM is placed at the N-terminal (40). The tunnel of the catalytic domain is shorter at 20 Å with two loops which are stabilized by two disulfide bridges (40). There are four defined

¹² Carboxymethyl cellulose, a soluble cellulose substituted with carboxymethyl groups, typically used in EG assays.

glucosyl binding sites, denoted -2 to + 2, with three tryptophans interacting with the glucosyl moieties (146). Hydrolysis is carried out by two aspartic acid residues, D175 and D221 by an inversion mechanism (59,147). In contrast (perhaps) to *TrCel7A*, *TrCel6A* is known to be *endo*-processive (53), in that the two loops can open to allow the catalytic domain direct access to the cellulose chain (146). However, once bound, the enzyme moves from the non-reducing end producing mainly cellobiose (29,55). In addition to these differences in structure and function, the CBM for *TrCel6A* has two tryptophan residues which replace the corresponding tyrosine residues on *TrCel7A* (40,148). The replacement of tyrosine by tryptophan has been reported to increase binding of the CBM to the cellulose surface (149). Of the two CBH's *TrCel6A* is less studied, possibly due to the fact non-reducing ends cannot be chemically modified or that the *endo-exo*-nature of this enzyme makes it more difficult to study.

2.2 Comparing *TrCel7A* and *TrCel6A*

The development of a thermochemical method to compare *Cel6A* and *Cel7A* wild types as well as further understand the interactions between cellulose and cellulase has been a focus in this study. To this end, the amplification system described in Article 2 (111) has been used. The reader may find it advantageous to read this article now in order to gain insight into the coupled assay and the potential it has for screening in an industrial setting. As a result of the amplification coupled assay, we can monitor the action of as little as 5 µg of enzyme; this is a very important factor where for example, protein engineering variants may not be plentiful. We can directly monitor the hydrolysis of insoluble unmodified cellulose with a time resolution presenting rate data using the non-destructive ITC method. At the very simplest, the data may be directly compared to evaluate enzymes' action on actual industrial substrates, as well as the more commonly used model substrates. We present a method to evaluate CBHs here, and show also how the data may be further analyzed to gain more insight into the mechanistic action of these enzymes.

Firstly, we present a study of the systematic evaluation of the action of both *TrCel7A* and *TrCel6A* on two substrate types, amorphous RAC, and crystalline BC. PCS (lignocellulose) will be dealt with separately after RAC and BC due to its more complex nature. The method employed here is straightforward; the enzyme is prepared in the same buffer as the substrate, and loaded into the ITC syringe. The cell is filled with substrate and the amplification mixture of enzymes (in order to increase the thermal signal), and allowed to come to thermal equilibrium. Upon injection of the enzyme a total of 50 nM is present in the cell. This presents the following issues:

- Although adsorption plays a pivotal role in cellulase kinetics and has been used in many models previously (126,150-153), the rate of adsorption of the enzyme at this dose (50 nM) is very fast¹³ (154),
- The heat associated with the adsorption of the cellulase to the cellulose is also minimal at this dose. Taking one of the higher reported values for the enthalpy of adsorption, -50 kJ/mol (155-157), and injecting a final dose of 50 nM to a cell of 0.957 mL over 10 s the error may be calculated:

$$\frac{50 \text{ nM} \times 0.000957 \text{ L} \times -50 \frac{\text{kJ}}{\text{mol}}}{10 \text{ s (injection time)}} = -0.24 \frac{\mu\text{J}}{\text{s}}$$

Equation 3. Heat associated with the adsorption of 50 nM CBH to cellulose.

A typical hydrolysis reaction which is amplified produces far in excess of 10 $\mu\text{J/s}$ in the first 10 s; so the heat of adsorption may be disregarded.

- The accessible surface areas of RAC and BC have been reported to be quite close to each other (25) at 240 and 200 m^2/g , respectively, and we have measured the DP_N of RAC with 180 ± 14 , BC with 236 ± 7 (111), so these two substrates may be compared to investigate crystallinity, where RAC has an I_cr of ≈ 0 , and BC has an I_cr of 0.87
- Due to the extreme low dose of enzyme, the conversion of the cellulose during the monitoring period is very low (< 3 %), the significance of this will be outlined later.

2.2.1 Hydrolysis results on RAC

The raw data are presented first in the form of the thermograms produced by the ITC. The curves are labeled according to the amount of cellulose present in the sample. Analysis of the raw data will be presented later.

Here we present a dose response curve for the hydrolysis of RAC¹⁴ by the individual cellobiohydrolases. There are a number of features illustrated here. Firstly, the time scale for the measurement of the rates is one point every 2 s (although the instruments time constant plays a role which is discussed later) on a completely opaque suspension and is independent of errors associated with further processing of the substrate for chemical analysis. Secondly, both graphs represent the rates of hydrolysis for the individual

¹³ 50 nM TrCel7A to 120 μM reducing ends of RAC (4 g/L) takes under 10 s to adsorb completely, measured using residual activity on the soluble substrate pNPL in the supernatant, Jens Elmerdahl Olsen, unpublished results.

¹⁴ As a reminder: RAC = Regenerated amorphous cellulose prepared from the commercial product Sigmacell, with effectively little or no crystalline regions.

CBHs in the presence of a β -glucosidase i.e. with no significant cellobiose product build up and therefore less product inhibition, as is often the case in industry. Thirdly, we can already see that under the investigated conditions where the enzymes are dosed equally, that the *TrCel7A* hydrolysis rates (as expressed by the heat flow, $\mu\text{J/s}$) appear to be relatively faster by simply looking at the ordinate and reading the thermal signal for the same cellulose doses. Lastly, the thermal signal scales proportionately to the amount of substrate S_0 present, as would also be expected in completely soluble systems, where more substrate would result in a faster initial rate (up to a saturation point). This is also a good indication that we have not yet reached the V_{max} for this system.

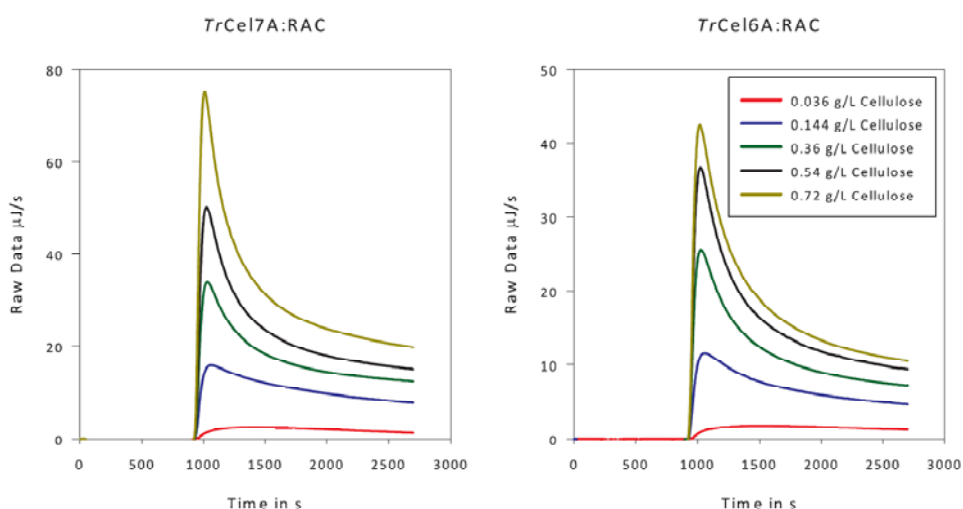


Figure 14. A direct comparison of the rates of hydrolysis for *TrCel7A* and *TrCel6A* on insoluble amorphous cellulose.

Note: Exothermic is up. NanoCal ITC, 250 rpm, pH 5.0 50 °C, 600 s baseline, 300 s 0.1 μL injection, monitoring time of 1800 s after 10 μL injection of enzyme at 900 s.

Now we take a closer look at the form of the hydrolysis curves. It is quite evident that both enzymes begin with large exothermic signals, an initial rate accelerating until an apex is reached, where we assume all enzymes (that can be) are now adsorbed and are involved in catalysis. This is, however, quite short lived as the hydrolysis rate declines relatively rapidly again. This is the characteristic burst phase of cellulases. These are enzymes which during a hydrolysis do *not* reach steady state, which would be indicated here by a flat line indicating a constant rate of heat production.

Using the 0.72 g/L cellulose curves as an example; the rates for both enzymes fall by approximately a factor 4 in the first 30 min of hydrolysis. This is not the case when we examine the lowest substrate dose, 0.036 g/L cellulose. The characteristic peak is missing here, and this is likely due to the time constant of the equipment and the time needed for the entire amplification system to reach a steady state and perhaps the low S:E ratio (we return to this later). The coupled assay relies on the amplification of the product

cellobiose, and at very low rates of production, the time to reach steady state is in the region of 200 – 300 s as outlined in Article 2 (111). This in effect means at low substrate concentrations, the initial rate is poorly reflected by the thermogram, and the peak disappears completely. Regardless of this, the heat signal represents the total hydrolysis and integrating the ITC data is free from instrumental interference under the monitoring periods presented here.

2.2.1 Hydrolysis results on BC

Again here we see the rates measured directly representing the hydrolysis of in this case crystalline ($I_{cr} = 0.87$) cellulose. Comparing the raw data as before, we can see the relative rate ($\mu\text{J/s}$) of *TrCel7A* appears again higher than that of *TrCel6A*. By comparing Figure 14 and Figure 15 we can compare the relative rates of the same enzyme on an amorphous and a crystalline substrate. With the naked eye we can see the $\mu\text{J/s}$ signal is approximately 6-7 times stronger for the amorphous cellulose.

We can see from both substrate graphs, there is a drastic decrease in rates, which is more pronounced at higher substrate concentrations. There are two rate decreases, the initial decrease right after the apex, and an underlying rate decrease coupled to this, seen in the longer time monitoring times where there is no steady state reached. Both appear to be affected by the substrate concentration indicating first order processes. In order to analyze the data, we first explain some background on cellulase kinetics.

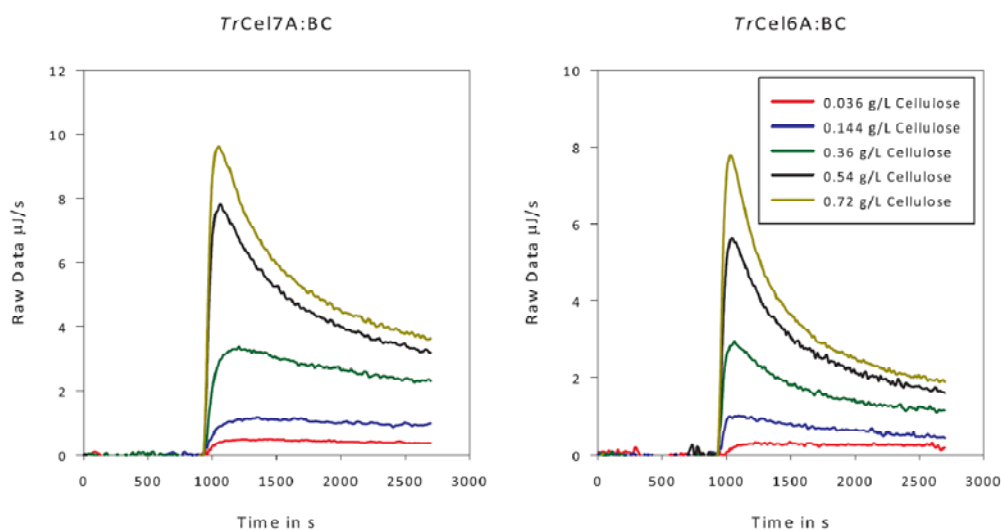


Figure 15. A direct comparison of the rates of hydrolysis for *TrCel7A* and *TrCel6A* on insoluble crystalline cellulose.

Note: Exothermic is up. NanoCal ITC, 250 rpm, pH 5.0, 50 °C, 600 s baseline, 300 s 0.1 μL injection, monitoring time of 1800 s after 10 μL injection of enzyme.

2.3 Kinetics of cellulases

The recalcitrant nature of cellulose is well reported (20,23-25). The degradation of cellulose under industrial conditions is such that over 50 % of the total glucose yield is produced in the first 8 h, while it

takes almost 96 h to achieve yields over 85 % (86). Cellulose hydrolysis is often described as having a “burst phase” a rapid initial rate followed by a slower rate of degradation (120,151,153,158-162). Some of the theories for this have been presented in Chapter 1. Cellulase kinetics are difficult to model as the enzyme and substrate interactions are *not constant* over time, and the substrate is an insoluble solid, leading to heterogeneous reaction conditions (151). This is already evident looking at the raw data presented here; there is no steady state level reached during the hydrolysis which would be represented by a flat line, or a constant production of heat (i.e. product).

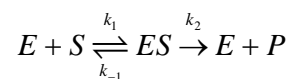
The major processes investigated in the current work are based on the assumption that there are four main processes involved in cellulase kinetics (151).

1. Adsorption of the enzyme to the substrate, this includes the formation of a viable ES complex and the location of a bond to hydrolyze.
2. Hydrolysis of the $\beta,1-4$ bond and in the case of cellobiohydrolases, procession along the cellulose chain.
3. Desorption of the enzyme, for example, upon reaching the end of the cellulose chain in the case of cellobiohydrolases, or reaching a “blocked” region due to the heterogeneous surface of the cellulose substrate (crossed chains, blockages). Or in the case of EG’s simply diffusing off the chain.
4. Decay or deactivation of the enzyme, herein inhibition.

In Article 3, we introduce a mechanistic interpretation for the kinetic action of EGs on insoluble cellulose, but for now we concentrate on CBHs. In Chapter 3 we investigate *TrCel7A* CBM protein engineering variants, and here we investigate the hydrolysis action of both *TrCel6A* and *TrCel7A*.

2.3.1 Burst phase kinetics, processivity model

In the Chapter 1 we introduced some of the substrate specific explanations for the observed decrease in hydrolysis; however, there are also enzyme specific kinetic reasons for a burst like behavior. In a normal Michaelis-Menten enzyme-substrate reaction the following scheme is used

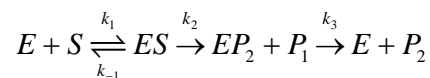


Equation 4. The Michaelis Menten equation.

This represents the model derived by Leonor Michaelis and Maud Leonora Menten based on Invertase around 1913 (163). For those less familiar with enzyme kinetics, we summarize as follows. Here an enzyme

(E) and a substrate (S) collide at a rate dictated by the second order rate constant k_1 , where the rate is given by $V = k_1[E][S]$. If the collision results in the formation of a viable ES complex, this complex may now proceed either in the reverse direction according to the first order rate constant k_{-1} at a rate of $k_{-1}[ES]$, or forward to form the product P, according to the first order rate constant k_2 at a rate of $k_2[ES]$. Already, here the assumption is that there is no re-formation of the ES complex dictated by the second order rate constant k_{-2} at the rate $k_{-2}[E][P]$. Briggs and Haldane in 1924 further simplified this by assuming a steady state is reached where the rate of change of $d[ES]/dt = 0$, that is to say the (ES) complex is being formed as fast as it is being broken down.

Now we proceed to a system where there is one substrate and two different products, P1 and P2. In an ordered uni-bi reaction¹⁵ (with soluble substrates, e.g. a hydrolysis reaction when water is not explicitly included as a substrate) the reaction is



Equation 5. The uni-bi ordered reaction equation.

Here there is an ordered sequential reaction occurring. The formation of the ES leads to the production of one product first, P1, followed by the generation of the second product P2. Thus if k_3 is small compared to k_1S_0 and k_2 , there is an initial build up of P1, relative to P2, and a large proportion of the enzyme remains in the EP2 complex. This leads to an initial fast rate of P1 production, which is followed by a slower apparent rate, V_{app} as the more and more of the free enzyme population is bound up in EP2, and slowly released. This forms the basis for the burst model presented here and outlined in detail in (162).

To look at cellobiohydrolase kinetics, a slightly different approach must be considered. Firstly, the formation of ES is not solely dependent on random collision; rather the enzyme must first find the correct attack point on an insoluble two dimensional surface. This may involve both collision and diffusion along the surface to find an attack point. The kinetic rate constants presented here for cellobiohydrolase hydrolysis of cellulose are k_1 , the rate constant describing adsorption, k_{-1} and k_3 are both rates constants for desorption (either through slipping the substrate or releasing from the substrate after a catalytic cleavage), and k_2 is the rate constant for catalysis. P1 is cellobiose and P2 is the remaining cellulose chain (a.k.a. the second “product”). Initially, the CBH adsorbs to the cellulose chain and upon formation of a productive ES, begins catalysis. As this progresses for many rounds of hydrolysis before the enzyme desorbs again (due to

¹⁵The term ordered uni-bi reaction comes from the ordered scheme where P1 is always released before P2, and one substrate (uni) produces two different products (bi).

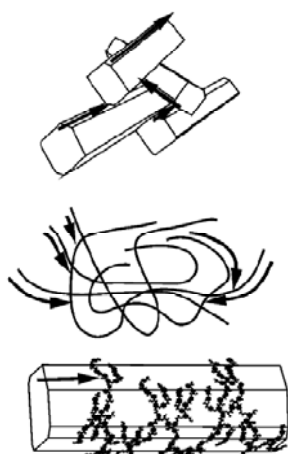


Figure 16. Possible hindrances affecting the procession of CBHs (165).

Top: Overlapping cellulose crystalline regions, chain ends. Middle: Amorphous cellulose represented by a disordered pattern of chains. Bottom: Non-cellulosic components, i.e. lignin, hemicellulose retarding the rate of CBH processivity.

The mathematical model presented in (162) is not used to fit the data generated by the ITC, however, this model is used to illustrate the parameters which will be presented later in the report, in particular k_2 and k_4 , to which the ITC data is better suited for determining. Here we present a more stylized rendering of the model.

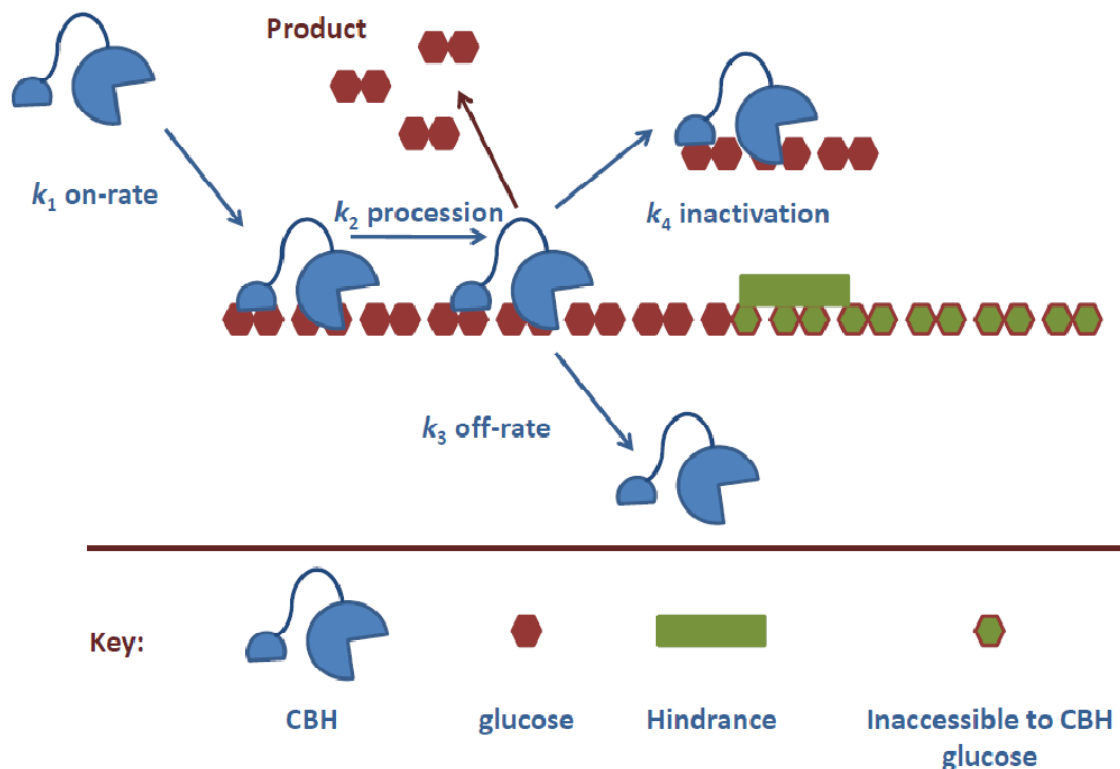


Figure 17. A model for processive cellulases. (162)

The probability of an enzyme becoming inactivated may be seen from Equation 6 to be $k_4/(k_2 + k_3 + k_4)$, thus a higher k_4 indicates an enzyme which is more likely to become inactivated in a shorter time. From a screening perspective, the k_4 parameter should therefore be as low as possible. Now we take k_2 as the amount of catalytic events the enzyme can perform at a completely unhindered rate with no other rate determining steps involved, and k_4 as the rate constant of inactivation. We can then calculate the average amount of hydrolytic cleavages each enzyme can perform before becoming inactivated, given by the ratio k_2/k_4 .

Using ITC, we directly measure the V_{app} , the rate of hydrolysis. This can be used to determine k_{cat} , given by the relationship $V_{max} = k_{cat} \cdot E_0$. Here we take the $V_{app} (max) = V_{max}$. In the initial part of the thermogram, given the low doses used here, all the enzymes are adsorbed (depending on S_0 , the amount of sites available) and assumed to be productive, so, initially this gives us the relationship $E_{abs} = E_{tot} = E_0$. Once the apex of the curve is reached, we assign this the value $V_{app} (max)$. So, once we have this value, we can divide the V_{app} rate by the total added enzyme concentration ($V_{app} (max)/E_0$) and report a $V_{max}(cat)$. At this peak of the thermogram, there is mainly influence from $k_1 S_0$ (remembering adsorption is rapid under our conditions) and k_2 before dissociation and inactivation begin to influence the rate determining step. We simplify by stating $V_{max}(cat) \approx k_2$ at this point.

There is a slight underestimation of this parameter which is caused by the physical limitations of the machine, as also described in Article 3, and we illustrate using this figure to explain.

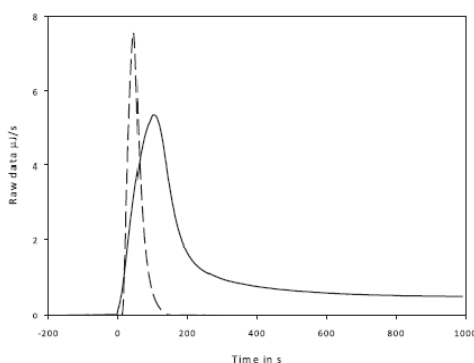


Figure 18 An illustration of the effect of the time constant for the ITC.

Both curves produce the exact same amount of heat during the first 150 s of the reaction. The solid line is the measured data for the *TrCel7B*, 100 nM on RAC 8 g/L, 30 °C, pH 5.0 run. The dashed line is a short pulse of heat generating a signal independent of enzyme and substrate action showing the response time of the instrument. The response time of the instrument may be measured by fitting the pulse to an exponential decay. Here it is recorded as 15 s.

Here we illustrate the slight underestimation of $V_{app} (max)$ from the ITC measurement. As ITC measures heat and is a differential technique, sudden “bursts” of heat such as those associated with cellulose

hydrolysis are influenced by the response time of the instrument. In an ideal system, the dashed line shows the response of the instrument if there were no enzyme or substrate factors involved, i.e. if the heat generation was instantaneous. This shows the underestimation in $V_{app}(\max)$, here measured to be approximately 5 $\mu\text{J/s}$, instead of the ideal 7 $\mu\text{J/s}$. This is a simplification (the enzyme reaction cannot reasonably be equated with a heat pulse), but in effect we conclude the time resolution of the instrument is insufficient to completely resolve the *initial* reaction rate. It is possible to correct for this using a so-called Tian correction by measuring the time constants for the instrument (166). However, from a screening point of view, all reactions are equally affected and so this analysis was not performed here.

Now, we propose the simplification stating $V_{\max}(\text{cat}) \approx k_2$ at the apex may be used in comparative analysis as all enzymes are equally affected by the response time of the instrument.

Now we may investigate enzymes based on the ratio of hydrolytic cleavages each enzyme can perform before becoming inactivated, given by the ratio $V_{\max}(\text{cat})/k_4$.

2.3.2 Modeling ITC data to the sum of two exponentials

In Article 1 (103), we introduce the idea of modeling the ITC data to the sum of two exponential decays. This could be construed as interpreting the data as the sum of two processes, one slow and one fast. For now, this analysis is treated empirically.

This type of decay has been reported by other methods and is not exclusive to ITC measurements. The decay in rate has been modeled to the sum of two exponentials before, for example; describing the action of Celluclast 1.5 L with added Novozym188 action on lignocellulose (167), and *TrCel7A* action on BC (161), and as shown in Chapter 1 with Celluclast 1.5 L and PASC. In brief, the ITC data is fitted to the following function using Origin Pro V 8.0,

$$y = A1.e^{(-at)} + A2.e^{(-bt)}$$

Equation 7. The sum of two exponentials used to model ITC data.

Where y is the heat flow, x is time, $A1$, $A2$, are amplitude constants and a , and b are decay time constants. The data is fitted from the apex of the curve.

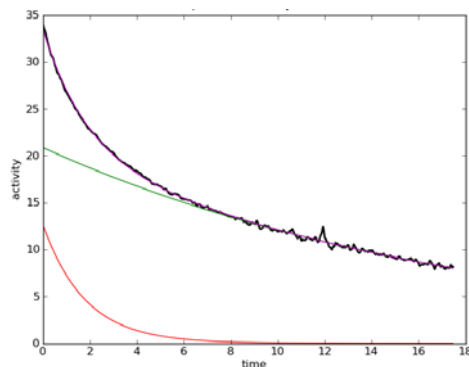


Figure 19. An example of the sum of two exponential decays model.

The red line is the fast decay, the green the slow decay and the black line is the measured data. The purple line is the model fit of the sum of both exponentials. *The units on the scale are arbitrary and are used only for illustrative purposes here.*

Given the thesis is based on thermochemical screening; the rate of enzymatic inactivation is also of paramount importance when selecting wild types or protein engineering variants. The value of the inactivation rate constant is b and may be used and explained as k_4 , and it should be noted the mathematical modeling using Equation 6 (k_4) and the empirical analysis using the sum of two exponentials (b) yield the same number (based on numerical analysis¹⁶). The fitting of the ITC data is throughout this report analyzed using this function; this is a rapid method to determine k_4 , and thus the probability of inactivation of the enzymes under investigation. Throughout the thesis this analysis has been employed and proven remarkably robust on various enzyme and substrate systems, using mixtures, mono components and the amplification coupled enzyme assay.

2.4 Data analysis for *TrCel6A* and *TrCel7A*

2.4.1 Direct conversion to rates

Now we have studied the raw data and explained some of the theory for the rate constants that will be used in the report. In order to further analyze the data, firstly, the ITC raw data is converted to a rate in for example nM/s, using Equation 1, with $\Delta_{\text{app}}H$ = molar enthalpy = -354 kJ/mol, determined in Article 2 (111) for the amplification coupled assay, and V_r = reaction volume = 0.957 mL. This gives us a direct measure for V_{app} , the rate of hydrolysis over the monitoring period. Now we can divide this number by 50 nM, the total amount of enzyme present in order to determine a representative k_{cat} . It should be noted k_2 , the actual catalytic rate constant does *not* change. What changes is the amount of enzyme actively hydrolyzing the cellulose. It follows if there is a larger population trapped or inactivated, the amount of enzyme actually working becomes less and less, leading effectively to a decrease in $[E_0]$ (active). Thus, k_{cat} , calculated from

¹⁶ Attempts to provide a rigorous proof of this have remained unsuccessful.

V_{app}/E_0 instead of $E_{0Active}$ no longer reflects the catalytic efficiency of the enzymes once inactivation begins, as may be seen in the large difference here after 30 min. As V_{app}/E_0 is not a true rate constant (due to the changing concentration of E_{Active}), we call this term the aforementioned $V_{max}(cat)$. However, the $V_{max}(cat)$ may be interpreted in the initial phase as k_2 . This allows the direct comparison of the two enzymes on both substrates as well as the comparison of the action of each enzyme depending on the substrate. The production of α -cellobiose by *TrCel6A* may be taken into account by using -180 kJ/mol as the molar enthalpy in this case.

Directly reading from the graphs below (Figure 20, Figure 21), we can summarize the apparent $V_{max}(cat)$ measurements from the 0.72 g/L cellulose thus:

Table 3. A summary of the hydrolysis rates of *TrCel6A* and *TrCel7A* on RAC and BC at 50 °C.

Enzyme	Substrate (0.72 g/L)	$V_{max}(cat)$ (apex)	$V_{max}(cat)$, at 30 min
<i>TrCel7A</i>	RAC	4.1 s ⁻¹	1.1 s ⁻¹
<i>TrCel6A</i>	RAC	4.6 s ⁻¹	1.2 s ⁻¹
<i>TrCel7A</i>	BC	0.5 s ⁻¹	0.2 s ⁻¹
<i>TrCel6A</i>	BC	0.8 s ⁻¹	0.2 s ⁻¹

Before beginning the more complex fitting of the data, already there are some interesting characteristics to be pointed out here. Both enzymes exhibit a marked decline in rate over time; this is evident for the hydrolysis of both substrates as well here, and may be the reason why such a variety of turnover numbers have been previously reported in the literature (44,69,168-170). Such values for (e.g.) the hydrolysis of amorphous cellulose by *TrCel6A* range from 8 s⁻¹ (69) (10 s incubation time) to 0.04 s⁻¹ (44) (3 h incubation time)¹⁷.

The turnover rates reported are very dependent on the incubation time (all other conditions equal) with the substrate; this is further examined in the case of EGs as well in Article 3. Here, on both substrates, *TrCel7A* has a faster initial rate of hydrolysis, seen by the higher V_{app} at the apex compared to *TrCel6A*. Both enzymes exhibit decaying rates on both substrates seen by the decrease in V_{app} , by a factor of approximately 4 over the 30 min monitoring period.

¹⁷ Calculated from 0.052 μ mol/mg/min, using a molar weight of 50 KDa.

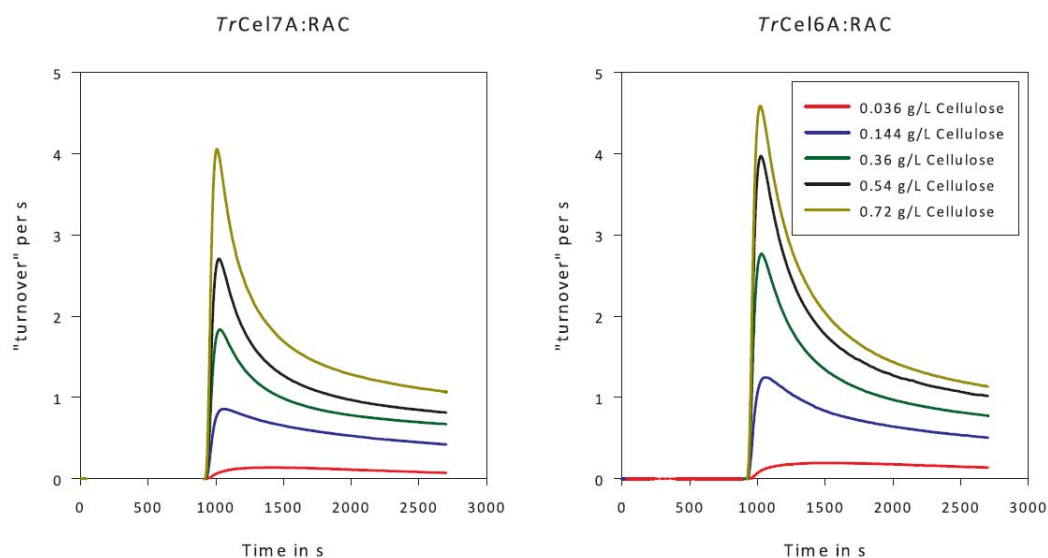


Figure 20. *TrCel7A* and *TrCel6A* action on RAC, 50 °C, pH 5, 50 nM enzyme.

The raw data are converted to an averaged $V_{\max}(\text{cat})$ as described in the text.

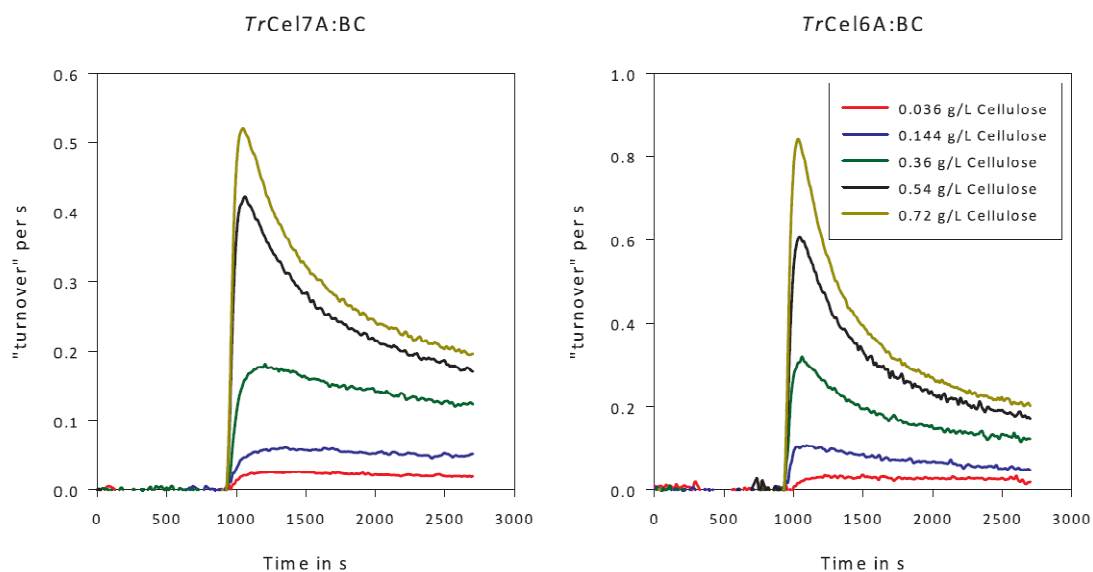


Figure 21. *TrCel7A* and *TrCel6A* action on BC, 50 °C, pH 5, 50 nM enzyme.

We have stated earlier that both substrates have a similar accessible surface area, which means the same amount of enzyme can adsorb to the surface of the substrate. We have also measured the DP_N to be quite close, at approximately 200 glucose units per chain. This is also important because it means there are equal numbers of reducing (and non-reducing) ends on each substrate, or in effect the same number of attack points for the enzymes (same effective $[S_0]$). Given the dose of enzyme is so low (50 nM), we assume all the enzymes are initially in action at the higher substrate concentrations, so it is reasonable to compare the rates on the two substrates directly as a measure for the overall catalytic rate of hydrolysis, V_{app} .

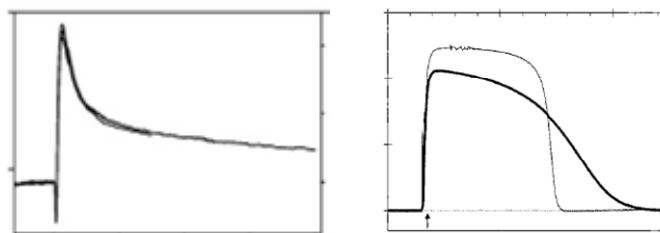


Figure 22. (L) ITC measured burst phase kinetics of cellulases (103). (R) A stylized adaptation of a typical ITC Michaelis-Menten kinetic curve (101).

Shown above is a graphical representation of the difference in soluble Michaelis-Menten kinetics and cellulase burst phase kinetics, both measured by ITC. The curve on the left represents the kinetic behavior of cellulases discussed below. On the left there are two curves, the faint line is an uninhibited reaction, the solid line shows the effects of inhibition on the enzyme. The integral (and thus product) for each is the same, it may be seen it is the rates that differ as a result of this inhibition.

To compare to more traditional enzyme kinetics, along the lines of soluble systems described by the Michaelis-Menten equation; upon addition of enzyme to the substrate, there is an initial fast rate followed by a steady state with no decline once the substrate is in excess, as demonstrated in Figure 22 (R). This is further illustrated by the steady state reached using β -glucosidase to hydrolyze cellobiose in Article 2 (111) as well as using D-glucono- δ -lactone hydrolase to hydrolyze D-glucono- δ -lactone to D-gluconic acid as shown in Chapter 4. The substrate is in excess for the higher concentrations used here, with the lowest cellulose g/L concentration of 0.036 g/L being expressed as 1.1 μ M reducing ends using the calculations shown below.

$$0.036 \frac{\text{g}}{\text{L}} \text{ cellulose} = \frac{0.036 \frac{\text{g}}{\text{L}}}{164.16 \frac{\text{g (glucose)}}{\text{mol}} \times \frac{200 \text{ (glucose)}}{\text{reducing end}}} = 1.09 \mu\text{M reducing end equivalents}$$

Equation 8. Calculation for the conversion of g/L cellulose to μ M reducing end equivalents.

This is still over 20 times the amount of enzyme present, although the accessibility of the substrate does become an issue at the lowest doses. This is why (in addition to the establishment of the steady state for the equilibrium system) the disappearance of the burst peak occurs. It may be the enzymes are lining up for access to substrate attack points, and thus the heat signal is more spread out as all the enzymes do not begin hydrolysis simultaneously.

From the $V_{\text{max}}(\text{cat})$ values we see *TrCel6A* has a higher V_{app} than *TrCel7A* under these conditions. To compare to previous values, this agrees with previously reported findings where *TrCel7A* performs slower than *TrCel6A* (44,69,171,172), recorded on filter paper, Avicel, and amorphous cellulose. We return to this in the discussion. For now, in order to further investigate this, first we fit the ITC data to the double exponential decay to get a value for the rate constant of inactivation, k_4 .

2.4.2 The rate constant of inactivation: k_4

k_4 is determined from the fit of the raw data as explained earlier in section 2.3.2 using Equation 7. The lower g/L cellulose levels of hydrolysis, with lower thermal signals could not be fit to this function (indicated by -). The results are presented below.

Table 4. The double exponential decay fits for *TrCel6A* and *TrCel7A* hydrolysis of RAC and BC.

Parameter Cellulose Concentration	μM reducing ends	k_4 RAC		k_4 BC	
		<i>TrCel7A</i>	<i>TrCel6A</i>	<i>TrCel7A</i>	<i>TrCel6A</i>
0.04 g/L Cellulose	1.1	-	-	-	-
0.14 g/L Cellulose	4.4	$2.8 \times 10^{-4} \text{ s}^{-1}$	$2.8 \times 10^{-4} \text{ s}^{-1}$	-	-
0.36 g/L Cellulose	11.0	$2.5 \times 10^{-4} \text{ s}^{-1}$	$3.0 \times 10^{-4} \text{ s}^{-1}$	-	-
0.54 g/L Cellulose	16.4	$2.5 \times 10^{-4} \text{ s}^{-1}$	$3.2 \times 10^{-4} \text{ s}^{-1}$	$2.6 \times 10^{-4} \text{ s}^{-1}$	$3.3 \times 10^{-4} \text{ s}^{-1}$
0.72 g/L Cellulose	21.9	$2.6 \times 10^{-4} \text{ s}^{-1}$	$3.2 \times 10^{-4} \text{ s}^{-1}$	$2.4 \times 10^{-4} \text{ s}^{-1}$	$3.3 \times 10^{-4} \text{ s}^{-1}$
Average		$2.6 \times 10^{-4} \text{ s}^{-1}$	$3.0 \times 10^{-4} \text{ s}^{-1}$	$2.5 \times 10^{-4} \text{ s}^{-1}$	$3.3 \times 10^{-4} \text{ s}^{-1}$
Standard Deviation		$1.6 \times 10^{-5} \text{ s}^{-1}$	$2.0 \times 10^{-5} \text{ s}^{-1}$	$1.2 \times 10^{-5} \text{ s}^{-1}$	$0.2 \times 10^{-5} \text{ s}^{-1}$
CV %		6 %	6 %	3 %	0.50 %
		k_4 RAC		k_4 BC	
Average k_4		$2.6 \pm 0.2 \times 10^{-4} \text{ s}^{-1}$	$3.0 \pm 0.2 \times 10^{-4} \text{ s}^{-1}$	$2.5 \pm 0.1 \times 10^{-4} \text{ s}^{-1}$	$3.3 \pm 0.02 \times 10^{-4} \text{ s}^{-1}$

The variation, here expressed by a coefficient of variation (CV) is under 10 % for the RAC samples. This is a good indication the k_4 the rate constant of inactivation is indeed an intrinsic property of the enzyme, and is independent of the substrate concentration. It has previously been reported that at over 15 μM reducing ends S_0 (*TrCel7A* hydrolyzing RAC at 30 °C) that the k_4 values attained were essentially equal (162), and we conclude the parameters presented here reflect the rate constant of inactivation for the two enzymes on the two substrates investigated. The value previously reported using the model outlined in Equation 6, for *TrCel7A* hydrolyzing RAC at 30 °C was $k_4 = 2 \pm 0.7 \times 10^{-4} \text{ s}^{-1}$, in very good agreement with the data presented here from the double exponential decay fit.

Taking the $V_{\text{max}}(\text{cat})$ from the 0.72 g/L cellulose hydrolysis shown in Table 3, we assume this is the highest measured k_2 , the catalytic rate constant. Now we can look at the relationship between $V_{\text{max}}(\text{cat})$ and k_4 . As stated earlier, we can calculate the average amount of hydrolytic cleavages each enzyme performs before becoming inactivated, given by the ratio k_2/k_4 .

Table 5. The number of hydrolytic events *TrCel7A* and *TrCel6A* may perform on RAC and BC based on $V_{\text{max}}(\text{cat})/k_4$ at 50 °C.

Enzyme	Substrate	$V_{\text{max}}(\text{cat})$	k_4	$V_{\text{max}}(\text{cat})/k_4$
<i>TrCel7A</i>	RAC	4.1 s^{-1}	$2.6 \pm 0.2 \times 10^{-4} \text{ s}^{-1}$	15769
<i>TrCel6A</i>	RAC	4.6 s^{-1}	$3.0 \pm 0.2 \times 10^{-4} \text{ s}^{-1}$	15334
<i>TrCel7A</i>	BC	0.5 s^{-1}	$2.5 \pm 0.1 \times 10^{-4} \text{ s}^{-1}$	2000
<i>TrCel6A</i>	BC	0.8 s^{-1}	$3.3 \pm 0.02 \times 10^{-4} \text{ s}^{-1}$	2424

The rate constants of inactivation k_4 (Table 4) are largely unchanged for *TrCel7A* and *TrCel6A* as a function of the substrate. The rate of inactivation V_{inact} , is a function of both the rate constant, and the amount of enzymes productively bound to the surface of the cellulose:

$$V_{inact} = k_4 \sum_1^n EC_n$$

Equation 9. The rate of inactivation.

From a screening perspective this ratio could be used to distinguish candidates with the ideal enzyme having both a high k_2 and a low k_4 . Here we see that *TrCel7A* can perform on average 16,000 catalytic events on RAC at 50 °C before becoming inactivated; this is slightly higher than reported values at lower temperatures in the order of 5,000-10,000 (162). This may reflect temperature dependent factors; in that the enzyme appears less susceptible to inactivation at higher temperatures, possibly due to being able to better overcome hindrances on the surface. *TrCel6A* has been reported to perform approximately 6,000 catalytic events before inactivation on soluble cello-oligosaccharides (173), the difference here (over factor 2) may be the result of the CBM playing a more pivotal role in the enzymatic inactivation on insoluble substrates.

When directly comparing the rate constants of inactivation for *TrCel6A* and *TrCel7A*, we see the *TrCel7A* rate constant; k_4 is 15 % lower than that of *TrCel6A* for RAC and 20 % lower for BC. This is already a very good indication that *TrCel7A* is less prone to inactivation on both of these two substrates, and indeed may explain why rates measured over longer monitoring times have reported *TrCel7A* to produce more cellobiose than *TrCel6A*. If *TrCel6A* becomes inactivated at a faster rate, at some point the *TrCel7A* V_{app} will overtake it as there will be effectively more active enzymes on the cellulose surface.

2.5 PCS analysis

Both *TrCel7A* and *TrCel6A* were added to PCS in the same manner as reported for RAC and BC. This was to establish if the same pattern would hold true for a lignocellulosic substrate, an imperative for screening. At the lower concentrations of PCS the burst is not evident; we attribute this to there being some non productive adsorption of the CBHs to the lignin fraction in combination with the aforementioned establishment of the equilibrium in the amplification system. As a result of this relatively higher concentrations of PCS were used. Here we also see we have reached a V_{max} for the system, as increasing the highest concentrations of substrate do not lead to an overall increase in V_{app} .

The method of analysis is the same as presented earlier; here we present the raw data already converted to a turnover number, and k_4 values from the double exponential fit.

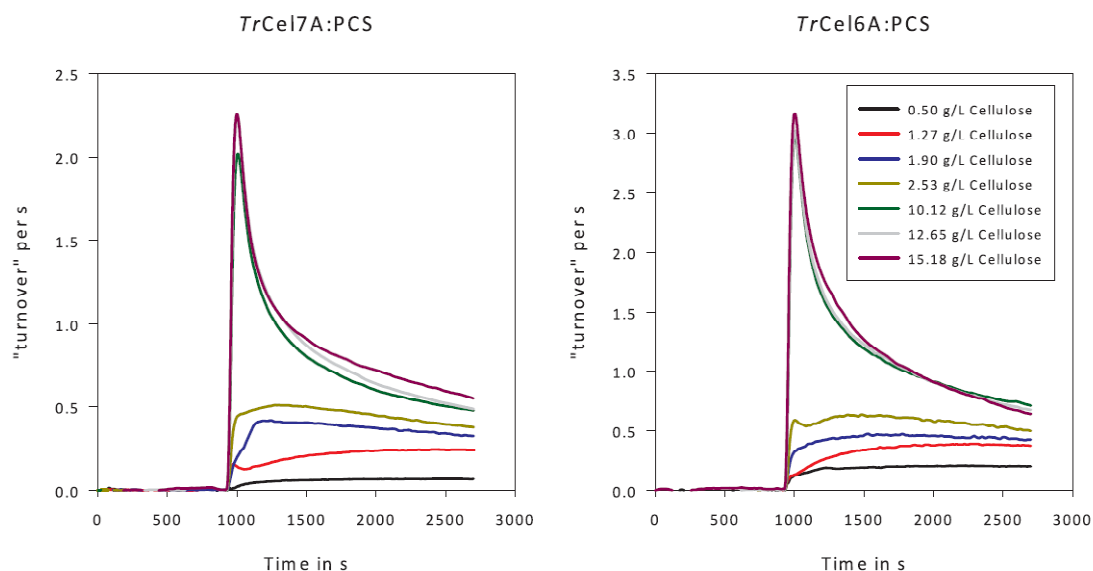


Figure 23. *TrCel7A* and *TrCel6A* action on PCS, 50 °C, pH 5, 50 nM enzyme.

Table 6. The double exponential decay fits and $V_{\max}(\text{cat})$ data for *TrCel6A* and *TrCel7A* hydrolysis of PCS.

Parameter Cellulose Concentration ¹⁸	<i>TrCel7A</i>		<i>TrCel6A</i>	
	$V_{\max}(\text{cat})$	k_4	$V_{\max}(\text{cat})$	k_4
0.50 g/L Cellulose	0.1 s^{-1}	-	0.2 s^{-1}	-
1.27 g/L Cellulose	0.2 s^{-1}	-	0.4 s^{-1}	-
1.90 g/L Cellulose	0.4 s^{-1}	-	0.4 s^{-1}	-
2.53 g/L Cellulose	0.5 s^{-1}	-	0.6 s^{-1}	-
10.12 g/L Cellulose	2.0 s^{-1}	$3.6 \times 10^{-4} \text{ s}^{-1}$	3.0 s^{-1}	$4.5 \times 10^{-4} \text{ s}^{-1}$
12.65 g/L Cellulose	2.2 s^{-1}	$4.2 \times 10^{-4} \text{ s}^{-1}$	3.0 s^{-1}	$4.9 \times 10^{-4} \text{ s}^{-1}$
15.18 g/L Cellulose	2.3 s^{-1}	$3.9 \times 10^{-4} \text{ s}^{-1}$	3.2 s^{-1}	$5.1 \times 10^{-4} \text{ s}^{-1}$
Average	2.2 s^{-1}	$3.9 \times 10^{-4} \text{ s}^{-1}$	1.5 s^{-1}	$4.8 \times 10^{-4} \text{ s}^{-1}$
Standard Deviation	0.1 s^{-1}	$0.3 \times 10^{-4} \text{ s}^{-1}$	0.05 s^{-1}	$0.3 \times 10^{-4} \text{ s}^{-1}$
CV %	6 %	8 %	3 %	6 %
		$V_{\max}(\text{cat})/k_4$		$V_{\max}(\text{cat})/k_4$
Average		5641		6250

We do not compare PCS directly to BC and RAC as the concentrations of cellulose are not the same and there is also lignin, hemicellulose and other hydrolysis factors to consider. However, the same trends appear here, as seen for RAC and BC hydrolysis. The rate constant of decay k_4 , is 20 % higher for *TrCel6A* compared to *TrCel7A*, indicating that on this, a third substrate, the enzyme has the same tendency as seen before. That is to say in all the analyzed substrates here, *TrCel6A* has a slightly higher V_{app} , than that of *TrCel7A*, and *TrCel7A* has a lower k_4 , varying from 15 % to 20 % lower than that of *TrCel6A* and thus is less

¹⁸ Based on the % solids measured and PCS = 57 w/w cellulose.

prone to inactivation. For PCS the $V_{\max}(\text{cat})/k_4$ ratio is 5641 for *TrCel7A* and 6250 for *TrCel6A*, again following the trend that both enzymes can perform an equal number of average catalytic events before becoming inactivated.

This may play a vital role in the future when determining which variant from protein engineering or which wild type enzyme should be chosen for a particular application. Looking at protein engineering variants, comparing the mutation to the mechanistic data may provide a good tool to further our understanding of cellulose:cellulase interactions.

2.6 Summary and conclusions

Here we have demonstrated a serious source of error when comparing cellulases. To report a k_{cat} or a V_{\max} without having specified the amount of contact time between the substrate and enzyme leads to a huge variety in kinetic values reported, up to 2 orders of magnitude in some cases. These values can also vary from substrate to substrate (of the same type) and in order to fully establish a system where cellulases can be directly compared, the substrate characteristics such as at least DP_N and I_{cr} should also be reported in such analyses.

Also, if the enzyme doses are higher (as they are in the previously mentioned experiments) there are other factors to consider. The jamming on the surface of inactivated enzymes clogging the pathways for catalytically active enzymes may play a more prominent role (161). This occurs when the enzymes become hindered, and block the processive nature of following enzymes. This is unlikely to have a major impact in our set-up due to the very small enzyme doses. At higher enzyme doses, there is the aforementioned jamming, competition between the enzymes for available substrate binding sites to produce a productive ES, as well as far more drastic changes on the substrate topography due to higher degrees of conversion. Topography changes may reveal such physical obstacles as other chain ends or crossover linkages which will have an effect on the enzymatic rates. We submit that in order to truly study the mechanics of the CBH enzymes such low doses are, in fact, necessary. By lowering the enzyme dose we limit the substrate effects, and focus on the actual enzymatic action, adding the possibility for mechanistic interpretation of the ITC data to ameliorate the screening data presented earlier.

Through conversion of ITC data to rates, we can directly compare the catalytic efficiency of the individual enzymes. To complement this we have demonstrated the use of the sum of two exponentials to attain a measure for the rate of inactivation. $V_{\max}(\text{cat})$ gives a good indication of the catalytic rate of the enzymes, while k_4 describes a measure for the rate of enzyme inactivation. Hence, we propose the reporting of both

$V_{\max}(\text{cat})$ and k_4 as critical parameters when using ITC to screen for variants or alternative wild types, with ideal candidates having a high $V_{\max}(\text{cat})$ (i.e. a high k_2) and a low k_4 . Although here, we present data where we compare two different enzyme classes, this simply serves to illustrate how such analyses may be carried out in future studies. By using model and complex substrates, we observe the hydrolysis trends here have been the same.

The slowdown of hydrolysis is apparent in the rapid decrease in the initial rate demonstrated here, followed by an underlying inactivation of the enzyme. The kinetic parameters k_3 and k_4 are the deciding factors here. The off rate, k_3 dictates the early (initial) rate decrease, where the rate at which the enzyme is released again to the liquid phase in an active form to re-initiate catalysis is prominent. Thus, processivity may be expressed as k_2/k_3 , and may be equated with the average amount of catalytic events each enzyme may perform before releasing the cellulose chain. Taking typical values for k_2 to be in the order of $1 - 10 \text{ s}^{-1}$ (52,69,162,165), and k_3 in the order of 10^{-2} s^{-1} to 10^{-3} s^{-1} (52,162), a typical processive enzyme can perform up to approximately 100 to 1000 catalytic events before releasing. The initial rate decrease seen after the apex in the presented figures here is mainly a function of k_3 , as has been proposed by the recent work outlined by Jalak and co-workers (165) and Præstgaard (162).

We have introduced the kinetic parameter, k_4 , the rate constant of inactivation. After the initial rate decrease, if there were no other factors involved in the hydrolysis of cellulose, there would be a steady state established. Here we see k_4 , the rate constant of inactivation coming to the fore. This is the rate constant describing the rate at which the enzyme population is effectively removed from the catalytic cycle, forming what is described as an inactive complex, IC_n in the model. The reason for this inactivation may be thermal denaturation, protein denaturation, or a form for trapping of the cellulase on the cellulose substrate where the enzyme gets stuck. Given the ratio of k_2/k_4 , we can express how many catalytic events each enzyme may perform before inactivation, presented here in the order of 2000 - 10,000 average catalytic events per enzyme.

Regarding the RAC and BC hydrolyses profiles presented here; we clearly can see the immediate effects of crystallinity. The same relative concentrations of amorphous (RAC) and crystalline (BC) cellulose are hydrolyzed at very different rates, by both enzymes. The overall V_{app} is lower for the more crystalline substrate for both *TrCel7A* and *TrCel6A*. The fact that two completely different enzymes are equally as affected by the composition of the cellulose substrate is interesting. If this is the case, I_{cr} may indeed reflect a critical parameter in determining hydrolysis rates in the future. Given the total population of enzymes (we assume all are adsorbed, all are initially active as outlined earlier) are hydrolyzing the substrates; there

must be a different rate determining step when hydrolyzing BC compared to RAC. Given the rate constants are the same, but the rate of inactivation V_{inact} , is not (which may be seen in the difference on overall V_{app});

there must therefore be a difference in $\sum_1^n EC_n$.

Despite having the same DP_N and similar reported values for the accessible surface area, one study using a CBM attached to a green fluorescent protein marker demonstrated an almost 18 fold difference in the amount of available binding sites (174) between RAC and BC. It may be the method of determining the DP_N , based on the availability of reducing ends for a comparatively small colored moiety may not be an accurate measurement for the amount of sites available for the larger CBM and Core of the CBH enzymes. This may account for the large difference in V_{app} seen here, although the enzyme to substrate ratio is still in excess.

The role of crystallinity remains complex. We report a V_{app} for the hydrolysis of amorphous cellulose approximately 6 times higher than that of the crystalline cellulose. Given the k_4 values are the same, but V_{app} is different, we propose the rate limiting step for hydrolysis on these two cellulose substrates is different. This may reflect different binding of the CBM (as outlined above), or other physical interactions such as the effect of the more ordered hydrogen bonding pattern in the crystalline substrate, which may slow hydrolysis rates. A recent study by Hall and co-workers outlines the decreasing rate as a direct consequence of increasing crystallinity, where the amount of adsorbed enzyme is measured and accounted for (130), although at far higher enzyme dosages than used here. This is in agreement with the observations presented for a cellulase mixture in chapter 1, where the rate of hydrolysis of a crystalline (Avicel) and an amorphous (PASC) substrate were quite different after taking the amount of adsorbed enzyme into account. Further investigation into this area is warranted, and the determination of k_1 (on-rate) and k_3 (off-rate) through a system with a faster time constant such as a cellobiose biosensor could provide vital clues into the on-off rate and determine if it is the binding of the CBHs among the causes of this drastic decrease in V_{app} .

The rate constant for inactivation k_4 appears independent of the cellulose substrate type. An interesting observation was reached by Harjunpää and co-workers, measuring *TrCel6A* action on soluble cello-oligosaccharides (173). Here, they explain the position of two tryptophans in the active site tunnel of *TrCel6A* playing a central role. They observe that when hydrolyzing cellohexaose, *TrCel6A* becomes inactivated at a rate in the order to 10^{-3} s^{-1} , and propose this is because sites A and F (see Figure 24) do not lineup exactly with rings 1 and 6 in the substrate, causing a conformational strain. Thus *TrCel6A* may

perform up to 5,000 catalytic events before the enzyme locks into position on the cellulose chain, and becomes inactively bound.

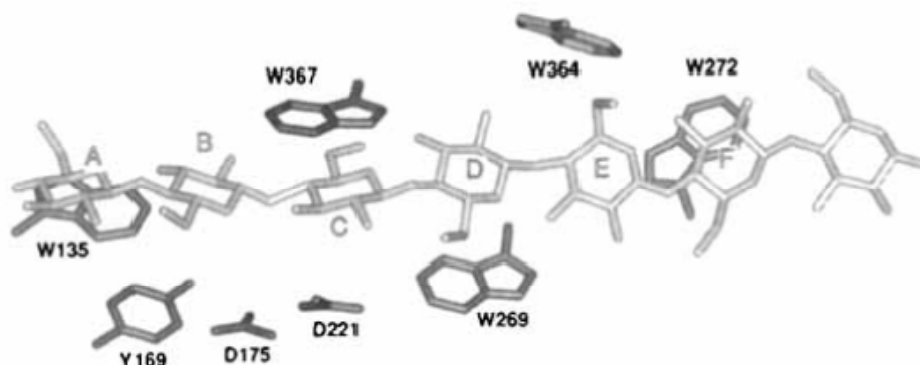


Figure 24. A, C, D and F show subsites of the TrCel6A active site where there are stacking interactions with glucose. These are tryptophan residues (W) W135, W367, W269 and W272 which interact with A, C, D and F, respectively.

There are similar interactions with tryptophans in the *TrCel7A* binding sites of the active tunnel (58). We propose the rate constant of inactivation is an intrinsic property of the enzyme, and represents a probability of becoming “stuck” on a cellulose chain in addition to denaturation factors for the enzyme. The processive nature of CBH’s is explained by the sliding action of the chain through the tunnel of the active site, through the complex interaction of stacking interactions, hydrogen bonding and van der Waals forces (58,175) resulting in an overall forward momentum. The intrinsic inactivation may therefore arise when this delicate balance is disrupted, and the CBH stalls or gets stuck, becoming a non-productively bound enzyme. It should be noted this is not the only source of inactivation as obstacles, jamming, and other factors play a role as outlined earlier which could be attributed the title extrinsic inactivation factors. We propose under the conditions we use here with low doses of enzyme over relatively short periods of time (i.e. 1 h compared to 24 h of hydrolysis), it is primarily the intrinsic k_4 being monitored, and further investigation into this parameter is warranted.

For PCS we see a significant increase in k_4 for both enzymes in the order of almost 50 % compared to the purer cellulose substrates. This may be as a result of the enzyme being bound to the lignin fraction, as has been described in the literature (176-178), either as the hydrolysis progresses and the enzyme runs into a lignin roadblock on the cellulose chain, or if there is lignin suspended in the liquid phase to which the enzyme binds instead of to cellulose. PCS also contains 7 % hemicellulose, also known to inhibit the action of cellulases. The hemicellulose is bound directly to the cellulose which may also lead to a roadblock situation, or xylo-oligosaccharides released into the liquid phase (from hemicellulose hydrolysis) have been shown to bind to *TrCel7A*, and inhibit the CBH activity, significantly (179). This increase in k_4 can therefore

be attributed to the sum of both extrinsic and intrinsic inactivation factors. We note the trends demonstrated by monitoring the hydrolysis of pure celluloses are accurately reflected in a complex lignocellulose matrix, thereby ratifying the use of these insoluble model substrates in future screening investigations.

In summary, we have demonstrated ITC and the amplification system may be used as a thermochemical screening tool. By comparing the two main cellobiohydrolases of *T. reesei*, we show the differences between their mode of action as well as a mechanistic interpretation of the data obtained. The resources used are minimal in that one run uses 5 μg of enzyme and substrates require little extra preparation. Rates measured on model substrates and parameters (rate constants) derived from them, can be directly compared to more complex lignocellulosic substrates. We submit *TrCel6A* attains a V_{app} slightly higher than *TrCel7A*, and that both enzymes can perform almost the same average amount of catalytic events before becoming inactivated. The k_4 parameter from pure cellulose substrates under these conditions appears to be an intrinsic enzyme property, and may provide a focus area for future protein engineering endeavors.

The technique provides more information than a simple test for which enzyme produces most sugar and may be used to further the current understanding of cellulose and cellulase interactions in addition to choosing the best candidate from a screening library.

Chapter 3. Thermochemical screening of *TrCel7A* CBM I variants.

Please note the variants in this chapter, and the methods used for screening are being patented by Novozymes A/S. CELLOBIOHYDROLASE AND CELLULOSE BINDING DOMAIN VARIANTS AND POLYNUCLEOTIDES ENCODING SAME, Docket No.: 12137-US-PRO.

3.1 Background

In Chapter 2 we introduced some of the uses of the ITC amplification system and provided the reader with a background to the parameters, $V_{\max}(\text{cat})$ and k_4 . We also concluded that this type of analysis may be used to determine important characteristics in particular for protein engineering variants, where there may not be large amounts of protein available. Here we follow up on this, and present an ITC investigation into *TrCel7A*-CBM variants, whilst focusing now on a more screening-like approach. We introduce a relative performance index, a normalization based on sugar production compared to the wild type enzyme. The variants have been generated using point mutation, which in effect allows the protein engineer to change a single amino acid. Here, we investigate 4 variants with mutations in different positions of the CBM wedge. As controls we have E212Q¹⁹, a catalytically inactive variant, and the wild type, or unaltered original *TrCel7A* enzyme. We outline a procedure to purify and quantitate the amount of active enzyme present in samples; which is of utmost importance when investigating protein engineering variants. We do not employ the exact method as outlined in the last chapter; here we use only one concentration of substrate, where S_0 is far in excess to ensure we are now measure V_{\max} .

3.1.1 Structure

To recap: *TrCel7A* is composed of three distinct regions, a catalytic domain (CD or Core), a linker region and a carbohydrate binding module (CBM). The catalytic domain as stated earlier is a 50 Å long tunnel form, containing essential tryptophan residues whose indole rings are essential in stacking interactions with cellulose. These help to orientate the chain in a position to be catalytically cleaved every cellobiose residue by the two glutamic acid residues E212 and E217 (144). The linker region separates the CD and CBM and is heavily *O*-glycosylated, (being composed of many serine and threonine residues) which serves to protect it from proteolysis (180,181). The CBM of *TrCel7A* was first reported separated from the functional or catalytic domain in (43), where the CD was reported to be 65 KDa and the CBM 10 KDa. This has been performed by Papain proteolytic cleavage on the linker (43,44,182). The CBM belongs to family I, characterized by wedge like structure where there are three aromatic residues positioned to interact with the cellulose surface (183-185). The small 10 KDa domain is a triple stranded β sheet CBM, stabilized by two disulfide bridges; here C485-C502 and C496-C512 (183,186). The position of the three tyrosine residues on

¹⁹ All the mutations are fully explained in Table 7.

the binding surface is consistent with binding to every second glucosyl moiety in the cellulose chain (186). See Figure 25 and Figure 26.

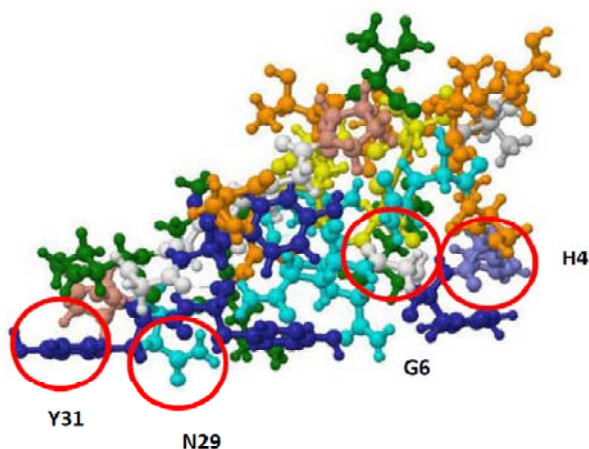


Figure 25. The CBM of *TrCel7A*.

Ringed residues are the variant targets to be investigated. Structure from (187) using Jmol 12.03.37. Color codes are presented at the end of the chapter.

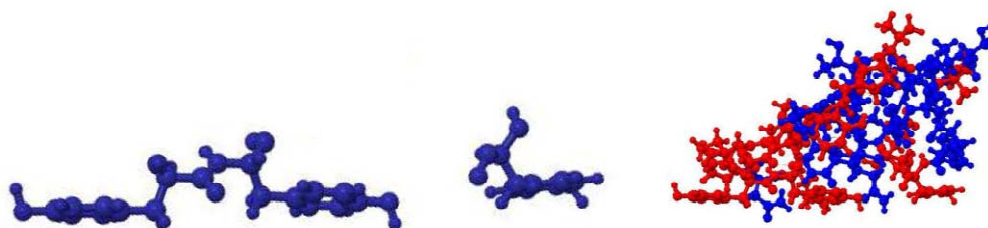


Figure 26. Hydrophobicity of *TrCel7A* CBM.

(L) Highlighted here are the three tyrosine residues involved in direct contact with the cellulose surface. (R) A hydrophobicity rendering of Figure 25. Red = hydrophobic, blue = hydrophilic. Hydropathy index from (188).

3.1.2 Function

The CBM facilitates binding to the insoluble surface, but has no significant affinity for soluble cellooligosaccharides (140). This binding is exothermic, in the order of 5 - 50 kJ/mol (155-157); and the role of water being released after the cellulose-CBM interaction driving the reaction entropically has been presented (155). The CBM is generally regarded as essential for the degradation of crystalline substrates, and binding is severely reduced when the CBM is removed (43,44,180,181,189,190). Both the CBM and the CD bind specifically to the cellulose surface and it is widely regarded that both interactions play a pivotal role in both adsorption and desorption of the complete cellulase enzyme (58,191). The CBM is also thought to play a role in disrupting the cellulose chains, either to “feed” into the CD tunnel, or to loosen them up for catalysis (55,141,142,175,192). Finally, there have been conflicting theories about the role of the CBM in

the mobility of cellulases during cellulose hydrolysis, in that it may or may not accommodate the processive movement of the enzyme through potential disruption of the substrate chains (170,193,194). It should be noted the exact position of the CBM and CD under a hydrolysis is not actually known and presented here are the most current theories.

It is clear however, as with all CBMs, the primary functions are involved with 1) maintaining the enzyme in close proximity to the cellulose surface, thus effectively decreasing the apparent K_M , 2) targeting specific areas of the cellulose chain for binding and 3) potentially increasing the catalytic efficiency of the cellulase through aiding the catalysis by some form of chain disruption (183).

Variants will be represented by the traditional single letter abbreviations shown in Table 7, where the first amino acid is the original, the position in the protein is indicated by a number and the second amino acid is the replacement.

3.2 *TrCel7A* point mutations analyzed in this study

In order to investigate the role of the CBM and potentially increase the rate of hydrolysis, a number of CBM variants (provided by Novozymes A/S) were generated using site directed mutagenesis. An overview is presented in Table 7:

Table 7. List of the mutations carried out on the CBM I of *TrCel7A* used in this study.

Variant Name/Site ²⁰	Comment/Main Changes.
Core	A CBM free variant.
E212Q	Glutamic acid (E) replaced by glutamine (Q). A catalytically inactive variant.(143)
TH110 WT	The wild type control. No mutations.
H4W	Histidine (H) replaced by tryptophan (W). Imidazole replaced with indole ring. Basic polar residue changed to a neutral slightly polar residue.
H4K	Histidine (H) replaced by lysine (K). Removal of the histidine imidazole ring. Basic polar residue maintained.
G6R	Glycine (G) replaced by arginine (R). Introduction of a much larger basic residue into the center of the wedge.
N29D	Asparagine (N) replaced by aspartic acid (D). Changed from amine (basic) to amide (acidic).
Y31A	Tyrosine (Y) replaced by alanine (A).Removal of the phenol group. Changed from polar to non-polar.

²⁰ For ease of reading the traditional 1 letter abbreviations of each amino acid will be used in the following discussions.

Note: For the purpose of this report, the numbering of the variants generated has been changed such that the first amino acid in the CBM sequence is number 1, rather than 477. The sequence of the CBM I (residues 477 – 513) of *TrCel7A* is TQSHYGQCGGIGYSGPTVCASGTTCQVLNPPYYSQCL. The full sequence of *TrCel7A* is available on <http://www.uniprot.org/uniprot/P62694>.

3.2.1 Purification of protein engineering variants

A one-step purification method was developed for rapid purification of variants. While this may lead to trace amounts of proteins such as BG contaminants, this source of error is accounted for by measuring the activity of the variants on a soluble substrate as described below. 1.2 M final concentration of ammonium sulfate was added to fermentation broths, slowly with vigorous stirring. After dissolution, the broth was filtered through a 75 μ m PES filter. pNPL activity was performed pre- and post- this procedure as outlined below. The filtrate was applied to a FF phenyl sepharose column equilibrated with 100 mM ammonium acetate + 1.2 M ammonium sulfate pH 5.5. The protein was eluted over 5 column volumes with a linear gradient of 100 mM ammonium acetate pH 5.5, and fractions run on SDS PAGE and tested for pNPL (CBH) and pNPG (residual BG) activity. There was no significant loss (< 5 %) in overall activity of the CBH under the purification procedure (the specific activity increases during purification).

Of major concern in protein engineering is determining the amount of *active* protein present (195). This is in order to screen variants for specific traits. Here we return to some of the colored soluble substrates mentioned in Chapter 1. pNPL, *p*-Nitrophenyl β -D-lactopyranoside, is used here to determine *TrCel7A* activity by measuring the release of *p*-nitrophenol through the hydrolysis of the agluconic bond (94). As this is a small molecule and completely soluble; the amino acid substitutions in the CBM have no effect on the catalytic activity (141). Activity for β -glucosidase was checked using a modified pNPG (4-Nitrophenyl β -D-glucopyranoside) assay (96,97,110). After pooling the fractions with the least (or no) BG background and highest CBH activity, normalization was carried out. It should be noted all variants had predominantly only the CBH band present as checked by SDS PAGE after staining with Coomassie Blue.

3.2.2 Soluble substrate assays

Briefly, final concentrations of 1 mM pNPG or pNPL were incubated after reaching thermal equilibrium in a thermomixer with 10 μ L of enzyme sample. Incubation was 15 min @ 50 $^{\circ}$ C, 1400 rpm. Reactions were terminated with 500 μ L of 200 mM NaOH and the release of the *p*-nitrophenol group quantified by measuring OD₄₁₀.

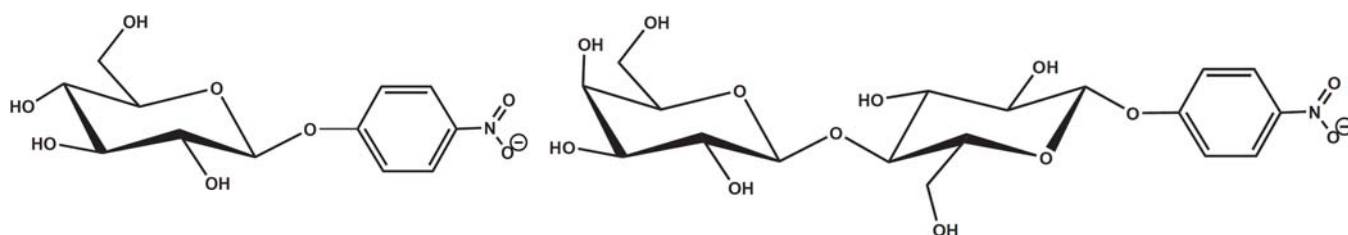


Figure 27. pNPG (L) and pNPL (R).

(L) pNPG, 4-Nitrophenyl β -D-glucopyranoside (N7006 Sigma) **(R)** pNPL, 4-Nitrophenyl β -D-lactopyranoside (N1752 Sigma).

3.3 Results and discussion

3.3.1 Normalization

Once the variants had been purified and buffer changed (using PD10²¹ columns) to 50 mM sodium acetate, 2 mM CaCl₂, 0.01 % triton X-100, pH 5; normalization was carried out. OD₂₈₀ should not be used as a measure of the total protein cannot be equated with a measure of the active variant. In order to overcome this limitation, activity on the soluble substrate was used to measure the concentration of active variant. The variants have all been mutated in the CBM which has no effect on their ability to degrade a soluble substrate (except with the obvious exception of E212Q which is inactive) (140,141). All samples were normalized based on the volume of sample needed to release the same amount of *p*-nitrophenol under the standard pNPL assays conditions. To ensure this is in the linear region, 3 time points were measured at 5, 10, and 15 min as this is not a continuous assay. The results are presented in Figure 28.

The presence of BG has no effect on the pNPL assay as BG negative controls confirm. It is important to remember also that in the amplification system, there is excess BG added to convert all cellobiose immediately to glucose, so the presence of a slight BG contaminant may be disregarded when interpreting the ITC results presented later. This normalization also means the dosing in the ITC is the same activity for each variant, rather than the same overall protein concentration being monitored.

²¹ These are commercially available small disposable Sephadex G-15 columns used for desalting.

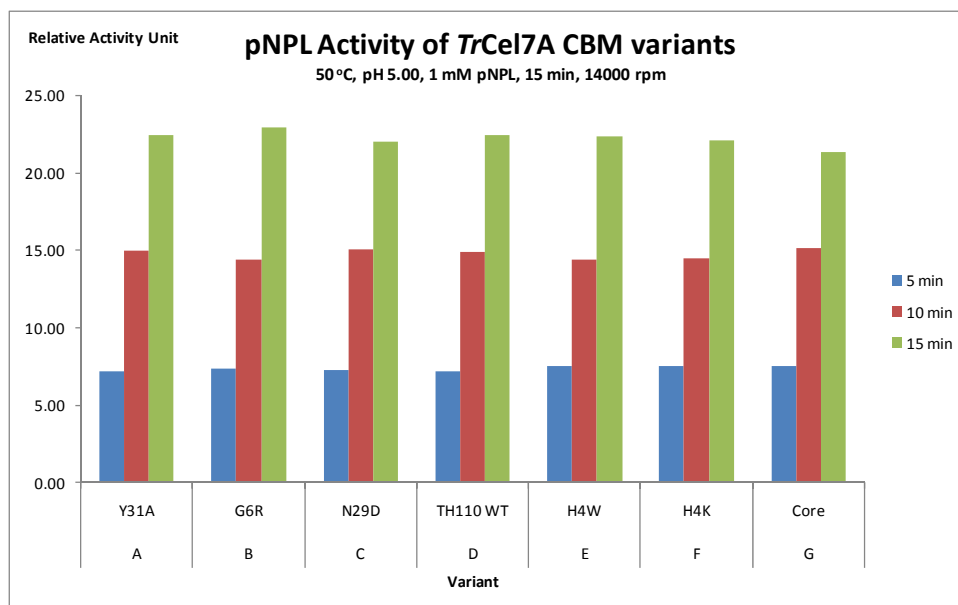


Figure 28. pNPL activity on the *TrCel7A* CBM I variants.

Note: no activity could be measured on the E212Q variant. The variation on triple analyses is under 5 %, error bars not shown.

3.3.2 Data analysis and ITC results

All reactions were carried out at the temperatures indicated on the results graphs i.e. 25 °C for RAC and 50 °C for PCS. Standard conditions were thermal equilibration of the substrate containing the amplification mixture described in Article 2 (111), in the cell followed by a single 10 μ L injection of the variant. Hydrolysis was then monitored for 30 min.

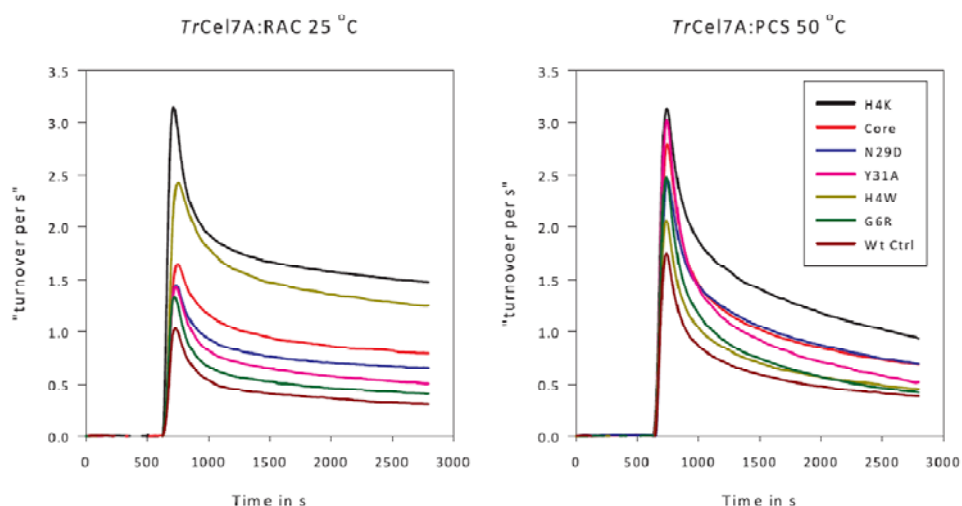


Figure 29. The raw data from the ITC *TrCel7A* CBM reactions converted to a k_{cat} .

(L) RAC 4 g/L at 25 °C monitored for 30 min, (R) 20 g/L PCS at 50 °C monitored for 30 min. As in Chapter 2, it is only the decay that is fitted, not the upswing. Both substrates had the amplification mixture of enzymes present in the cell. 25 nM was E_0 for the V_{max} (cat) calculations.

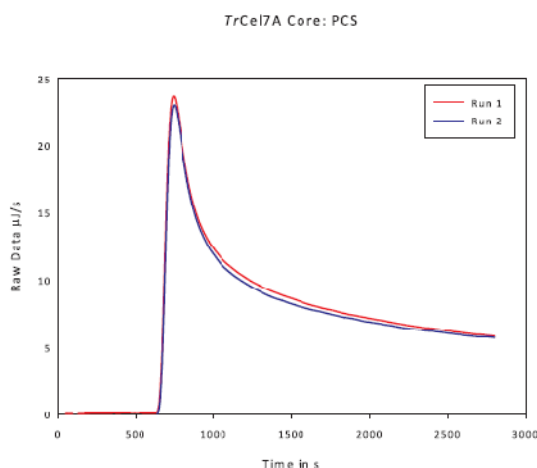


Figure 30. The reproducibility of the CBM variant analyses.

A repeat Core analysis on PCS hydrolysis, there is demonstrated minimal (< 2 %) variation on the $V_{\max}(\text{cat})$ and k_4 values from these two curves. see Table 8 for values.

Table 8. The $V_{\max}(\text{cat})$ and k_4 , inactivation rate constant for the RAC and PCS ITC fits.

$R^2 > 0.99$ in all cases. The results are ordered in ranking of $V_{\max}(\text{cat})/k_4$ for PCS, the industrial substrate.

Variants	4 g/L RAC 25 °C pH 5.0			20 g/L PCS 50 °C pH 5.0		
Parameter	$V_{\max}(\text{cat})$	k_4	$V_{\max}(\text{cat})/k_4$	$V_{\max}(\text{cat})$	k_4	$V_{\max}(\text{cat})/k_4$
H4K	1.3 s^{-1}	$1.07 \times 10^{-4} \text{ s}^{-1}$	11700	3.1 s^{-1}	$3.3 \times 10^{-4} \text{ s}^{-1}$	9539
Core 1	0.7 s^{-1}	$1.38 \times 10^{-4} \text{ s}^{-1}$	4777	2.8 s^{-1}	$3.3 \times 10^{-4} \text{ s}^{-1}$	8497
Core 2	-	-	-	2.7 s^{-1}	$3.3 \times 10^{-4} \text{ s}^{-1}$	8181
N29D	0.6 s^{-1}	$1.33 \times 10^{-4} \text{ s}^{-1}$	4324	2.5 s^{-1}	$3.5 \times 10^{-4} \text{ s}^{-1}$	7095
Y31A	0.6 s^{-1}	$2.07 \times 10^{-4} \text{ s}^{-1}$	2744	3.0 s^{-1}	$4.7 \times 10^{-4} \text{ s}^{-1}$	6409
H4W	1.0 s^{-1}	$1.31 \times 10^{-4} \text{ s}^{-1}$	7400	2.1 s^{-1}	$3.6 \times 10^{-4} \text{ s}^{-1}$	5751
G6R	0.5 s^{-1}	$2.15 \times 10^{-4} \text{ s}^{-1}$	2480	2.5 s^{-1}	$4.7 \times 10^{-4} \text{ s}^{-1}$	5226
TH110 WT	0.4 s^{-1}	$2.35 \times 10^{-4} \text{ s}^{-1}$	1741	1.8 s^{-1}	$3.7 \times 10^{-4} \text{ s}^{-1}$	4733
TrCel7A	4.1 s^{-1}	$2.6 \pm 0.2 \times 10^{-4} \text{ s}^{-1}$	15769	2.3 s^{-1}	$3.9 \pm 0.3 \times 10^{-4} \text{ s}^{-1}$	5782
	From Chapter 2, 0.72 g/L RAC, 50 °C			From Chapter 2, 15 g/L PCS, 50 °C		

There is a significant difference in values for all variants comparing the two substrates, RAC and PCS²². Here, in order to present a $V_{\max}(\text{cat})$ value, we use a standard enzyme concentration based on the dose of the wild type, 25 nM TH110 WT (Wt Ctrl). This will of course have a large effect on $V_{\max}(\text{cat})$ and given all the enzymes are dosed equally we present the data here, assuming $E_{\text{tot}} = E_{\text{Active}}$. The reproducibility of individual experiments was tested using duplicate analysis, one of which is shown in Figure 30, and

²²RAC is amorphous and contains no lignin, the temperature for screening was 25 °C and the concentration was 4 g/L cellulose. PCS contains 27 % lignin, the temperature for screening was 50 °C, and the concentration was 11.4 g/L cellulose (20 g/L PCS @ 57 % cellulose).

duplicates agreed to within 5 %. Before discussing the current results, we first refer to the earlier results presented in Chapter 2 (shown in grey in Table 8).

For PCS, where both experiments were run at 50 °C with excess amounts of substrate, the $V_{\max}(\text{cat})$ and k_4 values are essentially equal. This is a very good correlation between different batches and concentrations of both PCS (15 g/L and 20 g/L) and enzyme (50 nM and 25 nM), and shows the robustness of this type of analysis. For RAC, k_4 is largely unaffected by both temperature and substrate concentrations as we have seen earlier when we compared our 50 °C results to those obtained at 30 °C, where k_4 was reported to be $2.6 \pm 0.2 \times 10^{-4} \text{ s}^{-1}$ and $2 \pm 0.7 \times 10^{-4} \text{ s}^{-1}$, respectively. Looking at the V_{app} rates, it appears as though there is a drastic decrease in hydrolysis rate when sinking the temperature from 50 °C to 25 °C from 4.1 s^{-1} to 0.4 s^{-1} , however k_2 has been reported to be in the order of 0.5 - 1 s^{-1} at 30 °C using a similar method (162). To further investigate this we calculate the Q_{10} temperature coefficient²³.

$$Q_{10} = \left(\frac{V_{\max}(\text{cat}) 50^{\circ} \text{C}}{V_{\max}(\text{cat}) 25^{\circ} \text{C}} \right)^{\frac{10}{(323-298)}}$$

Equation 10. Calculating the Q_{10} temperature coefficient.

Here we use the $V_{\max}(\text{cat})$ as the rate, 323 and 298 as the temperature in Kelvin.

This gives us a Q_{10} value of 2.53, which is within the typical 1 – 3 seen in biological systems. This does, however, have a profound effect on the number of catalytic events which may be performed before inactivation, seen here by an almost 90 % reduction from 16,000 to 1700. The significance of this and a mechanistic interpretation for this is offered in the discussion.

There is a lot of data presented here, so we deal first with each substrate separately, before comparing the overall trends.

3.3.3 CBM variants action on RAC

There was a more pronounced difference in the variants action on RAC with the k_4 inactivation rate constant varying by a factor of up to three. All variants were seen to perform better than the original *TrCel7A*, including the Core. Y31A and G6R appear the most similar to the original wild type, having k_4 values only slightly lower, and consequently $V_{\max}(\text{cat})/k_4$ slightly higher. The histidine replacements appear to be far less prone to inactivation. They have k_4 values half (H4W), and even as low as one third (H4K) that of the original. H4K can perform on average 11700 catalytic events before being inactivated compared to the 1741 of the wild type, which is a drastic improvement. N29D, present on the same binding face as the

²³ The Q_{10} temperature coefficient is a measure of the rate of change of a biological or chemical system as a consequence of increasing the temperature by 10 °C

three binding aromatic tyrosine residues is also significantly better here, capable of performing twice the average amount of catalytic events based on this type of analysis.

3.3.4 CBM variants action on PCS

There was less of a difference between the variants in the k_4 inactivation rate constants with the PCS hydrolysis. Here, Y31A and G6R have the highest values, while H4K and the Core have the lowest. The overall relative values for $V_{\max}(\text{cat})/k_4$ are higher than those associated with RAC, and these higher k_4 values may indicate the *TrCel7A* becomes catalytically inactive faster on the PCS. This supports our conclusions in the last Chapter, where we state the inactivation rate on PCS may also include such extrinsic factors as either lignin or hemicellulose bound to the surface, blocking the processive nature of the cellobiohydrolase.

Here, while all the $V_{\max}(\text{cat})/k_4$ values are higher than the wild type again, it is interesting to note the rate constant of inactivation, k_4 is higher for Y31A and G6R (i.e. they are more prone to inactivation). G6R may serve to open the structure of the wedge (Arginine having a far larger side chain than Glycine) and in this case also appears to have a negative effect on the PCS hydrolysis. It is possible this mutation renders the CBM more prone to binding to the lignin fraction of the PCS by exposing more of the wedge structure to the polyphenolic structure. Y31A, on the other hand serves to reduce the binding of the overall enzyme to the cellulose fraction. This has been shown on a Y31A mutant previously generated (141), and tested on crystalline cellulose (BC)²⁴. One explanation for this observation is that if the enzyme is less strongly bound to the cellulose that it may come into contact with the lignin fraction more often and become inactivated in this manner.

3.3.5 CBM variants action on PCS (HPLC) hydrolysis results.

In order to confirm results determined by ITC as a viable method of screening for lignocellulosic biomass hydrolysis, the following field testing was carried out. The same dosing of *TrCel7A* variants based on pNPL activity was applied to PCS. 20 g/L, pH 5.00 buffer, incubated over 24 h at 50 °C, 1000 rpm in the thermomixer (0.5 mg/mL *AnBG* (*A. niger* BG purified as outlined in Article 2 (111)) was added to prevent cellobiose inhibition and to mimic the ITC set up). Here we report total sugars generated (all soluble), although it was mainly glucose measured by HPLC²⁵ as per Article 1 (103).

In order to directly compare the ITC and HPLC data, we introduce a relative performance index (RPI) where the variants are normalized after the total wild type sugar production. By this definition, a better

²⁴ BC, Bacterial cellulose, they report an I_{cr} of 1.0 i.e. 100 % crystalline.

²⁵ All HPLC samples in were triplicate, all samples analyzed with two separate injections, the averages of all 6 readings are presented here (error bars on graph).

performance is defined as an enzyme which produces more sugar under the monitoring period. The ITC data (Figure 29 (R)) is integrated and the μJ area value used for this purpose. This may be done even if the ΔH is not known for the system as the normalized total product is unit-less.

Here, note it is the total product formed after 30 min we normalize the ITC data with, and the total product after 24 h for the HPLC. It is necessary to run the hydrolysis this long for the HPLC in order to attain concentrations which may be detected accurately. First, we compare the relative performance index (RPI) in Figure 31 to the $V_{\max}(\text{cat})/k_4$ values presented in Table 8. The top two candidates, H4K and N29D are highlighted as performing better than the wild type. The correlation between the ITC after 30 min and the HPLC with the same dose after 24 h holds remarkably well for the first 5 variants, H4K, N29D, WT, G6R and H4W. Of these, the last two are within the boundaries of the error associated with both analyses.

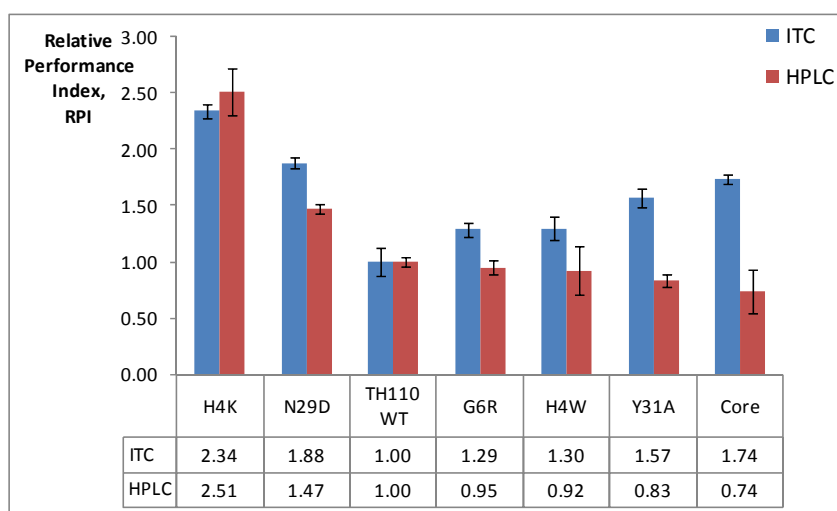


Figure 31. ITC 50 °C, 30 min amplified reactions on PCS compared to HPLC, 24 h hydrolysis reaction with the same dose of BG.

Finally, we have two exceptions to the ITC data. The Core and Y31A both perform worse than the wild type control over 24 h compared to the first 30 min monitored by the ITC. It may be possible these two variants are less thermally stable than their counterparts, leading to a decrease in the active enzyme population over the longer monitoring period of 24 h. We return to this in the discussion.

3.3.6 Overall substrate and temperature trends

Now we compare the trends from the two temperatures and the two substrates used in this study. The screening on RAC at 25 °C is carried out first for two main reasons. Firstly, the batch to batch variation of this substrate has been shown to be minimal allowing the comparison of old and new data. The DP_N is consistently 180 to 200 glucose units per cellulose chain, and the I_{cr} measured by NMR displays a steady almost completely amorphous structure.

Secondly, screening at 25 °C allows a higher throughput from a purely technical point of view as thermal equilibration to 25 °C by the ITC compared to 50 °C takes approximately 30 – 45 min less. This may then be followed up by screening the best performing RAC variants on the industrial substrate, PCS at the industrial conditions, i.e. 50 °C. We have shown the trends from substrate to substrate on RAC, BC and PCS were the same in the last Chapter, in that better performance on one substrate was reflected in all tested substrates.

Here, in order to directly compare the candidates from both ITC methods, we employ the same method as used in the last section and introduce the RPI again. This is a quick and simple method to compare the substrates, and we see the total product trends reflect the order of $V_{\max}(\text{cat})/k_4$ as well.

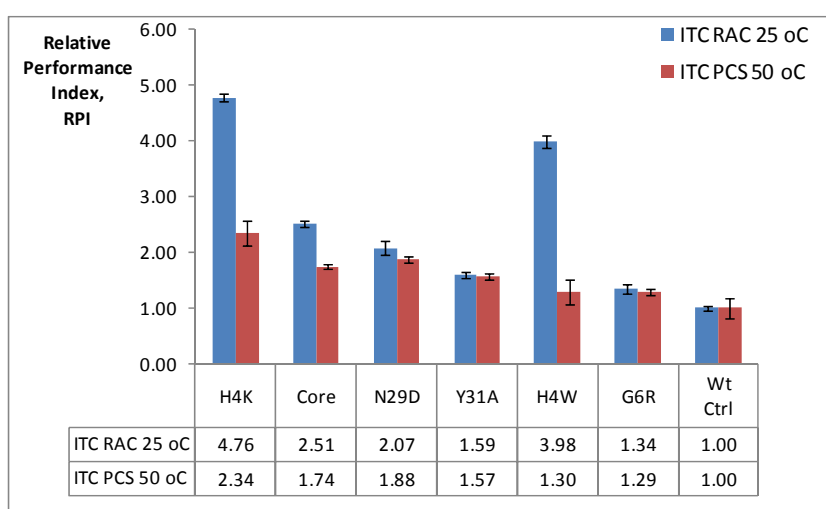


Figure 32. Integral of the RAC thermograms at 25 °C, compared to PCS integrals at 50 °C.

In general we see the trends for the two substrates follow each other. The Core outperforms the wild type far better on the RAC substrate. It has been previously reported the Core performs equally well as the intact wild type on insoluble amorphous cellulose and cello-oligosaccharides before (143,170,196,197), so this is not unexpected. Indeed, the lowering of the performance on PCS compared to RAC may reflect the higher amount of crystalline regions present in this substrate. In any case, under these initial 30 min conditions it may be seen the CBM is not essential for the hydrolysis of insoluble non crystalline cellulose.

The most marked exceptions are the histidine variants which both perform far better on RAC at 25 °C than PCS at 50 °C. We now examine all these trends in light of our results.

3.4 Discussion

There are three main trains of thought about the role of the CBM as outlined in the introduction. For a more structured discussion, we present them separately, but that is not to say they are mutually exclusive.

1) The CBM has no effect on the actual enzyme movement on the cellulose chain and serves only to increase the total amount of enzyme on the surface (170). This is based on monitoring the movement of the intact wild type and the Core with no CBM on the surface of crystalline cellulose using atomic force microscopy (AFM). Both the Core and the wild type move at the same observed speed, thus the author concludes the V_{app} difference must be a function of overall enzyme concentration on the surface rather than increased efficiency of the wild type compared to the Core on bacterial cellulose.

2) Measuring the crystallinity and hydrogen bonding pattern using x-ray diffraction (XRD) and Fourier transformed infra red spectroscopy (FTIR), respectively, the CBM functions to decrease the crystallinity of cellulose by the intermolecular splitting of hydrogen bonds, thus altering the surface structure of the substrate (148,192,194,198,199). Some of these studies have also been confirmed by visualization of the surface using scanning electron microscopy (SEM). Pretreatment of cellulose with CBMs alone has enhanced the hydrolysis rate through reduction in the crystalline regions to support this theory (192).

3) The CBM functions to aid in finding specific targeted areas of cellulose for binding. It is proposed CBMs alone do not bind to specific regions (200), but rather facilitate lateral diffusion along the two dimensional surface of the substrate until an appropriate binding site for the catalytic domain can be found.

We now discuss these theories in light of our results separately first.

3.4.1 CBM functions solely to increase the overall enzyme concentration

Firstly, we observe an increased rate V_{app} (higher initial rates, i.e. higher apex, see Figure 29) in the initial phase of the catalysis of both PCS and RAC for many of the mutants, and more importantly for the Core. This disagrees with the theory of CBM-increased affinity to the cellulose, or increased overall enzyme concentration, as if this were the case the overall Core V_{app} rate would be decreased.

The enzyme to substrate ratio is over 5000:1 based on the reducing ends available as measured by the BCA method. Thus, there is no apparent shortage of enzyme attack points. The substrate concentration of 4 g/L is over the 15 μM reducing ends (based on a DP_N of ca. 200), where the addition of more substrate to a constant low enzyme concentration (50 nM) has been shown not to lead to an increase in the overall rate (162), so V is independent of S_0 at these concentrations. The binding constant, K_B for the CBM alone on a cellulose surface is in the order of 10^7 M^{-1} (155), and given the Core and CBM both bind to the cellulose (i.e. one may assume this is cooperative and thus combined they have a larger K_B), it is reasonable to assume all enzymes are initially in action under these conditions. Given all enzymes are in action, there is no concentration difference and thus, the increase in V_{app} must be attributed to other factors.

To add to this; if all the enzymes functioned in a mechanistically similar manner and all V_{app} increases were solely a function of concentration, the rate constant of inactivation would not differ. The fact that CBM variants (and Core) have different rate constants of inactivation (k_4) would suggest there are different mechanisms involved here. This could be as a result of different binding affinities to the cellulose chain, different release rates, or altered procession rates as a result of these new interactions.

The CBM may play more of a role at higher enzyme to substrate ratios or on more crystalline substrates, but here we observe no concentration effect. The variants seen here have increased initial V_{app} rates, which cannot be attributed to an increase of enzyme concentration on the cellulose surface. We conclude therefore under our experimental conditions that the role of the CBM is not to increase the overall concentration of enzyme on the cellulose surface.

3.4.2 CBM functions to decrease intermolecular hydrogen bonding

A decrease in intermolecular hydrogen bonding would be seen as a decrease in effective crystallinity. To study this particular phenomenon it would have been optimal to have used a crystalline substrate such as BC, but that was not the initial aim of this study. The original aim was to screen CBM variants after performance on a model substrate and compare this to a lignocellulosic substrate for selection. RAC was used to this end as described earlier. Now we are in a situation where we are able to gain extra information from such a screening study and this of course leads to new insights which may be taken further in the fundamental study of this enzyme class.

We start with the Core which outperforms the wild type on RAC. This is seen by both the total product generated in the first 30 min (relative performance index, see Figure 32) and the increase in $V_{max(cat)}/k_4$ (See Table 8), indicating the Core can perform almost three times the amount of catalytic events than the wild type before inactivation on RAC at 25 °C. It is therefore reasonable to conclude the CBM has little, if any beneficial effect here. Judging from the PCS hydrolysis results we see the ITC again indicates increased hydrolysis in the absence of the CBM whereas the HPLC results indicate the opposite.

This is an inherent issue with comparing any screening method of 30 min to an industrial trial of 24 h. Although the screening may pinpoint the best variants after 30 min, over 24 h there are other issues which may play a larger role. In this case, it may be the Core is less thermally stable than the wild type, or that the conversion of cellulose may have a larger effect on the Core than the wild type. After 24 h under our conditions the conversion of cellulose to soluble sugar products is less than 5 %, so this is unlikely to be the cause of the measured decrease in product. Another possibility is the CBM does indeed loosen the cellulose

chains allowing for more product formation, but that this phenomenon is more widespread after the initial 30 min of hydrolysis which we monitor here.

This is supported by the Y31A results which also display a reduction in total product formed after 24 h compared to the wild type in the HPLC results. Y31A plays an essential role in the binding of the CBM to the cellulose, as has been demonstrated by other mutation studies (141,201,202). Thus, if the CBM is essential for “peeling” chains in complex matrices such as PCS, a drop in product formation would be expected in this variant.

The other variants all reflect the same trends in the ITC and HPLC. The two that stand out are H4K and N29D in PCS hydrolysis and these two and H4W in RAC hydrolysis. The difference in H4W rates on RAC compared to PCS may be the result of the extra tryptophan increasing the potential for the enzyme to bind to the lignin fraction, and therefore an increase in the extrinsic inactivation of the population. N29D is on the same face as the three conserved essential tyrosines involved in the binding of the CBM to the cellulose surface, and a previous N29A variant displayed reduced affinity (201). Here we change the amine to an amide, introducing the potential for another OH:H hydrogen bond. H4K has the most drastic increase in both RAC and PCS hydrolysis, confirmed also by HPLC results. We propose a mechanistic interpretation for this later.

3.4.3 CBM aids in targeting sites for productive binding

On an amorphous cellulose surface, the Core and wild type have been shown to perform almost equally (43,44). The absence of the CBM also has a drastic effect on the hydrolysis of crystalline cellulose (183,186). Here, we investigate the enzymes with a very large S:E ratio (in the order of 5000:1 based on the number of reducing ends of RAC i.e. attack points per unit enzyme). Under these conditions the lack of sites should not be an issue and thus a targeting function would not be revealed. A different type of study with a lower ratio on BC could be used in a fundamental context in order to further investigate this option.

However, given the difference in k_4 values displayed by the variants, we can state the mechanism is different for each CBM and CBM-free enzyme. A targeting function would have most effect in the start phase of the hydrolysis, leading to the formation of productive ES complexes faster, potentially facilitated through lateral diffusion along the surface of the two dimensional chain. This again would effectively be an initial concentration effect, which we do not see here, as explained earlier.

Thus, we conclude the most likely effect of altering the CBM is in the function of aiding the processive nature of the enzyme, through direct interaction with the cellulose chain, splitting or peeling chains. This is

supported by the changes in k_4 values seen for all variants and the Core, suggesting the changed amino acids contribute to changes in the rate constant of inactivation.

3.4.4 A mechanistic interpretation

Here, we propose a possible route for the cellulose in contact with the CBM (See Figure 33). Two of these three routes have been proposed before by Reinikainen and co-workers (141) who studied a Y31A mutation (there Y492A) and a proline residue on the other face of the CBM P477 (in close proximity to the red route). A similar mode of action was proposed by Mulakala and co-workers (175) based on docking studies of cello-oligosaccharides and supported by atomic force microscopy (AFM) observations (203) where the chains of cellulose appear to be lifted by the CBM. This supports the second theory presented above, that the role of the CBM is to disrupt the cellulose chains from the cellulose crystalline superstructure.

The blue route (open arrow, closed blue arrow) assumes the CBM simply increases the proximity of the Core to the cellulose surface. The red route (open arrow, closed red ringed green arrow) suggests the wedge opens the chain, effectively peeling off the layer before feeding it to the catalytic domain. Here we suggest a possible complementary route, the green route (either red or blue open arrows, with closed red ringed or blue ringed green arrows).

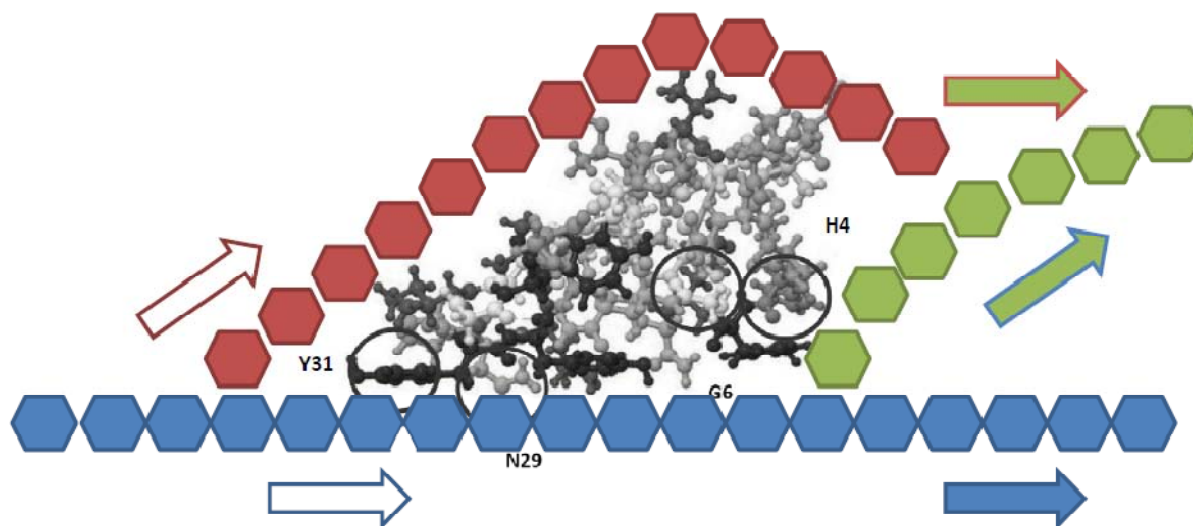


Figure 33. Proposed routes for cellulose association by the CBM. (141,175,203)

In all cases the arrows represent the direction of movement of the cellulose chain.

Taking the blue-green route first, the cellulose chain is bound at the hydrophobic face of the tyrosines present at Y13, Y31 and Y32, and then may be lifted to facilitate the feeding into the tunnel of the active

site. If this is the case, the H residue at H4 could play a critical role, and this is supported by our experimental observations, where we see increase V_{app} for RAC and PCS hydrolysis by changing this amino acid.

It is possible by introducing the mutation at H4 that we increase the probability of the cellulose chain to be lifted as shown in the green route as opposed to remaining bound to the cellulose super structure (denoted by the pure blue route). The H4W mutation introduces the possibility for more stacking interactions with the indole ring, which may serve to increase the lifting power of the back side of the wedge. Changing a tyrosine for a tryptophan has been seen to increase affinity of the CBM (149). Alternatively, the H4K mutation introduces a slightly more hydrophilic interaction and removes the weak stacking interaction between the imidazole ring and the glucose pyranose rings, our results indicate this too increases the overall rate of reaction, in particular on amorphous surfaces.

It is also possible the red-green route is complemented by the histidine variants. If the chain falls along the back side of the edge before being fed into the Core for catalysis, it is also possible here that the histidine lifts the chain as explained for the blue-green route. If the red-green route was the main route, it would seem likely the G6R mutant would play a more prominent role as this would possibly open the wedge structure and increase the disruption of the chain; this is not supported by our observations, where the hydrolysis with the G6R variant leads only to a very slight difference in the production of soluble sugars.

3.5 Summary and conclusions

We have developed a method to purify and quantify the active fraction of protein engineering variants. We have demonstrated how the activity on soluble substrate (pNPL) and insoluble cellulose do not reflect each other, precluding the use of small soluble substrates as accurate screening tools. ITC may be used to screen the variants for over all hydrolysis, changes in the decay rate, and the use of a lignocellulosic and amorphous substrate may be used to investigate different properties of the protein engineering enzymes. The use of ITC as a means to determine the effectiveness of hydrolysis on an industrial substrate, i.e. PCS is also demonstrated and the main advantage here is the possibility of determining kinetic parameters (k_4 , and $V_{max}(cat)$) as well as the small amount of resources needed (5 μ g of variant, 1 h).

The trends seen screening on RAC at 25 °C and PCS at 50 °C, hold true with the exception of H4W, which we postulate may have an increased affinity for binding to the lignin fraction of the PCS. Differences in the HPLC and ITC hydrolyses, we propose are the differences in a 24 h and a 30 min hydrolysis, and may reflect a change in the thermal stability variants which we highlight here using a simplified relative performance index normalization.

After screening the CBM point mutations, we conclude the function of the CBM under these conditions is neither to increase the overall concentration of the enzyme on the cellulose surface nor is it to target specific areas for productive binding of the complete enzyme. The use of a crystalline substrate and other enzyme to substrate ratios could be included in future analyses in order to further investigate this. From analysis of the ITC data we can determine the mutations at H4 to be the most beneficial for PCS hydrolysis, and in conclusion, it appears the back side of the wedge (the green route as discussed above) may play a critical role in the mechanical action of the CBM-Core interaction.

We see a profound difference in the turnover number based on a 25 °C temperature rise, while the rate of inactivation remains relatively constant; this is a very good argument for the development of thermally stable enzymes. This may be seen from looking at the ratio of k_2 and k_4 , which indicates on average how many catalytic events may be performed before the enzyme is inactivated. A rise in k_2 while k_4 remains the same will naturally lead to an improvement in the amount of catalytic events each enzyme may perform on average. A more thorough temperature series investigation is warranted.

3.6 Supplemental Information

For Figure 25: Amino acid residues by color: **ASP** **GLU** **CYS** **MET** **LYS** **ARG** **SER** **THR** **PHE** **TYR** **ASN** **GLN** **GLY**
LEU **VAL** **ILE** **ALA** **TRP** **HIS** **PRO**

Chapter 4. Thermochemical screening of D-glucono- δ -lactone hydrolases.

4.1 Background

We have outlined in the previous chapters the uses and advantages of the coupled amplification system developed for the monitoring of CBH action on cellulose. There are, however, two distinct disadvantages using this coupled technique. Firstly, the system inherently depletes oxygen from the cell (See Figure 34). For each mole of cellobiose produced, $\frac{1}{2}$ mol O_2 is removed, as the oxidation of glucose uses 1 mol O_2 and the breakdown of hydrogen peroxide replenishes only half of this. This can be alleviated, however, using oxygen enriched buffer as stated in Article 2 (111), increasing the amount of product which may be formed to maximum of 0.5 mM.

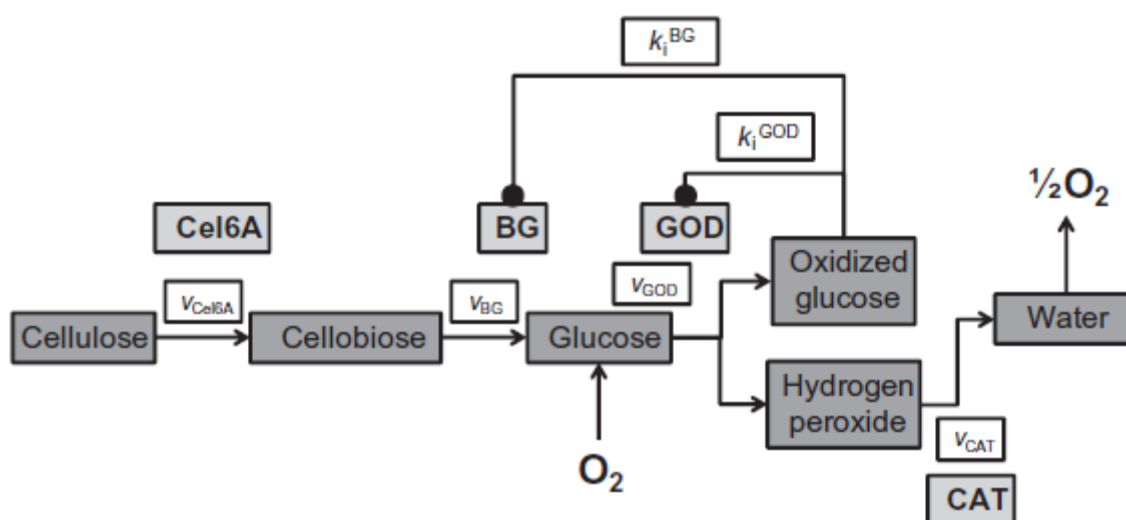


Figure 34. The coupled amplification system (111).

Cellobiose is hydrolyzed by β -glucosidase to glucose, glucose is oxidized to D-glucono- δ -lactone by glucose-1-oxidase, and hydrogen peroxide is broken down to water and oxygen, replenishing half the oxygen to the liquid phase.

Secondly and more critically, D-glucono- δ -lactone will build up long before this, and is a potent inhibitor of β -glucosidase ($K_i = 0.1$ mM). Very little information could be found about the rate of autohydrolysis of the D-glucono- δ -lactone to D-gluconic acid, other than very qualitative statements that it is “spontaneous” yet “slow” under our assay conditions (typically 25 °C, pH 5).

The original purpose of this investigation was to determine if this inhibition by the D-glucono- δ -lactone to the β -glucosidase in the amplification system, which is fully described in Article 2 (111) could be alleviated. This could provide the tool to monitoring for longer periods with higher enzyme activity, and thus a better measure of the k_4 kinetic parameter. In biological systems the D-glucono- δ -lactone is typically formed by

glucose dehydrogenase (204), although in the amplification system this is achieved by glucose-1-oxidase. In both cases, the D-glucono- δ -lactone is formed by the oxidation of glucose, which is spontaneously hydrolyzed to D-gluconic acid (205-207). This reaction is catalyzed by the enzyme D-glucono- δ -lactone hydrolase (E.C. 3.1.1.17) (208).

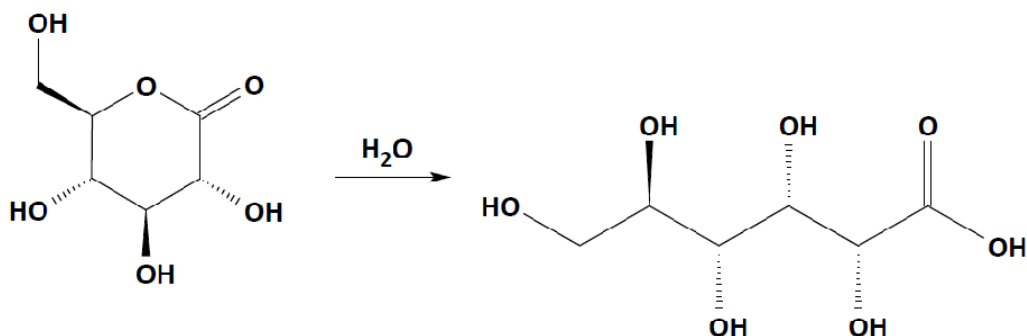


Figure 35. The hydrolysis of D-glucono- δ -lactone to D-gluconic acid.

The reaction also involves the formation of γ -lactone, but at pH 5.00 in acetate buffer at 25 °C, the δ -lactone:D-gluconic acid equilibrium is established long before the any appreciable amount of γ -lactone is formed (209).

The equilibrium constant is reported in the order of 1 to 3×10^4 M. This indicates under our conditions where there is a buildup of D-glucono- δ -lactone, and that the reaction goes towards the formation of the D-gluconic acid product, but not at what rate. Rates of hydrolysis have been measured either using colorimetric methods, or have monitored the fall in pH over time (204,206,208,210). Hestrin (210) originally determined the amount of remaining substrate with the limitation that the spectrophotometric method was hampered by the formation of bubbles on the cuvette (211) due to the release of N_2 . The formation of product has also been measured by using the pH indicator *p*-nitrophenol and measuring OD_{405} (211,212). However, this is limited to pH regions where the *p*-nitrophenol is colored ($> pH 6.6$ (98)), so this method may not be used in our context at pH 5.0. As stated in Chapter 1, this may be overcome by using a CNP (chloro-*p*NP, reduces pK_a to approximately 5.2) derivative (61), but again it is a form for product monitoring, the disadvantage of which we outline later.

Here, we use ITC to investigate the rate of autohydrolysis in the cell under pertinent assay conditions (for our amplified system) as well as the rates of enzyme catalyzed hydrolysis when catalyzed by two different D-glucono- δ -lactone hydrolase enzymes. The autohydrolysis is important for two reasons. Firstly, it may contribute to the thermal signal if the rate is fast enough, thus becoming a source of error to the kinetic readings. Secondly, the rate of autohydrolysis tells us how fast the β -glucosidase inhibitor is removed from

the system, as D-gluconic acid (comparatively) has no effect on the β -glucosidase or glucose-1-oxidase at these concentrations.

Then, we determine if the addition of D-glucono- δ -lactone hydrolase can further improve the amplification system by extending the monitoring time, by catalyzing the reaction and similarly removing D-glucono- δ -lactone hydrolase. The previous methods to investigate D-glucono- δ -lactone hydrolase have all measured product. This does not allow for the addition of product to investigate product inhibition. Here to the best of our knowledge, we demonstrate for the first time, a method to also monitor the product inhibition of this enzyme class.

4.2 Results and discussion

4.2.1 Determination of ΔH

To begin, a ΔH value must be measured in order to be able to convert $\mu\text{J/s}$ rates to mol/s rates. This is done using a depletion set up. Depletion is achieved by injecting the substrate to the enzyme and allowing the entire substrate to be hydrolyzed. The integral of the heat signal generated is the complete amount of heat for that amount of substrate and may be used to calibrate for future readings. This requires a relatively high (100 mM is high compared to our assay conditions) concentration of substrate in the syringe. Given there is such a concentration of D-glucono- δ -lactone in the syringe, we must correct for the autohydrolysis occurring there prior to the first injection, and measure the rate of autohydrolysis in the syringe to correct for future kinetic experiments.

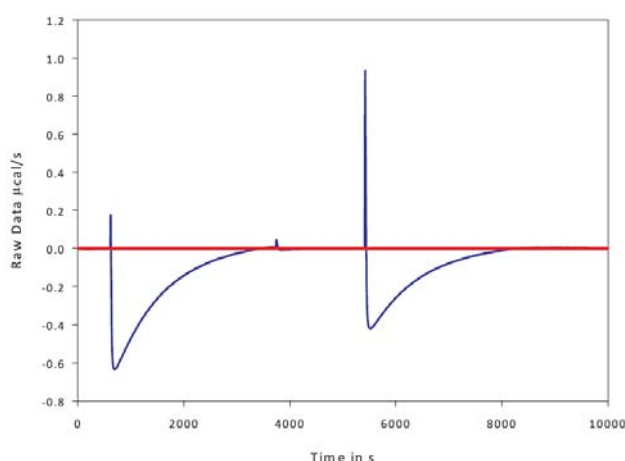


Figure 36. A depletion experiment for measuring autohydrolysis of D-glucono- δ -lactone in the syringe.

Raw data from the VP-ITC, exothermic signal is down. $2 \times 5 \mu\text{L}$ of 100 mM D-glucono- δ -lactone injected to 200 nM D-glucono- δ -lactone hydrolase (WT 1) in the cell. pH 5.0, 25 °C. Buffer = 100 mM sodium acetate, 2 mM CaCl_2 + 0.01 % triton X-100. The second injection is almost 30 % less than the first as a result of depleted substrate in the syringe.

All D-glucono- δ -lactone preparations were weighed out accurately and dissolved immediately prior to use to minimize autohydrolysis during the thermal equilibrium of the ITC; pH was also recorded. The rate of autohydrolysis in the syringe was first measured. This was achieved by multiple injections of the D-glucono- δ -lactone to the hydrolase enzyme in the cell. Unlike the stepwise kinetic experiments described below, here we use a slightly stronger enzyme concentration (200 nM) to completely hydrolyze the substrate. When the baseline is re-established (red line), the reaction has gone to completion and the integral is a measure for the total heat produced. Each subsequent injection is a smaller concentration of D-glucono- δ -lactone (blue lines), and thus the heat signal decreases proportionately. By integrating the heat signal and comparing it to previous injections, the rate of D-glucono- δ -lactone depletion in the syringe may be calculated. Then, we can retroactively calculate the concentration in the syringe for the first injection based on the thermal equilibration and baseline time from the time point where the D-glucono- δ -lactone was initially dissolved.

Using this method, ΔH was determined to be -5.1 ± 0.3 kJ/mol with a rate of autohydrolysis in the syringe determined to be $6 \mu\text{M/s}$ (100 mM D-glucono- δ -lactone, pH 5.00, 25 °C)

4.2.2 Determination of kinetic parameters

The determination of kinetic parameters for two different D-glucono- δ -lactone hydrolases (provided by Novozymes A/S) was performed using a stepwise ITC set up similar to the system described in (111). However, in this case, a rate of autohydrolysis in the cell must also be corrected for. This was achieved by titrating the D-glucono- δ -lactone to a cell containing only buffer, each injection was then allowed to come to a constant heat flow representing the rate of autohydrolysis at that concentration, seen as the red thermogram in Figure 37.

Table 9. Kinetic Parameters for the two tested D-glucono- δ -lactone hydrolases.

Presented are the fitted values from Figure 37 (R). Note other experiments yields very similar values with an overall CV % of less than 5%.

Enzyme	K_M	k_{cat}	k_{cat}/K_M
Wild Type 1	2.2 mM	295 s^{-1}	$134 \text{ s}^{-1} \text{ mM}^{-1}$
Wild Type 2	5.3 mM	148 s^{-1}	$28 \text{ s}^{-1} \text{ mM}^{-1}$

The method of calculation for Michaelis-Menten fits is outlined in the supplemental information at the end of the chapter.

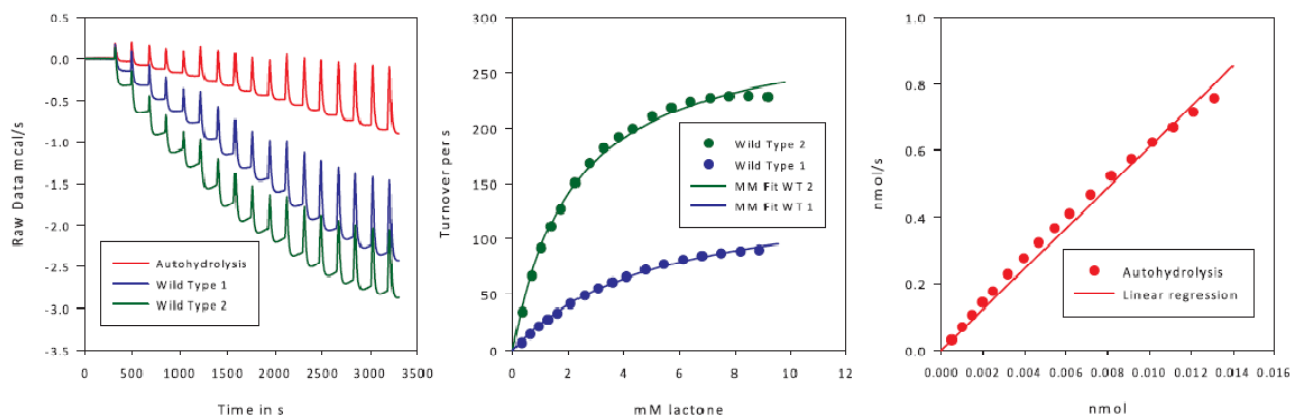


Figure 37. Michaelis-Menten (MM) fits for GDLH kinetics, $R^2 > 0.99$ in both cases.

(L) Raw data from the VP-ITC, exothermic signal is down. $5 \times 5 \mu\text{L}$, $5 \times 7.5 \mu\text{L}$ and $6 \times 10 \mu\text{L}$ injections of 100 mM D-glucono- δ -lactone dissolved in 100 mM pH 5.00 sodium acetate buffer + 2 mM calcium chloride, 0.01 % triton x-100 to the cell containing no enzyme (autohydrolysis), 5 nM wild type²⁶ (WT) 2 or 10 nM WT 1. **(M)** The raw data has been converted to rates per second and plotted against the substrate concentration. **(R)** The lactone autohydrolysis rate in the cell.

4.2.3 Calculating the potential error to amplified signals from the ITC

As we stated in the introduction, the rate of autohydrolysis may have an effect on the thermal signal monitored using the ITC. Now, the production of D-glucono- δ -lactone and rate of autohydrolysis during an experimental run using the amplification system may be determined to see what if any error is associated with this process. From the stoichiometry of the reaction there are two oxidized glucose produced for every cellobiose molecule (See Figure 34). We assume the worst case scenario, where the D-glucono- δ -lactone degrades rapidly, and assume the β -glucosidase-bound molecules are also subject to autohydrolysis. Using the ΔH for the amplification system determined to be -355 kJ/mol , and the ΔH for the D-glucono- δ -lactone hydrolysis of -5.1 kJ/mol , the effects of D-glucono- δ -lactone auto hydrolysis on the system may be calculated. Given the ΔH for both systems is negative, the contribution from the autohydrolysis will lead to a slightly larger overall heat signal. Typically, the system is monitored for 30 min, but in this case it is a run of 45 min that is investigated. Assuming the autohydrolysis is instantaneous yields the worst case scenario where the maximum error is

$$\text{Maximum \% Error} = \frac{\Delta H_{[\text{Lactone autohydrolysis}]}}{\Delta H_{[\text{amplification}]}} \times 100$$

Equation 11. Calculating the error associated with autohydrolysis of the D-glucono- δ -lactone.

This leads to a slight overestimation of less than 3 %.

²⁶ With respect to Novozymes A/S IP rights, the terms wild type 1 and 2 are employed here to distinguish between candidates.

The *actual* rate of autohydrolysis in the cell may be calculated by plotting the rates as a function of the concentration of substrate derived from Figure 37. This gives a linear plot, and when plotting nmol on the abscissa and nmol/s on the ordinate gives a slope of 62 s^{-1} ($R^2 = 0.99$). Under a typical hydrolysis reaction such as that outlined in the next section, the rate of autohydrolysis may be calculated by integrating the heat signal, and using the measured ΔH to provide a theoretical concentration of D-glucono- δ -lactone. Multiplying this by the rate of autohydrolysis (62 s^{-1}) gives the maximum value of 5 pmol/s, which given the enthalpy of -5.1 kJ/mol, is an interference of under 5 nJ/s, i.e. negligible compared to the resolution of the calorimeter.

4.2.4 Inhibition removal

In order to determine if it would be beneficial to remove the D-glucono- δ -lactone inhibition of the BG by addition of the D-glucono- δ -lactone hydrolase (GDLH) the following comparison was made. Using the following equations based on Michaelis-Menten kinetics where $S_0 \ll K_M$ to describe the system:

$$v_{BG} = \frac{V_{\max} \times [G2]}{K_M \left(1 + \frac{[G1OX]}{K_i(G1OX)}\right)} \quad v_{GDLH} = \frac{V_{\max} \times [G1OX]}{K_M}$$

Equation 12. Calculation of the rates for β -glucosidase and D-glucono- δ -lactone hydrolase in the ITC cell.

Where G1OX = oxidized glucose, G2 = cellobiose, and the other symbols have their usual meanings. The parameters for BG are taken from (111).

A typical set up is as follows: 35 nM of *TrCel7A* is titrated to 20 g/L PCS at 50 °C in the NanoITC. The PCS is suspended in the standard buffer of 50 mM sodium acetate + 2 mM CaCl_2 pH 5 0.01 % Triton X-100, and the amplification system with β -glucosidase is added as outlined in (111).

Table 10. The GDLH and BG kinetic data for the comparison of rates.

Enzyme	$k_{\text{cat}} \text{ s}^{-1}$	[E] mg/mL	Mw g/mol	V_{\max} mM/s	K_M	$K_i(\text{G1OX})$
BG	234	0.5	118000	991	0.8	0.1
GDLH	295	TBD	41458	TBD	2.2	N/A*

TBD = to be determined *See below.

The raw data from the heat signal may be expressed as mM/s using $\Delta H = -355 \text{ kJ/mol}$ and converted to a rate of production of G2, cellobiose. Then, multiplying this value by 2, gives the rate of production of the oxidized glucose product, G1OX. This allows us to calculate the v_{BG} and v_{GDLH} as a function of time. Given we know all the other values; the minimum concentration of GDLH to relieve inhibition of the BG may then be calculated. Based on Equation 12, at a GDLH dose of 0.19 mg/mL the rates are equal.

4.2.5 GDLH inhibition²⁷

In order to determine if the D-glucono- δ -lactone hydrolase enzyme is inhibited by its own product, D-gluconic acid, the same analyses as before was repeated with varied concentrations of product in the ITC cell. In order to correct for the autohydrolysis rate being influenced by the increased concentrations of product in the cell, control experiments with no enzyme were also carried out.

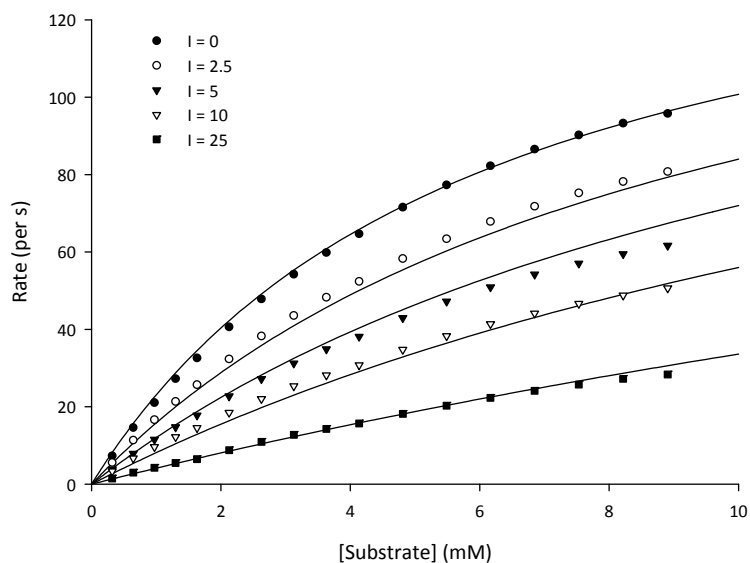


Figure 38. D-glucono- δ -lactone hydrolase Wild Type 2, inhibition studies.

D-glucono- δ -lactone hydrolase in the cell with D-gluconic acid, aliquots of D-glucono- δ -lactone titrated to the cell. The data has been fitted by non linear regression using Sigmaplot V 11.0 to the Michaelis-Menten competitive inhibition model shown here:

$$v = \frac{V_{\max} [S]}{K_M \left(1 + \frac{[I]}{K_i}\right)}$$

Equation 13. The Michaelis-Menten competitive inhibition model.

Table 11. Inhibition kinetic parameters for the two tested D-glucono- δ -lactone hydrolases.

The data has been fit to the Michaelis-Menten competitive inhibition model.

Enzyme	K_M	k_{cat}	K_i	R^2
Wild Type 1	2.5 mM	303 s^{-1}	3.1 mM	0.97
Wild Type 2	6.0 mM	161 s^{-1}	6.7 mM	0.99

²⁷These experiments were carried out by Kristian Filrup.

4.3 Conclusions

4.3.1 The general kinetics of GDLH

We have demonstrated here a fast and efficient method to screen GDLH wild types and characterize them kinetically. K_M values for GDLH have been reported in the region of 0.4 to 18 mM, and k_{cat} values have been reported in the area of 70 s^{-1} to 680 s^{-1} in good agreement with our findings²⁸ (204,207,208). Now, referring to the catalytic efficiency, defined as k_{cat}/K_M , of the two screened wild types shown in Table 9, it is evident which should be used for the degradation of D-glucono- δ -lactone, in that WT 1 is almost 5 times more efficient under these conditions.

We have also demonstrated a new method to determine the inhibition of the product on the GDLH. This has not previously been possible using methods which rely on the measurement of the product as this provides a huge background and thus interference to these assay types. Interestingly the K_i is very close to the K_M for both enzymes, but given the substrate and product are very structurally similar, this is not entirely unexpected. The data was fitted to competitive, uncompetitive, noncompetitive and mixed inhibition equations. All fits were quite good ($R^2 > 0.95$). We postulate because of the similarity between the product and substrate, that competition for the active site is more likely than the product binding to another site on the enzyme, or the ES complex, and thus present the result for competitive inhibition.

4.3.2 Potential for improving the amplification monitoring time

We return now to the inhibition aspect of D-glucono- δ -lactone on the amplification system, therein β -glucosidase. This investigation was initially to determine if GDLH could alleviate the inhibition of BG in the amplification mixture. We have determined in order for the GDLH to at least match the catalytic rate of the BG, and thus remove the D-glucono- δ -lactone as fast as it is formed, a dose of 0.2 mg/mL would be needed. Given the K_i for the BG is 0.1 mM and the lowest K_M for GDLH is 2.2 mM, this would in effect result in a type of competition for the D-glucono- δ -lactone in the amplification mixture. This cannot be a simple comparison though, as the GDLH will hydrolyze the D-glucono- δ -lactone and release the product, whereas the BG-bound D-glucono- δ -lactone is not immediately released, thus trapping the enzyme in the enzyme inhibitor (EI) complex. However, using the example presented above, the concentration of D-glucono- δ -lactone after 30 min of hydrolysis is far under the K_i or K_M for either enzyme, ($< 0.025\text{ mM}$). We have also demonstrated the interference from the autohydrolysis is negligible at these concentrations. We conclude therefore that the addition of an extra enzyme to the mixture to alleviate a negligible interference is unwarranted.

²⁸ k_{cat} calculated from $\mu\text{mol}/\text{min}/\text{mg}$ values, based on Mw of ca. 40 KDa.

4.3.3 Future perspectives

The use of GDLH in biomass hydrolysis may be beneficial in cases where there is a high starting concentration of oxidized glucose as a result of harsh pretreatment processes. Although we have seen under the conditions tested that the rate of autohydrolysis is significant, the addition of divalent metal ions may provide increased activity to the GDLH enzymes. Activation by Mn^{2+} (preferred (204,208) or Mg^{2+} (212) has been reported, although conflicting reports indicate this does not increase the activity of sufficiently pure enzymes (211). This could also easily be screened for using ITC, adding extra divalent ions to the cell, removing Ca^{2+} from the standard buffer, or adding EDTA to chelate free ions in solution.

4.4 Supplemental information

Calculations performed on the raw data to correct for fits:

4.4.1 Substrate concentrations

- 1) The weight of the D-glucono- δ -lactone is used calculate the 100 % value of the D-glucono- δ -lactone in the syringe.
- 2) The rate of autohydrolysis in the syringe is 6 $\mu M/s$, this is calculated for each injection and subtracted from the theoretical value of [S] added.
- 3) The rate of autohydrolysis in the cell is shown by the red curve in Figure 37 By multiplying this rate by the 180 s between injections, the amount of substrate present in the cell is corrected for.
- 4) For enzymatic reactions, the rate of enzymatic hydrolysis for the 180 s between injections is also corrected for. These are shown by the green and blue raw data curves in Figure 37.

4.4.2 Enzymatic rates

- 1) The rate in $\mu cal/s$ is converted to mol/s using ΔH of -5.1 kJ/mol.
- 2) The turnover is calculated based on the amount of enzyme present in the cell, in this case either 5 nM or 10 nM.

Concluding Remarks and Future Perspectives.

We have demonstrated ITC is a successful screening technique for determining the best candidate cellulase based on the hydrolysis of insoluble substrates. The strength of this method is in its versatility and simplicity, while providing extra information based on the enzymatic rates being measured. This is seen in simple completely soluble systems, shown here by determining the kinetics of both β -glucosidase (Article 2) and D-glucono- δ -lactone hydrolases (Chapter 4). ITC may also be used in inhibition studies (Chapter 4, Article 4), as the amount of product has no effect on the thermal signal, and we show here the possibility to screen for enzymes which are less sensitive to industrial product build up, thus pinpointing the weak links in future enzyme cocktails. The method does not currently allow for high throughput; being limited to six to eight experiments a day, and individual CBH enzymes action on insoluble substrates must be amplified in order to attain a relatively high thermal signal, and thus a high signal to noise ratio. For monitoring longer hydrolyses (> 24 h) other methods are better for determining total product formed, however, the strength of this method is the extra data gained in addition to the total product formed, i.e. mechanistic information.

There is a critical incubation time dependence of all reported kinetic values in the literature. We demonstrate the drastic and rapid changes in rate over time throughout the thesis, and in Article 3 propose this is one of the factors dictating the wide range of kinetic constants reported for cellulases. It is clear incubation time must be reported in such analyses in order to standardize any kind of constants derived in future endeavors.

We show (Chapters 2, 3, Articles 3, 5) all cellulases regardless of type are subject to both intrinsic and extrinsic inactivation. Extrinsic factors can include substrate parameters such as DP_N , I_{cr} , the amount of residual lignin and hemicellulose, and topographical changes in the two dimensional surface of the cellulose structure. We see this in the difference in inactivation rate constants for lignocellulose compared to crystalline and amorphous cellulose (Chapters 2, 3). Other intrinsic factors include thermal inactivation, protein denaturation and product inhibition. By monitoring the enzymes at very low doses on different cellulose substrates we demonstrate the ability to determine rate constants of inactivation of a primarily intrinsic nature; which are defined here as enzyme related. With ITC data we present $V_{max}(cat)$ as a measure of the turnover number, ($\approx k_2$) and k_4 , the rate constant of inactivation. The measurement of $V_{max}(cat)$ is affected by the instruments time constant but this is the same for all variants tested and thus may be used comparatively in screening. k_4 , the rate constant of decay is not so affected, being a far slower process and thus ITC is very well suited to monitoring the inactivation of cellulases. Through investigating the CBHs action on the different substrate types under the conditions here, we report both cellobiohydrolases are

equally prone to intrinsic inactivation, and thus may perform the same number of catalytic events on average per enzyme.

Endoglucanases are also prone to inactivation, as demonstrated in Article 3. These enzymes are not strictly processive, and thus do not become nonproductively bound as fast as the cellobiohydrolases, becoming trapped after a number of catalytic events in excess of the length of the chain of cellulose. This indicates the intrinsic inactivation is not linked to processivity. While these investigations focus on the initial kinetics of this enzyme class, a more thorough investigation in the later stage kinetics (i.e. longer monitoring of runs) of endoglucanases would allow for a direct comparison of k_4 values between EGs and CBHs.

The interplay of the cellulase on the cellulose surface is a combination of the binding of the Core and the CBM coupled to the catalysis. The breaking of the β , 1-4 bond has been previously proposed to power the processive nature of CBHs, and we see an intrinsic inactivation dependent on the number of catalytic events. This may reflect the delicate balance of forward motion and the interaction binding the cellulase to the surface of the substrate. The ratio k_2/k_4 presented here as $V_{\max}(\text{cat})/k_4$ are a measure of how many catalytic events the enzyme may perform before inactivation.

Given k_2 is affected by temperature, i.e. Q_{10} is high, and k_4 appears relatively unchanged, there is a strong argument for the development of temperature stable enzymes. This, however, requires a more thorough temperature series investigation. We see in Chapter 3, for every 10 degrees rise in temperature, the measured maximal rate for the number of catalytic events is more than doubled, while the rate constant of inactivation is largely unaffected. This in effect means the enzyme will be able to perform more than double the amount of catalytic events before inactivation, all other factors equal.

CBM variants have provided insight into the interaction between cellulose and cellulase, the rate of inactivation being influenced by both the catalytic core and the CBM. We propose a model for the mechanistic interaction of the CBM wedge with the cellulose chain and demonstrate the importance of the "back" side of the wedge, seen by the radical changes when H4 is changed. The studying of other cellulase Cores at low concentrations could provide fundamental insights in to intrinsic inactivation based solely on the catalysis action, rather than Core coupled with CBM interactions.

The use of the model presented in (*contribution to*) Article 5 will further the understanding of CBH kinetics. While the ITC data may be used to determine k_4 , a different method is needed to determine the initial kinetic constants of this enzyme class. The on-rate k_1 , and off-rate k_3 , may be determined using biosensor data which has a faster time constant, and coupled to ITC data could provide a more complete picture of

the role of, e.g. the CBM variants. Initial work on this area is presented in Article 5 using ITC data from *TrCel7A* action on cellulose substrates, and the coupled enzyme amplification system.

This kind of screening and improved fundamental understanding could further protein engineering undertakings in the future, and possibly aid in elucidating structure-function relationships in the cellulase world. This may lead to improved hydrolytic enzymes, and ultimately a more competitive second generation bioethanol industry.

A handwritten signature in black ink, reading "Jeffery Murphy". The signature is written in a cursive, flowing style with a large initial 'J'.

Acknowledgements

Thank you to Peter Westh and Kim Borch for excellent supervision, inspiration and ideas along the way. This has been a very enthusiastic project and I am grateful for having the opportunity to be a part of it. Special thanks to Martin J. Baumann for patiently reading almost all of to my thesis as well as getting almost all the articles RuB never had access to ☺. Thanks to Nicolaj Cruys-Bagger for all the excellent biosensor work. Thanks to Søren Nymand for great discussions and collaboration, as well as the group who have made this a fantastic project to be a part of; Christina Bohlin, Nina Lei, and Jens Olsen.

Thank you Søren Hvidt, for being a great co-supervisor on the projects we have had together and for help with all the viscometry we have used in this and other areas. Thanks to Erik Lumby Rasmussen and Eva Karlsen, for help in the lab; especially Erik who has played a huge role in the experimental side of my work. Thanks to Poul Erik Hansen and Kjeld Schaumburg for help with the solid state NMR and to Annette Christensen who ran the samples.

Thanks to Kristian Bertel Rømer Mørkeberg Krogh and Christine Pahle Toft who have greatly helped me in the purification part of this thesis, and to Peter Rahbek Østergaard who gave us the gift of glucose-1-oxidase.

Thank you to KC McFarland and Matt Sweeney for providing substrates, enzymes, and help along the way.

On a more personal note, thank you to my parents-in-law Anne and Preben for such unwavering support. Thanks to my children Trine and Peter, for not getting *too* sick this year ☺. To my mother who has prayed every day this month and more.

Thank you Dorte. You have never stopped supporting me the last 3 (well, 5 including my M.Sc. ☺) years through study, sick children, and the many ups and downs.

This work was supported by the Danish Agency for Science, Technology and Innovation (grant # 2104-07-0028 to PW) and the Carlsberg Foundation.

Material in this presentation is based upon work supported by the Department of Energy under Award Number DE-FC36-08GO18080. *Disclaimer:* This report was prepared as an account of work sponsored by an agency of the United States Government. Neither the United States Government nor any agency thereof, nor any of their employees, makes any warranty, express or implied, or assumes any legal liability or responsibility for the accuracy, completeness, or usefulness of any information, apparatus, product, or process disclosed, or represents that its use would not infringe privately owned rights. Reference herein to any specific commercial product, process, or service by trade name, trademark, manufacturer, or otherwise does not necessarily constitute or imply its endorsement, recommendation, or favoring by the United States Government or any agency thereof. The views and opinions of the authors expressed herein do not necessarily state or reflect those of the United States Government or any agency thereof.

Article 1: A calorimetric assay for enzymatic saccharification of biomass.

Leigh Murphy, Kim Borch, K.C. McFarland, Christina Bohlina, Peter Westh.



A calorimetric assay for enzymatic saccharification of biomass

Leigh Murphy^{a,b}, Kim Borch^b, K.C. McFarland^c, Christina Bohlin^{a,b}, Peter Westh^{a,*}

^a Roskilde University, NSM, Biomaterials, 1 Universitetsvej, DK-4000, Roskilde, Denmark

^b Novozymes A/S, Krogshøjvej 36, DK-2880, Bagsværd, Denmark

^c Novozymes Inc., 1445 Drew Avenue, Davis, CA 95 618, USA

ARTICLE INFO

Article history:

Received 10 July 2009

Received in revised form

15 September 2009

Accepted 16 September 2009

Keywords:

Microcalorimetry

Assay development

Hydrolysis of glycosidic bonds

Enzymatic mechanism

Lignocellulose

Cellulase

ABSTRACT

A limited selection of assay and screening methodologies for cellulolytic enzymes has been stated as a restriction in biomass research. In this report we test the potential of isothermal calorimetry for this purpose. The primary observable in this technique (the heat flow in Watts), scales with the rate of hydrolysis, and unlike other approaches, it provides a continuous picture of the hydrolytic rate. It was found that the activity of a standard enzyme cocktail against purified cellulose substrates and dilute acid pretreated corn stover (PCS) was readily detected in calorimeters of different types, and that the calorimetric signal scaled with the enzyme activity measured by established analytical techniques. Hence, it was concluded that the heat flow provided a valid measure of the hydrolytic rate also in a complex biomass. The hydrolysis process was consistently found to be exothermic, but the amount of heat released per mole of soluble sugar produced varied for different types of substrates. This variation probably reflects heat contributions from processes which are coupled to the hydrolysis of the glycosidic bond (e.g. dissolution of crystalline substrate or physical transitions in the solid matrix). Calorimetric determinations of absolute reaction rates therefore require initial calibration against another method for each new substrate. However, the main potential of the method lies in real-time measurements of relative changes in hydrolysis rates. This approach may be used both for different starting conditions and the titration of enzyme, substrate, promoters or inhibitors to reacting samples in different stages of the hydrolysis. These experiments are technically straight forward, do not require separate calibrations against other techniques and appear to be useful for studies of the regulation and functional mechanism of cellulases.

© 2009 Elsevier Inc. All rights reserved.

1. Introduction

Cellulases are essential in natural carbon cycling, and they have attracted significant research interest over several decades [1]. Recently, this interest has been intensified as a result of the commercial and environmental potential of lignocellulosic residue from agriculture and forestry. This low-cost, renewable resource can be used as a feedstock for the production of ethanol and other bio-products, but the depolymerization (saccharification) of recalcitrant lignocellulose to fermentable sugars remains a bottleneck to its utilization [2]. One of the most promising solutions to this problem is the use of cellulolytic enzymes.

One of the challenges in cellulase and saccharification research is the limited availability of simple, quantitative assays [1,3]. Different assay strategies have been successful in separate areas. For example, the use of small soluble substrates or substrate analogues has been very productive in studies of basic catalytic mechanisms and certain regulatory aspects of pure enzymes (see, e.g. [4,5]). However, a recent review on assay techniques [1] concluded that there is no clear relationship between cellulase activity towards respectively, soluble and insoluble substrates, and this obviously puts strong limitations on the use of this data on soluble model substrates in biomass research. For insoluble substrates, the most common assay strategy is to quantify the product concentration in quenched subsets of a reaction mixture. This can be done for example by chromatographic sugar analysis of filtered samples or by analysis of the amount of reducing sugars. Other less common approaches include measurements of the loss of substrate or changes in physical properties (e.g. viscosity) of the sample. Many of the advances and drawbacks of these approaches have previously been discussed in detail, and it was suggested that improved assay technologies is a central element in biomass research [1,6].

In the current work we test the applicability of calorimetry to measure the rate of enzymatic saccharification of biomass.

Abbreviations: PCS, dilute acid pretreated corn stover; GS-PCS, ground sieved PCS; WGS-PCS, washed ground sieved PCS; PASC, phosphoric acid swollen cellulose; EGU, endoglucanase units; CBU, cellobiose units; FPU, filter paper units; DNS, dinitrosalicylic acid; BCA, bicinchoninic acid; Cell/N188, 15 FPU/g cellulose Celluclast® 1.5 L + 1/4 (v/v) Novozym® 188; ITC, isothermal titration calorimeter; TAM, thermal activity monitor.

* Corresponding author. Tel.: +45 4674 3011; fax: +45 4674 3011.

E-mail address: pwesth@ruc.dk (P. Westh).

Calorimetry has proven useful as a general tool in enzyme kinetics in a number of studies [7–9] and it may offer some special advantages for biomass research. It does not require special probes or modified substrates and more importantly it may be applied to multi-component, opaque, viscous and chemically complex samples [10]. The technique does not require any post experiment procedures and the primary observable (energy per time) scales with the rate of the reaction—not the concentration of substrate or products [8]. This means that calorimetry provides a detailed and continuous picture of the time-course, and this may be of value for cellulosytic enzyme reactions, which are known to exhibit a highly non-linear progression particularly in the initial phase [11–13]. Another potential asset of the method may be the option of titrating different liquids to a reacting system. This may allow an easy, and (in the time scale of a typical cellulase assay) essentially real-time view on the effects of e.g. promoters, inhibitors, enzyme synergy and substrate quality.

Among the expected limitations of calorimetry, the small enthalpy change accompanying the hydrolysis of the β -1–4 glycosidic bond may be the most important. Earlier calorimetric investigations of pure, soluble oligosaccharides have suggested an exothermic enthalpy change $\Delta H \approx -2.5$ kJ/mol for the hydrolysis of this bond type in either cello-oligosaccharides or *N,N*-diacetylchitobiose [14–16]. Although coupled reactions and intermolecular interactions could make the enthalpy change quite different for a complex, partly crystalline substrate like lignocellulose, this value suggests that the hydrolysis will produce a limited heat flow. The sensitivity of modern calorimeters, however, has been improved to well below the μ J/s level, and hydrolysis rates of 10–100 pmol of glycosidic bonds per second could therefore be measurable.

To investigate the balance between these possible advantages and limitations, and hence evaluate calorimetry in biomass saccharification research, we have monitored the enzymatic hydrolysis of a soluble substrate, two purified insoluble cellulose substrates, and biomass (pretreated corn stover) in a number of commercial microcalorimeters.

2. Methods and materials

2.1. Substrates

The soluble substrate was cellobiose, HPLC grade (Sigma, St. Louis, USA).

The (partially) crystalline cellulose substrate was commercial Avicel PH-101 (Fluka Biochemika, Ireland). Amorphous cellulose, phosphoric acid swollen cellulose (PASC) was prepared according to an established method from Avicel PH-101 [17].

The dry weight measurement of PASC determined the concentration to be 13.32 ± 0.13 g/L, PCS was determined to be 20.82 ± 0.18 g/L.

Dry senescent corn stover was pretreated by National Renewable Energy Laboratory (NREL) by addition of sulfuric acid to 1.2% (w/w), water and heat to 192 °C in a Sunds reactor for 3 min. The resulting slurry, 29% total solids, pretreated corn stover was mechanically ground and sieved to 60-mesh to produce (ground sieved) GS-PCS. PCS was washed by repeated suspension in MilliQ water (Millipore, Copenhagen, Denmark) and settling until the pH was higher than 4.0, then the washed slurry was mechanically ground and sieved to 60-mesh to produce washed ground sieved (WGS)-PCS. Composition of the PCS was determined by NREL Laboratory Analytical Procedures (LAP) [18,19] to be 41.5% cellulose equivalent, 23.5% xylan equivalent, and after washing to be 27.2% lignin, 57.5% cellulose equivalent and 7.0% xylan equivalent. It is important to note the cellulose content was necessary to determine the dose of enzyme per gram cellulose.

All substrates were homogenized using an Ultra Turrax T8 homogenizer (IKA Labortechnik, Uppsala, Sweden) for 10 min on ice. All standard experiments were conducted in a 50 mM sodium acetate 2 mM calcium chloride pH 5.00 buffer.

2.2. Enzymes

The enzymes used for hydrolysis reactions were Celluclast® 1.5L (A cellulase mixture from *T. reesei* with 700 endoglucanase units (EGU), $\rho = 1.2$ g/mL) and Novozym® 188 (A β -glucosidase from *A. niger* with 250 cellobiose units (CBU)). In cellulose hydrolysis, such a complex mixture of glycoside hydrolases is necessary to achieve saccharification. The cellulase activity of Celluclast® 1.5L was measured using the filter paper unit (FPU) assay [3,20,21]

to be 82.1 FPU/mL. Enzymes were supplied from Novozymes A/S, Bagsværd, Denmark.

2.3. HPLC

HPLC analysis was adapted from the NREL LAP [22]. Samples were centrifuged (13,500 rpm for 10 min) then filtered through a 0.45 μ m filter. The column was an Aminex HPX-87H (Bio-Rad, Copenhagen, Denmark) with a mobile phase of 5 mM H₂SO₄. Flow conditions were 60 °C, 0.6 mL/min and the detector was an Agilent 1100 series Refractive Index (Agilent Technologies, CA, USA) run at approximately 40 °C. Calibrations using saccharides (glucose, cellobiose, xylose and arabinose) were performed, and separately prepared external controls of 6 mg/mL were monitored during each batch at periodic intervals in addition to an internal fucose control. All saccharides supplied from Sigma (St. Louis, USA) purity >98%.

For the correlation with thermogram data, samples were taken from the ITC or TAM cells, heated to 99 °C for 5 min to stop the enzymatic hydrolysis and processed for HPLC. Varying degrees of hydrolysis were achieved either by stopping the reaction at different times or by dosing other FPU/g concentrations of enzyme.

2.4. Determination of reducing sugars

Total reducing sugars were determined using the dinitrosalicylic acid (DNS) assay adapted from Ghose [3] and Miller [21]. The DNS reagent was prepared according to Ghose [3] using analytical grade chemicals. Three mL of DNS reagent were added to 1 mL of sample and boiled for 5 min. The OD₅₄₀ was monitored on a Shimadzu PharmaSpec 1700 (Shimadzu Scientific instruments, MD, USA) and reducing sugars quantitated based on a glucose standard curve.

2.5. Degree of polymerization (DP)

The degree of polymerization assay was carried out as described in [23,24]. Glucosyl monomers were determined by the phenol-sulfuric acid method [23,24]. Total reducing ends were determined using the bicinchoninic acid (BCA, Sigma, St. Louis, USA) method [24]. All protein was removed from hydrolysis samples as described in [24]. The number average degree of polymerization calculated from the ratio of reducing ends to total monomers.

2.6. Viscosity

Viscosity measurements were carried out using a Bohlin Rheometer model VOR (Bohlin-Reologi, Lund, Sweden). A 1.434 g torsion element was used in a 15 mL chamber. A rate sweep of PASC at 50 °C was carried out, and 14.6 s⁻¹ was determined to be the optimal shear rate for monitoring the hydrolysis. Hydrolysis reactions using PASC and Celluclast® 1.5L with 1/4 (v/v) Novozym® 188 (at different FPU/g cellulose doses) were carried out in the torsion chamber at 50 °C and viscosity measurements recorded every 10 s for 30 min. All viscosity measurements were corrected using PASC with no added enzyme measured in the same way.

2.7. Calorimetry

Hydrolytic activity was monitored on several state-of-the-art calorimeters both a passive heat flow instrument (TAM 2277 from TA Instruments, New Castel, DE, USA) and power compensated equipments (Nano-ITC 2G from TA Instruments and VP-ITC and ITC₂₀₀ both from MicroCal Inc., Northampton, MA, USA).

2.7.1. Calibration and controls

For all experiments in aqueous solutions, the reference cells were filled with degassed MilliQ water. All calibrations were carried out at both 25 and 50 °C. The calorimeters were electrically calibrated according to the manufacturer's instructions. It was followed by a chemical calibration using propan-1-ol (Fisher Scientific, Slangerup, Denmark) as outlined by Briggner and Wadso [25]. Three aliquots of 10% propan-1-ol were injected into cells filled with water, it was repeated twice and the enthalpy of dilution calculated from the integral of the resulting six peaks. Control injections of water to water were carried out and the background heat of mixing corrected for. Comparing this value to the theoretical value yields a calibration factor for each instrument.

Enzymatic standardization was carried out as described by Jeoh et al. [14]. All solutions were degassed immediately before use. Ten aliquots of 10 μ L of 10 mM cellobiose in 50 mM sodium acetate with 2 mM calcium chloride, pH 5.00 were injected to a solution of 0.5 mg/mL *A. niger* β -glucosidase (the active component from Novozym® 188) in the same buffer. The reaction was allowed to go to completion (monitored by allowing the peak to return to a stable baseline) to achieve total hydrolysis of the known amount of cellobiose. The integral of the peak for each injection is the amount of heat produced by this hydrolysis. The average of 10 injections was then used to calculate the molar enthalpy of the hydrolysis of a β -1–4 bond. Control injections of cellobiose to buffer and buffer to enzyme were carried out and the heat of dilution corrected for (baselines as shown in inset of Fig. 1).

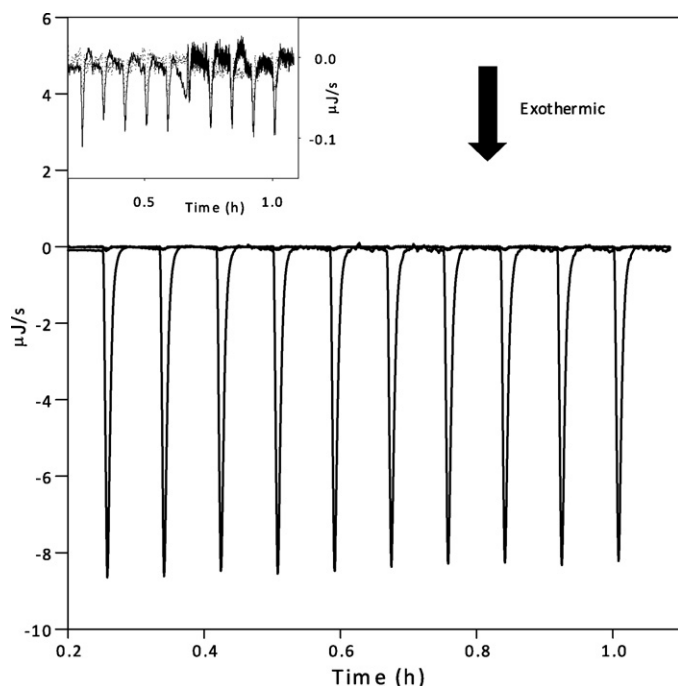


Fig. 1. Heat flow traces reflecting the hydrolysis of cellobiose (ten 10 μL aliquots of a 10 mM cellobiose solution at pH 5 and 50 $^{\circ}\text{C}$ injected to 0.5 mg/ml β -glucosidase). The inset shows the two control experiments where buffer is injected into enzyme solution and cellobiose solution is injected into buffer. Both controls generate negligible heats, but have been corrected for.

2.7.2. Standard hydrolysis experiment

A typical hydrolysis experiment was carried out as follows. All solutions were prepared in 50 mM sodium acetate with 2 mM calcium chloride, pH 5.00. Substrates were degassed and placed in the sample cell at the appropriate temperature. The enzymes were degassed and placed in the syringe. After the establishment of a stable baseline whilst the system equilibrated at the desired temperature, the enzymes were then injected to the substrate, typically at 15 FPU/g cellulose Celluclast[®] 1.5 L with 1/4 (v/v) Novozym[®] 188 (this mixture of 15 FPU/g Celluclast[®] 1.5 L with 1/4 (v/v) Novozym[®] 188 will be abbreviated to Cell/N188). The resulting thermogram was then recorded.

3. Results and discussion

3.1. Soluble substrate

Calorimetric measurements of cellulolytic enzyme activity relies on the enthalpy change, $\Delta_{\text{hydrolysis}}H_{\beta-1-4}$, associated with the hydrolysis of the β -1–4 glycosidic bond. However, it will also depend on coupled processes such as the hydrolysis-induced dissolution of crystalline cellulose, structural changes in other macromolecular matrices and possible mutarotation equilibria in the released saccharides. To single out some of these effects, we first studied the hydrolysis of the simplest substrate, cellobiose, in the different types of isothermal calorimeters mentioned above. Representative data for β -glucosidase activity is illustrated in Fig. 1 which shows the thermal response for the addition of ten 10 μL aliquots of 10 mM cellobiose into 0.5 mg/ml *A. niger* β -glucosidase in a VP-ITC. Here (as in the subsequent thermograms) the deflection from the baseline signal on the ordinate is proportional to the reaction rate while the accumulated area under the curve (seen as peaks in Fig. 1) specifies the total number of hydrolyzed glycosidic bonds at a given experimental time. Average $\Delta_{\text{hydrolysis}}H_{\beta-1-4}$ at 25 $^{\circ}\text{C}$ ranged from -2.36 ± 0.03 kJ/mol (VP-ITC) to -2.62 ± 0.21 kJ/mol (TAM 2277) in excellent agreement with previously published results for the hydrolysis of the β -1–4 glycosidic bond in cellobiose (-2.4 to -2.6 kJ/mol) [14,26] and chito-oligosaccharides (-2.3 to -2.4 kJ/mol) [16,27]. Karim et al. on the other hand, reported a

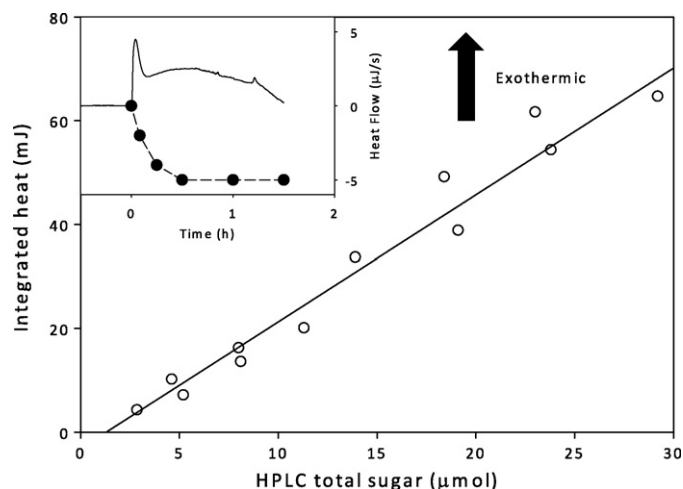


Fig. 2. The inset shows raw data from the hydrolysis of 1.3% PASC at 50 $^{\circ}\text{C}$, pH 5.00 in the Nanocal ITC 2G. The solid line (inset) represents the hydrolysis which is started by addition of the Cell/N188 cocktail at 30 min and stopped after 90 min hydrolysis. The solid dots connected by a dashed line is a baseline constructed on the basis of separate trials (see main text for details). The area between the two curves was determined for a number of hydrolysis experiments and plotted as a function of the concentration of soluble sugars (measured by HPLC) in the main panel.

much less exothermic hydrolysis (-0.6 to -0.8 kJ/mol) of cello-oligosaccharides, and suggested this to be caused by contributions from mutarotation in the product. At the weakly acidic pH used here, however, uncatalyzed mutarotation is most likely too slow to affect the calorimetric [28].

Measurements at 25 to 50 $^{\circ}\text{C}$ did not reveal any detectable temperature effect on $\Delta_{\text{hydrolysis}}H_{\beta-1-4}$ and this is also in accord with earlier observations [26]. The reproducibility of $\Delta_{\text{hydrolysis}}H_{\beta-1-4}$ during sequential injection of cellobiose was ± 1 –2% for the power compensated calorimeters and ± 8 –10% in the passive heat flow instrument.

3.2. Purified insoluble substrates

The inset of Fig. 2 shows an example of the heat flow generated when the Cell/N188 enzyme cocktail was added to a PASC suspension in the Nano-ITC instrument at pH 5 and 50 $^{\circ}\text{C}$. Complete hydrolysis under these conditions took about 6 h and calorimetric trials of that duration consistently had a final heat flow which was constant and about -5 $\mu\text{J/s}$ lower than the initial level (corresponding to the dashed line in the inset of Fig. 2). This endothermic shift in baseline was assigned to the frictional heat of stirring the gel-like samples, which decreases as the sample becomes depolymerized and hence less viscous. PASC was determined to have an initial DP of 235 which is quite close to that of 205 reported by [24]. This interpretation was based on parallel measurements outside the calorimeter (not shown), which demonstrated that both the fraction of insoluble substrate and the sample viscosity followed the same time-course as the (dashed) baseline in the inset of Fig. 2.

In order to establish the correct baseline and thus enable a meaningful integration of the PASC trials, we determined the heat of stirring by loading partially hydrolyzed samples into the calorimeter. To this end, samples were pre-hydrolyzed in a disposable test tube for a given period, heat inactivated (boiling for 5 min) and then loaded into the calorimeter (without any titration of enzymes). The thermogram was recorded until a stable baseline was reached and this $\mu\text{J/s}$ value was recorded as one data point on the baseline. By stopping the reaction at different times, data points were collected for varying times of the hydrolysis and plotted as shown is the inset of Fig. 2. These data points were then connected by straight lines (the dashed lines of the extrapolated baseline in Fig. 2). The heat

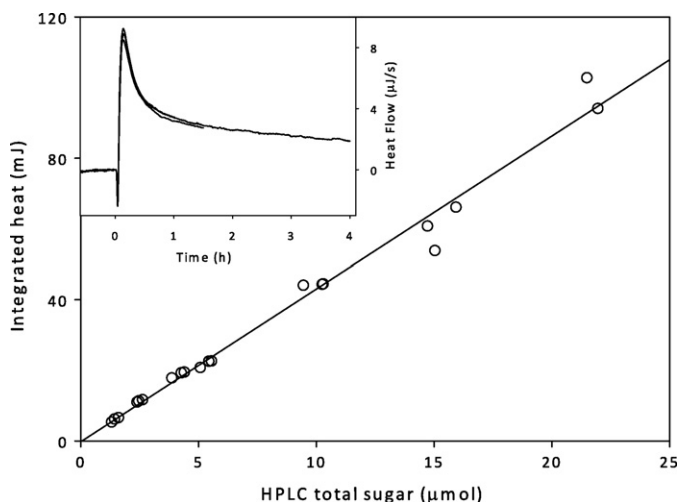


Fig. 3. Raw data (inset) and comparison of calorimetric and chromatographic results for the hydrolysis of Avicel by the Cell/N188 enzyme cocktail at 25 °C. The three trials in the inset were started time = 0, at stopped at $t = 60$ min, $t = 90$ min and $t = 4$ h respectively. The slope of the fitted line is 4.32 ± 0.13 kJ/mol. Unlike in the results in Fig. 2, no shift in baseline occurred for the Avicel measurements.

flow during stirring of such samples takes into account variations of the frictional heat for the partially hydrolyzed substrate and thus provides a realistic reproduction of the baseline underlying hydrolysis traces like the one in the inset of Fig. 2. The area between the hydrolysis trace (solid line in the inset of Fig. 2) and the reproduced baseline (dashed line in the inset of Fig. 2) was calculated for a number of runs and plotted as a function of the amount of soluble sugars in the sample as determined by HPLC. It appears that the integrated heat is proportional to the amount of soluble sugars and hence that the calorimetric heat flow provides a direct measure of the extent of the hydrolysis. The slope in Fig. 2 corresponds to an exothermic heat of hydrolysis of 2.52 kJ/mol and the average (exothermic) slope for five trials with enzyme loads of respectively 10, 15, 20, 25 and 30 FPU/g was 2.65 ± 0.29 kJ/mol in perfect accordance with $\Delta_{\text{hydrolysis}}H_{\beta-1-4}$ for soluble cellodextrins (discussed above). We conclude that the heat signal provides a useful measure of the hydrolytic rate for PASC and that processes other than the hydrolysis of the β -1–4 glycosidic bond contribute negligibly to the signal.

As another example of a pure insoluble substrate we studied the hydrolysis of 2% (w/w) Avicel suspensions. Like in the case of PASC, the approach for the basic benchmarking was to compare the integral heat with the sugar contents measured by HPLC in quenched samples. We mention in passing that less viscous substrates such as Avicel and PCS suspensions (discussed below) did not show detectable shifts in the baseline. For the Avicel work, we tested a passive heat flow calorimeter (TAM 2277) and used unstirred samples. The Cell/N188 enzyme cocktail was injected to 1.0 ml thermally equilibrated sample (25 °C) and mixed for 3 min (45 rpm, 8 mm propeller) during and immediately after the injection. The stirring was then turned off and the hydrolysis was allowed to proceed over different periods ranging from 15 min to 12 h. The (small) heat generated by the stirring as well as the heat of dilution for injecting respectively buffer into Avicel suspension and enzyme solution into buffer was determined in separate trials and subtracted from the total heat in the hydrolysis experiments. Some examples of raw data from these trials are shown in the inset of Fig. 3 and the area under the calorimetric traces are plotted as a function of the measured content of soluble sugars in the main panel. Like in the case of PASC, the proportionality of the integral heat and the concentration of soluble sugars confirms that the heat signal provides a valid measure of the hydrolytic activity. The

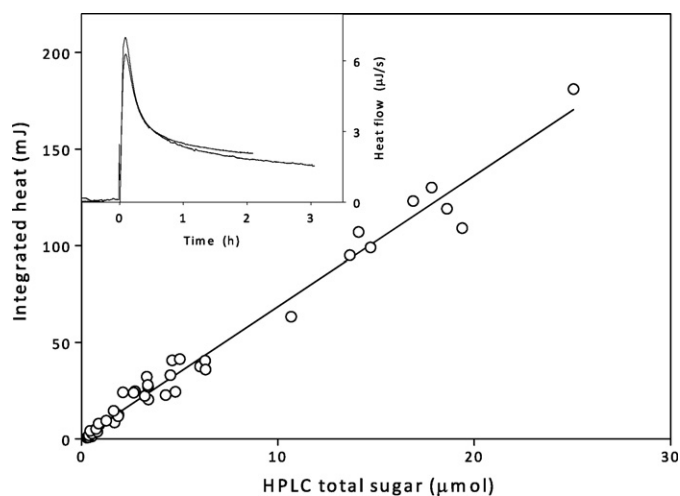


Fig. 4. The inset shows two typical thermograms for the hydrolysis of PCS (2%) with the Cell/N188 enzyme cocktail injected at $t = 0$ h. The experimental temperature was 25 °C. The main panel shows the accumulated heat (peak area) as a function of the concentration of soluble sugars.

(exothermic) slope in Fig. 4 was 4.32 ± 0.13 kJ/mol or about 65% more than $\Delta_{\text{hydrolysis}}H_{\beta-1-4}$. Deviations from $\Delta_{\text{hydrolysis}}H_{\beta-1-4}$ are to be expected for complex and partially crystalline substrates and will be discussed in the next section. The noise and reproducibility of the Avicel trials was estimated to be between 0.2 and 0.5 $\mu\text{J/s}$ (Fig. 3, inset) and this suggests a sensitivity of the TAM 2277 calorimeter corresponding to a hydrolytic activity of 50–100 pmol glycosidic bonds per second. For the power compensated instruments the sensitivity was generally 2–5 times better.

3.3. Biomass

We have used pretreated corn stover to test the potential of calorimetry to monitor enzymatic saccharification of complex biomass. Again, the fundamental requirement is proportionality between the extent of the hydrolysis and the integrated heat flow. Fig. 4 shows that this is the case in a series where 2% (w/w total solids) PCS was hydrolyzed with Cell/N188 enzyme cocktail in the TAM 2277 instrument. The procedure and conditions were the same as in the Avicel measurements described above.

The sugar content was also analyzed by DNS and the (molar) concentration ratio of reducing ends (DNS) and soluble sugars (HPLC) averaged for all samples was 1.13 ± 0.18 .

The slope of the fitted line in Fig. 4 is 6.7 ± 0.2 kJ/mol, which is more than twice the size of $\Delta_{\text{hydrolysis}}H_{\beta-1-4}$ value for cellobiose. This suggests, the hydrolysis of glycosidic bonds in PCS couples to other exothermic processes, possibly structural changes in the insoluble matrix or hydration of newly exposed polymer as cellodextrins dissolve. Moreover, the observed (exothermic) enthalpy change is expected include an endothermic contribution from the lattice energy of crystalline cellulose [29], which disintegrates during hydrolysis. We conclude that the proportionality between heat and sugar content implies that calorimetry is useful for studies of enzymatic saccharification of biomass, but that the coefficient, which relates reaction rate and heat flow is composed by several contributions other than $\Delta_{\text{hydrolysis}}H_{\beta-1-4}$, and hence must be measured for a given substrate system in a calibration trial akin to the one shown in Fig. 4.

The results in Figs. 2–4 confirm that the primary observable in calorimetry (the heat flow) scales with the rate of reaction and this fact also dictates the principal advantages and limitations of the approach. Regarding the latter, calorimetry may not be the method of choice for measurements of the cumulative degree of saccharifi-

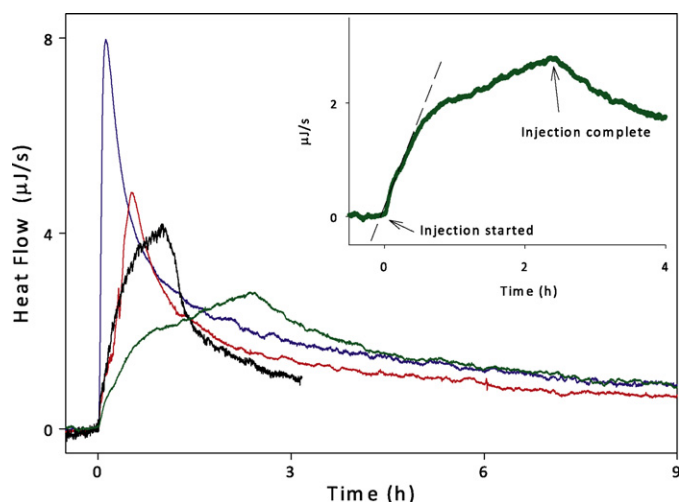


Fig. 5. Effect of enzyme delivery rate on the hydrolysis rate. In all cases, 1 ml of 2% PCS was titrated with the Cell/N188 cocktail to a final enzyme load of 15 FPU/g cellulose. The enzyme concentration was increased linearly over a period of respectively (left to right) 1.5, 30, 65 and 150 min. The inset shows an enlargement of the 150 min trial with the initial linear region defined by a dashed line.

cation following prolonged hydrolysis. This is due to integration problems in particular establishing a precise area at late stages where the hydrolysis heat signal is low. For this purpose, HPLC and other methods that accumulate the signal over the whole course of reaction are better suited. Conversely, we suggest that calorimetry has an ample potential to elucidate interrelationships between the hydrolysis rate and the concentration of e.g. enzyme, substrate, promoters or inhibitors. Such applications will generally focus on relative changes and therefore not require separate calibration trials. Neither will they require integration of the calorimetric traces. In fact, integration is only recommendable during initial benchmarking trials since this procedure abolishes the ability to resolve small changes over a background of glucose produced earlier in the hydrolysis. This ability is indeed a key advantage of the method and it may be exploited through the design of more sophisticated injection protocols involving for example slow, parallel or sequential additions of effectors at different stages of saccharification. In the following, we give a few examples of this approach and stress that the current scope is to illustrate methodical possibilities rather than to conduct systematic investigations.

First, we illustrate relationships between reaction rate and the enzyme load by delivering the enzyme cocktail at different rates. Fig. 5 shows an example of this type of measurements where the Cell/N188 enzyme cocktail was delivered at constant rate by a syringe pump over times ranging from 1.5 to 150 min. It appears that the initial burst in hydrolysis is stronger when the enzyme is delivered rapidly, and that no systematic dependence on the original delivery rate could be detected at later stages. It follows that in samples with slow delivery, the moderate initial burst is not compensated by a higher hydrolysis rate at a later stage. This is in accord with the suggestion that factors such as “crowding” or “jamming” of surface bound cellulases [11,30,31] rather than substrate heterogeneity [13] underlie the declining rates for PCS.

The inset in Fig. 5 shows an enlargement of the slow (150 min) injection trial. It appears that the reaction rate increases linearly with the protein concentration up to ~40 min at which point the enzyme load is ~4 FPU/g cellulose. This behavior is in accord with a simple picture of maximal turn-over rate for the added enzymes under conditions of excess substrate. At higher enzyme concentrations, the rate of hydrolysis increases less, but interestingly, the curve enters another (shallower) linear regime up to the point where the delivery of enzyme is complete and the hydrolysis rate

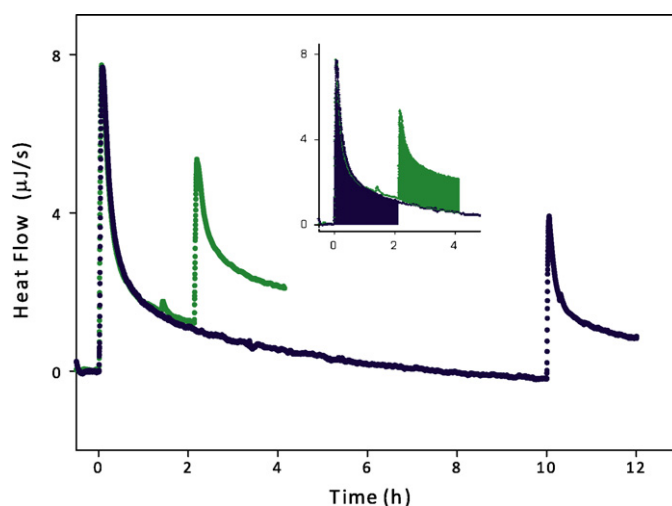


Fig. 6. Results from double-injection trials where one initial injection of Cell/N188 enzyme (15 FPU/g) is followed by a second injection respectively 2 h (green symbols in main panel—light grey in black-and-white representations) or 10 h (blue symbols—dark grey) subsequent to the first dosage. It appears that the second injection produces a burst in activity which is qualitatively similar, but smaller than the first. The extent of hydrolysis over 2 h following the first injection is specified by the blue (dark grey) area in the inset, while the additional activity (over 2 h) caused by the adding the second enzyme dose is defined by the green (light grey) area. (For interpretation of the references to color in this figure legend, the reader is referred to the web version of the article.)

instantly starts to decrease. Further measurements of “real-time dose–response curves” such as Fig. 5 may establish if there is a critical value of about 4 FPU/g for PCS hydrolysis and the approach appears to be generally promising for the elucidation of non-linear kinetics of cellulases.

In a related study, we investigated the effect of adding fresh enzyme to partially hydrolyzed samples of PCS. Fig. 6 show results where two doses of Cell/N188 enzyme cocktail (each 15 FPU/g) were added to 2% PCS with several hours separation. The extent of hydrolysis brought about by the first and second injection respectively, was defined as the blue and green areas in the inset (dark- and light grey in black-and-white). Analysis of several trials with 2–5 h separation between the two injections suggested that the degree of hydrolysis over 2 h attributed to the second injection was 75–85% of the hydrolysis over 2 h attributed to the first injection (i.e. the green (light grey) area is ~20% smaller than the blue (dark) area). When the separation was increased to 40 h, this value fell to 50%. One study where all enzyme was removed from the surface of the substrate and a fresh addition of enzyme was added show the burst phase is re-established 100% [13]. We conclude that addition of fresh enzyme reactivates a stalled PCS hydrolysis but that the effectiveness of the second enzyme dose tapers off with the degree of hydrolysis. This approach may provide an avenue to investigate the importance of substrate heterogeneity and enzyme dose at different stages of the saccharification process.

Calorimetry provides better time resolution than e.g. HPLC and DNS, and this may be useful in attempts to model cellulolytic processes. As a final example, we demonstrate that the course of PCS saccharification could be consistently described by a simple mathematical function. Fig. 7 shows a typical result for a 10 h hydrolysis trial in which data points (black symbols) prior to the maximum (c.f. Fig. 3) have been deleted. The red (dashed) curve is the best fit of a function, which is the sum of two exponential decays ($HF = ae^{-bt} + ce^{-dt}$, where HF is the heat flow and a, b, c and d are constants). The two blue curves are the separate exponential functions on the right-hand side of the fitting expression. We found that this sum of two exponentials accounted remarkably well

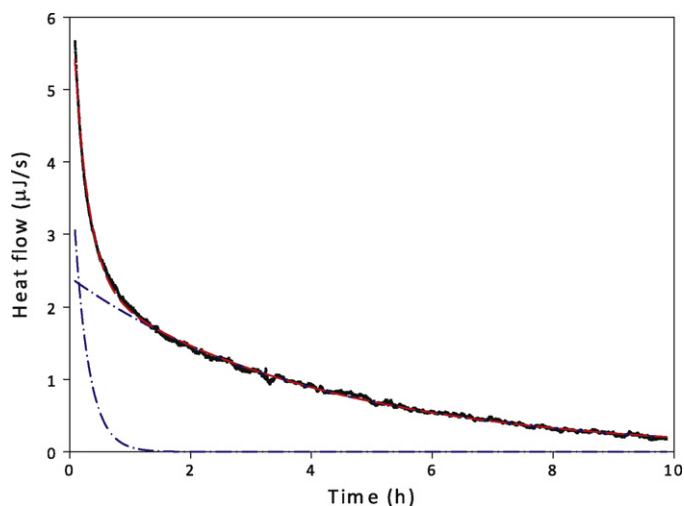


Fig. 7. Heat flow for the hydrolysis of 1 ml, 2% PCS at 25 °C, started by the injection of Cell/N188 at time = 0 h. The experimental data (black symbols, solid line in black-and-white) fitted a function with two exponential decays, $HF = ae^{-bt} + ce^{-dt}$. The fitted function (red, dashed) and each of the two exponential decay functions (blue, dash-dot) are also shown. Half times for the fast and slow component were respectively 10 min and 3 h. (For interpretation of the references to color in this figure legend, the reader is referred to the web version of the article.)

for all our data, including data obtained in different instruments and for different substrates and temperatures. Also, the fits consistently identified halftimes of about 10 min and 3–4 h respectively for the fast and slow decay at 25 °C. Currently, these observations are entirely empirical but the quality of the fits and consistency of the parameters may suggest that the two exponential contributions actually represents identifiable physical processes which show first order kinetics. A similar conclusion was reached previously in a study on the activity of purified CBH1 against bacterial microcrystalline cellulose [30] and further work to identify the underlying mechanisms appears warranted.

In conclusion we have established that calorimetry may be used to monitor the activity of cellulolytic enzymes on insoluble substrates including complex biomass. The apparent enthalpy of glucose production was found to vary from substrate to substrate. For cellobiose and the amorphous PASC, we found enthalpy changes close to the table value of $\Delta_{\text{hydrolysis}}H_{\beta-1-4}$. For Avicel and PCS, the (exothermic) heat per hydrolyzed glycosidic bond was higher, probably as a result of enthalpy changes associated with coupled covalent and physical transformations. Hence, if the absolute reaction rate is to be derived from calorimetric measurements the method has to be calibrated (against e.g. HPLC) for each substrate. The most promising applications, however, involves continuous detection of changes in the hydrolysis rate when the sample is titrated with relevant components such as enzymes, substrates, inhibitors or promoters. This approach generally does not rely on separate calibrations. Rather, the relative change in hydrolytic heat output may be analyzed directly, and we suggest that this type of information will be particularly useful in studies of mechanistic and regulatory aspects of the saccharification process.

Acknowledgements

This work was supported by the Danish Agency for Science, Technology and Innovation (grant # 2104-07-0028 to PW) and the Carlsberg Foundation. Drs. Søren Nymand Olsen and Søren Hvidt provided a number of insightful comments and suggestions to this work and we highly appreciate the excellent technical assistance of Erik L. Rasmussen.

References

- [1] Zhang YHP, Himmel ME, Mielenz JR. Outlook for cellulase improvement: screening and selection strategies. *Biotechnol Adv* 2006;24:452–81.
- [2] Wyman CE. What is (and is not) vital to advancing cellulosic ethanol. *Trends Biotechnol* 2007;25:153–7.
- [3] Ghose TK. Measurement of cellulase activities. *Pure Appl Chem* 1987;59:257–68.
- [4] Tomme P, Driver DP, Amandoron EA, Miller RC, Antony R, Warren J, et al. Comparison of a fungal (family-I) and bacterial (family-II) cellulose-binding domain. *J Biotechnol* 1995;177:4356–63.
- [5] Wolfgang DE, Wilson DB. Mechanistic studies of active site mutants of *Thermomonospora fusca* endocellulase E2. *Biochemistry* 1999;38:9746–51.
- [6] Kabel MA, van der Maarel M, Klip G, Voragen AGJ, Schols HA. Standard assays do not predict the efficiency of commercial cellulase preparations towards plant materials. *Biotechnol Bioeng* 2006;93:56–63.
- [7] Beezer AE, Steenson TI, Tyrrell HJV. Application of flow-microcalorimetry to analytical problems. 2. Urea-urease system. *Talanta* 1974;21:467–74.
- [8] Todd MJ, Gomez J. Enzyme kinetics determined using calorimetry: a general assay for enzyme activity? *Anal Biochem* 2001;296:179–87.
- [9] Williams BA, Toone EJ. Calorimetric evaluation of enzyme-kinetic parameters. *J Org Chem* 1993;58:3507–10.
- [10] Olsen SN. Applications of isothermal titration calorimetry to measure enzyme kinetics and activity in complex solutions. *Thermochim Acta* 2006;448:12–8.
- [11] Eriksson T, Karlsson J, Tjerneld F. A model explaining declining rate in hydrolysis of lignocellulose substrates with cellobiohydrolase I (Cel7A) and endoglucanase I (Cel7B) of *Trichoderma reesei*. *Appl Biochem Biotechnol* 2002;101:41–60.
- [12] Valjamae P, Pettersson G, Johansson G. Mechanism of substrate inhibition in cellulose synergistic degradation. *Eur J Biochem* 2001;268:4520–6.
- [13] Zhang S, Wolfgang DE, Wilson DB. Substrate heterogeneity causes the nonlinear kinetics of insoluble cellulose hydrolysis. *Biotechnol Bioeng* 1999;66:35–41.
- [14] Jeoh T, Baker JO, Ali MK, Himmel ME, Adney WS. Beta-D-glucosidase reaction kinetics from isothermal titration microcalorimetry. *Anal Biochem* 2005;347:244–53.
- [15] Karim N, Kidokoro S. Precise and continuous observation of cellulase-catalyzed hydrolysis of cello-oligosaccharides using isothermal titration calorimetry. *Thermochim Acta* 2004;412:91–6.
- [16] Lonhienne T, Baise E, Feller G, Bouriotis V, Gerday C. Enzyme activity determination on macromolecular substrates by isothermal titration calorimetry: application to mesophilic and psychrophilic chitinases. *Biochim Biophys Acta Protein Struct Mol Enzymol* 2001;1545:349–56.
- [17] Schulein M. Enzymatic properties of cellulases from *Hemicola insolens*. *J Biotechnol* 1997;57:71–81.
- [18] Selig MJ, Viamajala S, Decker SR, Tucker MP, Himmel ME, Vinzant TB. Deposition of lignin droplets produced during dilute acid pretreatment of maize stems retards enzymatic hydrolysis of cellulose. *Biotechnol Prog* 2007;23:1333–9.
- [19] Sluiter A, Sluiter J. Determination of starch in solid biomass samples by HPLC. 2005. http://www.nrel.gov/biomass/analytical_procedures.html.
- [20] Adney B, Baker J. Measurement of cellulase activities. 2008. http://www.nrel.gov/biomass/analytical_procedures.html.
- [21] Miller GL. Use of dinitrosalicylic acid reagent for determination of reducing sugar. *Anal Chem* 1959;31:426–8.
- [22] Sluiter A, Hames B, Ruiz R, Scarlata C, Sluiter J, Templeton D. Determination of sugars, byproducts, and degradation products in liquid fraction process samples. 2006. http://www.nrel.gov/biomass/analytical_procedures.html.
- [23] Dubois M, Gilles KA, Hamilton JK, Rebers PA, Smith F. Colorimetric method for determination of sugars and related substances. *Anal Chem* 1956;28:350–6.
- [24] Zhang YHP, Lynd LR. Determination of the number-average degree of polymerization of cellooligosaccharides and cellulose with application to enzymatic hydrolysis. *Biomacromolecules* 2005;6:1510–5.
- [25] Briggner LE, Wadso I. Test and calibration processes for microcalorimeters, with special reference to heat-conduction instruments used with aqueous systems. *J Biochem Bioph Methods* 1991;22:101–18.
- [26] Tewari YB, Goldberg RN. Thermodynamics of hydrolysis of disaccharides—cellobiose, gentiobiose, isomaltose, and maltose. *J Biol Chem* 1989;264:3966–71.
- [27] Krokeide IM, Eijsink VGH, Sorlie M. Enzyme assay for chitinase catalyzed hydrolysis of tetra-n-acetylchitotetraose by isothermal titration calorimetry. *Thermochim Acta* 2007;454:144–6.
- [28] Karim N, Okada H, Kidokoro S. Calorimetric evaluation of the activity and the mechanism of cellulases for the hydrolysis of cello-oligosaccharides accompanied by the mutarotation reaction of the hydrolyzed products. *Thermochim Acta* 2005;431:9–20.
- [29] Calvet E, Hermans PH. Heat of crystallization of cellulose. *J Polym Sci* 1951;6:33–8.
- [30] Valjamae P, Sild V, Pettersson G, Johansson G. The initial kinetics of hydrolysis by cellobiohydrolases i and ii is consistent with a cellulose surface-erosion model. *Eur J Biochem* 1998;253:469–75.
- [31] Xu F, Ding HS. A new kinetic model for heterogeneous (or spatially confined) enzymatic catalysis: contributions from the fractal and jamming (overcrowding) effects. *Appl Catal A* 2007;317:70–81.

Article 2: An enzymatic signal amplification system for calorimetric studies of cellobiohydrolases.

Leigh Murphy, Martin J. Baumann, Kim Borch, Matt Sweeney, Peter Westh.



An enzymatic signal amplification system for calorimetric studies of cellobiohydrolases

Leigh Murphy^{a,b}, Martin J. Baumann^{a,b}, Kim Borch^b, Matt Sweeney^c, Peter Westh^{a,*}

^a Department of Science, Systems, and Models (NSM), Biomaterials, Roskilde University, DK-4000 Roskilde, Denmark

^b Novozymes, DK-2880 Bagsværd, Denmark

^c Novozymes, Davis, CA 95618, USA

ARTICLE INFO

Article history:

Received 18 January 2010

Received in revised form 14 April 2010

Accepted 18 April 2010

Available online 8 May 2010

Keywords:

Isothermal titration calorimetry

Signal amplification

Cellobiohydrolase

Coupled enzyme reactions

ABSTRACT

The study of cellulolytic enzymes has traditionally been carried out using endpoint measurements by quantitation of reaction products using high-performance liquid chromatography (HPLC) or overall determination of produced reducing ends. To measure catalytic activity, model substrates such as solubilized cellulose derivatives, soluble chromogenic, and fluorogenic oligomeric substrates are often employed even though they do not reflect the natural insoluble substrate hydrolysis. Thermochemical methods using, for example, isothermal titration calorimetry (ITC) yield data where the primary observable is heat production. This can be converted to the rate of reaction and allows direct and continuous monitoring of the hydrolysis of complex substrates. To overcome the low molar enthalpy of the hydrolysis of the glycosidic bond, which is typically on the order of -2.5 kJ mol^{-1} , an enzymatic signal amplification method has been developed to measure even slow hydrolytically active enzymes such as cellobiohydrolases. This method is explained in detail for the amplification of the heat signal by more than 130 times by using glucose oxidase and catalase. The kinetics of this complex coupled reaction system is thoroughly investigated, and the potential use to generate kinetic models of enzymatic hydrolysis of unmodified cellulosic substrates is demonstrated.

© 2010 Elsevier Inc. All rights reserved.

The hydrolysis of cellulose is a complex process involving the synergistic action of three main classes of enzymes, collectively called cellulases (glycoside hydrolases, EC 3.2.1.–) [1]. These are *endo*-glucanases (EGs, ¹ EC 3.2.1.4, 1,4- β -D-glucan 4-glucanohydrolase), which rapidly decrease the degree of polymerization of cellulose, cleaving the chain internally at random; *exo*-glucanases (CBHs, EC 3.2.1.91, 1,4- β -D-glucan cellobiohydrolase), which target the reducing and nonreducing ends of the cellulose chains, producing predominantly cellobiose; and β -glucosidase (BG, EC 3.2.1.21, 1,4- β -D-glucoside glucohydrolase), which cleaves the cellobiose

product, known to inhibit both *endo*- and *exo*-cellulases, to individual glucose monomers [2].

In the current study, the focus is on the development of a fundamental method to monitor the hydrolysis action of the cellobiohydrolase enzyme, Cel6A. There have been many methods and substrates used to monitor the activity of this class of enzyme, from chromogenic substrates to modified soluble oligosaccharides [3–5]. Although these assays may be used to study individual enzymes in a comparative way, it is known that they do not reflect the hydrolysis of biomass or more complex cellulose substrates [6]. Typically, Avicel, filter paper, or amorphous cellulose substrates have been used to determine the activity of these enzymes through monitoring of the sugar produced over time using high-performance liquid chromatography (HPLC) or reducing sugars using, for example, dinitrosalicylic acid (DNS) [7–11].

With isothermal titration calorimetry (ITC), the rate of substrate use may be monitored continuously even if the substrate is complex or opaque [12], and the heat generated is converted directly to the hydrolysis rate [13,14]. However, one of the shortcomings of ITC in the study of low-hydrolytic-activity cellulolytic enzymes is the low molar enthalpy of the β 1–4 bond, typically in the order of -2.5 kJ mol^{-1} [12,15]. As a result, the heat flow at low hydrolysis rates is too slow to be quantified precisely, and to overcome this

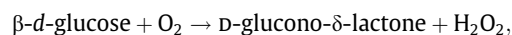
* Corresponding author. Fax: +45 4674 3011.

E-mail address: pwesth@ruc.dk (P. Westh).

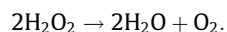
¹ Abbreviations used: EG, *endo*-glucanase; CBH, *exo*-glucanase; BG, β -glucosidase; HPLC, high-performance liquid chromatography; DNS, dinitrosalicylic acid; ITC, isothermal titration calorimetry; GOD, glucose oxidase; FAD, flavin adenine dinucleotide; SDS-PAGE, sodium dodecyl sulfate-polyacrylamide gel electrophoresis; FPLC, fast protein liquid chromatography; RAC, regenerated amorphous cellulose; BC, bacterial cellulose; DP, degree of polymerization; I_{cr} , crystallinity index; CP/MAS, cross-polarization/magic angle spinning; NMR, nuclear magnetic resonance; HPAEC-PAD, high-performance anion exchange chromatography with pulsed amperometric detection; ABTS, 2,2'-azino-bis(3-ethylbenzthiazoline-6-sulfonic acid); BCA, bicinchoninic acid; CAT, catalase; G1, glucose; G2, cellobiose; G1OX, D-glucono- δ -lactone/gluconic acid; DO, dissolved oxygen.

issue an enzymatic ITC signal amplification method has been developed. The basic principles are analogous to those applied in first-generation biosensor technology [4].

Glucose oxidase (GOD, EC 1.1.3.4, β -D-glucose/oxygen 1-oxidoreductase) catalyzes the oxidation of β -D-glucose as follows:



which is followed by the spontaneous hydrolysis of D-glucono- δ -lactone to D-gluconic acid in aqueous solutions [16]. This reaction is strongly exothermic, and literature values of the enthalpy change range from 80 to 125 kJ mol⁻¹ [1,17]. Hydrogen peroxide is inhibitory to GOD [18–20] but may be rapidly removed by catalase (EC 1.11.1.6) via the following reaction:



This reaction is also highly exothermic, with reported ΔH values of 83.7 to 100.4 kJ mol⁻¹ [1,4]. Both reactions, when coupled, have been reported to generate from 180 to 223 kJ mol⁻¹ [1,4]. The reader should note that the ΔH is a fixed value, and reported variations are due to variable precision in methods or instruments.

Using a β -glucosidase to convert Cel6A-produced cellobiose to glucose, followed by GOD and catalase action as outlined here, the heat generated from a single hydrolytic event is amplified from –2.5 to –360 kJ mol⁻¹, a factor of more than 130. This in effect allows *direct* monitoring of very low hydrolytic rate cellulolytic enzymes with a high time resolution and sensitivity. Given that there are three enzymes used to amplify the hydrolysis signal of Cel6A, the system was thoroughly investigated to ensure that the rate-limiting enzyme is Cel6A and that the signal measured was not governed by the kinetics of the other enzymes in the system. One major criterion for coupled reactions is that the V_{\max} of a subsequent enzyme reaction must be 10 times the rate of the preceding enzyme for first-order kinetics to hold [21]; this and the different inhibition effects were investigated.

D-Glucono- δ -lactone is a potent inhibitor of BG [22], mimicking the high energy transition state of its substrate, cellobiose [3], and D-gluconic acid has also been reported to weakly inhibit GOD [16]. Possible implications of these inhibitory effects are investigated at the concentrations relevant to the amplification assay.

It should be noted from the stoichiometry of the reactions that one molecule of oxygen is consumed for every two rounds of oxidation. This has proved to be an extra challenge in calorimetry where the typical setup involves the removal of all gas in the liquids involved so as to remove interference from air bubbles. The use of ultrasound to remove bubbles and the potential for using headspace to overcome this issue are investigated.

Finally, a method to directly monitor the action of cellobiohydrolases on unmodified cellulose substrates is reported. Kinetic data determined by ITC for Cel6A are reported, and the possibility of this method being used for future fundamental studies of such enzymes is demonstrated.

Materials and methods

Unless otherwise stated, all chemicals were supplied by Sigma-Aldrich (St. Louis, MO, USA).

Enzymes

GOD from *Aspergillus niger*

The GOD was heterologously expressed in *Aspergillus oryzae*. The fermentation broth was centrifuged and the supernatant was filtered through a 0.2- μ m filter unit to remove traces of the production organism. The pH in the filtrate was adjusted to 5.0 with 3 M Tris base, and the enzyme solution was diluted with Milli-Q

water to reduce the conductivity to 1.1 ms/cm. The filtrate was applied to an anion exchanger Q Sepharose Fast Flow (GE Healthcare Life Sciences, Buckinghamshire, UK). The protein was eluted using a linear gradient over 5 column volumes to 20 mM sodium acetate (pH 5.0) with 0.25 M NaCl. Fractions were collected based initially on the presence of the yellow color characteristic of the cofactor flavin adenine dinucleotide (FAD) bound to GOD. Yellow fractions that showed only one band on a Coomassie blue-stained sodium dodecyl sulfate–polyacrylamide gel electrophoresis (SDS–PAGE) gel were pooled as the purified product. The purified product was tested for absence of catalase activity.

The activity was determined to be 260 GODU/mg, where GODU is the amount of enzyme that forms 1 μ mol of H₂O₂ per minute at pH 5.0 with a substrate of 90 mM glucose at 30 °C, and was incubated for 20 min.

Catalase Terminox Ultra 50 L

Commercial product was supplied by Novozymes (Bagsværd, Denmark). The activity was declared to be 50 KCIU/g, where CIU is the amount of enzyme that degrades 1 μ mol of H₂O₂ per minute at pH 7.0 with the substrate of 10.3 mM H₂O₂ decreasing to 9.2 mM at 25 °C, monitored by absorbance change at 240 nm.

BG from *A. niger*

The BG was heterologously expressed in *A. oryzae*. The fermentation broth was buffer exchanged to 25 mM Hepes (pH 7.0) using ultrafiltration over a 10-kDa PES filter (3051463901E-SG Sartocoon Slice, Sartorius Stedim Biotech, Goettingen, Germany). The retentate was applied to an anion exchanger Q Sepharose Fast Flow using an ÄKTA Prime fast protein liquid chromatography (FPLC) system. The BG was eluted using a linear gradient over 5 column volumes to 25 mM Hepes (pH 7.0) with 1 M NaCl. Fractions were pooled based on SDS–PAGE. The pooled fractions were dialyzed to a 50-mM acetate buffer (pH 4.0) using a dialysis tube (50 kDa MWCO, SpectraPor, Spectrum Europe, Breda, Netherlands) overnight at 4 °C. The dialyzed pool was applied to a hydrophobic charge induction chromatography matrix; Xpressline–ProA (Upfront Chromatography, Copenhagen, Denmark). The protein was batch-eluted with 100 mM Tris (pH 8.0). Fractions were pooled based on SDS–PAGE. To remove excess color, 1% (w/v) activated carbon (FGV-120, PICA, Saint-Maurice Cedex, France) was added to the pooled fractions and gently agitated for 15 min. This was followed by centrifugation to remove the activated carbon.

The activity was determined to be 35.1 \pm 0.8 BGU/mg, where BGU is the amount of enzyme that releases 1 μ mol of *para*-nitrophenol per minute at pH 6.0 with a substrate of 1 mM 2-nitrophenyl β -D-glucopyranoside at 37 °C, and was incubated for 15 min.

Cel6A from *Hypocrea jecorina*

The *Hypocrea jecorina cel6A* cellobiohydrolase II gene (GenBank P07987) was isolated from *Hypocrea jecorina* RutC30 as described in WO 2005/056772 (<http://www.wipo.int/pctdb/en/wo.jsp?wo=2005056772>). The *cel6A* gene was expressed in *Fusarium venenatum* using pEJG61 as an expression vector and was fermented as described in U.S. patent application 20060156437 (http://www.hichem.com/tech_patent/download1.php?autoid=123). Culture supernatant was desalted by and concentrated in an ultrafiltration cell (Amicon) into 20 mM Tris–HCl (pH 8.0). Desalted culture supernatant was then applied to a Mono Q column (GE Healthcare Life Sciences). The column was washed with 20 mM Tris–HCl (pH 8.0) and eluted using a linear gradient over 5 column volumes to 20 mM Tris–HCl with 0.6 M NaCl. Cel6A-containing fractions were pooled (by SDS–PAGE) and then were concentrated and desalted into 20 mM Tris (pH 8.0) by centrifugal ultrafiltration. The concentration of Cel6A was determined by OD₂₈₀ using the

theoretical molar extinction coefficient of $97,290 \text{ M}^{-1} \text{ cm}^{-1}$ derived from the amino acid sequence.

All enzymes, prior to use, were buffer-exchanged using PD-10 columns (GE Healthcare Life Sciences) to a 50-mM sodium acetate buffer containing 2 mM calcium chloride (pH 5.0). This was to minimize the heat of dilution effects on ITC measurements.

Substrates

Soluble substrates

Glucose and cellobiose (HPLC grade, minimum > 98% purity) were supplied by Sigma (St. Louis, MO, USA). Hydrogen peroxide (30%) was supplied by Merck (Darmstadt, Germany).

Insoluble substrate

Regenerated amorphous cellulose (RAC) was prepared from Sigma-cell 20 by the method described by Zhang and Lynd [23] with the following changes. RAC was resuspended in 50 mM sodium acetate buffer with 2 mM calcium chloride (pH 5.0), centrifuged, and resuspended in the same buffer again. The pH was adjusted to 5.0 using HCl or NaOH. To prolong shelf life, the RAC suspension was heated to 80 °C for 20 min, followed by three consecutive centrifugation/resuspension washes with a buffer which had been filtered through a 0.22 μm filter. Sodium azide was not added because this inhibits catalase [24].

Bacterial cellulose (BC) was prepared from commercially available Nato de Coco (Pinoy Mini Mall, Snaith, UK). The cubes were washed in Milli-Q water at room temperature for 2 to 4 h with three water changes. This was followed by three washes in 0.25 M NaOH for 2 to 4 h, followed by one wash overnight. The cubes were washed over a period of a week with frequent water changes and finally were blended to homogeneity. Sucrose contamination was checked for using HPLC, and the suspension was finally washed three times with buffer and treated as outlined for RAC. The BC was homogenized using an Ultra Turrax T8 homogenizer (IKA Labortechnik, Uppsala, Sweden) for 10 min on ice.

Insoluble cellulose substrate characterization

Total glucose and degree of polymerization

The total glucose content of RAC and BC and the number average degree of polymerization (DP_N) were determined as described previously [12,23,25].

Crystallinity index

The crystallinity index (I_{cr}) of RAC and BC was determined using solid-state ^{13}C cross-polarization/magic angle spinning (CP/MAS) nuclear magnetic resonance (NMR). Samples were freeze-dried for analysis. The solid-state NMR settings were adopted from Matulova et al. [26]. Spectra were measured on a 300-MHz Varian Unity Inova spectrometer (Varian, Oxford, UK) operating at 75.42 MHz. The scans were performed at 8 kHz at room temperature using a variable-amplitude CP sequence and a standard pulse program with a 2.3- μs proton 90° pulse, a 1-ms contact time, and a 5-s relaxation delay. Chemical shifts were referenced to the external standard hexamethylbenzene (δ 17.6 ppm).

The crystallinity was determined using the method described by VanderHart and Atalla [27].

HPAEC–PAD

Cellobiose was analyzed for glucose contamination on a Dionex HPLC system (Dionex, Sunnyvale, CA, USA) with a GP40 four-channel gradient pump and an ED40 electrochemical detector with a gold working electrode (standard carbohydrate settings). The sugars were separated on a CarboPac PA10 column (4 mm \times 25 cm,

Dionex) with the following gradient program at a flow rate of 1 ml/min: 0 to 10 min of isocratic 20 mM sodium hydroxide, 10 to 11 min of 500 mM sodium acetate in 150 mM sodium hydroxide, and 11 to 15 min of reequilibration with 20 mM sodium hydroxide. Cellobiose was prepared at 200 mM (due to solubility), and 5 GODU/ml was added to oxidize trace glucose at 35 °C for 1 h. The enzyme was then inactivated by heating to 99 °C for 10 min. High-performance anion exchange chromatography with pulsed amperometric detection (HPAEC–PAD) analysis was carried out before and after this procedure to confirm the removal of trace glucose in cellobiose concentrations of 10 mM, 1 mM, and 100 μM . The detection limit was 0.5 to 1 μM .

ITC

ITC was carried out using power-compensated equipment (VP–ITC from MicroCal, Northampton, MA, USA). The VP–ITC has a Hastelloy cell of volume 1.428 ml. Standard conditions were as follows: 250 μl syringe, 310 rpm stirring rate, and collection of data with a point every 1 s.

Calibration and controls

Because all experiments were performed in aqueous solutions, the reference cells were filled with degassed Milli-Q water. All calibrations were carried out at 25 °C. The calorimeters were initially calibrated by the built-in electrical heater according to the manufacturer's instructions. This was followed by a chemical calibration using propan-1-ol (Fisher Scientific, Slangerup, Denmark) as outlined by Briggner and Wadso [28] and as described previously [12]. All data have been corrected for using the chemical calibration factor.

Molar enthalpies

Contrary to standard practice, the solutions were not vacuum-degassed prior to use, as explained in the introductory paragraphs. Ultrasonics (Ultrasonic Cleaner 8890E-MT, Cole Parmer, Vernon Hills, IL, USA) were used to remove excess bubbles in solution, and a DO meter (HQ20 Portable DO/pH Meter, Hach, Loveland, CO, USA) was used to determine the effect on the amount of available oxygen in solution.

Five aliquots of 10 mM cellobiose, glucose, or hydrogen peroxide in 50 mM sodium acetate with 2 mM calcium chloride (pH 5.0) were injected into a solution of 25 BGU/ml BG, 25 GODU/ml GOD, or 25 CIU/ml catalase in the same buffer at 25 °C. The reaction was allowed to go to completion (monitored by allowing the peak to return to a stable baseline) to achieve total conversion of the known amount of substrate. The integral of the peak for each injection is the amount of heat produced by the enzymatic reaction. The average of five injections was used to calculate the molar enthalpy of the reaction. Control injections of substrate to buffer and buffer to enzyme were carried out, and the heat of dilution was corrected for.

In addition to these standard molar enthalpies, the total combined reaction enthalpy was measured by titrating cellobiose to the standard amplification mixture of enzymes: 25 BGU/ml BG, 25 GODU/ml GOD, and 25 CIU/ml catalase.

ITC kinetic assays

Stepwise addition experiments

To determine the kinetic parameters of BG, the method described by Jeoh et al. [15] was adopted. Enzyme and substrate were prepared in 50 mM sodium acetate with 2 mM calcium chloride buffer (pH 5.0). All assays were performed at 25 °C.

BG kinetics

Cellobiose (50 mM) was titrated in 20 aliquots to 0.25 $\mu\text{g}/\text{ml}$ enzyme with 180 s between injections (see Fig. 1). This setup was used to determine K_M and V_{max} . The experiment was repeated with BG in the presence of 0.05, 0.1, 0.15, and 0.2 mM D-glucono- δ -lactone to test for inhibition. All D-glucono- δ -lactone solutions were prepared freshly for each experiment to minimize the amount of D-gluconic acid present. Although the hydrolysis is spontaneous; this is a slow process at pH 5.0 and 25 $^{\circ}\text{C}$ [5].

GOD kinetic assays

Kinetic parameters for GOD with glucose and cellobiose as substrates were determined using a 2,2'-azinobis(3-ethylbenzthiazoline-6-sulfonic acid) (ABTS) assay adapted from Zhu et al. [29]. The substrates were glucose (0–300 mM) and glucose-free cellobiose (0–200 mM). All enzymes and substrates were prepared in 50 mM sodium acetate buffer with 2 mM calcium chloride (pH 5.0). The reaction was started by adding GOD (2 or 0.2 $\mu\text{g}/\text{ml}$) to the wells, and the change of absorbance was measured at 405 nm and 25 $^{\circ}\text{C}$ for 5 min. Inhibition was tested by repeating the glucose experiment in the presence of 5 mM D-glucono- δ -lactone.

No kinetic assays were deemed necessary on the catalase, Terminus 50 L, because this enzyme is not rate limiting under the assay conditions due to the very high turnover number [30].

Determination of Cel6A kinetics

ITC kinetic assays were performed at 25 $^{\circ}\text{C}$ using the standard amplification mixture with the addition of Cel6A in the cell. The RAC was titrated to the cell (typically in 5- μl aliquots), allowed to achieve a steady state of hydrolysis (with a flat line indicating a constant rate of cellobiose production), and monitored for a total of 20 min per injection.

Settling of RAC in the syringe was tested by allowing the experiments to be started after different incubation times of RAC in the

syringe. Settling does occur slowly over a period of hours. This was effectively eliminated by thorough mixing, minimizing the time from loading to injection, and changing the syringe contents between experiments.

The Cel6A was present in the cell at 2 to 5 μM . Alternatively, the Cel6A was titrated to a cell containing either RAC or BC. Aliquots (12 μl) of 2 μM Cel6A were titrated to 2.4 g/L RAC or 0.7 g/L BC. The final concentration of Cel6A in the calorimeter was in the range of 20 nM in these trials.

The control experiments used exactly the same setup with no Cel6A present and were used as baselines for correction.

Product effects

To determine the effects of the products on the substrate and Cel6A, the following trials were conducted.

Hydrogen peroxide effects on the substrate

The steady-state concentration of hydrogen peroxide was estimated, and 100 nM was used in the trials. The RAC or cellobiose at assay-relevant concentrations was incubated in the presence of 100 nM hydrogen peroxide at 25 $^{\circ}\text{C}$ for 1 h. The oxidation effect of this amount of peroxide was tested by determining the amount of reducing ends in the presence or absence of H_2O_2 . This was done using the bicinchoninic acid (BCA) method [12,23].

Product effects on Cel6A

The effects of 100 nM hydrogen peroxide, 0.05 and 0.15 mM D-glucono- δ -lactone, and 0.05 and 0.15 mM D-gluconic acid were tested on the action of Cel6A. D-Glucono- δ -lactone was made freshly just prior to use at pH 5.0. D-Gluconic acid was prepared by dissolving the lactone in 100 mM phosphate buffer (pH 12.0) and allowing an equilibration time of 1 h. Both the lactone and acid were prepared at 100 \times , and further dilution removed any pH effects. Cel6A (2 μM) was incubated in the presence of 2 g/L RAC in 50 mM sodium acetate buffer containing 2 mM calcium chloride (pH 5.0) with and without the concentrations of the above prod-

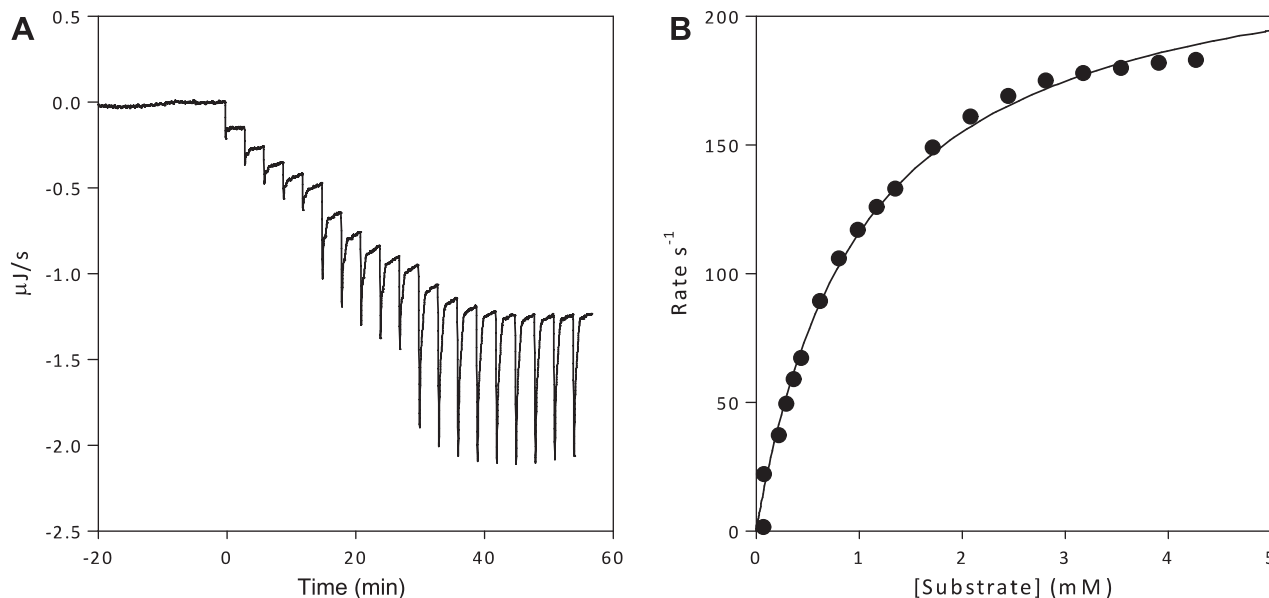


Fig. 1. (A) Example of a single ITC kinetic assay experiment for BG and cellobiose. Cellobiose (50 mM) is titrated directly to 0.25 $\mu\text{g}/\text{ml}$ BG at pH 5.0 and 25 $^{\circ}\text{C}$ (1×0.2 -, 5×2 -, 5×5 -, and 9×10 - μl injections). The final 10- μl injection is not included in the fit. (B) Using Eq. (1), the rate of heat production is converted to the glucose production rate. The curve shows the best fit to the Michaelis–Menten equation ($R^2 = 0.99$).

ucts at 25 °C for 1 h. The reactions were stopped by adding 100 μ l of 10 M NaOH to the 1-ml samples. The cellobiose concentration was then determined using HPAEC–PAD.

All curve fitting and analysis was performed using the Enzyme Kinetics add-on module (version 1.3) for SigmaPlot (version 11.0) and OriginPro (version 8.0).

Results and discussion

Kinetics of the amplification system

Given that there are four enzymes at work in the cell to produce one signal, the kinetic interplay of the system was thoroughly investigated. For the amplification signal to be a true reflection of Cel6A action, there are two conditions that must be met. First, the cellobiose must be hydrolyzed preferentially by the BG. In particular, this hydrolysis should be much faster than the oxidation of cellobiose by GOD. Second, each subsequent enzyme's maximum rate in the chain must be greater than 10 times the rate of the preceding enzyme for first-order kinetics to hold and, thus, must be solely dependent on substrate concentration [21].

Determination of BG kinetic parameters

Fig. 1A shows a typical ITC kinetic experiment. The first injection of substrate causes a deflection from the baseline. This is a direct result of the exothermic reaction taking place as the ITC adjusts to equalize the temperature between the reactant cell and the reference cell. Each subsequent injection of substrate causes a further increase in the deflection from the baseline, registered as a power change and expressed as dQ/dt . Each dQ/dt may be converted to a rate of product formation, $d[P]/dt$, for that specific substrate concentration using

$$\frac{d[P_i]}{dt} = \frac{1}{V \cdot \Delta_{app}H} \cdot \frac{dQ_i}{dt}, \quad (1)$$

where V is the reaction volume (cell) and $\Delta_{app}H$ is the measured molar enthalpy. This type of experiment using soluble substrates has been described in detail; for a complete derivation and explanation of stepwise addition ITC experiments, the reader is directed to Todd and Gomez [14] and Olsen [13].

Taking the average of the i th injection dQ_i/dt for the last 30 s prior to the $i + 1$ injection, a pseudo-steady-state rate of product formation may accurately be determined. Determining the slope of this averaged deflection (1 data point every second) was used to determine whether the hydrolysis was at a constant rate. Determination of the averaged deflection from the baseline for each injection was done automatically by a customized Python script (www.python.org). Using these data, a plot of reaction rate versus substrate concentration may be prepared (see Fig. 1B). The data were prepared from nonlinear regression of the Michaelis–Menten standard kinetic equation.

Determination of GOD kinetic parameters

The use of the ABTS assay to determine the kinetic parameters of GOD has been described before [29]. In brief, the system was calibrated using hydrogen peroxide, which was used to quantitate the product formation rate at 405 nm. A plot of substrate concentration, either glucose or cellobiose, may be plotted against the product formation rate and a nonlinear regression of the Michaelis–Menten standard kinetic equation may be performed (Table 1).

Table 1
Kinetic parameters of BG and GOD (pH 5.0, 25 °C).

Enzyme	Substrate	k_{cat} (s^{-1})	K_M (mM)	k_{cat}/K_M ($s^{-1} mM^{-1}$)
GOD ^a	Glucose	633	18.5	34.2
GOD ^a	Cellobiose ^b	27	187.4	0.14
BG ^c	Cellobiose	234	0.8	292.5

^a Derived from ABTS assay.

^b Cellobiose was determined to contain $0.66 \pm 0.03\%$ glucose, and this was consequently decreased to below the detection limit by the GOD treatment ($<0.01\%$).

^c Derived from ITC assay.

The enzymatic amplification system

In the presence of both substrates, GOD is *specific* for glucose. However, in the ITC assay setup (see Fig. 2), cellobiose is produced first and in small amounts. Both BG and GOD compete for the substrate, and with two enzymes competing, the main considerations are concentration and affinity and then turnover rates. The molar ratio of the enzymes in the assay is 2 BG/GOD, and given that the specificity of BG for cellobiose is far higher, interference from this potential side reaction may be ignored under these experimental conditions.

However, as the reaction proceeds, D-glucono- δ -lactone/D-gluconic acid begins to accumulate and subsequently inhibit predominantly the BG. To describe the system, the following nomenclature has been adopted: X_{ENZ}^{RCT} , where X denotes the kinetic parameter of interest, RCT denotes the reactant (substrate, inhibitor), and ENZ denotes the enzyme involved. Given that Cel6A has reported values of turnover number on the order of $1 s^{-1}$ [9,31,32], it can be stated with confidence for BG, GOD, and catalase that $[E] \gg [S_0]$. The following kinetic models are used to describe the system (Tables 2 and 3).

The following assumptions are made. Substrate inhibition of BG is insignificant at the low levels of cellobiose in the assay. Substrate inhibition of GOD has been reported under oxygen-limiting conditions of less than 0.02 mM. This is not reached under the current assay setup [33] because there is 0.25 mM oxygen present in the aqueous phase, allowing the production of 0.5 mM product. Hydrogen peroxide is also assumed to be present in negligible amounts due to the rapid action of catalase. It should be noted that the model presented here for GOD is very simplified but sufficient to investigate this system. For a detailed description of GOD kinetics with two substrates playing a role, the reader is directed to a recent study by Tao et al. [2]. The last step in the amplification system involving catalase is assumed not to be rate limiting ($v_{max-CAT} \gg 10v_{GOD}$, where CAT is catalase); thus, the main rates to be investigated are v_{BG} and v_{GOD} . The equations shown in Table 3 are reduced to

$$v_{BG} = \frac{V_{maxBG} \cdot [G2]}{K_{MBG} \cdot \left(1 + \frac{[G1OX]}{K_{IG1BG}}\right)}, \quad v_{GOD} = \frac{V_{maxGOD} \cdot [G1]}{K_{MGOD} \cdot \left(1 + \frac{[G1OX]}{K_{IG1GOD}}\right)},$$

where G1 is glucose, G2 is cellobiose, and G1OX is D-glucono- δ -lactone/gluconic acid. To illustrate $V_{maxGOD} > 10v_{BG}$, the following may be shown. Cellulose is in abundance compared with Cel6A concentration; therefore, it is assumed that the highest v_{Cel6A} is $V_{maxCel6A}$. At the highest dose used in the assay, and assuming $1 s^{-1}$ turnover number, $V_{maxCel6A}$ is $2 \times 10^{-6} M s^{-1}$. V_{maxGOD} at the dose used in the assay and using $633 s^{-1}$ turnover number from the ABTS assay is $1.65 \times 10^{-3} M s^{-1}$. Using the V_{maxBG} and K_{MBG} values from the ITC kinetic assay, v_{BG} is initially $2.9 \times 10^{-2} [G2] s^{-1}$. For $10 v_{BG} > V_{maxGOD}$, and thus to render the signal amplification erroneous, $[G2]$ must reach a concentration of more than 6 mM. In the ITC assay, the concentrations are in the micromolar (μM) concentration range; therefore, the assumption of first-order kinetics is justified.

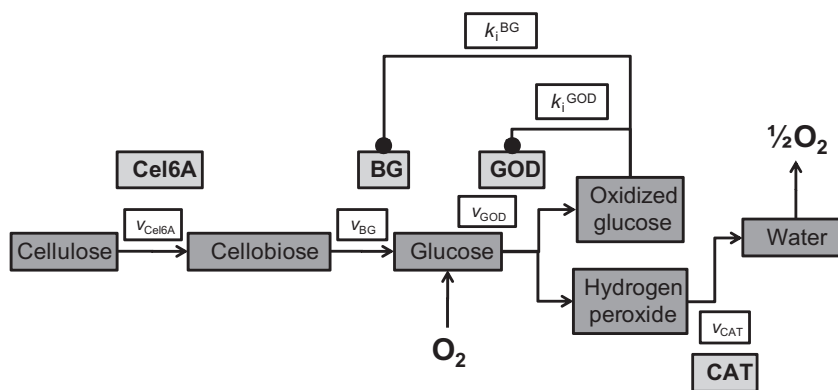


Fig. 2. Simplified overview of the amplification of the heat signal generated by Cel6A. Cellobiose produced by Cel6A is converted to two glucose molecules that are oxidized, and the hydrogen peroxide is broken down to water and oxygen. The oxidized glucose product inhibits both GOD and BG. See text for further details.

Table 2
Kinetics models used to describe the system.

Kinetic model	Formula
Michaelis–Menten ($S_0 \ll K_M$)	$v = \frac{V_{max} \cdot [S]}{K_M}$
Michaelis–Menten Product inhibition ($S_0 \ll K_M$)	$v = \frac{V_{max} \cdot [S]}{K_M \left(1 + \frac{[P]}{K_i}\right)}$
Michaelis–Menten Substrate inhibition ($S_0 \ll K_M$)	$v = \frac{V_{max} \cdot [S]}{K_M \left(1 + \frac{[S]}{K_i}\right)}$

Table 3
Rate equations.

Enzyme	Substrate	Formula
BG	Cellobiose	$v_{BG} = \frac{V_{maxBG} \cdot [G2]}{K_{M_{BG}} \cdot \left(1 + \frac{[G1]}{K_{i_{BG}^{G1}}} + \frac{[G1OX]}{K_{i_{BG}^{G1OX}}} + \frac{[G2]^2}{K_{i_{BG}^{G2}}}\right)}$
GOD	Glucose	$v_{GOD} = \frac{V_{maxGOD} \cdot [G1]}{K_{M_{GOD}} \cdot \left(1 + \frac{[G1OX]}{K_{i_{GOD}^{G1OX}}} + \frac{[PXD]}{K_{i_{GOD}^{PXD}}} + \frac{[G1]^2}{K_{i_{GOD}^{G1}}}\right)}$
CAT	Hydrogen peroxide	$v_{CAT} = \frac{V_{maxCAT} \cdot [PXD]}{K_{M_{CAT}}}$

Note. G2, cellobiose; G1, glucose; G1OX, D-glucono- δ -lactone/gluconic acid; PXD, hydrogen peroxide; CAT, catalase.

Because D-glucono- δ -lactone is a strong competitive inhibitor of BG [3] and a weak competitive inhibitor of GOD [20], the most critical kinetic factor for the amplification is $k_{i_{BG}^{G1OX}}$. This was determined to be 0.1 mM and competitive (Michaelis–Menten $R^2 = 0.97$), in good agreement with previous findings [3]. $k_{i_{GOD}^{G1OX}}$ may be ignored because the addition of 5 mM D-glucono- δ -lactone to the ABTS assay containing GOD did not exhibit any inhibition.

The above analyses of kinetic parameters suggest that the initial calorimetric heat flow in the amplified assay indeed reflects the rate of cellobiose production and that the first limitation that occurs during continuous measurement is an accumulation of a critical level of D-glucono- δ -lactone (0.1 mM). This interpretation is based on the application of conventional inhibition models, but it is also possible to conduct direct experimental (model-free) validation of this key correlation. To this end, slow continuous injection of cellobiose to the amplification mixture in the calorimetric cell was used.

Examples of this in Fig. 3 show that when cellobiose is delivered at 8.1 pmol s^{-1} , the heat signal reaches a constant level of $3.2 \text{ } \mu\text{J s}^{-1}$ after approximately 100 s. This observation has two important implications. First, the overall response time of the system (including thermal response of the instrument, mixing, amplification reactions, etc.) is approximately 100 s. Second, the heat signal during

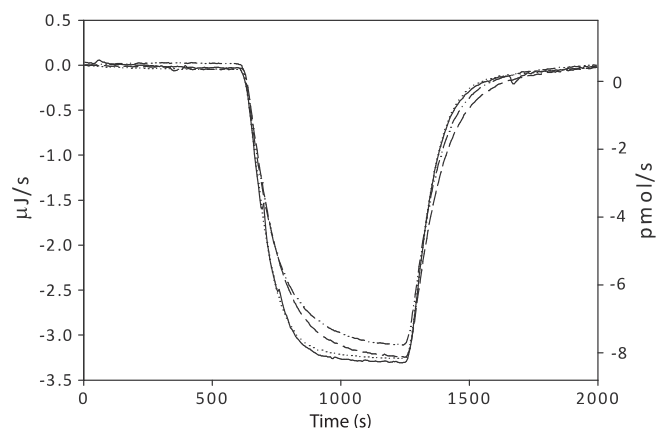


Fig. 3. Titration of cellobiose to the amplification mixture. Cellobiose is injected to the amplification mixture at a constant rate of 8.1 pmol s^{-1} over 10 min, and then the baseline is allowed to reestablish. The cellobiose is titrated at a rate equivalent to the higher observed rates in the Cel6A assay, and steady state is reached within 300 s. The measured and theoretical values of the steady-state heat flow are within 2% of each other. Solid line: no inhibitor; dotted line: 0.05 mM D-glucono- δ -lactone; dashed line: 0.1 mM D-glucono- δ -lactone; dash-dotted line: 0.15 mM D-glucono- δ -lactone. The instrument response time was determined to be $18.8 \pm 2 \text{ s}$ using a standard electrical pulse program varying from 1 to $20 \text{ } \mu\text{J s}^{-1}$. Fitting the rate of heat produced initially until steady state was attained (constant heat production, the plateau) to a single exponential decay allows calculation of the time constant, τ . The observed τ is expressed as the response time.

continuous cellobiose “production” is -362 kJ mol^{-1} of the disaccharide. This latter value is in excellent agreement with the more precise sum of the separate reactions of the amplification system measured independently in titration trials and listed in Table 4. This accordance strongly supports the assumption that cellobiose is quickly and quantitatively converted by the amplification mixture. The results in Fig. 3 also illustrate the effect of D-glucono- δ -lactone on the amplification system. It appears that no significant changes are observed for 0.05 mM lactone. At 0.1 mM, the response time is increased to approximately 120 s, but the uninhibited steady-state heat flow is still reached. A still higher lactone concentration (0.15 mM) further slows the response time ($\sim 140 \text{ s}$) and, more important, diminishes the final heat flow. This latter observation suggests incomplete hydrolysis and/or oxidation of the added cellobiose (cf. Fig. 2), most likely due to the inhibition of β -glucosidase.

Other factors in the design include maximizing the availability of oxygen as dissolved oxygen (DO) in the liquid phase. This was introduced by removing the vacuum degassing step used in ITC experiments. The DO measured in the amplification experiments

Table 4
Measured molar enthalpies.

Enzyme(s)	Substrate	$\Delta_{\text{app}}H$ (kJ mol ⁻¹): current study	Reference values (kJ mol ⁻¹)
BG	Cellobiose	-2.6 ± 0.02	-2.36 [12], -2.63 [15]
GOD	Glucose	-82.5 ± 1.7	-80 [4], -125 [1]
CAT	Peroxide	-106.7 ± 0.6	-100 [1,4], -84 [1], -89 [1]
GOD + CAT + BG	Cellobiose	-355.3 ± 2.0	

Note. Ref. [1] is a database and, thus, presents different values. CAT, catalase.

was 7.9 ± 0.2 mg/L at 25 °C, with a negligible decrease of 0.1 mg/L after ultrasonic treatment. The background noise registered after the ultrasonic treatment was on the same order of magnitude as observed after vacuum degassing. The enzymes' activity was not changed after 1 min of ultrasound treatment (data not shown).

Initially, headspace was introduced as a method to overcome the oxygen depletion limitation of the enzymatic amplification system. The sensitivity of the measurements was severely affected, and there was a significant increase in the background noise. The air/liquid two-phase reactant cell could not be thermally controlled as accurately as a single-phase filled liquid cell by the instrument.

There was no oxidation of the substrates RAC and cellobiose in the presence of more than twice the estimated steady-state concentration of hydrogen peroxide. Similarly, trials conducted on Cel6A in the presence of hydrogen peroxide, D-glucono-δ-lactone, and D-gluconic acid showed no decrease in enzyme activity based on cellobiose production results.

Finally, BG was determined to produce a negligible amount of glucose from RAC, using both ITC and HPAEC-PAD, which is corrected by running a control experiment with the amplification mix for each new substrate.

It is concluded that the combination of β-glucosidase, GOD, and catalase provides a useful amplification system that increases the heat flow to an extent where cellobiose produced by cellobiohydrolases such as Cel6A may be monitored calorimetrically even at a low cellulase load. In a well-aerated (or oxygen-enriched) sample, the primary experimental limitation is the inhibitory effect of D-glucono-δ-lactone. This inhibition becomes significant when the lactone concentration exceeds 0.1 mM, but because the experimental sensitivity corresponds to the production of approximately 0.1 pmol of cellobiose per second (and optimal signals are in the range of 1–10 pmol s⁻¹), the reaction may be monitored for many hours before lactone inhibition interferes with the measurements. The accumulated amount of lactone scales with the area under the calorimetric trace, and hence its concentration in any given trial, can be readily checked.

Cel6A kinetics on unmodified cellulose

The accurate determination of kinetic parameters requires precise calibration and controls. The conversion of heat flow to reaction rate relies on the enthalpy of the reactions. Table 4 presents the molar enthalpies determined as outlined earlier.

Substrate characterization

To accurately express the kinetics of cellulose hydrolysis, it is necessary to have a well-characterized substrate. RAC was chosen because it is claimed to be the most homogeneous amorphous substrate available to date [34], and BC was chosen to represent a pure cellulose crystalline substrate. Table 5 summarizes the analyses carried out.

Sigmacell 20 has been reported to have a DP of 209 ± 10 [23], and commercially prepared cellulose has been reported to have

Table 5
Substrate characteristics.

Material	% Dry weight for assay	Total glucose (g/L)	DP _N	I _{cr}
Sigmacell 20	0.16 ± 0.02	1.62 ± 0.17	189 ± 13	0.57
RAC	0.47 ± 0.014	4.67 ± 0.33	180 ± 14	0.00 ^a
BC	0.14 ± 0.02	1.38 ± 0.095	236 ± 7	0.87

^a There was no evidence of a C4 peak at 92 to 86 ppm, indicating a completely amorphous substrate.

an I_{cr} of between 0.50 and 0.60 [11]. RAC has been reported to have a DP of 215 ± 9 [23] and to be completely amorphous [34]. BC has been reported to have a DP_N of 600 to 2000 and an I_{cr} of 0.80 to 0.95 [6]. It is proposed that the DP_N of BC is less than previously reported as a result of the mechanical action of the Ultra Turrax T8 homogenizer.

Many mechanistic and regulatory aspects of cellulolytic enzymes remain incompletely resolved, and this may be due in part to the shortage of precise quantitative assays [6]. It is suggested that calorimetry may be a useful approach for some studies because it offers real-time data and directly measures the rate of the reaction (not the concentration of the product). In the following examples, it is shown how the amplified assay quantifies the activity of Cel6A. Fig. 4A shows an example where 5-μl aliquots of 4.7 mg/ml RAC are titrated into the calorimetric cell containing the amplification system and 2 μM Cel6A.

The substrate for Cel6A is cellulose that will be degraded from the nonreducing ends of the strands [35], and the "concentration" of such ends (calculated from the DP_N [Table 5]) is much lower than the concentration of Cel6A. Thus, following the first injection of RAC, the molar ratio of Cel6A to nonreducing ends ([E]/[S₀]) is approximately 25. The results in Fig. 4 show that under these conditions, the injection of RAC is associated with an initial exothermic process (the peaks in Fig. 4A) that occurs too quickly to be resolved reliably in time (e.g., faster than the response time of ~100 s). The control experiments (dotted line in Fig. 4A) show that this initial exotherm is not due to a mixing enthalpy. Other possibilities include cellulase adsorption to RAC and an initial burst in Cel6A's production of cellobiose, but the assignment of this process awaits studies that systematically vary [E] and [S₀].

Subsequent to the peak in Fig. 4A, the signal reaches a constant level of cellobiose production that increases linearly with the amount of added RAC (Fig. 4C). Taking the slope of the averaged data set in Fig. 4B, there is 3.94 nM s⁻¹ (i.e., 5.6 pmol s⁻¹ in the 1.42-ml calorimetric vessel) cellobiose being produced per micromolar (μM) of reducing end equivalents. Given that there is an excess of Cel6A, one may assume all accessible nonreducing ends to be "in use" and, thus, that the absolute maximum number of active cellulases is equal to the number of reducing ends. Shielding or steric hindrance by unproductively adsorbed enzymes may affect this number. Under this assumption, the enzymatic turnover number is best described as the ratio of the reaction rate and the concentration of reducing end equivalents (~0.24 min⁻¹ for the data in Fig 4). In other words, these results suggest that at the pseudo-steady state defined by the horizontal part of the curve in Fig. 4A, each active Cel6A produces only approximately 14 cellobiose molecules per hour.

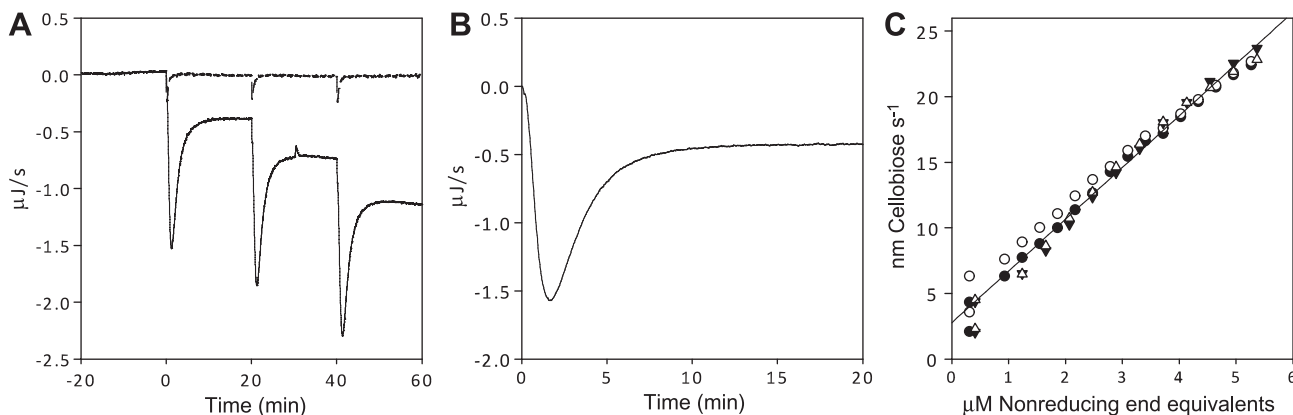


Fig. 4. (A) Solid line: three injections of RAC to the amplification mix and Cel6A in the ITC cell. Injections (5 μl) were added with 20 min between each one. Dashed line: control experiment in the absence of Cel6A. The area caused by the addition of RAC to the cell in the absence of Cel6A has been subtracted from the total area in calculations. (B) Single injection of RAC enlarged to demonstrate the steady state of cellobiose production reached after 10 min. (C) Product rate formation plotted as a function of substrate concentration. For the Cel6A experiments, it is the last 5 min prior to the $i + 1$ injection that is used to determine the constant rate of product formation. There is 2 μM Cel6A in the cell. Shown are four replicates and a linear fit of the averaged data ($R^2 = 0.99$).

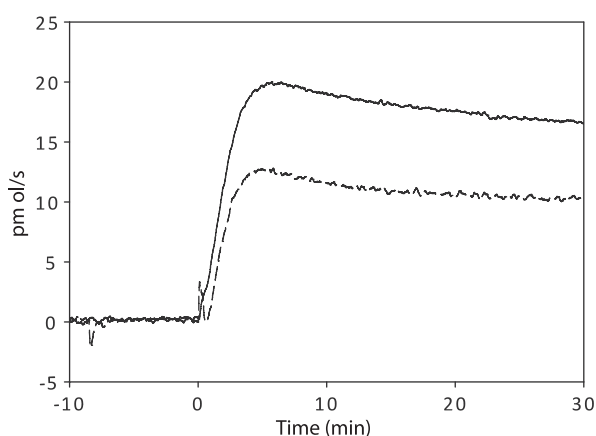


Fig. 5. Two runs of $S \gg E$ kinetic studies. Solid line: 30 pmol of Cel6A added to 80 μM NRE (RAC) with amplification system in the cell; dashed line: 15 pmol of Cel6A titrated to the cell.

To test this further, the activity of Cel6A was measured under conditions of excess nonreducing ends (i.e., $[E] \ll [S_0]$). Fig. 5 shows results for the addition of 15 and 30 pmol of Cel6A to an RAC suspension with 80 μM nonreducing end equivalents. It should be noted that the consumption of Cel6A in these experiments is only approximately 1 μg per trial and, hence, that the assay may be useful in studies of protein variants and other material with limited availability. Also, the results for $[E] \ll [S_0]$ (Fig. 5) are quite different from those in Fig. 4 ($[E] \gg [S_0]$). For example, the initial exothermic peak seen in Fig. 4 is absent and, unlike in Fig. 4, the reaction rate in Fig. 5 decays slightly throughout the 30-min recording. Moreover, the turnover number derived by normalizing the reaction rate in Fig. 5 with respect to the concentration of Cel6A (maximum value $\sim 40 \text{ min}^{-1}$) is more than two orders of magnitude larger than the value in Fig. 4 (0.24 min^{-1}). Previous reports on the turnover number for Cel6A have shown some variation [9,10,31,32,36] but are generally in line with the high value found here. The slow turnover when $[E] \gg [S_0]$ could reflect limited substrate availability (e.g., inaccessibility of a large fraction of the nonreducing ends) or “jamming” of cellulases on a crowded surface. It should be noted that K_m may play a significant role when interpreting the ratio between E/S results. At lower overall substrate concentrations, the reported turnover number could also reflect conditions under K_m where some or many of the Cel6A

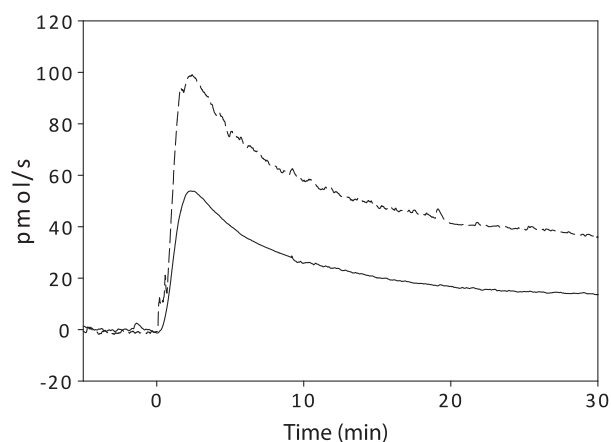


Fig. 6. Two runs of $S \gg E$ kinetic studies. Solid line: 300 pmol of Cel6A added to 85 μM NRE (BC) with amplification system in the cell at 25 $^{\circ}\text{C}$; dashed line: same experiment at 50 $^{\circ}\text{C}$.

molecules might not be bound. Again, it appears that comparative studies along these lines (with variable $[E]$, $[S_0]$, and DP_N) have the potential to resolve this question, which is relevant inasmuch as studies of cellulases are frequently conducted under conditions of $[E] \gg [S_0]$. For BC, the rate was slower, with a maximum value of 10 min^{-1} being determined, but this was followed by a rapid decrease in hydrolysis rate, as seen in Fig. 6. Here we also demonstrate the applicability of the assay at higher temperatures (i.e., 50 $^{\circ}\text{C}$).

In conclusion, it has been demonstrated that the ITC amplification method may be used to monitor the enzymatic production of cellobiose down to rates below 1 pmol s^{-1} . The amplification system was analyzed both on the basis of kinetic models and by direct experimental detection of the hydrolysis and oxidation of continuously added cellobiose. These tests collectively suggest that the heat flow provides a true measure of the rate of cellobiose production provided that the sample is well aerated prior to the experiment and the concentration of the product D-glucono- δ -lactone does not exceed approximately 0.1 mM. One key advantage of the method is that it measures the reaction rate directly and in real time. It is anticipated that this may become valuable in attempts to resolve some of the highly complex regulatory and mechanistic aspects of cellulolytic enzyme action.

Acknowledgments

This work was supported by the Danish Agency for Science, Technology, and Innovation (Grant 2104-07-0028 to P.W.) and the Carlsberg Foundation. We thank Poul Erik Hansen and Kjeld Schaumburg for collaboration with NMR studies as well as Annette Christensen for technical assistance. We also thank Peter Rahbek Østergaard for the GOD enzyme and Kristian Bertel Rømer Mørkeberg Krogh (Novozymes) for help and guidance in purifying the BG.

References

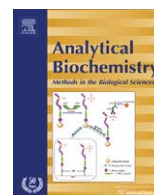
- [1] R.N. Goldberg, Y.B. Tewari, T.N. Bhat, Thermodynamics of enzyme-catalyzed reactions: a database for quantitative biochemistry, *Bioinformatics* 20 (2004) 2874–2877.
- [2] Z.M. Tao, R.A. Raffel, A.K. Souid, J. Goodisman, Kinetic studies on enzyme-catalyzed reactions: oxidation of glucose, decomposition of hydrogen peroxide, and their combination, *Biophys. J.* 96 (2009) 2977–2988.
- [3] E.B. de Melo, A.D. Gomes, I. Carvalho, α - and β -glucosidase inhibitors: chemical structure and biological activity, *Tetrahedron* 62 (2006) 10277–10302.
- [4] L.J. Blum, P.R. Coulet (Eds.), *Biosensor Principles and Applications*, Marcel Dekker, New York, 1991.
- [5] R. Wilson, A.P.F. Turner, Glucose oxidase: an ideal enzyme, *Biosens. Bioelectron.* 7 (1992) 165–185.
- [6] Y.H.P. Zhang, M.E. Himmel, J.R. Mielenz, Outlook for cellulase improvement: screening and selection strategies, *Biotechnol. Adv.* 24 (2006) 452–481.
- [7] G. Beldman, M.F. Searle van Leeuwen, F.M. Rombouts, F.G.J. Voragen, The cellulase of *Trichoderma viride*: purification, characterization, and comparison of all detectable endoglucanases, exoglucanases, and β -glucosidases, *Eur. J. Biochem.* 146 (1985) 301–308.
- [8] S. Shoemaker, K. Watt, G. Tsitovsky, R. Cox, Characterization and properties of cellulases purified from *Trichoderma reesei* strain L27, *Nat. Biotechnol.* 1 (1983) 687–690.
- [9] P. Tomme, H. Vantilbeurgh, G. Pettersson, J. Vandamme, J. Vandekerckhove, J. Knowles, T. Teeri, M. Claeysens, Studies of the cellulolytic system of *Trichoderma reesei* QM 9414: analysis of domain function in two cellobiohydrolases by limited proteolysis, *Eur. J. Biochem.* 170 (1988) 575–581.
- [10] B. Nidetzky, W. Steiner, M. Claeysens, Cellulose hydrolysis by the cellulases from *Trichoderma reesei*: adsorptions of two cellobiohydrolases, two endoglucanases, and their core proteins on filter paper and their relation to hydrolysis, *Biochem. J.* 303 (1994) 817–823.
- [11] Y.H.P. Zhang, L.R. Lynd, Toward an aggregated understanding of enzymatic hydrolysis of cellulose: noncomplexed cellulase systems, *Biotechnol. Bioeng.* 88 (2004) 797–824.
- [12] L. Murphy, K. Borch, K.C. McFarland, C. Bohlin, P. Westh, A calorimetric assay for enzymatic saccharification of biomass, *Enzyme Microb. Technol.* 46 (2010) 141–146.
- [13] S.N. Olsen, Applications of isothermal titration calorimetry to measure enzyme kinetics and activity in complex solutions, *Thermochim. Acta* 448 (2006) 12–18.
- [14] M.J. Todd, J. Gomez, Enzyme kinetics determined using calorimetry: a general assay for enzyme activity?, *Anal. Biochem.* 296 (2001) 179–187.
- [15] T. Jeoh, J.O. Baker, M.K. Ali, M.E. Himmel, W.S. Adney, β -D-Glucosidase reaction kinetics from isothermal titration microcalorimetry, *Anal. Biochem.* 347 (2005) 244–253.
- [16] C.M. Wong, K.H. Wong, X.D. Chen, Glucose oxidase: natural occurrence, function, properties, and industrial applications, *Appl. Microbiol. Biotechnol.* 78 (2008) 927–938.
- [17] B. Danielsson, Enzyme thermistor devices, in: L.J. Blum, P.R. Coulet (Eds.), *Biosensor Principles and Applications*, Marcel Dekker, New York, 1991, pp. 83–105.
- [18] J. Bao, K. Furumoto, M. Yoshimoto, K. Fukunaga, K. Nakao, Competitive inhibition by hydrogen peroxide produced in glucose oxidation catalyzed by glucose oxidase, *Biochem. Eng. J.* 13 (2003) 69–72.
- [19] J. Bao, K. Furumoto, K. Fukunaga, K. Nakao, A kinetic study on air oxidation of glucose catalyzed by immobilized glucose oxidase for production of calcium gluconate, *Biochem. Eng. J.* 8 (2001) 91–102.
- [20] J. Miron, M.P. Gonzalez, J.A. Vazquez, L. Pastrana, M.A. Murado, A mathematical model for glucose oxidase kinetics, including inhibitory, deactivant, and diffusional effects, and their interactions, *Enzyme Microb. Technol.* 34 (2004) 513–522.
- [21] A.C. Storer, A. Cornish-Bowden, Kinetics of coupled enzyme reactions: applications to assay of glucokinase, with glucose-6-phosphate dehydrogenase as coupling enzyme, *Biochem. J.* 141 (1974) 205–209.
- [22] M.L. Sinnott, Catalytic mechanisms of enzymatic glycosyl transfer, *Chem. Rev.* 90 (1990) 1171–1202.
- [23] Y.H.P. Zhang, L.R. Lynd, Determination of the number-average degree of polymerization of cellodextrins and cellulose with application to enzymatic hydrolysis, *Biomacromolecules* 6 (2005) 1510–1515.
- [24] H.C. Lichstein, M.H. Soule, Studies of the effect of sodium azide on microbial growth and respiration: I. The action of sodium azide on microbial growth, *J. Bacteriol.* 47 (1944) 221–230.
- [25] M. Dubois, K.A. Gilles, J.K. Hamilton, P.A. Rebers, F. Smith, Colorimetric method for determination of sugars and related substances, *Anal. Chem.* 28 (1956) 350–356.
- [26] M. Matulova, R. Nouaille, P. Capek, M. Pean, A.M. Delort, E. Forano, NMR study of cellulose and wheat straw degradation by *Ruminococcus albus* 20, *FEBS J.* 275 (2008) 3503–3511.
- [27] D.L. VanderHart, R.H. Atalla, Studies of microstructure in native celluloses using solid-state carbon-13 NMR, *Macromolecules* 17 (1984) 1465–1472.
- [28] L.E. Briggner, I. Wadso, Test and calibration processes for microcalorimeters, with special reference to heat-conduction instruments used with aqueous systems, *J. Biochem. Biophys. Methods* 22 (1991) 101–118.
- [29] Z.W. Zhu, C. Momeu, M. Zakhartsev, U. Schwaneberg, Making glucose oxidase fit for biofuel cell applications by directed protein evolution, *Biosens. Bioelectron.* 21 (2006) 2046–2051.
- [30] P. Chelikani, I. Fita, P.C. Loewen, Diversity of structures and properties among catalases, *Cell. Mol. Life Sci.* 61 (2004) 192–208.
- [31] H. Vantilbeurgh, R. Bhikhabhai, L.G. Pettersson, M. Claeysens, Separation of endo-type and exo-type cellulases using a new affinity-chromatography method, *FEBS Lett.* 169 (1984) 215–218.
- [32] M. Gruno, P. Valjamae, G. Pettersson, G. Johansson, Inhibition of the *Trichoderma reesei* cellulases by cellobiose is strongly dependent on the nature of the substrate, *Biotechnol. Bioeng.* 86 (2004) 503–511.
- [33] M.J. Nicol, F.R. Duke, Substrate inhibition with glucose oxidase, *J. Biol. Chem.* 241 (1966) 4292–4293.
- [34] Y.H.P. Zhang, J.B. Cui, L.R. Lynd, L.R. Kuang, A transition from cellulose swelling to cellulose dissolution by σ -phosphoric acid: evidence from enzymatic hydrolysis and supramolecular structure, *Biomacromolecules* 7 (2006) 644–648.
- [35] B.K. Barr, Y.L. Hsieh, B. Ganem, D.B. Wilson, Identification of two functionally different classes of exocellulases, *Biochemistry* 35 (1996) 586–592.
- [36] J.O. Baker, C.I. Ehrman, W.S. Adney, S.R. Thomas, M.E. Himmel, Hydrolysis of cellulose using ternary mixtures of purified cellulases, *Appl. Biochem. Biotechnol.* 70–72 (1998) 395–403.



Contents lists available at ScienceDirect

Analytical Biochemistry

journal homepage: www.elsevier.com/locate/yabio



Corrigendum

Corrigendum to “An enzymatic signal amplification system for calorimetric studies of cellobiohydrolases” [Anal. Biochem. 404 (2010) 140–148]

Leigh Murphy^{a,b}, Martin J. Baumann^{a,b}, Kim Borch^b, Matt Sweeney^c, Peter Westh^{a,*}

^a Department of Science, Systems, and Models (NSM), Biomaterials, Roskilde University, DK-4000 Roskilde, Denmark

^b Novozymes, DK-2880 Bagsværd, Denmark

^c Novozymes, Davis, CA 95618, USA

The numbering of the following references is cited incorrectly:

Reference [1] page 140, paragraph 1, line 3 should refer to reference [11].

Reference [2] page 140, paragraph 1, line 11 should refer to reference [36].

References [3–5] page 140, paragraph 2, line 6 should refer to references [9,10,35].

References [4] and [17] are the same, but individual references to each are correct.

All other references are cited correctly to the current numbering.

DOI of original article: 10.1016/j.ab.2010.04.020

* Corresponding author. Fax: +45 4674 3011.

E-mail address: pwesth@ruc.dk (P. Westh).

Article 3: Burst kinetics of *T. reesei* endoglucanases on insoluble cellulose.

Leigh Murphy, Nicolaj Cruys-Bagger, Martin J. Baumann, Søren Nymand Olsen, Kim Borch, Matt Sweeney, Hirosuke Tatsumi , Peter Westh.

BURST KINETICS OF *T. REESEI* ENDOGLUCANASES ON INSOLUBLE CELLULOSE.

Leigh Murphy¹, Nicolaj Cruys-Bagger¹, Martin J. Baumann², Søren Nymand Olsen², Kim Borch², Matt Sweeney³, Hirosuke Tatsumi⁴ & Peter Westh^{1*}.

¹Roskilde University, NSM, Biomaterials, 1 Universitetsvej, DK-4000, Roskilde, Denmark. ²Novozymes A/S, Krogshøjvej 36, DK-2880, Denmark. ³Novozymes Inc. 1445 Drew Ave., Davis, CA 95 618, USA. ⁴International Young Researchers Empowerment Center, Shinshu University, Mastumoto, Nagano 390-8621, Japan.

*Corresponding author. Email: pwesth@ruc.dk Fax: +45 4674 3011

The kinetics of cellulose hydrolysis have long been described by an initial fast hydrolysis rate, tapering rapidly off, leading to a process that takes days rather than hours to complete. This behavior has been mainly attributed to the action of cellobiohydrolases, and often linked to the processive mechanism of this *exo*-acting group of enzymes. The initial kinetics of *endo*-glucanases (EGs) is far less investigated, partly due to a limited availability of quantitative assay technologies. We have used isothermal calorimetry to monitor the early time course of the hydrolysis of insoluble cellulose by the three main EGs from *Trichoderma reesei* (*Tr*); *TrCel7B* (formerly EG I), *TrCel5A* (EG II), and *TrCel12A* (EG III). These *endo*-glucanases show a distinctive initial burst with a maximal rate which is about 5-fold higher than the rate after 5 min of hydrolysis. The burst is particularly conspicuous for *TrCel7B*, which reaches a maximal turnover of about 20 s⁻¹ at 30 °C, and conducts about 1200 catalytic cycles per enzyme molecule in the initial fast phase. For *TrCel5A* and *TrCel12A* the extent of the burst is 2-300 cycles per enzyme molecule. The availability of continuous data on EG activity allows an analysis of the mechanisms underlying the initial kinetics, and it is suggested that the slowdown is linked to transient inactivation of enzyme on the cellulose surface. The frequency of structures on the substrate surface that cause inactivation determines the extent of the burst phase.

Biomass provides a carbon neutral alternative to fossil fuels, and the optimization of the enzymatic breakdown of lignocellulose has intensified greatly in recent times (1,2). The hydrolysis of cellulose is a complex process involving the synergistic action of a combination of glycoside hydrolases (1) collectively called cellulases (2,3). Endo-1,4- β -D-glucan-4-glucanohydrolases

(EG) (EC 3.2.1.4) randomly cleave the cellulose polymer backbone in the amorphous areas (2,4). In addition to this, there are normally two *exo*-enzymes, *exo*-1,4- β -D-glucan-cellobiohydrolase (CBH I and II) (EC 3.2.1.91) which cleave cellobiose from the reducing and non-reducing ends (5) of the cellulose chain, and degrade the crystalline areas of cellulose (3,6). Finally, β -D-glucoside glucohydrolase (*cellobiase*) (EC 3.2.1.21) hydrolyzes the cellobiose into glucose monomers (6).

The activity of many cellulolytic enzymes shows an unusual time course including an initial burst and a subsequent slowdown. The latter can sometimes be detected already within seconds or minutes of the reaction onset and the gradual reduction in the hydrolytic rate often persists for days (7,8). This behavior is of particular interest both in attempts to elucidate the molecular mechanisms and regulation of cellulolytic enzymes, and in the application of cellulases for the industrial breakdown of biomass. Thus, a typical biomass saccharification starts with a conversion of up to 50 % in the first 24 h, but takes 2 - 5 days to achieve appreciable yields (> 80%) of glucose (9). For the breakdown of complex biomass the slowdown is undoubtedly controlled by a variety of factors, but the observation of a distinct burst and slowdown for pure cellulose/cellulase systems at very low degrees of conversion, has directed the focus to the intrinsic molecular properties of the enzymes and substrate (10-14). The general conclusion in this work is that the early slowdown in pure systems depends on the processive mode of action for the CBHs (*i.e.* their tendency to sequentially hydrolyze stretches of one cellulose strand without dissociation). Clearly, this explanation is not immediately applicable to EGs, which are thought to hydrolyze glycosidic bonds randomly (that is non-processively). Here we study the initial kinetics of the three main EG's produced by

Hypocrea jecorina (Anamorph: *Trichoderma reesei*). *TrCel7B*, *TrCel5A*, and *TrCel12A* (4), belong to glycoside hydrolase (GH) families 7 (15), 5 (16), and 12 (17) respectively. *TrCel7B* has a C-terminal carbohydrate binding module (CBM I), and shares 40 % to 45 % overall homology to the exo-cellulase *TrCel7A* (18,19). *TrCel5A* has the least homology to the other *T. reesei* cellulases, and has an N-terminal CBM I (16). *TrCel12A* is smaller (25 KDa), and has no CBM (20) All three are retaining glycoside hydrolases (21,22).

Methods to determine the activity of EGs have been based on the quantitative spectrophotometric measurement of reducing ends produced on soluble and insoluble substrates (23-29). These assays often do not correlate well with each other, are often subject to *exo*-enzyme interferences (30), and are often influenced by different stoichiometric reactivities based on the cello-oligomer length (31,32). Being spectrophotometric, they are also subject to optical limitations, in that complex biomass samples cannot be assayed in this way, and being end point assays, time resolution must be estimated by differentiating a series of stopped aliquots or separate parallel reactions. EG activity is also often determined through the use of viscometry, based on the depolymerisation of carboxymethyl cellulose (CMC) or hydroxyethyl cellulose (HEC) substrates (30,33-35). CMC provides a cellulose that cannot be significantly depolymerised by processive (e.g. CBH) enzymes, due to the steric hindrance of the carboxymethyl groups (36,37), and EGs have even been referred to as CMCases (30,38). However, it is a model substrate, so the activity of an enzyme on it does not reflect the activity on a more realistic insoluble substrate (39,40). CMC, being an ionic substituted substrate, is also subject to changes in viscosity dependent on ionic strength, pH and polyvalent cations (41).

In order to follow the initial kinetics of EG action on an unmodified cellulose substrate, we have used Isothermal titration calorimetry (ITC). The heat-flow measured may be directly converted to a rate of hydrolysis (42-44). In the current study, this new method is introduced and validated against both the widely used PAHBAH (24,25) and BCA (29) reducing sugar assays. Based on the time course of the calorimetric results and data

from chromatography and continuous amperometric detection of glucose production, we analyze molecular origins of the initial burst and rapid decline in the activity of endoglucanases on insoluble cellulose.

Material and Methods

Enzymes

TrCel7B

TrCel7B was cloned and expressed in *A. oryzae* as described in WO 2005/067531. The broth was filtered then buffer exchanged using a 10 kDa polyethersulfone membrane with 20 mM Tris-HCl pH 8.5. The sample was loaded onto a Q sepharose® High Performance column (GE Healthcare, Piscataway, NJ, USA) and bound proteins were eluted with a linear gradient from 0-600 mM NaCl. The fractions were desalted into 20 mM Tris pH 8.0, 150 mM NaCl.

TrCel5A

TrCel5A was cloned and expressed in *A. oryzae*. Filtered broth was desalted and buffer-exchanged into 20 mM Tris-HCl pH 8.0. Desalted *TrCel5A* was loaded onto a MonoQ™ HR 16/10 ion exchange column (GE Healthcare, Piscataway, NJ, USA) and eluted with a 0-300 mM NaCl gradient in 20 mM Tris-HCl pH 8.0

TrCel12A

TrCel12A was cloned and expressed in *A. oryzae*. The purification procedure was adapted from (45). The protein was eluted from the phenyl sepharose FF column (GE Healthcare Life Sciences, Buckinghamshire, UK) with 20 mM sodium phosphate pH 6.00, followed by 50:50 % v/v 20 mM sodium phosphate pH 6.0:95 % ethanol. Fractions were pooled based on the activity measured by AZCL-HE-Cellulose from Megazyme (Bray, Co. Wicklow, Ireland) and buffer exchanged using a sephadex G25 column (GE Healthcare Life Sciences, Buckinghamshire, UK) into 12 mM sodium acetate pH 4.8.

Prior to ITC analysis, all proteins were buffer changed to 50 mM sodium acetate, 2 mM calcium chloride pH 5.0. The concentration of all enzymes were determined from OD₂₈₀ using the molar

absorption coefficients of 72770 M⁻¹cm⁻¹ (*TrCel7B*), 81360 M⁻¹cm⁻¹ (*TrCel5A*) and 73340 M⁻¹cm⁻¹ (*TrCel12A*).

Megazyme EG Assay The assay was carried out as per manufacturer's instructions using 0.1 % AZCL-HE-Cellulose w/v substrate for 15 min at 50 °C, 1400 rpm in 1.5 mL eppendorf tubes. The solutions were centrifuged at 13,500 rpm for 5 min, and OD₅₉₅ read.

Substrates Regenerated Amorphous Cellulose (RAC) was prepared as described previously (46). Total glucose was quantified (46-48) using a glucose (Sigma Aldrich, St. Louis, MO, USA) standard curve at OD₄₉₀. The number averaged degree of polymerization (DP_N) was calculated from the ratio of reducing ends measured by BCA (see below) and total sugars. The crystallinity index of RAC was determined using solid-state ¹³C cross-polarization/magic angle spinning (CP/MAS) nuclear magnetic resonance (NMR) with settings adapted from (49) and described in (46). Cello-oligosaccharides (COS) were prepared according to (50), and purity determined using HPAEC-PAD (46).

Reducing Ends Assays p-hydroxy benzoic acid hydrazide assay. The PAHBAH assay was adapted from (24,25) and samples quantified using a glucose and cellotetraose standard curve at OD₄₁₀. 2,2' Bicinchoninic acid assay. The BCA assay was performed as outlined in (48) at 80 °C in a thermomixer at 1400 rpm, and a 30 min incubation time. Samples were quantified using a glucose and cellotetraose standard curve at OD₅₆₀.

Reducing Ends Assays Control Experiments. The sensitivity of the assays to mixtures of soluble and insoluble reducing ends was tested. To determine if the assays were affected by a constant RAC background, they were calibrated from 10 μM to 50 μM glucose and cellotetraose in the presence and absence of 1 g/L RAC. To test if the assays were incorrectly measuring mixtures of insoluble and soluble reducing ends 40 μM of glucose or cellotetraose was added to varied amounts of RAC (0.2 – 1 g/L). The % recovery measured by determining how much of the added 40 μM could be re-found in the mixtures after subtracting the background.

Reducing ends assays on hydrolysis reactions Reactions were performed in the ITC cell (with

and without 400 rpm mixing) and after data collection, the samples were immediately quenched. This was achieved by taking a 1 mL sample, and pipetting 3 × 50 μL aliquots to 450 μL buffer with 500 μL BCA reagent, and the remaining 850 μL was quenched using 50 μL of 2 M Na₂CO₃. BCA and PAHBAH reducing sugar determination were carried out on the quenched aliquots. The effect of 2 M Na₂CO₃ on the substrate was checked by allowing contact over several hours before assaying, compared to a sample of RAC with freshly added 2 M Na₂CO₃. Protein controls were run to correct for BCA-protein interference.

Reducing ends assays to determine soluble and insoluble fractions The enzymes and 8 g/L RAC were pre-incubated separately in a thermomixer at 30 °C with no stirring and quenched immediately after 15 min of hydrolysis. The total reducing ends were immediately determined from the collected samples. Samples were then centrifuged and the supernatant filtered through a 0.22 μm filter to remove all insoluble matter before determination of soluble reducing ends products.

ITC hydrolysis monitoring. ITC was carried out using power-compensated equipment (Nano ITC^{2G} from TA Instruments, New Castle, DE, USA). The Nano ITC^{2G} has a gold cell of volume 0.957 mL. It has previously been reported that the rapid decrease in polymerization as a result of EG activity has a profound effect on the baseline in ITC experiments which may be corrected for manually (44). To overcome this limitation a new method has been developed. A stable baseline with no stirring is established, and then the enzyme is injected under maximum stirring and mixed for a total of 60 s. The stirring is then turned off and the hydrolysis monitored continuously. Standard conditions were as follows: 100 μL syringe, no stirring, 30 °C in 50 mM sodium acetate, 2 mM calcium chloride pH 5.0, and collection of data with a point every 2 s. All data has been corrected for heat of dilution and calibration factors (46,51,52).

ITC Depletion Experiments. The ITC cell was filled with degassed 800 μM COS 3, 4, or 5 in 50 mM sodium acetate, 2 mM calcium chloride pH 5.0. After thermal equilibration at 30 °C with 400 rpm stirring, 100 nM of enzyme was added. Data was collected every 2 s until the substrate was

depleted. The depletion of a soluble substrate monitored by ITC has often been used to determine kinetic constants (43,52-55) and the derivation of the equations used in this analysis (Fig. 6) is presented elsewhere (43).

Glucose measurements using an amperometric biosensor Preparation of an amperometric glucose biosensor and the electrochemical measurements were performed as described in (56) with a few minor modifications. Briefly, the glucose biosensor was based on a mediator-modified carbon paste electrode with surface immobilized and cross-linked glucose oxidase. After a stable baseline with 8 g/L RAC was established, an aliquot of enzyme was added to the 30 °C, temperature controlled, 4 mL reaction vessel stirred at 900 rpm. The current due to the enzymatic oxidation of glucose by the glucose oxidase-catalyzed reaction was recorded as a function of time.

All data analysis has been performed using Origin Pro V 8.0 and Sigmaplot V 11.

Results and Discussion

RAC The RAC substrate was determined to have a DP_N of 181 ± 9 , and the complete disappearance of the crystalline peak at C-4 in CP/MAS NMR was interpreted as producing a near completely amorphous substrate.

Reducing Ends Assays The PAHBAH and BCA assays were calibrated using both glucose (G1) and cellotetraose (G4) initially to determine the effect of soluble cello-oligosaccharide length on the spectrophotometric response. Both assays provided near identical calibration curves for the G1 and G4 standards; see Fig. 1, panel D. It was determined the PAHBAH assay was affected by the presence of mixtures of insoluble and soluble substrates, the two calibrations carried out in the absence and presence of RAC differing in slope values by a factor of 1.5. The BCA assay displayed no such bias, both glucose and cellotetraose calibrations in the presence and absence of RAC agreeing to within 5 %, and the recovery of 40 μ M cellotetraose with varied RAC background was complete, $96 \pm 3\%$. The BCA assay was approximately ten times more sensitive than the PAHBAH assay. The results from the BCA assay for measuring hydrolysis products are

shown in Fig.1 and Table 1 lists the soluble and insoluble reducing sugar equivalents determined.

Calibration It may be seen from Fig. 1 that there is a direct proportionality between the area under the ITC signal and the moles of reducing ends produced for each enzyme. The total activity, measured as the sum of both soluble and insoluble reducing sugar equivalents is thus measured continuously by the calorimeter. The slopes of the calibration plots, expressed in kJ/mol as the molar enthalpy of the reaction ($\Delta_{app}H$), are different for each enzyme with -1.7 kJ/mol measured for *TrCel7B*, -3.0 kJ/mol for *TrCel5A* and -5.4 kJ/mol *TrCel12A*. Clearly, the covalent change (hydrolysis of β -1,4 glycosidic bonds) is the same in all cases and the difference in the apparent enthalpy must rely on non-covalent interactions. Such interaction energies may be sizable for the breakdown of cellulose. Thus, the lattice energy of crystalline cellulose is about 25 kJ/(mol glucosyl unit) (57) and the energy changes associated with both the creation of a cavity in water that can accommodate a small oligosaccharide and the hydration of the dissolved sugar is in the 10-20 kJ/mol range and dependent on the size of the oligosaccharide (58,59). The three EGs tested here produce different profiles of products (Tab. 1, (45)), and this most likely accounts for the observed differences of a few kJ/mol in $\Delta_{app}H$. Comparisons of the apparent enthalpies in Fig. 1 and the product profile in Tab. 1 suggest that the enthalpy becomes less negative the smaller the average product size. This relationship may be used in future calorimetric product profiling, but it also calls for caution in prolonged calorimetric measurements with high degrees of conversion, where the product profile may shift as the process progresses.

The calorimetric data (Fig. 2) immediate shows that the rate of hydrolysis changes conspicuously even at very low conversion. Thus, if the results for *TrCel7B* (Fig. 2C) are normalized with respect to the enzyme concentration we find maximal a turnover of 15 - 20 s^{-1} . This value falls 5-10 fold (depending on the enzyme concentration) over the following 5 min although the total conversion at this point is only under 3-5 % for the maximum enzyme dose. *TrCel5A* also showed an initial burst with a 5-10 fold reduction in activity, but the maximal turnover for this enzyme was significantly lower (maximal rate 2.5 - 4 s^{-1}). For

TrCel12A the burst was weaker and the maximal reaction rate in the early part of the hydrolysis was only 3-4 times larger than the rate after 15 min. The enzyme also had the lowest absolute rate with a maximal turnover of 2.2 - 2.8 s⁻¹. Changes in reaction rate near the maximum are too rapid to be fully resolved by the ITC instrument. This smearing is due to the thermal inertia of the calorimetric vessel and it is conventionally corrected on the basis of the instrument time constants (60). This dynamic correction suggested that the maximum for *TrCel7B* occurred after 30-40 s and this is in accord with results from the biosensor measurements (Fig. 3), which showed that glucose production reached the maximal level after about 25 sec.

We suggest that the characteristic initial kinetics (the burst phase) illustrated in Fig. 2 is the origin of pronounced variation in kinetic parameters (particularly k_{cat}) found for EGs in the literature (c.f. Tab. 2). Thus, the rate may decrease strongly as the hydrolysis progresses, and end-point measurements obtained at different stages of the hydrolysis cannot be meaningfully converted to turn-over numbers or k_{cat} values. This conclusion is substantiated by further analysis of the data in Tab. 2. If the turnover number from different works using filter paper as substrate are plotted as a function of the experimental time, the course is close to a single-exponential decay ($R^2 = 0.93$), and this correlation occurs in spite of differences in temperature and experimental set-up. We conclude that kinetic analyses of EGs must include rapid and frequent data sampling over the first few minutes, and preferably be based on a continuous assay technology.

The kinetic behavior illustrated in Fig. 2 may be interpreted as an initial burst phase which subsequently falls off towards a nearly constant reaction rate, which reflects a (near) steady state situation with (nearly) constant concentrations of free enzyme and enzyme intermediates. This behavior is in contrast to simple enzyme kinetics, where the rate of product formation increases monotonously in the pre steady-state regime. Hence, the key question that arises from Fig. 2 is why this pronounced overshoot in reaction rate occurs. We suggest that the possible reasons for this can in principle be arranged into three groups. These are:

i) The burst may be linked to the degree of conversion. If, for example, the EG has a high activity towards certain structures in the insoluble substrate, and these good attack points are scarce, the rate of hydrolysis may decrease quickly as they are depleted as a result of topological changes in the substrate surface (surface-erosion). Other conversion-dependent causes for a slowdown include inhibition by accumulated product. (61-65)

ii) The burst may rely on the fact that both the insoluble substrate (in this case RAC) and some of the products (soluble cello-oligosaccharides (COS) of a certain DP) are substrates to the EGs. This may generate a complex interplay between the release (or initial presence) of COS and its rapid breakdown in the aqueous phase, where k_{cat} values may reach up to 50 - 100 s⁻¹ (45).

iii) Finally, the burst could depend on inactivation of enzyme. Irreversible inactivation, dependent on e.g. conventional protein stability issues would be expected to give a single exponential decay unlike the biphasic course in Fig. 2. A more likely interpretation is a reversible inactivation model where rapid hydrolysis prevails until the enzyme encounters some structure in the substrate (an "obstacle" or "trap"), which dictates a protracted (but finite) inactive period (13,14). In this case the activity is high over some initial period, but it will decrease as more and more enzyme gets stalled by obstacles. Eventually, when the population of inactivate enzyme approaches a constant (steady-state) level, the reaction rate will reach a constant (low) value.

To assess the importance of i) we first note that the highest concentration of soluble sugars in the current experiments is about 1-3 mM. This is much lower than reported product inhibition constants for the investigated enzymes (13,66,67), and it therefore seems unlikely that the slowdown depends on product inhibition. This reasoning is supported in Fig. 4, which shows that the addition of a second enzyme dose to a sample with about 0.5 mM product generates a second burst phase. The initial kinetic is re-established approximately 95 % of the original activity and there is 1 % conversion at this time, that is to say the two enzyme doses are kinetically identical within experimental boundaries. More importantly, this figure also shows that the slowdown cannot

depend on surface erosion or the depletion of good attack-points on the substrate. If there was erosion (or other factors making the substrate less reactive), adding more enzyme could not reestablish an equivalent burst for the second enzyme dosage. Taken together, we did not find evidence for a link between the slowdown after about 1 min and the degree of conversion (which is indeed very low at this stage).

With respect to ii) we first note that no background COS could be detected in the supernatant of centrifuged substrates, neither by BCA-analysis nor calorimetric measurements. We therefore rule out soluble COS in the substrate samples. The current results also speak against an initial release of hydrolysable COS (e.g. COS 4-6) and their subsequent rapid hydrolysis as the origin of the burst. This is seen, for example, from Tab. 1, which shows that *TrCel7B* (that shows the strongest burst) generates almost exclusively (97 %) soluble reducing ends. If the enzyme released COS as a "true endoglucanase" with hydrolysis of random glycosidic bonds; there would be a more pronounced production of insoluble reducing ends. The depletion experiments shown in Fig. 5 show that COS break-down, even at concentrations far in excess of those potentially found in the burst phase is not fast enough to account for the peaks in Fig. 2. Taking the 100 nM run from Fig.2 and Fig. 3, we see the rate of glucose production is 250 nM/s and the total rate from the ITC is far in excess of 1000 nM/s. The total rate of 1000 nM/s would require a COS concentration of over 200 μ M, based on Fig 6, this value cannot be reached given *TrCel7B* produces mainly cellobiose and glucose. The COS hydrolyses also produce significant amounts of glucose (measured by HPAEC and the biosensor). The latter implies a coupling of the glucose production and the total enzyme activity. However, a comparison of results from ITC and biosensor measurements (Fig.2 and Fig. 3) does not suggest a burst in glucose production that scales with the total activity. In conclusion, the current results do not suggest a link between the initial burst and rapid hydrolysis of soluble COS.

This leaves us with the reversible inactivation model sketched out under point *iii*). To evaluate this, we first assess the magnitude of the burst. This is done by empirically by defining 0-230 s in Fig. 2 as the burst phase. The area under the ITC-

curves in this time range (which quantify the amount of glycosidic bonds hydrolyzed during the burst) were found to scale proportionally to the enzyme concentration when the concentration of substrate was kept constant. The increments were 1239 ± 200 (n=18) for *TrCel7B*, 242 ± 38 (n=20) for *TrCel5A* and 280 ± 29 (n=5) for *TrCel12A*, respectively. These figures specify the number of catalytic cycles conducted by each enzyme molecule during the burst. If instead we varied the substrate concentration from 4 g/L to 6 g/L and 8 g/L, and maintained the concentration of *TrCel7B* at 200 nM, we found that the ITC-areas from 0 to 230 sec remained constant (data not shown). When normalizing these latter areas with respect to the enzyme concentration we again found 1332 ± 200 for *TrCel7B*. We conclude that under the investigated conditions the extent of the burst is proportional to the enzyme concentration and independent of the substrate concentration. This behavior is in perfect accord with the reversible inactivation model. Hence, in this picture each enzyme is predicted to perform a certain number of rapid cycles determined by the frequency of "traps" and not the concentration of substrate. For *TrCel5A* and *TrCel12A* this frequency is about 1:250 hydrolysable bonds and if the slowdown depends on reversible inactivation, changing the substrate concentration (as long as it is in excess) would not alter the average number of hydrolytic steps preceding the encounter with a "trap". For *TrCel7B*, the extent of the burst is significantly larger. This suggests that this enzyme is either less susceptible to reversible inactivation or that it has a preferential affinity for substrate regions with fewer "traps". The reversible inactivation model is also in line with the reestablished burst upon a second enzyme injection (Fig. 4) inasmuch as a new population of enzymes is predicted to run through the same initial phase as long as the substrate is in excess. We conclude that the observations concurrently support *iii*).

A similar course of burst and inactivation has previously been suggested for processive exoglucanases (11,12,14,66,68). *TrCel6A*, formerly cellobiohydrolase II (CBH) II, (36) has two loops enclosing the active site, one of which can move, allowing for endo-attack initiation on insoluble substrates (69,70). *TrCel6A* is classified as an endo-processive enzyme (12), being able to degrade CMC, HEC and bacterial cellulose in an endo fashion (71,72). Similar claims have been

made for *TrCel7A* (formerly CBH I (73)), with a recorded 90 % *endo*-attack initiation on amorphous substrates recently being recorded . There are four loops enclosing the catalytic domain of *TrCel7A*, which are shortened on *TrCel7B* (14,74). The processivity of the *endo*-glucanases investigated here remains to be fully elucidated, but under the conventional definition (3,4), EGs hydrolyze randomly and are as such non-processive. However, strict boundaries between *endo*- and (processive) *exo*-cellulases are becoming blurred as their mode of action is better elucidated.

The processivity under the current experimental conditions may be approximated from the ratio of soluble and insoluble reducing ends (75-78). This analysis suggests (Tab 1) that *TrCel7B* shows pronounced processivity on RAC (33) while the other enzymes appears to perform only a few (4-6) sequential steps on the same strand. A recent analysis of *endo*-processivity on *TrCel5A* and *TrCel12A* has reported apparent processivity values very close to this 3-5 (14). Our analysis should be considered an indication only, as the product profiles change over time and the concentration of soluble reducing ends may rely on both processive enzyme action and the hydrolysis of soluble COS produced non-processively. Nevertheless, these numbers demonstrate that all three EGs (*TrCel7B* in particular) show some degree of processivity and hence do not attack accessible glycosidic bonds randomly.

In conclusion we have found that the three most common endoglucanases from *T. reesei* exhibit a pronounced non-monotonic initial activity on amorphous cellulose with a maximum after about 0.5 - 1 min. Subsequently, the enzymatic turnover decreases 2-10 fold over a few minutes as the reaction appears to enter a (near) steady-state condition. This maximum (or burst) must be taken into account in kinetic analysis of EG, and we suggest that the pronounced variation in reported values of *e.g.* k_{cat} based on end-point measurements could depend on the failure to do so. This aspect is particularly relevant when estimates of kinetic constants are used in functional models for the break-down of cellulose (c.f.(79-81)), and the results in Fig. 2 and Tab 2 show that parameters estimated at different time scales may vary by orders of magnitude (Fig.2

Tab. 2). On the basis of complementary experimental data we suggest that that the burst reflects a balance between rapid hydrolysis with moderate processivity on one hand and the transient inactivation of enzyme on the other. The mechanism of the temporary inactivation cannot be assessed, but we note that the interpretation is in line with the notion of non-productively bound enzyme, which has been repeatedly discussed for cellulases (11,12,14,66,68). The number of catalytic cycles in the burst phase was much higher (about 2 orders of magnitude) than processivity for all three enzymes. This implies that upon addition to the substrate, the EG will perform many (tens or hundreds) *endo*-processive runs at a turnover rate that is over 20 s⁻¹ for *TrCel7B*. It follows, that unlike earlier interpretations for *exo*-cellulases (11,13,14,62), the early slowdown for the enzymes studied here, is not necessarily linked to processivity. As the process progresses, an increasing population of the enzyme gets randomly trapped in unproductive positions for extended periods and the turnover rates consequently begins to fall. After several minutes the trapped population approaches a constant level and the turnover rate levels off towards a constant value well below the maximum. At this stage the rate limiting step is the release from the non-productively bound position. We stress that this interpretation only pertains to the strong initial reduction in hydrolytic which is studied here. Longer trials with significant changes in the structure and amounts of substrate and concentration of soluble products are likely to be affected by a range of other inhibitory mechanisms. In a wider perspective, this interpretation is analogous to the original description of burst-phase kinetics over 50 years ago (82). This work pointed out that an ordered two-step (bi-bi) enzyme reaction could produce an initial burst if the first product is released from the enzyme complex faster than the second. Obviously the EG reactions studied here are more complex, but the basic course for the initial maximum in the turnover rate may result from an ordered sequence of a rapid (*endo*-processive hydrolysis) and a slower (release from non-productively bound positions) process.

REFERENCES

1. Henrissat, B. (1991) *Biochem. J.* **280**, 309-316
2. Rabinovich, M. L., Melnik, M. S., and Boloboba, A. V. (2002) *Appl. Biochem. Microbiol.* **38**, 305-321
3. Lynd, L. R., Weimer, P. J., van Zyl, W. H., and Pretorius, I. S. (2002) *Microbiol. Mol. Biol. Rev.* **66**, 506-577
4. Zhang, Y. H. P., and Lynd, L. R. (2004) *Biotechnol. Bioeng.* **88**, 797-824
5. Barr, B. K., Hsieh, Y. L., Ganem, B., and Wilson, D. B. (1996) *Biochemistry* **35**, 586-592
6. Cao, Y., and Tan, H. (2002) *Carbohydr. Res.* **337**, 1291-1296
7. Valjamae, P., Sild, V., Pettersson, G., and Johansson, G. (1998) *Eur. J. Biochem.* **253**, 469-475
8. Lee, Y. H., and Fan, L. T. (1983) *Biotechnol. Bioeng.* **25**, 939-966
9. Xiao, Z. Z., Zhang, X., Gregg, D. J., and Saddler, J. N. (2004) *Appl. Biochem. Biotechnol.*, 1115-1126
10. Eriksson, T., Borjesson, J., and Tjerneld, F. (2002) *Enzyme. Microb. Technol.* **31**, 353-364
11. Jalak, J., and Valjamae, P. (2010) *Biotechnol. Bioeng.* **106**, 871-883
12. Kipper, K., Valjamae, P., and Johansson, G. (2005) *Biochem. J.* **385**, 527-535
13. Praestgaard, E., Elmerdahl, J., Murphy, L., Nymand, S., McFarland, K. C., Borch, K., and Westh, P. (2011) *FEBS J.* **278**, 1547-1560
14. Kurasin, M., and Valjamae, P. (2011) *J. Biol. Chem.* **286**, 169-177
15. Penttila, M., Lehtovaara, P., Nevalainen, H., Bhikhabhai, R., and Knowles, J. (1986) *Gene* **45**, 253-263
16. Saloheimo, M., Lehtovaara, P., Penttila, M., Teeri, T. T., Stahlberg, J., Johansson, G., Pettersson, G., Claeysens, M., Tomme, P., and Knowles, J. K. C. (1988) *Gene* **63**, 11-21
17. Sandgren, M., Shaw, A., Ropp, T. H., Bott, S. W. R., Cameron, A. D., Stahlberg, J., Mitchinson, C., and Jones, T. A. (2001) *J. Mol. Biol.* **308**, 295-310
18. Divne, C., Sinning, I., Stahlberg, J., Pettersson, G., Bailey, M., Siikaaho, M., Margollesclark, E., Teeri, T., and Jones, T. A. (1993) *J. Mol. Biol.* **234**, 905-907
19. Stahlberg, J., Johansson, G., and Pettersson, G. (1988) *Eur. J. Biochem.* **173**, 179-183
20. Nakazawa, H., Okada, K., Onodera, T., Ogasawara, W., Okada, H., and Morikawa, Y. (2009) *Appl. Microbiol. Biotechnol.* **83**, 649-657
21. Okada, H., Mori, K., Tada, K., Nogawa, M., and Morikawa, Y. (2000) *J. Mol. Catal. B-Enzym.* **10**, 249-255
22. Bayer, E. A., Chanzy, H., Lamed, R., and Shoham, Y. (1998) *Curr. Opin. Struct. Biol.* **8**, 548-557
23. Miller, G. L. (1959) *Anal. Chem.* **31**, 426-428
24. Lever, M. (1972) *Anal. Biochem.* **47**, 273-&
25. Lever, M. (1973) *Biochem. Med.* **7**, 274-281
26. Nelson, N. (1944) *J. Biol. Chem.* **153**, 375-380
27. Somogyi, M. (1952) *J. Biol. Chem.* **195**, 19-23
28. Anthon, G. E., and Barrett, D. M. (2002) *Anal. Biochem.* **305**, 287-289
29. Doner, L. W., and Irwin, P. L. (1992) *Anal. Biochem.* **202**, 50-53
30. Sharrock, K. R. (1988) *J. Biochem. Biophys. Methods* **17**, 81-105
31. Coward-Kelly, G., Aiello-Mazzari, C., Kim, S., Granda, C., and Holtzapple, M. (2003) *Biotechnol. Bioeng.* **82**, 745-749
32. Sengupta, S., Jana, M. L., Sengupta, D., and Naskar, A. K. (2000) *Appl. Microbiol. Biotechnol.* **53**, 732-735
33. Miller, G. L., Blum, R., Glennon, W. E., and Burton, A. L. (1960) *Anal. Biochem.* **1**, 127-132
34. Lee, J. M., Heitmann, J. A., and Pawlak, J. J. (2007) *BioResources* **2**, 20-33

35. Joos, P., Sierens, W., and Ruysen, R. (1969) *J. Pharm. Pharmacol.* **21**, 848-&
36. Rouvinen, J., Bergfors, T., Teeri, T., Knowles, J. K. C., and Jones, T. A. (1990) *Science* **249**, 380-386
37. Vlasenko, E. Y., Ryan, A. I., Shoemaker, C. F., and Shoemaker, S. P. (1998) *Enzyme. Microb. Technol.* **23**, 350-359
38. Mullings, R. (1985) *Enzyme. Microb. Technol.* **7**, 586-591
39. Zhang, Y. H. P., Himmel, M. E., and Mielenz, J. R. (2006) *Biotechnol. Adv.* **24**, 452-481
40. Eveleigh, D. E., Mandels, M., Andreotti, R., and Roche, C. (2009) *Biotechnol. Biofuels* **2**, 8
41. Child, J. J., Eveleigh, D. E., and Sieben, A. S. (1973) *Can. J. Biochem.* **51**, 39-43
42. Todd, M. J., and Gomez, J. (2001) *Anal. Biochem.* **296**, 179-187
43. Olsen, S. N. (2006) *Thermochim. Acta* **448**, 12-18
44. Murphy, L., Borch, K., McFarland, K. C., Bohlin, C., and Westh, P. (2010) *Enzyme. Microb. Technol.* **46**, 141-146
45. Karlsson, J., Siika-aho, M., Tenkanen, M., and Tjerneld, F. (2002) *J. Biotechnol.* **99**, 63-78
46. Murphy, L., Baumann, M. J., Borch, K., Sweeney, M., and Westh, P. (2010) *Anal. Biochem.* **404**, 140-148
47. Dubois, M., Gilles, K. A., Hamilton, J. K., Rebers, P. A., and Smith, F. (1956) *Anal. Chem.* **28**, 350-356
48. Zhang, Y. H. P., and Lynd, L. R. (2005) *Biomacromolecules* **6**, 1510-1515
49. Matulova, M., Nouaille, R., Capek, P., Pean, M., Delort, A. M., and Forano, E. (2008) *FEBS J.* **275**, 3503-3511
50. Zhang, Y. H. P., and Lynd, L. R. (2003) *Anal. Biochem.* **322**, 225-232
51. Briggner, L. E., and Wadsö, I. (1991) *J. Biochem. Biophys. Methods* **22**, 101-118
52. Jeoh, T., Baker, J. O., Ali, M. K., Himmel, M. E., and Adney, W. S. (2005) *Anal. Biochem.* **347**, 244-253
53. Bohlin, C., Olsen, S. N., Morant, M. D., Patkar, S., Borch, K., and Westh, P. (2010) *Biotechnol. Bioeng.* **107**, 943-952
54. Karim, N., Okada, H., and Kidokoro, S. (2005) *Thermochim. Acta* **431**, 9-20
55. Karim, N., and Kidokoro, S. (2004) *Thermochim. Acta* **412**, 91-96
56. Tatsumi, H., and Katano, H. (2005) *Journal of Agricultural and Food Chemistry* **53**, 8123-8127
57. Calvet, E., and Hermans, P. H. (1951) *Journal of Polymer Science* **6**, 33-38
58. Dale, B. E., and Tsao, G. T. (1982) *J. Appl. Polym. Sci.* **27**, 1233-1241
59. Taylor, J. B. (1957) *Transactions of the Faraday Society* **53**, 1198-1203
60. Loblich, K. R. (1994) *Thermochim. Acta* **231**, 7-20
61. Igarashi, K., Wada, M., Hori, R., and Samejima, M. (2006) *FEBS J.* **273**, 2869-2878
62. Eriksson, T., Karlsson, J., and Tjerneld, F. (2002) *Appl. Biochem. Biotechnol.* **101**, 41-60
63. Nidetzky, B., and Steiner, W. (1993) *Biotechnol. Bioeng.* **42**, 469-479
64. Zhang, S., Wolfgang, D. E., and Wilson, D. B. (1999) *Biotechnol. Bioeng.* **66**, 35-41
65. Yang, B., Willies, D. M., and Wyman, C. E. (2006) *Biotechnol. Bioeng.* **94**, 1122-1128
66. Gruno, M., Valjamae, P., Pettersson, G., and Johansson, G. (2004) *Biotechnol. Bioeng.* **86**, 503-511
67. Holtzapple, M. T., Caram, H. S., and Humphrey, A. E. (1984) *Biotechnol. Bioeng.* **26**, 753-757
68. Valjamae, P., Pettersson, G., and Johansson, G. (2001) *Eur. J. Biochem.* **268**, 4520-4526
69. Breyer, W. A., and Matthews, B. W. (2001) *Protein Sci.* **10**, 1699-1711
70. Zou, J. Y., Kleywegt, G. J., Stahlberg, J., Driguez, H., Nerinckx, W., Claeysens, M., Koivula, A., Teerii, T. T., and Jones, T. A. (1999) *Struct. Fold. Des.* **7**, 1035-1045
71. KlemanLeyer, K. M., SiikaAho, M., Teeri, T. T., and Kirk, T. K. (1996) *Appl. Environ. Microbiol.* **62**, 2883-2887
72. Bailey, M. J., Siikaaho, M., Valkeajarvi, A., and Penttila, M. E. (1993) *Biotechnol. Appl. Biochem.* **17**, 65-76
73. Shoemaker, S., Watt, K., Tsitovsky, G., and Cox, R. (1983) *Bio-Technology* **1**, 687-690
74. Mackenzie, L. F., Sulzenbacher, G., Divne, C., Jones, T. A., Woldike, H. F., Schulein, M., Withers, S. G., and Davies, G. J. (1998) *Biochem. J.* **335**, 409-416
75. Zhang, S., Irwin, D. C., and Wilson, D. B. (2000) *Eur. J. Biochem.* **267**, 3101-3115

76. Irwin, D. C., Spezio, M., Walker, L. P., and Wilson, D. B. (1993) *Biotechnol. Bioeng.* **42**, 1002-1013
77. Zhou, W. L., Irwin, D. C., Escovar-Kousen, J., and Wilson, D. B. (2004) *Biochemistry* **43**, 9655-9663
78. Watson, B. J., Zhang, H. T., Longmire, A. G., Moon, Y. H., and Hutcheson, S. W. (2009) *J. Bacteriol.* **191**, 5697-5705
79. Levine, S. E., Fox, J. M., Blanch, H. W., and Clark, D. S. (2010) *Biotechnol. Bioeng.* **107**, 37-51
80. Peri, S., Karra, S., Lee, Y. Y., and Karim, M. N. (2007) *Biotechnol. Prog.* **23**, 626-637
81. Zhang, Y. H. P., and Lynd, L. R. (2006) *Biotechnol. Bioeng.* **94**, 888-898
82. Hartley, B. S., and Kilby, B. A. (1954) *Biochem. J.* **56**, 288-297
83. Ryu, D. D. Y., Kim, C., and Mandels, M. (1984) *Biotechnol. Bioeng.* **26**, 488-496
84. Nikupaavola, M. L., Lappalainen, A., Enari, T. M., and Nummi, M. (1985) *Biochem. J.* **231**, 75-81
85. Henrissat, B., Driguez, H., Viet, C., and Schulein, M. (1985) *Bio-Technology* **3**, 722-726
86. Baker, J. O., Ehrman, C. I., Adney, W. S., Thomas, S. R., and Himmel, M. E. (1998) *Appl. Biochem. Biotechnol.* **70-2**, 395-403
87. Nidetzky, B., Steiner, W., and Claeysens, M. (1994) *Biochem. J.* **303**, 817-823

FOOTNOTES

This work was supported by the Danish Agency for Science, Technology and Innovation (grant # 2104-07-0028 to PW) and the Carlsberg Foundation. We thank Erik Lumby Rasmussen for excellent technical assistance.

Abbreviations used are: EG, endo-glucanase, CBH, cellobiohydrolase, CMC, carboxymethyl cellulose, HEC, hydroxyethyl cellulose, CBM, carbohydrate binding module, ITC, isothermal titration calorimetry, PAHBAH, *p*-hydroxy benzoic acid hydrazide, HPAEC-PAD, High Performance Anion Exchange Chromatography with Pulsed Amperometric Detection, BCA, 2,2' Bicinchoninic acid, AZCL-HE-cellulose, Azurine-Crosslinked hydroxyethyl cellulose, RAC, regenerated amorphous cellulose, COS, cello-oligosaccharide, CP/MAS NMR cross-polarization/magic angle spinning nuclear magnetic resonance, GH, glycoside hydrolase.

FIGURE LEGENDS

Figure 1. Calibration Data. A-C Shown are the calibration plots to determine $\Delta_{app}H$ for each enzyme. Data on the ordinate is integrated values from the ITC runs shown in Fig.2, the data on the abscissa has been measured using the BCA assay on the same samples. All analyses are performed on 8 g/L RAC, 30 °C, pH 5.0. **Panel A** Varied doses (200-1000 nM) of *TrCel5A* added to RAC. **Panel B** Varied doses of (100-500 nM) *TrCel12A* added to RAC. **Panel C** Varied doses of *TrCel7B* (100-500 nM) added to 8g/L RAC. In both A and C the different symbols represent runs on different batches of substrate. **Panel D.** Calibration of the reducing ends assays with glucose (open symbols) and cellotetraose (closed symbols) for BCA (circles) and PAHBAH (triangles). μmol values in A, B and C were measured in triplicate, the CV was under 5% in all cases (error bars not shown). From the slopes: $\Delta_{app}H$ of *TrCel7B* = -1.7 kJ/mol, *TrCel5A* = -3.0 kJ/mol and *TrCel12A* = -5.4 kJ/mol.

Figure 2. ITC Data. (L-R) Varied doses of *TrCel12A*, *TrCel5A* and *TrCel7B* added to 8 g/L RAC at 30 °C, pH 5.0. The raw data ($\mu\text{J/S}$) has been converted to nM/s using the $\Delta_{app}H$ determined from Fig. 1. Here the distinctive burst of all three EGs is evident.

Figure 3. Biosensor Data. (L) Varied doses of *TrCel7B* added to 8 g/L RAC, pH 5.0, 30 °C, monitored for glucose production only. **(R)** The raw data has been converted to a rate by differentiating. Shown are the first 110 s, depicting a constant production of glucose for all doses after 25 s.

Figure 4. ITC Data (exothermic up) (L) A double injection analysis. 75 nM *TrCel7B* is injected to 8 g/L RAC at 30 °C, pH 5.0 at $t = 0$ s, and again at $t = 1100$ s. **(R)** Extrapolation of the baselines and plotting the curves on top of each other for comparison. Dashed line = injection at $t = 0$ s, solid line = injection at $t = 1100$ s. The relative areas have been calculated by integrating the peaks.

Figure 5. ITC Data (exothermic down) (L) 100 nM of *TrCel7B* is titrated to 800 μM COS 5 (solid line) or COS 4 (dashed line) at 30 °C at 400 rpm. The return to the baseline indicates the substrate has been completely hydrolyzed.**(R)** The raw data has been converted to rates and substrate concentrations using the $\Delta_{app}H$ measured from Fig.2. Note there can be no meaningful kinetic constants derived as we appear to be under the K_M value for both COS 5 and 4, given there is no V_{max} reached. Previously reported values have varied from μM (45) to mM (16), so this is not unreasonable.

TABLES

Table 1. Total soluble and insoluble reducing ends of *TrEG*'s determined using BCA. Product profile determined using HPAEC-PAD. n.d. = not detected.

Hydrolysis was carried out for 15 min in a thermomixer at 30 °C, pH 5.0 with no stirring, and stopped aliquots measured for soluble (centrifuged and filtered) and total (prior to separation of solid and liquid phases) reducing sugar equivalents.

Enzyme	<i>Soluble reducing ends</i> <i>Total Reducing Ends</i>	Soluble Cello-oligosaccharide profile (fraction)					
		G1	G2	G3	G4	G5	G6
100 nM <i>TrCel7B</i>	0.97 ± 0.06	0.29	0.69	0.02	n.d.	n.d.	n.d.
200 nM <i>TrCel5A</i>	0.71 ± 0.05	0.18	0.44	0.29	0.09	n.d.	n.d.
100 nM <i>TrCel12A</i>	0.82 ± 0.06	0.09	0.45	0.20	0.25	n.d.	n.d.

Table 2. Summary of some reported kinetic measurements for *TrEG*s action on cellulose.

Enzyme	Temp.	Substrate/incubation time	Turnover	Ref.
<i>TrEG</i>	50 °C	Filter paper/1 h	0.14 s ⁻¹	(83)‡
<i>TrEG</i>	50 °C	Amorphous Cellulose/20 h	2.8 s ⁻¹	(84) ‡
<i>TrCel7B</i>	45 °C	Avicel/30 min	0.13 s ⁻¹	(73) ‡
		Amorphous Cellulose/30 min	19.95 s ⁻¹	
<i>TrCel7B</i>	40 °C	Avicel/8 h	0.004 s ⁻¹	(85) ‡
		Filter paper/8 h	0.002 s ⁻¹	
<i>TrCel7B</i>	50 °C	Avicel/120 h	0.45 s ⁻¹	(86) ‡
<i>TrCel7B</i>	50 °C	Filter Paper/40 min	0.92 s ⁻¹	(87) ‡
<i>TrCel5A</i>	50 °C	Filter Paper/40 min	0.46 s ⁻¹	
<i>TrCel7B</i>	25 °C	Amorphous Cellulose/5-10 s	20 s ⁻¹	(66)†
<i>TrCel5A</i>	25 °C	Amorphous Cellulose/5 – 10 s	8 s ⁻¹	

† These are values reported directly in the article.

‡ These are values calculated based on values reported in μmol/mg/min in (4) and for the purposes of calculation *TrCel7B* calculations were based on based on Mw = 46032 Da, *TrCel5A* Mw = 42185 Da.

FIGURE 1.

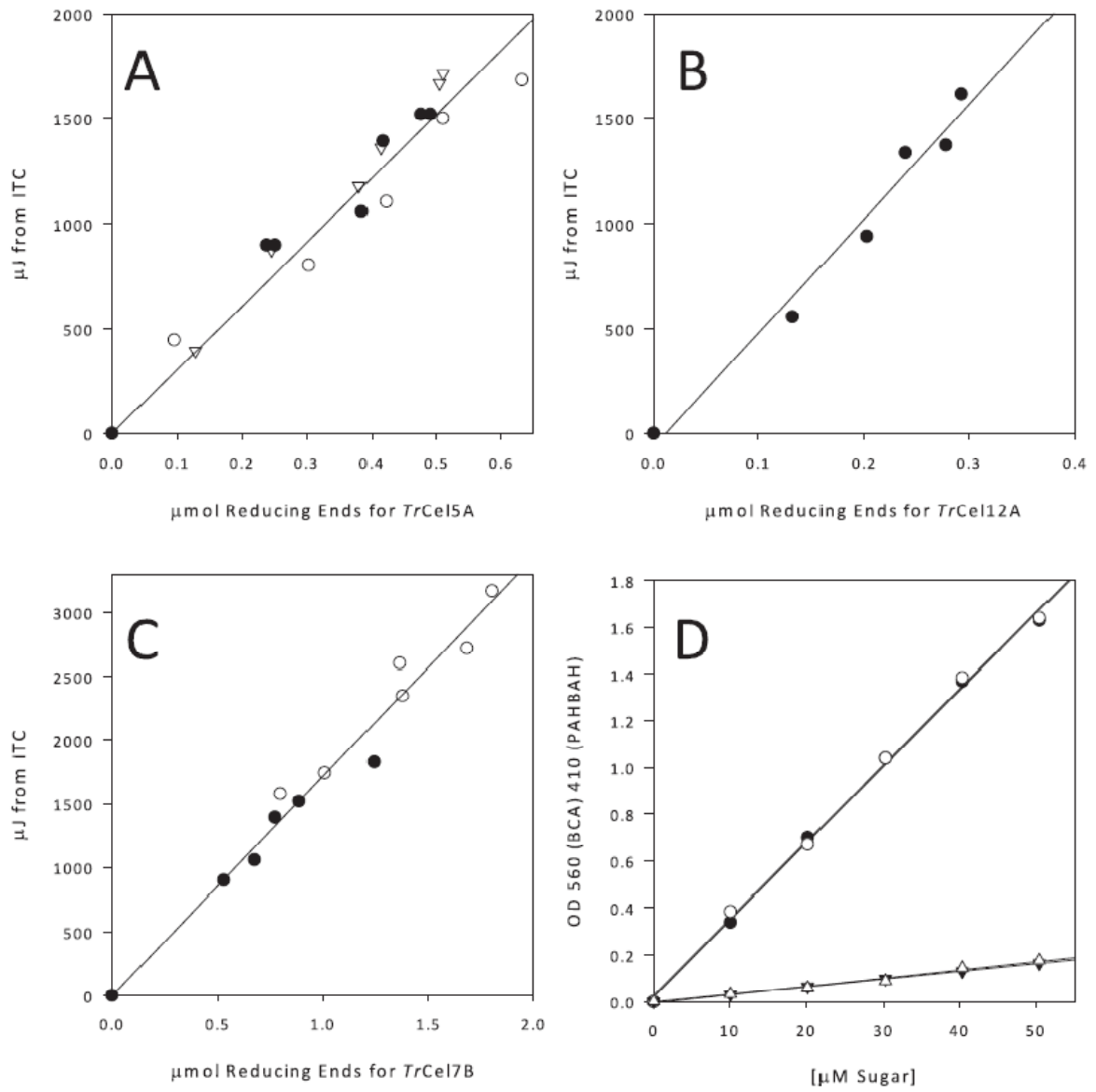


FIGURE 2.

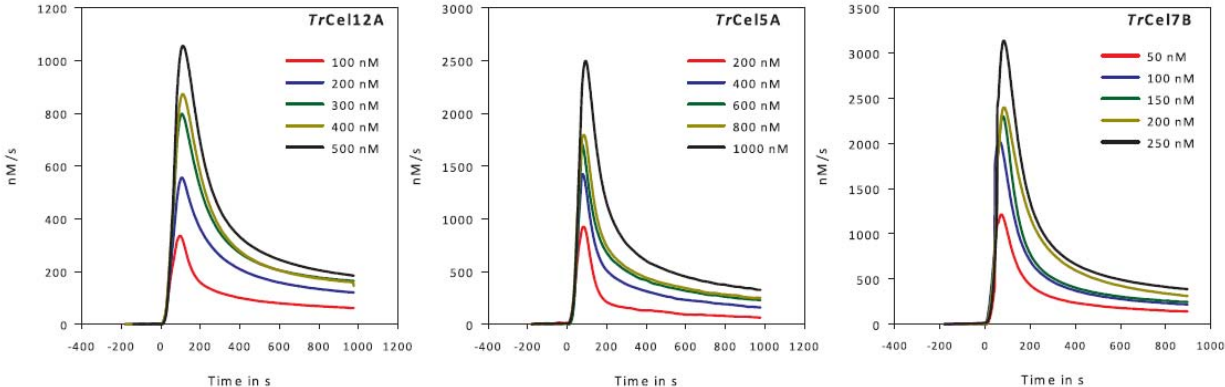


FIGURE 3.

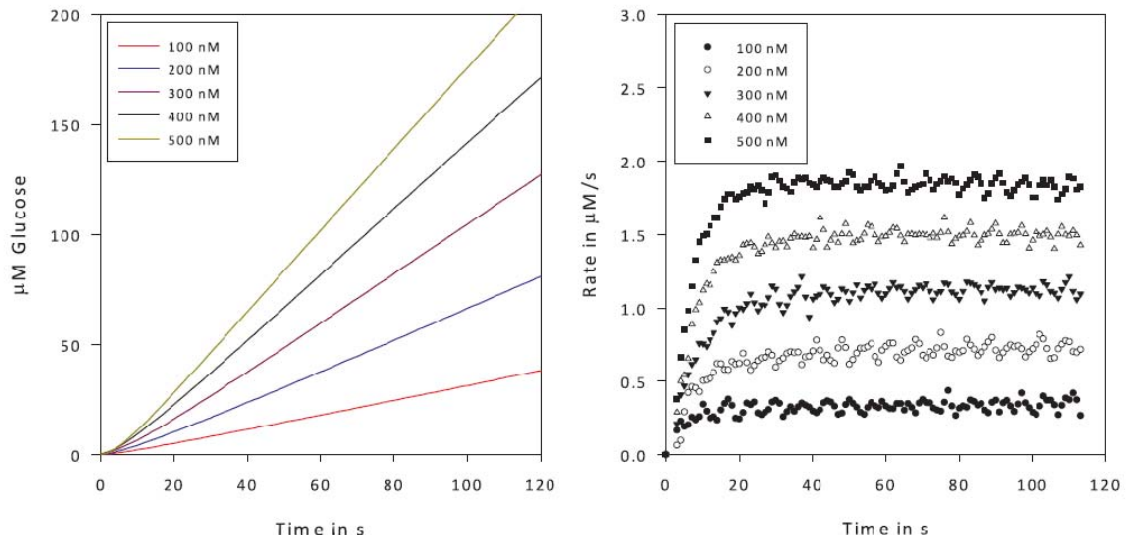


FIGURE 4.

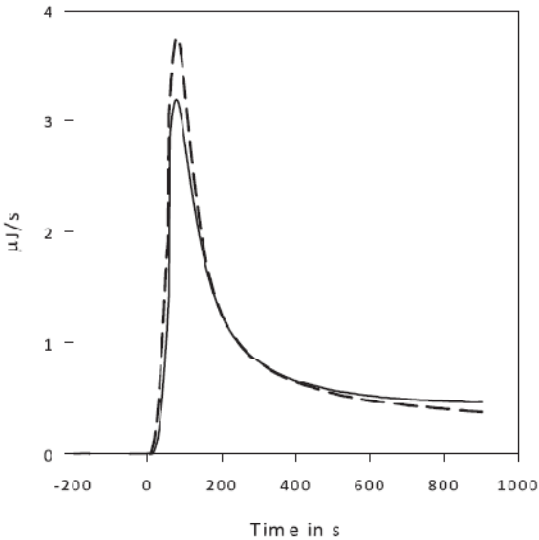
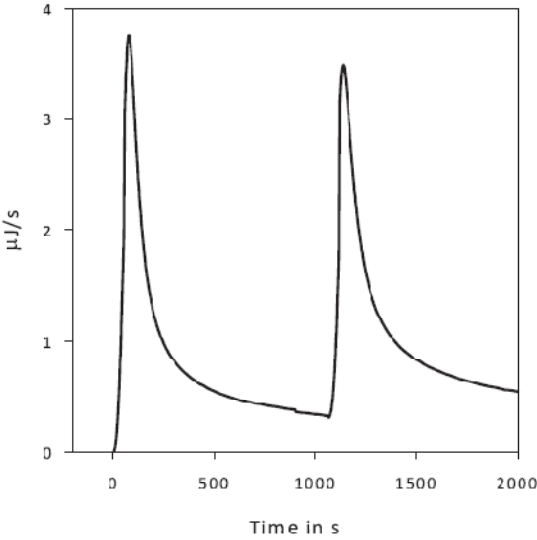
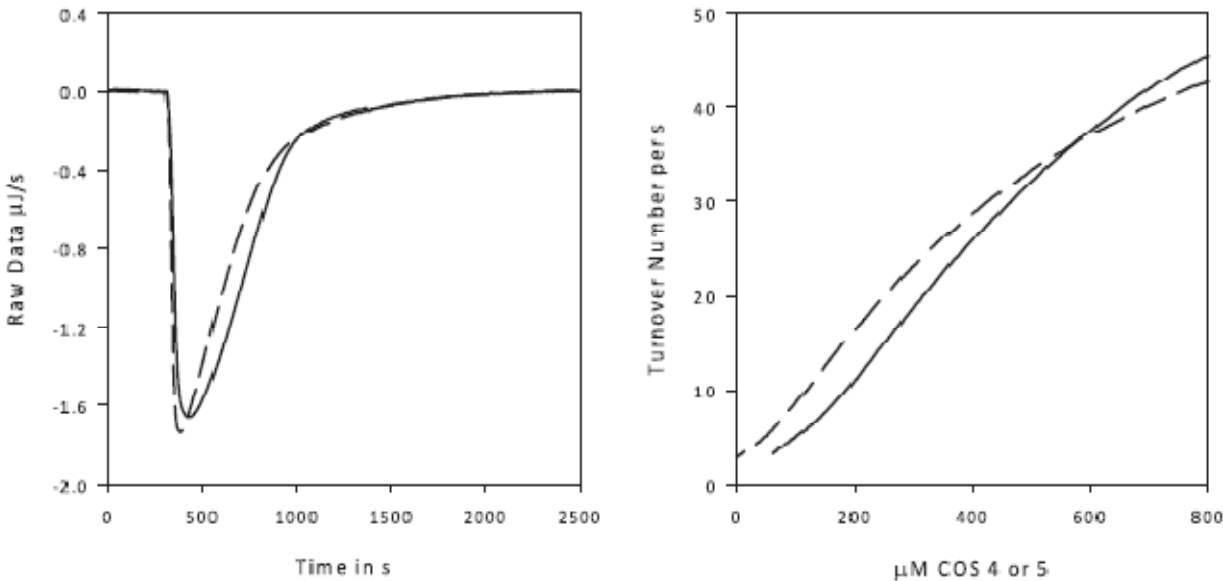


FIGURE 5.



Article 4: Product inhibition of *T. reesei* endoglucanases.

Leigh Murphy, Kim Borch, Peter Westh.

Product inhibition of *T. reesei* endoglucanases.

Leigh Murphy¹, Kim Borch², & Peter Westh^{1*}.

¹Roskilde University, NSM, Biomaterials, 1 Universitetsvej, DK-4000, Roskilde, Denmark. ²Novozymes A/S,
Krogshøjvej 36, DK-2880, Denmark,

*Corresponding author. Email: pwesth@ruc.dk Fax: +45 4674 3011

Abstract

Product inhibition has long been deemed one of the most critical factors in the slowdown of biomass hydrolysis. Many investigations have been conducted into elucidating this rate retardation, empirically, or using complex kinetic models. These studies have been conducted primarily using crude preparations or commercial mixed cellulase products, and many investigated on lignocellulosic substrates. While this is of interest to Industry, to model a mixture of enzymes and their action on a complex insoluble biomass substrate cannot pinpoint the weak links in cellulose hydrolysis. We propose the necessity of investigating the individual enzymes on a fundamental level first, in order to assess the level of inhibition displayed by each component of the cellulase complex. Only when this has been accomplished will it then be possible to identify which of the cellulase components are limited by product build-up on an industrial scale. Here we report a new method to monitor the inhibition of *T. reesei* endoglucanases, *TrCel7B* (EG I), *TrCel5A* (EG II) and *TrCel12A* (EG III). Through the use of an amorphous insoluble cellulose substrate, and industrially relevant concentrations of glucose and cellobiose, we present new insights into EG sensitivity to product inhibition. All three EG's are largely unaffected by glucose, while cellobiose is determined to be a more potent inhibitor. The concentration of product at which the hydrolysis rate is halved ($V_{0.5}$) is 113 ± 6 mM cellobiose and 2.67 ± 0.21 M glucose for *TrCel5A*, 118 ± 22 mM cellobiose and < 200 mM glucose for *TrCel12A*, whereas *TrCel7B* displays a non-uniform inhibition pattern, initially inhibited but lessening over time.

Keywords

Endoglucanase, Inhibition, *T. reesei*, Isothermal titration calorimetry.

Background The slowdown of cellulose hydrolysis is of primary concern to making second generation bio-ethanol commercially viable (Wyman 2007). A typical lignocellulose enzymatic hydrolysis generates 50 % of the available glucose in the first 8 h, but then takes up to 96 h to reach yields over 85 % glucose (Xiao et al. 2004). This slowdown has been ascribed to a variety of factors, either substrate or enzyme related (Lynd et al. 2002; Rabinovich et al. 2002; Zhang and Lynd 2004). Lignin, present after pretreatment (Mosier et al. 2005) has been reported to inhibit enzyme action on lignocellulose, proposed to be a result of non specific interactions between the enzyme and lignin fractions (Berlin et al. 2006). Baumann et al. 2011 demonstrated that xylan oligosaccharides generated from xylan can significantly reduce the activity of the most abundant *T. reesi* cellobiohydrolase *TrCel7A* (Baumann et al, in preparation). The recalcitrance of the cellulose substrate itself has been associated with the crystallinity (I_{cr}), the degradation into less a hydrolysable cellulose structure, or changes in the accessible surface area and thus a change in the overall enzyme to substrate ratio (Eriksson et al. 2002; Fan and Lee 1983; Hall et al. 2010; Lee and Fan 1982; Lee and Fan 1983; Zhu et al. 2009). Enzymatic slowdown has also been attributed to product inhibition, jamming of the cellulases on the substrate surface, or other deactivation mechanisms of the enzymes, either by non productive ES complex formation or denaturation over time (Andric et al. 2010; Asenjo 1983; Gruno et al. 2004; Gusakov and Sinitsyn 1992; Holtzapple et al. 1990; Holtzapple et al. 1984b; Praestgaard et al. 2011). Product inhibition has become more of a focus in recent times due to the higher concentrations present in high solids (> 10 % dry weight) hydrolysis reactions (Olsen et al. 2010). Here we investigate product inhibition of cellobiose and glucose on endoglucanases.

The enzymatic degradation of cellulose involves three types of glycoside hydrolase (GH) (Henrissat 1991). The endoglucanases, Endo-1,4- β -D-glucan-4-glucanohydrolases (EG) (EC 3.2.1.4) attack randomly on amorphous regions rapidly decreasing the degree of polymerization, producing new reducing and non-reducing ends (Cao and Tan 2002). The cellobiohydrolases, (CBH I and II) (EC 3.2.1.91) cleave mainly cellobiose from these reducing and non-reducing ends, respectively (Barr et al. 1996), and BG,

β -D-glucoside glucohydrolase (cellobiase) (EC 3.2.1.21) hydrolyzes the cellobiose to glucose (Bohlin et al. 2010). Inhibition of BG has been well reported and is not the focus of the current work (Bohlin et al. 2010; Decker et al. 2000; Decker et al. 2001; Jeoh et al. 2005).

We present a new method to directly monitor the inhibition of endoglucanases. The focus is on a study of the action of the three main EG's produced by *Hypocrea jecorina* (Anamorph: *Trichoderma reesei*) (Zhang and Lynd 2004), which belong to glycoside hydrolase families 7 (*TrCel7B*) (Penttila et al. 1986) 5 (*TrCel5A*) (Saloheimo et al. 1988), and 12 (*TrCel12A*) (Sandgren et al. 2001) respectively. The addition of typical hydrolysis products such as cellobiose and glucose will provide a large reducing end background to traditional EG assays (Anthon and Barrett 2002; Doner and Irwin 1992; Ghose 1987; Lever 1972; Lever 1973; Miller 1959; Nelson 1944; Somogyi 1952) , making product inhibition studies without modifying the substrate difficult, and dye substituted cellulose derivatives with bulky dye groups (Gusakov and Sinitsyn 1992; Holtzapple et al. 1990; Holtzapple et al. 1984b) may also affect the rates of EG hydrolysis.

Cellulose itself is a complex heterogeneous, insoluble substrate, and enzyme-substrate interactions do not follow typical Michaelis-Menten kinetics (Holtzapple et al. 1984a; Holtzapple et al. 1984c; Lee and Fan 1982; Lee and Fan 1983; Murphy et al. 2010b). Many product inhibition studies have been limited to crude preparations and mixes of cellulases (Andric et al. 2010; Bezerra and Dias 2005; Frennesson et al. 1985; Scheiding et al. 1984; Takagi 1984; Xiao et al. 2004), which inherently describe a system of at least three enzymes' action on substrate acting in synergy. These analyses either treat cellulases as a single enzyme or divide them into EGs and CBHs without distinguishing between the particular enzymes of each class. While this can provide a rudimentary guide to overall inhibition, there can be no identification of a single weak link in the mixture, or no real quantification of which sugar inhibits which enzyme and by how much.

There have been very few product inhibition studies on mono-component cellulase enzymes. Bezerra and co-workers (Bezerra and Dias 2004; Bezerra and Dias 2005) have investigated cellobiose inhibition of *TrCel7A* (CBH I), Zhao and co-workers (Zhao et al. 2004) have investigated cellobiose inhibition of

Trichoderma pseudokoningii Cel7A (although in the presence of *TpCel7B*), and Gruno and co-workers (Gruno et al. 2004), have investigated the inhibition of the primary mono components of the *T. reesei* system, and is perhaps the most comprehensive investigation of *T. reesei* cellulases product inhibition to date. This does not include inhibition studies conducted using soluble substrates, such as pNPL (Claeyssens et al. 1989; Vantilbeurgh and Claeyssens 1985) or pNPG (Decker et al. 2000; Decker et al. 2001), as these have been shown to be subject to a different type of inhibition, which may be seen in the large difference in reported K_i 's determined using soluble and insoluble substrates. For *TrCel7A*, small soluble substrates report competitive inhibition in the 20 μ M (Claeyssens et al. 1989; Rabinowitch et al. 1986; Teeri 1997; Vantilbeurgh and Claeyssens 1985; Vonhoff et al. 1999) range, compared to the insoluble substrates reporting in the range of 2 mM after 5-10 s hydrolysis (Gruno et al. 2004).

Using Isothermal titration calorimetry (ITC), the action of EG's on an unmodified amorphous cellulose substrate may be monitored continuously using small amounts (μ g) of enzyme. This heat may be directly converted to a rate of hydrolysis (Murphy et al. 2010b; Olsen 2006; Todd and Gomez 2001). As ITC monitors the heat associated with each individual hydrolysis event, the addition of typical hydrolysis products such as cellobiose and glucose will have no effect on the measurement technique. Cellobiose and glucose are the two main soluble sugars present in an industrial hydrolysis situation (Zhang et al. 2010), so the inhibition of both these sugars is investigated. Varying the inhibitor concentrations over a typical range of the product concentrations while maintaining an excess of substrate, allows for the interpretation of the kinetic data, and the inhibition data for *TrCel7B*, *TrCel5A*, and *TrCel12A* for both glucose and cellobiose is presented here.

Material and Methods

Chemicals Cellobiose and glucose (HPLC grade, minimum > 98% purity) were provided by Sigma Aldrich, (St. Louis, MO, USA). All other chemicals unless otherwise stated were also provided by Sigma-Aldrich.

Enzymes

Preparation of *Trichoderma reesei* TrCel7B (Endoglucanase I)

TrCel7B (endoglucanase I, EGI) was cloned and expressed in *Aspergillus oryzae* JaL250 as described in WO 2005/067531. Filtered broth was concentrated and buffer exchanged using a tangential flow concentrator equipped with a 10 kDa polyethersulfone membrane with 20 mM Tris-HCl pH 8.5. The sample was loaded onto a Q Sepharose® High Performance column (GE Healthcare, Piscataway, NJ, USA) equilibrated in 20 mM Tris pH 8.5, and bound proteins were eluted with a linear gradient from 0-600 mM sodium chloride. The fractions were concentrated and desalted into 20 mM Tris pH 8.0, 150 mM NaCl using VIVASPIN® 20 10 kDa MWCO centrifugal concentration filter.

Preparation of *Trichoderma reesei* TrCel5A Endoglucanase II

TrCel5A (endoglucanase II, EGII) was cloned and expressed in *Aspergillus oryzae* JaL250. Fermentation broth was harvested from the vessel and centrifuged at 3000 x g to remove the biomass. The supernatant was sterile filtered using a 0.22 µm EXPRESS™ Plus Membrane, and stored at 4°C. The supernatant was desalted and buffer-exchanged into 20 mM Tris-HCl pH 8.0 using a 400 ml Sephadex G25 desalting column (GE Healthcare, Piscataway, NJ, USA) according to the manufacturer's instructions. Desalted TrCel5A was loaded onto a MonoQ™ HR 16/10 ion exchange column (GE Healthcare, Piscataway, NJ, USA) and eluted with a 300 ml linear 0-300 mM NaCl gradient in 20 mM Tris-HCl pH 8 with collection of 10 ml fractions. Fractions were pooled based on SDS-PAGE.

Preparation of *Trichoderma reesei* TrCel12A Endoglucanase III

TrCel12A (endoglucanase III, EGIII) was cloned and expressed in *Aspergillus oryzae* JaL250. The purification procedure was adapted from (Karlsson et al. 2002). Ammonium sulfate to a concentration of 350 mM was added to the 0.2 µm filtered broth. The treated cultivation broth was filtered and applied to a phenyl sepharose FF column (GE Healthcare Life Sciences, Buckinghamshire, UK) equilibrated with 20 mM sodium phosphate pH 6.0 with 350 mM ammonium sulfate. The protein was eluted over 5 column volumes with 20

mM sodium phosphate pH 6.00, followed by 5 column volumes of 50:50 % v/v 20 mM sodium phosphate pH 6.0:95 % ethanol. *TrCel12A* was eluted in both steps. The fractions were applied to an SDS PAGE and the activity was estimated using AZCL-HE-Cellulose from Megazyme (Bray,Co. Wicklow, Ireland) (see below). Fractions were pooled based on the activity and buffer exchanged using a sephadex G25 column (GE Healthcare Life Sciences, Buckinghamshire, UK) into 12 mM sodium acetate pH 4.8. The buffer exchanged solution was concentrated to 6 mg/mL on a Sartorius tandem sartoflow Slice 200 crossflow filtration system using a pelican XL 10 KDa Millipore Biomax 50 cm² filter.

Megazyme EG Assay

The assay was carried out as per manufacturer's instructions with the following modifications. 5 µL of fractions were added to 45 µL of 50 mM ammonium acetate pH 5.00 buffer and 750 µL of 0.1 % AZCL-HE-Cellulose w/v substrate. The solutions were incubated in a thermomixer after individual thermal equilibration for 15 min at 50 °C, 1400 rpm in 1.5 mL eppendorf tubes. The solutions were centrifuged at 13,500 rpm for 5 min, 200 µL of the supernatant was added to a microtiter plate and the OD₅₉₅ read.

Substrates

Regenerated Amorphous Cellulose. RAC was prepared as described previously, (Murphy et al. 2010a) adapted from the procedure outlined by Zhang and coworkers (Zhang et al. 2006).

Substrate Characterization

Total Sugars The total sugars assay was adapted from (Dubois et al. 1956; Murphy et al. 2010a; Zhang and Lynd 2005). The following modifications were made. The RAC was diluted 1/5 or 1/10 in Milli-Q water to 1.6 or 0.8 g/L, respectively. 1.5 mL of concentrated H₂SO₄ was added to 0.5 mL of each dilution and allowed to digest for 10 min. 3 mL of Milli-Q water was added to the digestions. 3 × 200 µL of each sample was added to 3 × 1.5 mL eppendorf tubes, 200 µL of freshly made 5 % phenol was added to each tube with a positive

displacement pipette and mixed well. The tubes were briefly centrifuged to ensure all liquid was collected in the bottom. 1 mL of conc. H₂SO₄ was added rapidly under the surface of each sample, then the samples were allowed to rest for 10 min, mixed well, and OD₄₉₀ was read. Total glucose was quantified using a glucose standard curve.

Reducing Ends Assays 2,2' Bicinchoninic acid assay (BCA). The BCA assay was performed as outlined in (Zhang and Lynd 2005) at 75 °C with a 30 min incubation time. The 0.75 mL samples were heated in a thermomixer with 0.75 mL of freshly made BCA reagent. After cooling the OD₅₆₀ was measured on a Shimadzu PharmaSpec 1700 (Shimadzu Scientific instruments, MD, USA) and samples quantified using a glucose standard curve.

Degree of polymerization The number averaged degree of polymerization (DP_N) was calculated from the ratio of reducing ends measured by BCA and total sugars as outlined above, and described previously (Murphy et al. 2010a).

Crystallinity Index, I_{cr} The crystallinity index of RAC was determined using solid-state ¹³C cross-polarization/magic angle spinning (CP/MAS) nuclear magnetic resonance (NMR) with settings adapted from (Matulova et al. 2008) and described in (Murphy et al. 2010a).

ITC Methods ITC was carried out using power-compensated equipment (Nano ITC^{2G} from TA Instruments, New Castle, DE, USA). The Nano ITC^{2G} has a gold cell of volume 0.957 mL. Standard conditions were as follows: 100 µL syringe, 400 rpm stirring rate^{*}, 30 °C, and collection of data with a point every 2 s.

Prior to ITC analysis, all proteins were buffer changed to 50 mM sodium acetate, 2 mM calcium chloride pH 5.00 using the VIVASPIN® 20 10 kDa MWCO centrifugal concentration filter. The concentration of all enzymes were determined from OD₂₈₀ using the molar absorption coefficients of 72770 M⁻¹cm⁻¹ (*TrCel7B*), 81360 M⁻¹cm⁻¹ (*TrCel5A*) and 73340 M⁻¹cm⁻¹ (*TrCel12A*).

Calibration and controls Because all experiments were performed in aqueous solutions, the reference cells were filled with degassed Milli-Q water. All calibrations were carried out at 30 °C. The calorimeters were initially calibrated by the built-in electrical heater according to the manufacturer's instructions. This was followed by a chemical calibration (Briggner and Wadso 1991; Murphy et al. 2010a) and an enzymatic calibration (Jeoh et al. 2005; Murphy et al. 2010b) as described previously. Heats of dilution were measured by titrating the same volume of buffer (or buffer with inhibitor) to RAC as the enzyme injections (applying the same stirring parameters), and also by injecting enzyme to buffer. All data has been corrected for heat of dilution and calibration factors.

ITC hydrolysis reactions It has previously been reported that the rapid decrease in polymerization as a result of EG activity has a profound effect on the baseline in ITC experiments (Murphy et al. 2010b). This may be overcome as before, using quenched subsets of the reaction to establish a baseline, however, when varying the enzyme dose, or adding inhibitors to the cell, the amount of work involved establishing a baseline for each set of conditions quickly becomes unfeasible. To overcome this limitation a new method has been developed. A stable baseline with no stirring is established, and then the enzyme is injected under maximum stirring and mixed for a total of 60 s. The stirring is then turned off and the hydrolysis monitored continuously without the baseline change caused by reduction of the viscosity.

Inhibition Experiments Inhibition experiments were set up as follows. The cell was filled with RAC and the appropriate amount of either cellobiose or glucose. For glucose this was 200 mM to 1 M, for cellobiose 5 mM to 65 mM. The final concentration of RAC was 4 g/L in the cell. The final enzyme concentration in the cell after injection was 200 nM. The syringe was filled with the enzyme in buffer and the same concentration of sugar. This was to minimize the heat of dilution as well as to mimic inhibition in the liquid phase. Hydrolysis was then carried out as outlined above. Results presented have been confirmed by duplicate analysis.

All data analysis has been performed using Origin Pro V 8.0 and Sigmaplot V 11.

Results and Discussion

RAC The *RAC* substrate was determined to have a DPN of 186 ± 4 , and the complete disappearance of the crystalline peak at C-4 in CP/MAS NMR was interpreted as producing a near completely amorphous substrate.

Experimental Design

The concentrations of soluble sugar chosen for this investigation are based on the levels of cellobiose and glucose found under relevant lignocellulose saccharification conditions. In order to increase productivity, while lowering water and power inputs, higher amounts of dry matter are being used in industry today (Jorgensen et al. 2007; Kristensen et al. 2009; Olsen et al. 2010). This leads to higher concentrations of glucose and cellobiose in the liquid phase, in the order of 500 mM glucose and up to 50 mM cellobiose, based on a typical hydrolysis of 20 % dry matter with 60 % cellulose, and 80 % conversion with a molar ratio of 10:1 glucose:cellobiose (Kristensen et al. 2009). To match this, we have investigated glucose concentrations varying from 200 mM to 1000 mM, and cellobiose from 5 mM to 65 mM.

Typical Michaelis-Menten inhibition experiments would vary the substrate concentration in order to determine the type of inhibition in a soluble substrate, soluble inhibitor system (Cornish-Bowden 2004). However, as this is a study of an insoluble substrate and a soluble inhibitor, a new approach had to be adopted. There are two distinct phases in cellulose hydrolysis, a solid phase where the enzyme may interact with the two dimensional surface of the substrate, and the liquid phase where the inhibitor and enzyme may interact in a three dimensional setting (Zhang and Lynd 2004). The enzymes adsorb onto the cellulose surface, their CBM decreasing the apparent K_m , and catalyze the hydrolysis of the $\beta,1-4$ bond (Rabinovich et al. 2002). After this or subsequent rounds of catalysis, they release to the liquid phase where the inhibitor is encountered. Thus simplified, inhibition may be seen as the probability of the enzyme returning to the insoluble surface again, or remaining in the liquid phase bound to the soluble ligand.

RAC was chosen for this investigation as it represents the most amorphous cellulose substrate recorded to date and is thus the most easily hydrolysable substrate for EGs (Zhang et al. 2006). The monitoring of 15 min of 4 g/L RAC with 200 nM EG is optimal as there is less than 1% conversion of the substrate, and therefore substrate modification as a result of hydrolysis does not play a role here. The enzymes were prepared in buffer containing the inhibitor prior to addition to the substrate. This was to mimic the conditions in the liquid phase, where the EGs encounter the inhibitor effectively in the absence of substrate.

ITC monitoring of Inhibition

In order to assess the inhibition of cellobiose and glucose on the EGs, a series of experiments was carried out varying the sugar concentration, while maintaining a constant excess of substrate. Fig. 1 shows the raw data for the hydrolysis of RAC by the three EGs as monitored by ITC. The observed heat-flow can be readily converted into a reaction rate when the enthalpy change of the reaction under the relevant conditions is known (Olsen 2006; Todd and Gomez 2001). However, this conversion is inevitably associated with an error, particularly so as the enthalpy change depends on the product profile and hence is different for the three enzymes considered here (Murphy et al, in preparation). In the current discussion we will use relative rate changes (see below), and we therefore refrain from converting the results in Fig. 1 to absolute rates. Inspection of the data in Fig. 1 immediately shows that the activity of the EG's depends strongly on time. Thus, the reaction rate quickly increases to a maximum (after 50-100 sec) which is 3-10 times higher than the rate after 15 min. The origin and extent of this distinct burst in activity is discussed elsewhere (Murphy et al, in preparation). In the current context of product inhibition the burst is important because it reflects that the rate limiting step for the enzymatic catalysis changes over the 15 min course monitored here. It follows that a time-dependence in the product inhibition may be observed if the effect of product on the burst phase is different from the effect at later stages of the hydrolysis where the reaction rate approaches a constant value (at pseudo steady state). As it appears below, we indeed observed both time dependent

and time independent inhibition and we will refer to this as respectively non-uniform and monotonous inhibition.

The three EGs investigated here all employ the retaining mechanism and it is therefore possible that they conduct transglycosylation where a sugar molecule (rather than water) acts as the nucleophile when the covalent enzyme-substrate complex is broken down (Withers 2001). This process is essentially athermal ($\Delta H \sim 0$) (Tewari et al. 2008) and therefore mute in a calorimetric experiment (Bohlin et al. 2010). It follows that, the inhibition discussed below includes any slowdown in hydrolytic activity whether it pertains to a lower frequency of the catalytic cycle (as in conventional inhibition) or a flow through the glycosyl-transfer reaction path.

Data Analysis of Cellobiose Inhibition

There two main features in Fig. 1 which may be interpreted. Firstly, it may be seen the pattern for the inhibition of *TrCel7B* is not uniform; rather it appears the inhibition is lessened over time, even in the short 15 min monitored here. This is seen by the merging of the rates of hydrolysis towards the end of the monitoring period. Secondly, and conversely, both *TrCel5A* and *TrCel12A* appear to be monotonously inhibited, seen by the decreased, and apparently parallel rates of hydrolysis.

Monotonous Inhibition

It is possible to quantify the inhibition of *TrCel5A* and *TrCel12A* as the rates are affected uniformly over time. An empirical analysis may be performed on the raw data by adapting the following. 1) The decrease in rate is as a result of part of the enzyme population no longer being available to take part in the hydrolysis. 2) The rate with no inhibitor is assigned V , the other rates are apparent rates in the presence of inhibitor, and are assigned V_{app} . V_{app}/V is thus a measure of the inhibition when the rates are parallel. By plotting V_{app}/V against $[I]$ and extrapolating until $V_{app}/V = 0.5$ a numerical evaluation of the inhibition may be reported (i.e. $V_{0.5}$). By taking an average of the V_{app}/V from 200 to 900 s and plotting against $[I]$, the $V_{0.5}$ for

TrCel5A is 113 ± 6 mM, and for *TrCel12A*, 118 ± 22 mM. Prior to 200 s we are still in the burst phase of the endoglucanases, where the rates are increasing initially, and there is some effect of the stirring which has yet to return to a constant baseline. This process is completely finished after 200 s and may be seen by the control experiment shown in Fig. 4 (right), and here we monitor the effect of the inhibitor on the hydrolysis process. It should be noted that because the inhibition is monotonous, the same $V_{0.5}$ values are attained when using concentration values. In Fig. 2 this is applied by integrating the entire thermogram and plotting C_{app}/C as a function of the inhibitor concentration $[I]$, which in turn yields $C_{0.5}$ for *TrCel5A* of 105 ± 2 mM, and *TrCel12A* of 101 ± 12 mM. Here $V_{0.5} = C_{0.5}$ and this indicates the inhibition is constant over time, as the same values are obtained from monitoring the change in rates ($V_{0.5}$) and the change in overall concentration ($C_{0.5}$). This is not always the case as will be seen for *TrCel7B*.

Care should be taken when characterizing such values as K_i , rather than $V_{0.5}$ as this is an empirical interpretation of the inhibition for the purpose of identifying which, if any EG is most affected by the presence of inhibitor. Interestingly, the hydrolysis rate of *TrCel5A* is linearly dependent on the concentration of the inhibitor (Fig. 2), and this would be described as competitive in a soluble:soluble system (Cornish 1974). *TrCel12A* on the other hand, displays a sharper decrease in rate for the first 20 mM than is reflected by the addition of up to 45 mM more cellobiose (Fig. 2). This is also seen in the $V_{0.5}$ values where the standard deviation for *TrCel12A* is higher. This is because a linear regression has been used for extrapolation (Fig. 2), and the fit for *TrCel5A* ($R^2 = 0.98$) was better than that for *TrCel12A* ($R^2 = 0.89$).

Non-Uniform Inhibition

The errors associated with determining concentrations, rather than hydrolysis rates when the inhibition is non-uniform are highlighted in Fig. 3. Here we have integrated the raw data from Fig. 1 for *TrCel7B*, and normalized after the 200 nM EG with no inhibition (concentration of product with no inhibitor, C) after 5 min of hydrolysis. By plotting C_{app}/C as a function of the inhibitor concentration $[I]$, a typical inhibition curve was expected. By then defining the inhibitor concentration where the activity (here expressed as the

fraction C_{app}/C is halved as $C_{0.5}$ again, the apparent inhibition of *TrCel7B* at this time is approximately 15 – 20 mM. This value is in good accordance with the value reported after 5 – 10 s of hydrolysis by Gruno and co-workers of 11 ± 3 mM (Gruno et al. 2004). However, we propose this does not entirely reflect the cellobiose inhibition of *TrCel7B*. This may be illustrated by reading the rate of hydrolysis at 15 min with the highest inhibitor concentration used in the study which shows a nominal decrease (V/V_{app}) of 17 % after 15 min, compared to that of 57 % after 5 min; this is illustrated in Fig. 3 (open circles). We conclude that cellobiose is a strong inhibitor of the initial burst in *TrCel7B* activity, but has a much lower effect at a later stage where the rate approaches a constant level.

Glucose Inhibition

Fig. 4 shows the inhibition pattern for glucose on the three EGs. Here it may be seen *TrCel5A* and *TrCel12A* appear inhibited in a similar fashion to that of cellobiose, that is to say they are monotonously inhibited over the monitoring time. Using the same method as has been described for constant cellobiose inhibition, $V_{0.5}$ may be reported here as 2.67 ± 0.21 M for *TrCel5A*. The same type of analysis may not be performed for *TrCel12A* here as the first inhibitor concentration of 200 mM has already reduced the V_{app}/V to under 0.5. This indicates in the $V_{0.5}$ in this case is less than 200 mM glucose. In a manner similar to cellobiose, it appears the inhibition of *TrCel12A* is more pronounced at the lower concentrations, and levels out after the addition of more inhibitor. Once more, *TrCel7B* shows a different inhibition behavior. The overall rate of hydrolysis is more decreased here in the presence of higher amounts of glucose compared to the same amounts cellobiose, but again, the rates are merging towards the end of the hydrolysis monitoring period, indicating a lessening of inhibition.

TABLE 1.

A summary of the inhibition of EGs used in the study as determined by ITC measurements.

Enzyme	$V/V_{app} = V_{0.5}$	$V/V_{app} = V_{0.5}$	Comment
	Cellobiose	Glucose	
<i>TrCel5A</i>	113 ± 6 mM	2.67 ± 0.21 M	N/A
<i>TrCel12A</i>	118 ± 22 mM	< 200 mM	N/A
<i>TrCel7B</i>	Varies with time	Varies with time	See text for details.

TrCel5A appears to be monotonously inhibited by both cellobiose and glucose although at relatively high levels of both. *TrCel12A*, has been thought to play a special role in the hydrolysis of cellulose as it is a smaller protein (25 KDa compared to ca. 50 KDa), and has no CBM (Karlsson et al. 2002). This could potentially allow it access to areas the bulkier EGs cannot reach. *TrCel12A* makes up a small part of the secreted *Hypocrea jecorina* cellulase cocktail, representing only about 1 % of the cellulase enzyme fraction, compared to the 12 % of *TrCel7B* (Zhang and Lynd 2004). *TrCel7B* inhibition by cellobiose has previously been described as complex (Claeyssens et al. 1990) and in contrast to these two, *TrCel7B* appears to display a change in the rate limiting step, in that products affect the initial rate limiting step more than the "steady state" rate limiting step.

The study of individual cellulase enzymes is useful as there is a cascade effect in crude mixtures; e.g. if the BG is first inhibited, then there is a build-up of cellobiose which is a stronger CBH inhibitor (Andric et al. 2010; Frennesson et al. 1985; Takagi 1984), or if the EG is inhibited, then the EG:CBH synergy is reduced as less new attack points are generated for the CBH enzyme in the form of new reducing or non reducing ends.

Both *TrCel7B* and *TrCel5A* have a CBM from family I (Boraston et al. 2004) . Given the inhibition pattern seen for *TrCel5A* and *TrCel12A* (with no CBM) reported here are similar, it is reasonable to assume the CBM does not play a significant role in this mechanism. It has also previously been shown that up to 0.5 M

cellobiose has no effect on enzyme binding to the substrate (Vantilbeurgh et al. 1986). The catalytic domains for *TrCel5A* and *TrCel12A* both have five glucosyl binding sites in the active site cleft (Macarron et al. 1993; Sandgren et al. 2001) compared to *TrCel7B*'s four (Kleywegt et al. 1997). Looking at the product profile of these EGs on insoluble cellulose, *TrCel5A* and *TrCel12A* both produce a distribution of soluble cello-oligosaccharides compared to the almost exclusive cellobiose and glucose produced by *TrCel7B* (Karlsson et al. 2002). It may be these differences that contribute to the divergence in inhibition patterns seen here, although this would require further investigation of the binding affinity of the inhibitors to the individual enzymes.

In conclusion

ITC is a good tool to study inhibition as it is unaffected by the addition of up to 1 M product added here and may be used to determine inhibition patterns. By investigating inhibition using this set up, it may be determined if the nature of the inhibition is monotonous or not. Non uniform inhibition would be recorded as an apparent increase in the hydrolysis rate over time while the EG adsorbs onto the surface of the cellulose and ejects the inhibitor. In contrast to this, monotonous inhibition would be distinguished by an overall and constant drop in the hydrolysis rate representing a portion of the enzyme population removed from the possibility of performing catalysis.

Interpretation of these patterns at this point is largely conjectural, but may prove useful in screening protein engineering variants in the future, as well as providing an experimental basis for the assessment of theories on inhibitory mechanisms. The resources used are minimal, given a complete (5 inhibitor concentrations and control) experimental trial uses less than 60 µg of enzyme. The preparation is also minimal in that the substrate is not modified. Two of the EGs tested here did not display significant inhibition at levels of cellobiose and glucose up to 65 mM and 1 M respectively, while *TrCel12A* was inhibited at lower concentrations of glucose (< 200 mM).

The addition of other biomass relevant inhibitors such as lignocellulosic residue or other pretreatment residues may be investigated in this type of comparative analysis, and may play an important role in elucidating weaknesses in future enzyme cocktails. We propose such empirical analyses can be used to compare EGs of the same glycoside hydrolase family from different wild types or protein engineering variants, and may play an important role in designing future enzyme products.

References

- Andric P, Meyer AS, Jensen PA, Dam-Johansen K. 2010. Effect and modeling of glucose inhibition and in situ glucose removal during enzymatic hydrolysis of pretreated wheat straw. *Applied Biochemistry and Biotechnology* 160(1):280-297.
- Anthon GE, Barrett DM. 2002. Determination of reducing sugars with 3-methyl-2-benzothiazolinonehydrazone. *Analytical Biochemistry* 305(2):287-289.
- Asenjo JA. 1983. Maximizing the formation of glucose in the enzymatic-hydrolysis of insoluble cellulose. *Biotechnology and Bioengineering* 25(12):3185-3190.
- Barr BK, Hsieh YL, Ganem B, Wilson DB. 1996. Identification of two functionally different classes of exocellulases. *Biochemistry* 35(2):586-592.
- Berlin A, Balakshin M, Gilkes N, Kadla J, Maximenko V, Kubo S, Saddler J. 2006. Inhibition of cellulase, xylanase and beta-glucosidase activities by softwood lignin preparations. *Journal of Biotechnology* 125(2):198-209.
- Bezerra RMF, Dias AA. 2004. Discrimination among eight modified michaelis-menten kinetics models of cellulose hydrolysis with a large range of substrate/enzyme ratios. *Applied Biochemistry and Biotechnology* 112(3):173-184.
- Bezerra RMF, Dias AA. 2005. Enzymatic kinetic of cellulose hydrolysis - inhibition by ethanol and cellobiose. *Applied Biochemistry and Biotechnology* 126(1):49-59.
- Bohlin C, Olsen SN, Morant MD, Patkar S, Borch K, Westh P. 2010. A comparative study of activity and apparent inhibition of fungal β -glucosidases. *Biotechnology and Bioengineering* n/a.
- Boraston AB, Bolam DN, Gilbert HJ, Davies GJ. 2004. Carbohydrate-binding modules: Fine-tuning polysaccharide recognition. *Biochemical Journal* 382:769-781.
- Briggner LE, Wadso I. 1991. Test and calibration processes for microcalorimeters, with special reference to heat-conduction instruments used with aqueous systems. *Journal of Biochemical and Biophysical Methods* 22(2):101-118.
- Cao Y, Tan H. 2002. Effects of cellulase on the modification of cellulose. *Carbohydrate Research* 337(14):1291-1296.
- Claeysens M, Vantilbeurgh H, Kamerling JP, Berg J, Vrsanska M, Biely P. 1990. Studies of the cellulolytic system of the filamentous fungus *trichoderma-reesei* qm-9414 - substrate-specificity and transfer activity of endoglucanase-i. *Biochemical Journal* 270(1):251-256.
- Claeysens M, Vantilbeurgh H, Tomme P, Wood TM, McRae SI. 1989. Fungal cellulase systems - comparison of the specificities of the cellobiohydrolases isolated from *penicillium-pinophilum* and *trichoderma-reesei*. *Biochemical Journal* 261(3):819-825.
- Cornish-Bowden A. 2004. *Fundamentals of enzyme kinetics*: Portland Press.
- Cornish A. 1974. Simple graphical method for determining inhibition constants of mixed, uncompetitive and non-competitive inhibitors. *Biochemical Journal* 137(1):143-144.
- Decker CH, Visser J, Schreier P. 2000. B-glucosidases from five black *aspergillus* species: Study of their physico-chemical and biocatalytic properties. *Journal of Agricultural and Food Chemistry* 48(10):4929-4936.
- Decker CH, Visser J, Schreier P. 2001. B-glucosidase multiplicity from *aspergillus tubingensis* cbs 643.92: Purification and characterization of four β -glucosidases and their differentiation with respect to substrate specificity, glucose inhibition and acid tolerance. *Applied Microbiology and Biotechnology* 55(2):157-163.
- Doner LW, Irwin PL. 1992. Assay of reducing end-groups in oligosaccharide homologs with 2,2'-bichinoninate. *Analytical Biochemistry* 202(1):50-53.
- Dubois M, Gilles KA, Hamilton JK, Rebers PA, Smith F. 1956. Colorimetric method for determination of sugars and related substances. *Analytical Chemistry* 28(3):350-356.

- Eriksson T, Karlsson J, Tjerneld F. 2002. A model explaining declining rate in hydrolysis of lignocellulose substrates with cellobiohydrolase i (cel7a) and endoglucanase i (cel7b) of trichoderma reesei. *Applied Biochemistry and Biotechnology* 101(1):41-60.
- Fan LT, Lee YH. 1983. Kinetic-studies of enzymatic-hydrolysis of insoluble cellulose - derivation of a mechanistic kinetic-model. *Biotechnology and Bioengineering* 25(11):2707-2733.
- Frennesson I, Tragardh G, Hahnagerdal B. 1985. An ultrafiltration membrane reactor for obtaining experimental reaction-rates at defined concentrations of inhibiting sugars during enzymatic saccharification of alkali-pretreated sawdust - formulation of a simple empirical rate-equation. *Biotechnology and Bioengineering* 27(9):1328-1334.
- Ghose TK. 1987. Measurement of cellulase activities. *Pure and Applied Chemistry* 59(2):257-268.
- Grano M, Valjamae P, Pettersson G, Johansson G. 2004. Inhibition of the trichoderma reesei cellulases by cellobiose is strongly dependent on the nature of the substrate. *Biotechnology and Bioengineering* 86(5):503-511.
- Gusakov AV, Sinitsyn AP. 1992. A theoretical-analysis of cellulase product inhibition - effect of cellulase binding constant, enzyme substrate ratio, and beta-glucosidase activity on the inhibition pattern. *Biotechnology and Bioengineering* 40(6):663-671.
- Hall M, Bansal P, Lee JH, Realff MJ, Bommarius AS. 2010. Cellulose crystallinity - a key predictor of the enzymatic hydrolysis rate. *FEBS Journal* 277(6):1571-1582.
- Henrissat B. 1991. A classification of glycosyl hydrolases based on amino-acid-sequence similarities. *Biochemical Journal* 280:309-316.
- Holtzapfel M, Cognata M, Shu Y, Hendrickson C. 1990. Inhibition of trichoderma-reesei cellulase by sugars and solvents. *Biotechnology and Bioengineering* 36(3):275-287.
- Holtzapfel MT, Caram HS, Humphrey AE. 1984a. A comparison of 2 empirical-models for the enzymatic-hydrolysis of pretreated poplar wood. *Biotechnology and Bioengineering* 26(8):936-941.
- Holtzapfel MT, Caram HS, Humphrey AE. 1984b. Determining the inhibition constants in the hch-1 model of cellulose hydrolysis. *Biotechnology and Bioengineering* 26(7):753-757.
- Holtzapfel MT, Caram HS, Humphrey AE. 1984c. The hch-1 model of enzymatic cellulose hydrolysis. *Biotechnology and Bioengineering* 26(7):775-780.
- Jeoh T, Baker JO, Ali MK, Himmel ME, Adney WS. 2005. Beta-d-glucosidase reaction kinetics from isothermal titration microcalorimetry. *Analytical Biochemistry* 347(2):244-253.
- Jorgensen H, Kristensen JB, Felby C. 2007. Enzymatic conversion of lignocellulose into fermentable sugars: Challenges and opportunities. *Biofuels Bioproducts & Biorefining-Biofpr* 1(2):119-134.
- Karlsson J, Siika-aho M, Tenkanen M, Tjerneld F. 2002. Enzymatic properties of the low molecular mass endoglucanases cel12a (eg iii) and cel45a (eg v) of trichoderma reesei. *Journal of Biotechnology* 99(1):63-78.
- Kleywegt GJ, Zou JY, Divne C, Davies GJ, Sinning I, Stahlberg J, Reinikainen T, Srisodsuk M, Teeri TT, Jones TA. 1997. The crystal structure of the catalytic core domain of endoglucanase i from trichoderma reesei at 3.6 angstrom resolution, and a comparison with related enzymes. *Journal of Molecular Biology* 272(3):383-397.
- Kristensen JB, Felby C, Jorgensen H. 2009. Yield-determining factors in high-solids enzymatic hydrolysis of lignocellulose. *Biotechnology for Biofuels* 2.
- Lee YH, Fan LT. 1982. Kinetic-studies of enzymatic-hydrolysis of insoluble cellulose - analysis of the initial rates. *Biotechnology and Bioengineering* 24(11):2383-2406.
- Lee YH, Fan LT. 1983. Kinetic-studies of enzymatic-hydrolysis of insoluble cellulose .2. Analysis of extended hydrolysis times. *Biotechnology and Bioengineering* 25(4):939-966.
- Lever M. 1972. New reaction for colorimetric determination of carbohydrates. *Analytical Biochemistry* 47(1):273-&.
- Lever M. 1973. Colorimetric and fluorometric carbohydrate determination with para-hydroxybenzoic acid hydrazide. *Biochemical Medicine* 7(2):274-281.

- Lynd LR, Weimer PJ, van Zyl WH, Pretorius IS. 2002. Microbial cellulose utilization: Fundamentals and biotechnology. *Microbiology and Molecular Biology Reviews* 66(3):506-577.
- Macarron R, Acebal C, Castillon MP, Dominguez JM, Delamata I, Pettersson G, Tomme P, Claeysens M. 1993. Mode of action of endoglucanase-iii from trichoderma-reesei. *Biochemical Journal* 289:867-873.
- Matulova M, Nouaille R, Capek P, Pean M, Delort AM, Forano E. 2008. Nmr study of cellulose and wheat straw degradation by ruminococcus albus 20. *FEBS Journal* 275(13):3503-3511.
- Miller GL. 1959. Use of dinitrosalicylic acid reagent for determination of reducing sugar. *Analytical Chemistry* 31(3):426-428.
- Mosier N, Wyman C, Dale B, Elander R, Lee YY, Holtzapple M, Ladisch M. 2005. Features of promising technologies for pretreatment of lignocellulosic biomass. *Bioresource Technology* 96(6):673-686.
- Murphy L, Baumann MJ, Borch K, Sweeney M, Westh P. 2010a. An enzymatic signal amplification system for calorimetric studies of cellobiohydrolases. *Analytical Biochemistry* 404(2):140-148.
- Murphy L, Borch K, McFarland KC, Bohlin C, Westh P. 2010b. A calorimetric assay for enzymatic saccharification of biomass. *Enzyme and Microbial Technology* 46(2):141-146.
- Nelson N. 1944. A photometric adaptation of the somogyi method for the determination of glucose. *Journal of Biological Chemistry* 153(2):375-380.
- Olsen SN. 2006. Applications of isothermal titration calorimetry to measure enzyme kinetics and activity in complex solutions. *Thermochimica Acta* 448(1):12-18.
- Olsen SN, Lumby E, McFarland K, Borch K, Westh P. 2010. Kinetics of enzymatic high-solid hydrolysis of lignocellulosic biomass studied by calorimetry. *Applied Biochemistry and Biotechnology* 163(5):626-635.
- Penttila M, Lehtovaara P, Nevalainen H, Bhikhabhai R, Knowles J. 1986. Homology between cellulase genes of trichoderma-reesei - complete nucleotide-sequence of the endoglucanase-i gene. *Gene* 45(3):253-263.
- Praestgaard E, Elmerdahl J, Murphy L, Nymand S, McFarland KC, Borch K, Westh P. 2011. A kinetic model for the burst phase of processive cellulases. *FEBS Journal:Accepted manuscript*.
- Rabinovich ML, Melnik MS, Boloboba AV. 2002. Microbial cellulases (review). *Applied Biochemistry and Microbiology* 38(4):305-321.
- Rabinowitch ML, Klyosov AA, Melnick MS. 1986. The titration of the active-centers of cellobiohydrolase from trichoderma-reesei. *Analytical Biochemistry* 156(2):489-494.
- Saloheimo M, Lehtovaara P, Penttila M, Teeri TT, Stahlberg J, Johansson G, Pettersson G, Claeysens M, Tomme P, Knowles JKC. 1988. Egiii, a new endoglucanase from trichoderma-reesei - the characterization of both gene and enzyme. *Gene* 63(1):11-21.
- Sandgren M, Shaw A, Ropp TH, Bott SWR, Cameron AD, Stahlberg J, Mitchinson C, Jones TA. 2001. The x-ray crystal structure of the trichoderma reesei family 12 endoglucanase 3, cel12a, at 1.9 angstrom resolution. *Journal of Molecular Biology* 308(2):295-310.
- Scheiding W, Thoma M, Ross A, Schugerl K. 1984. Modeling of the enzymatic-hydrolysis of cellobiose and cellulose by a complex enzyme mixture of trichoderma-reesei qm 9414. *Applied Microbiology and Biotechnology* 20(3):176-182.
- Somogyi M. 1952. Notes on sugar determination. *Journal of Biological Chemistry* 195(1):19-23.
- Takagi M. 1984. Inhibition of cellulase by fermentation products. *Biotechnology and Bioengineering* 26(12):1506-1507.
- Teeri TT. 1997. Crystalline cellulose degradation: New insight into the function of cellobiohydrolases. *Trends in Biotechnology* 15(5):160-167.
- Tewari YB, Lang BE, Decker SR, Goldberg RN. 2008. Thermodynamics of the hydrolysis reactions of 1,4-beta-d-xylobiose, 1,4-beta-d-xylotriose, d-cellobiose, and d-maltose. *Journal of Chemical Thermodynamics* 40(10):1517-1526.
- Todd MJ, Gomez J. 2001. Enzyme kinetics determined using calorimetry: A general assay for enzyme activity? *Analytical Biochemistry* 296(2):179-187.

- Vantilbeurgh H, Claeysens M. 1985. Detection and differentiation of cellulase components using low-molecular mass fluorogenic substrates. *FEBS Letters* 187(2):283-288.
- Vantilbeurgh H, Tomme P, Claeysens M, Bhikhabhai R, Pettersson G. 1986. Limited proteolysis of the cellobiohydrolase I from *Trichoderma reesei* - separation of functional domains. *FEBS Letters* 204(2):223-227.
- Vonhoff S, Piens K, Pipelier M, Braet C, Claeysens M, Vasella A. 1999. Inhibition of cellobiohydrolases from *Trichoderma reesei*. Synthesis and evaluation of some glucose-, cellobiose-, and cellotriose-derived hydroxymolactams and imidazoles. *Helvetica Chimica Acta* 82(7):963-980.
- Withers SG. 2001. Mechanisms of glycosyl transferases and hydrolases. *Carbohydrate Polymers* 44(4):325-337.
- Wyman CE. 2007. What is (and is not) vital to advancing cellulosic ethanol. *Trends in Biotechnology* 25(4):153-157.
- Xiao ZZ, Zhang X, Gregg DJ, Saddler JN. 2004. Effects of sugar inhibition on cellulases and beta-glucosidase during enzymatic hydrolysis of softwood substrates. *Applied Biochemistry and Biotechnology*:1115-1126.
- Zhang MJ, Su RX, Qi W, He ZM. 2010. Enhanced enzymatic hydrolysis of lignocellulose by optimizing enzyme complexes. *Applied Biochemistry and Biotechnology* 160(5):1407-1414.
- Zhang YHP, Cui JB, Lynd LR, Kuang LR. 2006. A transition from cellulose swelling to cellulose dissolution by o-phosphoric acid: Evidence from enzymatic hydrolysis and supramolecular structure. *Biomacromolecules* 7(2):644-648.
- Zhang YHP, Lynd LR. 2004. Toward an aggregated understanding of enzymatic hydrolysis of cellulose: Noncomplexed cellulase systems. *Biotechnology and Bioengineering* 88(7):797-824.
- Zhang YHP, Lynd LR. 2005. Determination of the number-average degree of polymerization of cellodextrins and cellulose with application to enzymatic hydrolysis. *Biomacromolecules* 6(3):1510-1515.
- Zhao Y, Wu B, Yan BX, Gao PJ. 2004. Mechanism of cellobiose inhibition in cellulose hydrolysis by cellobiohydrolase. *Science in China Series C-Life Sciences* 47(1):18-24.
- Zhu ZG, Sathitsuksanoh N, Vinzant T, Schell DJ, McMillan JD, Zhang YHP. 2009. Comparative study of corn stover pretreated by dilute acid and cellulose solvent-based lignocellulose fractionation: Enzymatic hydrolysis, supramolecular structure, and substrate accessibility. *Biotechnology and Bioengineering* 103(4):715-724.

Footnotes

This work was supported by the Danish Agency for Science, Technology and Innovation (grant # 2104-07-0028 to PW) and the Carlsberg Foundation. We thank Erik Lumby Rasmussen for excellent technical assistance.

Abbreviations used are: EG, endo-glucanase, CBH, cellobiohydrolase, CBM, carbohydrate binding module, ITC, isothermal titration calorimetry, BCA, 2,2' Bicinchoninic acid, AZCL-HE-cellulose, Azurine-Crosslinked hydroxyethyl cellulose, RAC, regenerated amorphous cellulose, COS, cello-oligosaccharide, CP/MAS NMR cross-polarization/magic angle spinning nuclear magnetic resonance, GH, glycoside hydrolase.

Figure Legends

Figure 1. The isothermal titration calorimetry (ITC) raw data for the inhibition of cellobiose. The 4 g/L substrate is placed in the cell with the indicated amount of cellobiose added. This is allowed to come to thermal equilibrium at 30 °C (pH 5.0), indicated by the flat baseline for the first 180 s (designated -180 to 0 s). At this time 10 µL of enzyme with inhibitor is injected, to a final concentration of 200 nM EG. The heat generated by the reaction is monitored continuously then for 15 min. The exothermic nature of the reaction is indicated by the thermogram as heat applied (µJ/s) to the reference cell in order to maintain the temperature differential. Right: *TrCel12A*, Middle: *TrCel5A*, Left: *TrCel7B*.

Figure 2. A simplified method for analysis of the cellobiose inhibition of *TrCel5A* and *TrCel12A*. V is the rate with no inhibitor present, and V_{app} is the rate in the presence of the indicated amount of inhibitor. By normalizing against the original V rate, the degree of inhibition may be estimated by extrapolating until $V_{app} = 0.5 V$. Left: *Trcel5A*, right *TrCel12A*. Closed circles are rates determined from figure 1, averaged over 200 – 900s. Open circles are the normalized total product formed, derived from the integrating the thermograms in figure 1.

Figure 3. Left: Illustrating the inhibition of *TrCel7B*, the blue (vertical) line represents the point at which the integrals have been performed in order to determine the relative concentrations after 5 min. Right ● A plot of C_{app}/C_0 Vs $[I]$. The horizontal red line represents the point at which $C_{app} = 0.5 C$, defined as $V_{0.5}$. ○ A plot of V_{app}/V_0 Vs $[I]$. Here we illustrate the relative rates merge already after 15 min.

Figure 4. The isothermal titration calorimetry (ITC) raw data for the inhibition of glucose. The 4 g/L substrate is placed in the cell with the indicated amount of glucose added. These are allowed to come to thermal equilibrium at 30 °C (pH 5.0), as outlined in Fig. 1. At this time 10 µL of enzyme with inhibitor is injected, to a final concentration of 200 nM. The heat generated by the reaction is monitored continuously then for 15 min. Shown in the *TrCel12A* panel is a control injection of buffer + 1 M glucose to RAC + 1 M glucose Right: *TrCel12A*, Middle: *TrCel5A*, Left: *TrCel7B*.

Figure 1.

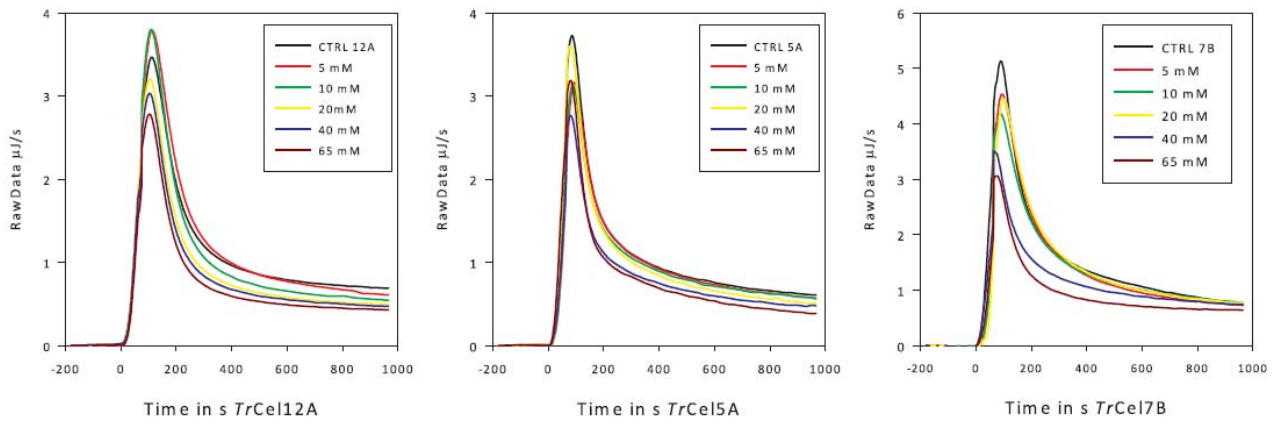


Figure 2.

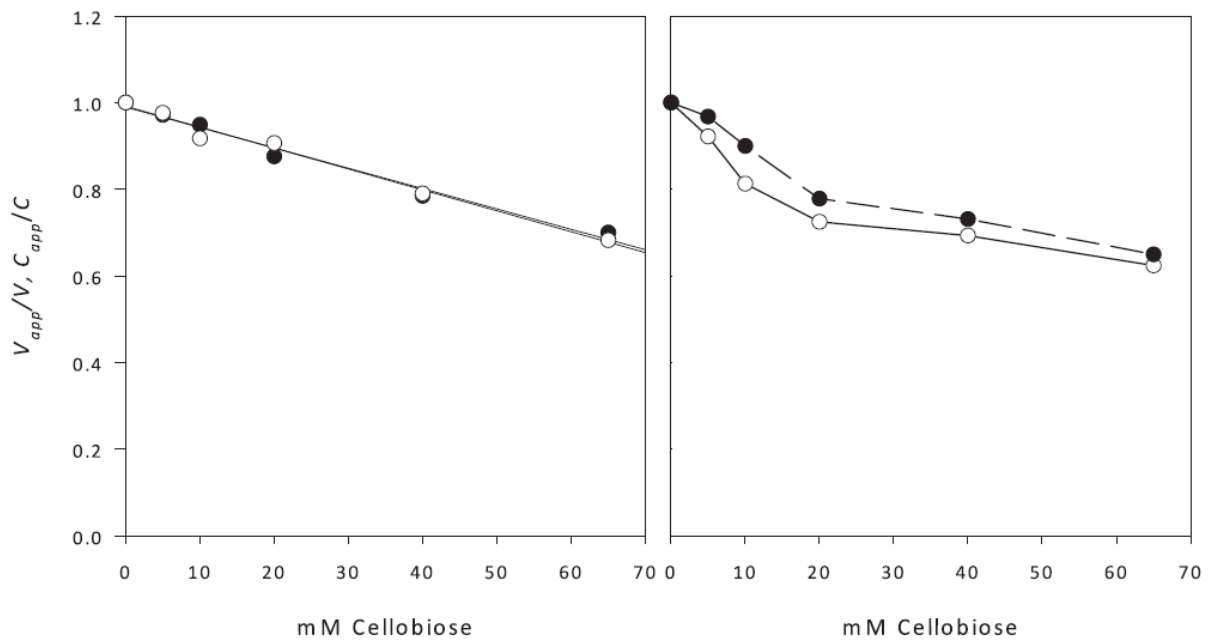


Figure 3.

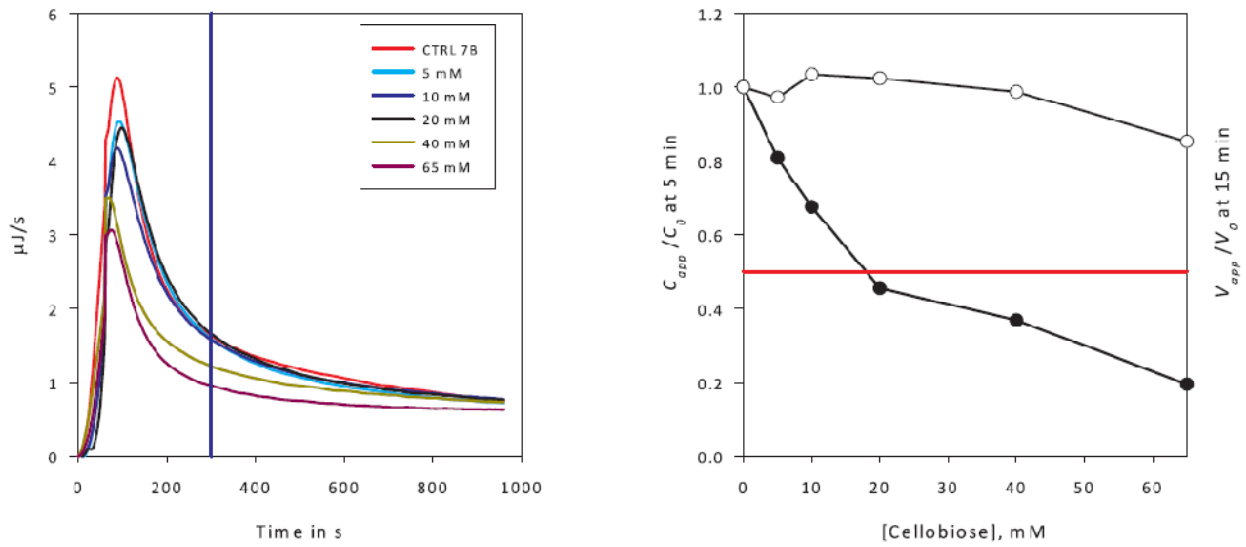
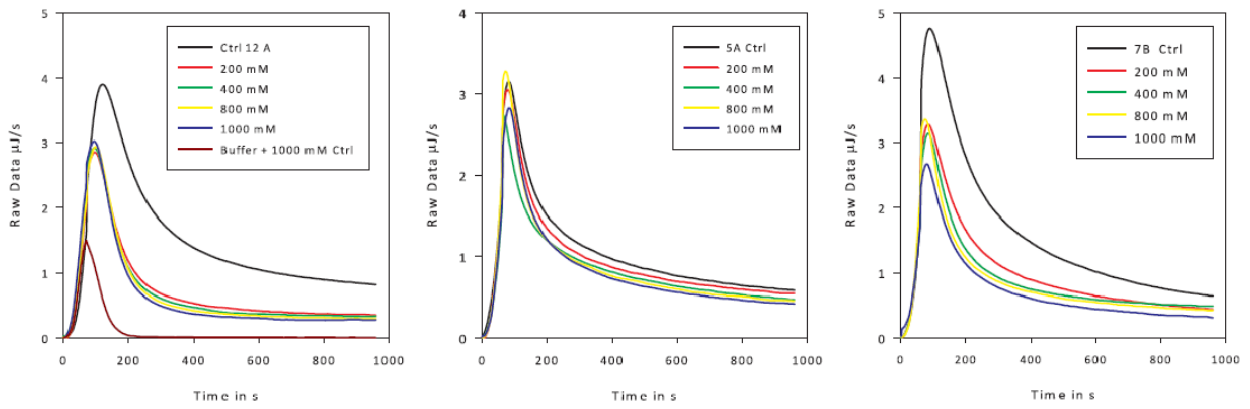


Figure 4.



Contribution to Article 5: A kinetic model for the burst phase of processive cellulases.

Egil Praestgaard, Jens Elmerdahl, **Leigh Murphy**, Søren Nymand, K. C. McFarland, Kim Borch, Peter Westh.

A kinetic model for the burst phase of processive cellulases

Eigil Praestgaard¹, Jens Elmerdahl¹, Leigh Murphy¹, Søren Nyman¹, K. C. McFarland², Kim Borch³ and Peter Westh¹

¹ Roskilde University, NSM, Research Unit for Biomaterials, Roskilde, Denmark

² Novozymes Inc., Davis, CA, USA

³ Novozymes A/S, Bagsværd, Denmark

Keywords

burst phase; calorimetry; cellulase; kinetic equations; slowdown of cellulolysis

Correspondence

P. Westh, Roskilde University, Building 18.1,
PO Box 260, 1 Universitetsvej, DK-4000
Roskilde, Denmark
Fax: +45 4674 3011
Tel: +45 4674 2879
E-mail: pwesth@ruc.dk

(Received 30 October 2010, revised 21
February 2011, accepted 25 February
2011)

doi:10.1111/j.1742-4658.2011.08078.x

Cellobiohydrolases (exocellulases) hydrolyze cellulose processively, i.e. by sequential cleaving of soluble sugars from one end of a cellulose strand. Their activity generally shows an initial burst, followed by a pronounced slowdown, even when substrate is abundant and product accumulation is negligible. Here, we propose an explicit kinetic model for this behavior, which uses classical burst phase theory as the starting point. The model is tested against calorimetric measurements of the activity of the cellobiohydrolase Cel7A from *Trichoderma reesei* on amorphous cellulose. A simple version of the model, which can be solved analytically, shows that the burst and slowdown can be explained by the relative rates of the sequential reactions in the hydrolysis process and the occurrence of obstacles for the processive movement along the cellulose strand. More specifically, the maximum enzyme activity reflects a balance between a rapid processive movement, on the one hand, and a slow release of enzyme which is stalled by obstacles, on the other. This model only partially accounts for the experimental data, and we therefore also test a modified version that takes into account random enzyme inactivation. This approach generally accounts well for the initial time course (approximately 1 h) of the hydrolysis. We suggest that the models will be useful in attempts to rationalize the initial kinetics of processive cellulases, and demonstrate their application to some open questions, including the effect of repeated enzyme dosages and the 'double exponential decay' in the rate of cellulolysis.

Database

The mathematical model described here has been submitted to the Online Cellular Systems Modelling Database and can be accessed at <http://jij.biochem.sun.ac.za/database/Praestgaard/index.html> free of charge.

Introduction

The enzymatic hydrolysis of cellulose to soluble sugars has attracted increasing interest, because it is a critical step in the conversion of biomass to biofuels. One major challenge for both the fundamental understanding and application of cellulases is that their activity tapers off early in the process, even when the substrate

is plentiful. Typically, the rate of hydrolysis decreases by an order of magnitude or more at low cellulose conversion, and experimental analysis has led to quite divergent interpretations of this behavior. One line of evidence has suggested that the slowdown is a result of the heterogeneous nature of the insoluble substrate.

Abbreviations

CBH, cellobiohydrolase; Cel7A, cellobiohydrolase I; ITC, isothermal titration calorimetry; RAC, reconstituted amorphous cellulose.

Thus, if various structures in the substrate have different susceptibility to enzymatic attack, the slowdown may reflect a phased depletion of the preferred types of substrate [1,2]. Other investigations have emphasized enzyme inactivation as a major cause of the decreasing rates [3]. This inactivation could reflect the formation of nonproductive enzyme–substrate complexes [4–6] or the adsorption of cellulases on noncellulosic components, such as lignin [7,8], although the role of lignin remains controversial [9]. Recently, Bansal *et al.* [10] have provided a comprehensive review of theories for cellulase kinetics, and it was concluded that no generalization could be made regarding the origin of the slowdown. In particular, so-called ‘restart’ or ‘resuspension’ experiments, in which a substrate is first partially hydrolyzed, then cleared of cellulases and finally exposed to a second enzyme dose, have alternatively suggested that enzyme inactivation and substrate heterogeneity are the main causes of decreasing hydrolysis rates (see refs. [10,11]).

Further analysis of different contributions to the slowdown appears to require a better theoretical framework for the interpretation of the experimental material. In this study, we introduce one approach and test it against experimental data for the cellobiohydrolase Cel7A (formerly CBHI) from *Trichoderma reesei*. Our starting point is classical burst phase theory for soluble substrates [12], and we extend this framework to account for the characteristics of cellobiohydrolases, such as adsorption onto insoluble substrates, irreversible inactivation and processive action. The latter implies a propensity to complete many catalytic cycles without the dissociation of enzyme and substrate. For cellobiohydrolases, the processive action may involve the successive release of dozens or even hundreds of cellobiose molecules from one strand [13], and some previous reports have suggested a possible link between this and the slowdown in hydrolysis [8,13,14].

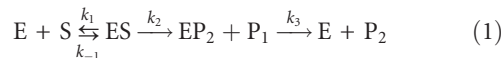
Results and Discussion

Theory

Burst phase for soluble substrates and nonprocessive enzymes

The concept of a burst phase was introduced more than 50 years ago, when it was demonstrated that an enzyme reaction with two products may show a rapid production of one of the products in the pre-steady-state regime [15,16]. Later work has shown that this is quite common for hydrolytic enzymes with an ordered ‘ping–pong bi–bi’ reaction sequence [12]. At a constant water concentration, this type of hydrolysis may be

described by Eqn (1), which does not explicitly include water as a substrate (the process is considered as an ordered uni–bi reaction):



In an ordered mechanism, the product P_1 is always released from the complex before the product P_2 , and it follows that, if k_3 is small (compared with k_1S_0 and k_2), there will be a rapid production of P_1 (a burst phase) when E and S are first mixed. Subsequently, at steady state, a large fraction of the enzyme population will be trapped in the EP_2 complex, which is only slowly converted to P_2 and free E, and the (steady state) rate of P_1 production will be lower. The result is a maximum in the rate of production of P_1 but not P_2 (see Fig. 1). To analyze this maximum, we need an expression for the rate of P_1 production: $P_1'(t)$. Here, and in the following analyses of the reaction schemes, we first try to derive analytical solutions, as this approach provides rigorous expressions that may help to identify the molecular origin of the burst and slowdown. In cases in which analytical expressions cannot

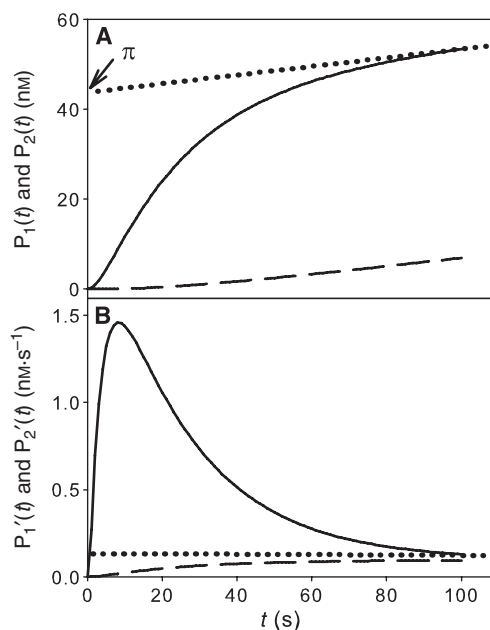


Fig. 1. Initial time course of the concentrations $P_1(t)$ and $P_2(t)$ (A) and the rates $P_1'(t)$ and $P_2'(t)$ (B) calculated from Eqns <10>–<13> in Data S1. Full and broken lines indicate P_1 and P_2 , respectively, and the dotted line shows the steady-state condition with constant concentrations of the intermediates ES and EP_2 , and hence constant rates. The intersection π is a measure of the extent of the burst (see text for details). The parameters were $S_0 = 20 \mu\text{M}$, $E_0 = 0.050 \mu\text{M}$, $k_2 = 0.3 \text{ s}^{-1}$, $k_1 = 0.002 \text{ s}^{-1}\mu\text{M}^{-1}$, $k_{-1} = k_3 = 0.002 \text{ s}^{-1}$; these values are similar to those found below for Cel7A.

in Eqn (3)] or enter the next catalytic cycle [horizontal step to the right in Eqn (3)], which releases one more cellobiose. A typical cellulose strand is hundreds or thousands of glycosyl units long, and it follows that the local environment experienced by the cellulase may be similar for many sequential catalytic steps. Therefore, we use the same rate constants k_2 and k_3 for consecutive hydrolytic or dissociation steps. This version of the model neglects the fact that the C_{n-1} , C_{n-2} , ... strands are also substrates (free E is not allowed to associate with these partially hydrolyzed strands). This simplification is acceptable in the early part of the process where $C_n \gg E_0$. After n processive steps, the enzyme reaches the 'check block', and this necessitates a (slow) desorption from the remaining cellulose strand (designated C_x) before the enzyme can continue cellobiose production from a new C_n strand. In other words, the strand consists of $n + x$ cellobiose units in total, but because of the 'check block', only the first n units are available for enzymatic hydrolysis. This interpretation of obstacles and processivity is similar to that recently put forward by Jalak & Valjamae [14].

A kinetic treatment of Eqn (3) requires the specification of the substrate concentration. This is not trivial for an insoluble substrate, but, as the enzyme used here attacks the reducing end of the strand, we use the molar concentration of ends for S_0 throughout this work. This problem may be further addressed by introducing noninteger (fractal) kinetic orders that account for the special limitations of the heterogeneous reaction (see refs. [31,32]). For this model, this is readily performed by introducing apparent orders in Eqn (5). However, the current treatment is limited to the simple case in which the kinetic order is equal to the molecularity of the reactions in Eqn (3). This implies that the adsorption of enzyme onto the substrate is described by a kinetic (rather than equilibrium) approach (c.f. Ref. [21]). Based on this and the simplifications mentioned above, the kinetic equations for each step in Eqn (3) were written and solved with respect to the EC_{n-i} intermediates as shown in Data S1. As cellobiose production in Eqn (3) comes from these EC_{n-i} complexes, which all decay with the same rate constant k_2 , the rate of cellobiose production $C'(t)$ follows the equation:

$$C'(t) = k_2 \sum_{i=0}^{n-1} EC_{n-i}(t) \quad (4)$$

Using the expressions in Data S1, the sum in Eqn (4) may be written as:

where $\text{Gamma}[n, xt] = \int_x^\infty t^{n-1} e^{-t} dt$ is the so-called upper incomplete gamma function [22]. Equations (4) and (5) provide a description of the burst phase for processive enzymes. In the simple case, this approach will eventually reach steady state with constant concentrations of all EC_{n-i} complexes and hence constant $C'(t)$. We emphasize, however, that there are no steady-state assumptions in the derivation of Eqn (5) and, indeed, we use it to elucidate the burst in the pre-steady-state regime. As discussed below, Eqn (3) is found to be too idealized to account for experimental data, and some modifications are introduced. Nevertheless, Eqn (5) is the main result of the current work and is the backbone in the subsequent analyses.

Examination of a processive burst phase as specified by Eqns (4) and (5) reveals some similarity to the simple burst behaviour in Fig. 1. Hence, if we insert the same rate constants as in Fig. 1, and use an obstacle-free path length of $n = 100$ cellobiose units, the rate of cellobiose production $C'(t)$ (full curve in Fig. 2) exhibits a maximum akin to that observed for $P_1'(t)$ in Fig. 1B. However, the occurrence of fast sequential steps in the processive model produces a more pronounced maximum in both duration and amplitude. Figure 2 also illustrates the meaning of the three terms that are summed in Eqn (5). The chain line shows the contribution from the first (simple exponential) term on the right-hand side of Eqn (5), which describes the kinetics devoid of any effect from obstacles (corresponding to $n \rightarrow \infty$). The broken line is the sum of the last two terms (the terms with gamma functions) and quantifies the (negative) effect on the hydrolysis rate arising from the 'check blocks'. For the parameters used in Fig. 2, this contribution only becomes important above $t \approx 300$ s, and this simply reflects the minimal time required for a significant population of enzyme to bind and perform the 100 processive steps to reach the 'check block'. After about 600 s, essentially all enzymes have reached their first encounter

$$\begin{aligned} \sum_{i=0}^{n-1} EC_{n-i}(t) = & \frac{[1 - e^{-(k_3+k_1S_0)t}] E_0 k_1 S_0}{(k_3 + k_1 S_0)} + \frac{E_0 \left(\frac{k_2}{k_2+k_3}\right)^n k_1 S_0 \left(-1 + \frac{\text{Gamma}[(n), (k_2+k_3)t]}{\text{Gamma}[n]}\right)}{(k_3 + k_1 S_0)} \\ & + \frac{1}{(k_3 + k_1 S_0)} e^{-(k_3+k_1S_0)t} E_0 k_1 S_0 \left(\frac{k_2}{k_2 - k_1 S_0}\right)^n \left(1 - \frac{\text{Gamma}[(n), (k_2 - k_1 S_0)t]}{\text{Gamma}[n]}\right) \end{aligned} \quad (5)$$

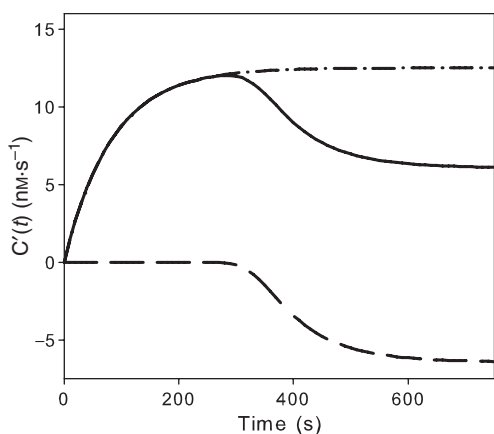


Fig. 2. The rate of cellobiose production $C'(t)$ (solid curve) calculated according to Eqns (4) and (5) and plotted against time. The rate constants are the same as in Fig. 1 and the initial concentrations were $E_0 = 0.050 \mu\text{M}$ and $S_0 = 5 \mu\text{M}$ reducing ends. The obstacle-free path n was set to 100 cellobiose units. The chain curve shows the first term in Eqn (5), which signifies the rate of cellobiose production on an 'obstacle-free' substrate (i.e. for $n \rightarrow \infty$). The broken curve, which is the sum of the last two terms in Eqn (5), signifies the inhibitory effect of the obstacles. The two curves sum to the full curve.

with a 'check block' and we observe an abeyance with reduced $C'(t)$ because a significant (and constant) fraction of the enzyme is unproductively bound in front of a 'check block'.

The extent of the processive burst may be assessed from the intersect $\pi_{\text{processive}}$ defined in the same way as π for the simple reaction (see Fig. 1A). As shown in Data S1, $\pi_{\text{processive}}$ may be written as:

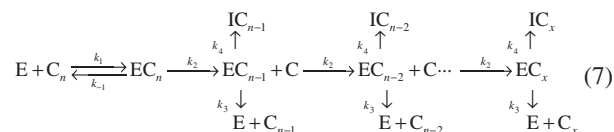
$$\pi_{\text{processive}} = E_0 \frac{S_0 k_1 k_2 \left[-1 + \left(\frac{k_2}{k_2 + k_3} \right)^n \left(1 + \frac{n(k_3 + k_1 S_0)}{k_2 + k_3} \right) \right]}{(k_3 + k_1 S_0)^2} \quad (6)$$

We note that $\pi_{\text{processive}}$ is proportional to E_0 and, if we again consider the case in which adsorption and hydrolysis are fast compared with desorption (i.e. $k_1 S_0 \gg k_3$ and $k_2 \gg k_3$), Eqn (6) reduces to $\pi_{\text{processive}} = nE_0$. This implies that, under these special conditions, every enzyme rapidly makes one run towards the 'check block', and thus produces the number of cellobiose molecules n which are available to hydrolysis in the obstacle-free path.

Modifications of the model

In analogy with the simple case in Eqn (1), the rate $C'(t)$ specified by Eqn (3) runs through a maximum and falls towards a steady-state level (Fig. 2) in which the concentrations of all intermediates EC_{n-i} and the

rate $C'(t)$ are independent of time. This behavior, however, is at odds with countless experimental reports, as well as the current measurements, which suggest that the activity of Cel7A does not reach a constant rate. Instead, the reaction rate continues to decrease. This suggests that, in addition to the burst behavior described in Eqn (3), other mechanisms must be involved in the slowdown. The nature of such inhibitory mechanisms has been discussed extensively and much evidence has pointed towards product inhibition, reduced substrate reactivity or enzyme inactivation (see, for example, refs. [10,11,23] for reviews). In the current work, we observed this continuous slowdown even in experiments with very low substrate conversion ($< 1\%$), where the hydrolysis rates are unlikely to be affected by inhibition or substrate modification (an inference that is experimentally supported in Fig. 9 below). In the coupled calorimetric assay used here, the product (cellobiose) is converted to gluconic acid. The concentration is in the micromolar range, and previous tests have shown that this is not inhibitory to cellulolysis or the coupled reactions (see Ref. [48]). Therefore, the continuous decrease in the rate of hydrolysis was modeled as protein inactivation. To this end, we essentially implemented the conclusions of a recent experimental study by Ma *et al.* [24] in the model. As with earlier reports [3,14,25–27], Ma *et al.* discussed unproductively bound cellulases, and found that substrate-associated Cel7A could be separated into two populations of reversibly and irreversibly adsorbed enzyme. The latter population, which grew gradually over time, was found to lose most catalytic activity. This behavior was introduced into the model through a new rate constant k_4 , which pertains to the conversion of an active enzyme–cellulose complex (EC_{n-i}) into a complex of cellulose and inactive protein (IC_{n-i}). In other words, any EC_{n-i} complex in Eqn (7) is allowed three alternative decay routes, namely hydrolysis (k_2), dissociation (k_3) or irreversible inactivation (k_4). We also introduced a separate rate constant k_{-1} for the dissociation of substrate and enzyme EC_n before the first hydrolytic step. With these modifications, we may write the reaction:



We were not able to find an analytical solution for $C'(t)$ on the basis of Eqn (7), and we instead used a numerical treatment with the appropriate initial conditions [i.e. all initial concentrations except $E(t)$ and $C_n(t)$ are zero].

One final modification of the model was introduced to examine the effect of ‘polydispersity’ in n . Thus, n as defined in Eqns (3) and (7) is a constant, and this implies that all enzymes must perform exactly n catalytic cycles before running into the ‘check block’. This is evidently a rather coarse simplification and, to consider the effects of this, we also tested an approach which used a distribution of different n values. For example, the substrate was divided into five equal subsets (i.e. each 20% of S_0) with n values ranging from 40% to 160% of the average value. We also analyzed different distributions and subsets of different sizes (with a larger fraction close to the average n and less of the longest/shortest strands). In all of these analyses, the rate of cellobiose production from each subset was calculated independently and summed to obtain the total $C'(t)$.

Experimental

Two parameters from the model, namely the substrate and enzyme concentrations (E_0 and S_0), can be readily varied in experiments, and we therefore firstly compared measurements and modeling in trials in which S_0 and E_0 were systematically changed. Figure 3A shows a family of calorimetric measurements in which Cel7A was titrated to different initial substrate concentrations (S_0 in μM of reducing ends – this unit can be readily converted into a weight concentration using the molar mass of a glycosyl unit and the average chain length for the current substrate, $\text{DP} = 220$ glycosyl units). The concentration of Cel7A was 50 nM in these experiments and the experimental temperature was 25 °C. Figure 3B shows model results for the same values of E_0 and S_0 . Here, we used the model in Eqn (3) [Eqns (4) and (5)] and manually adjusted the kinetic constants and n by trial and error. The parameters in Fig. 3B are $k_1 = 0.0004 \text{ s}^{-1} \cdot \mu\text{M}^{-1}$, $k_2 = 0.55 \text{ s}^{-1}$, $k_3 = 0.0034 \text{ s}^{-1}$ and $n = 150$. Comparison of the two panels shows that the idealized description of processive hydrolysis in Eqn (3) cannot account for the overall course of the process, but some characteristics, both qualitative and quantitative, are captured by the model. For example, the model accounts well for the diminished burst (i.e. the disappearance of the maximum) at low S_0 (below 5–10 μM). In these dilute samples, the rate of cellobiose production $C'(t)$ increases slowly to a level which is essentially constant over the time considered in Fig. 3. At higher S_0 , a clear maximum in $C'(t)$ signifies a burst phase in both model and experiment. On a quantitative level, comparisons of the maximal rate at the peak of the burst ($t = 150 \text{ s}$ in Fig. 3C) and after the burst ($t = 1400 \text{ s}$ in Fig. 3C) showed a rea-

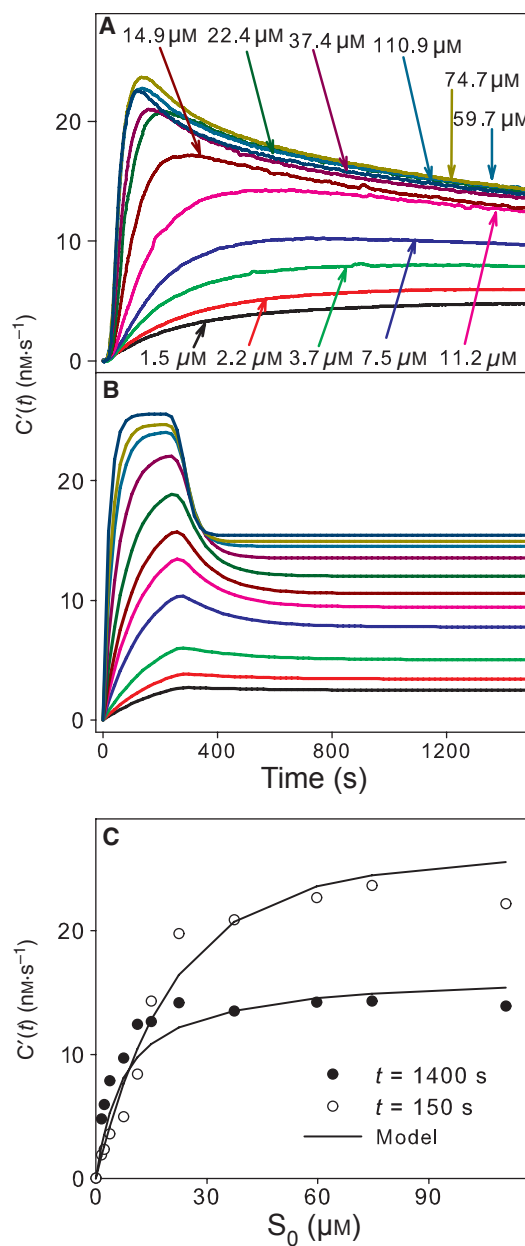


Fig. 3. Comparison of the results from experiment and model [Eqn (3)] for different substrate concentrations (S_0 in μM reducing ends). The enzyme concentration E_0 was 50 nM. Experimental (A) and model (B) $C'(t)$ results from Eqns (4) and (5) using the parameters $k_1 = 0.0004 \text{ s}^{-1} \cdot \mu\text{M}^{-1}$, $k_2 = 0.55 \text{ s}^{-1}$, $k_3 = 0.003 \text{ s}^{-1}$ and $n = 150$ cellobiose units. (C) Experimental (circles) and modeled (lines) rates at two time points plotted as a function of S_0 .

sonable accordance between experiments and model. In addition, the substrate concentration that gives half the maximal rate (5–10 mM) is similar to within experimental scatter (Fig. 3C). Conversely, two features of the experiments do not appear to be captured by Eqn (3). Firstly, the model predicts a sharp termination of the

burst phase, which tends to produce a rectangular shape of the $C'(t)$ function at high S_0 (Fig. 3B). This is in contrast with the experiments which all show a gradual decrease in $C'(t)$ after the maximum. Secondly, the model suggests a constant $C'(t)$ well within the time frame covered in Fig. 3, but no constancy was observed in the experiments. We return to this after discussing the effect of changing E_0 .

Figure 4 shows a comparison of the calorimetric measurements and model results for a series in which the enzyme load was varied and S_0 was kept constant at $40.8 \mu\text{M}$ reducing ends. The model calculations were based on the same parameters as in Fig. 3 without any additional fitting, and it appears that $C'(t)$ increases proportionally to E_0 . This behavior, which was seen in both model and experiment, implies that the turnover number $C'(t)/E_0$ is constant over the studied range of time and concentration, and this, in turn, suggests that the extent of the burst scales with E_0 . To analyze this further, $\pi_{\text{processive}}$ was estimated from the data in Fig. 4. For the model results (Fig. 4B), this is simply done by inserting the kinetic parameters in Eqn (6). For the experimental data, we first numerically integrated the rates in Fig. 4A to obtain the concentration

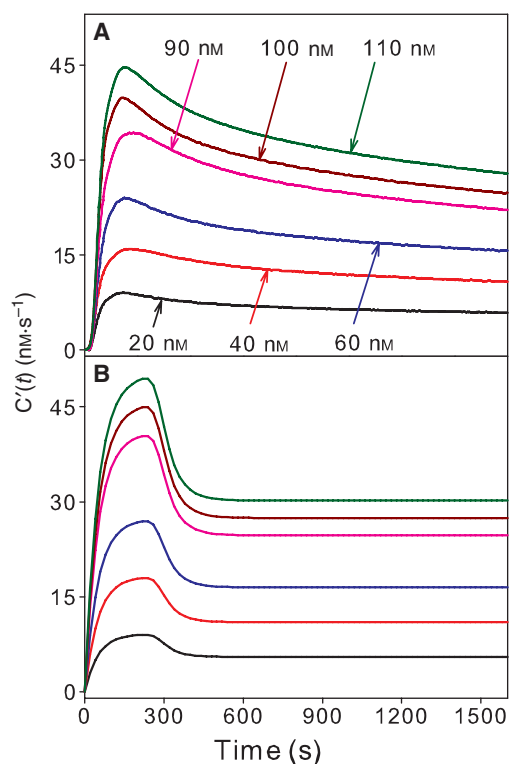


Fig. 4. Comparison of experimental and model results for different enzyme concentrations (E_0). The substrate concentration was $40.8 \mu\text{M}$ reducing ends. Experimental (A) and model (B) $C'(t)$ results using the same parameters as in Fig. 3.

of cellobiose $C(t)$, and then extrapolated linear fits to the data between 1400 and 1600 s to the ordinate as illustrated in the inset of Fig. 5. In analogy with the procedure used for nonprocessive enzymes (Fig. 1A), this intercept between the extrapolation and the $C(t)$ axis was taken as a measure of the experimental $\pi_{\text{processive}}$.

The proportionality of the theoretical $\pi_{\text{processive}}$ and E_0 seen in Fig. 5 follows directly from Eqn (6). The slope of the theoretical curve is about 42, suggesting that each enzyme molecule completes 42 catalytic cycles (produces 42 cellobiose molecules) during the burst phase. This is about three times less than the obstacle-free path (n), which is 150 in these calculations, and this discrepancy simply reflects that $k_1 S_0$ is too small for the simple relationship $\pi_{\text{processive}} = n E_0$ to be valid (see Theory section). Thus, low k_1 and the concomitant slow 'on rate' tend to smear out the burst and, consequently, $\pi_{\text{processive}}/E_0 < n$. This is a general weakness of the extrapolation procedure [17,18], also visible in Fig. 1, where the dotted line intersects the ordinate at a value slightly less than E_0 . It occurs when the rate constants and S_0 attain values that make the fractions on the right-hand side of Eqns (2) and (6) smaller than unity (this implies that the criteria for a simple π expression, $k_1 S_0 \gg k_3 + k_{-1}$ and $k_2 \gg k_3$, discussed in the Theory section, are not met [17,18]). More importantly, the experimental data also show proportionality between $\pi_{\text{processive}}$ and E_0 with a comparable slope (about 65), and this supports the general validity of Eqn (3).

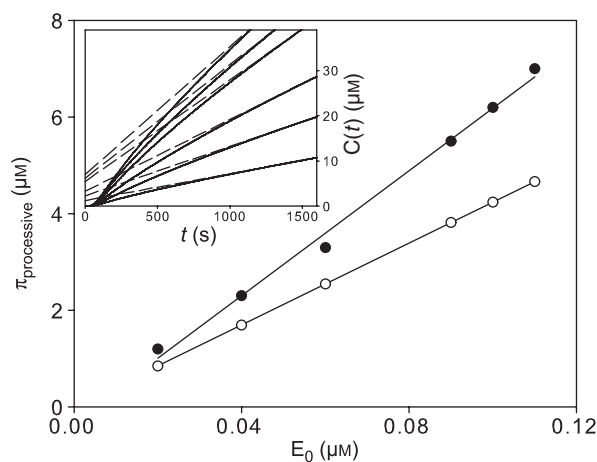


Fig. 5. Theoretical (open symbols) and experimental (filled symbols) estimates for the extent of the burst ($\pi_{\text{processive}}$) based on the results in Fig. 4. Theoretical values were obtained by insertion of the kinetic constants from Fig. 3 into Eqn (4), and the experimental values represent extrapolation of the $C'(t)$ function to $t = 0$ as illustrated in the inset. The extrapolations were based on linear fits to $C'(t)$ from 1400 to 1600 s.

We now return to the two general shortcomings of Eqn (3) which were identified above: (a) the abrupt termination of the modeled burst phase (Fig. 3B), which is evident for high S_0 and not seen in the experiments; and (b) the regime with constant $C'(t)$ (see, for example, $t > 500$ s in Fig. 4B and inset in Fig. 6), which is also absent in the measurements. We suggest that, at least to some extent, (a) is a consequence of the ‘polydispersity’ in n in a real substrate and (b) depends on the random inactivation of the enzyme. As discussed in the Theory section, simplified descriptions of these properties may be included in the model, and these modifications considerably improve the concordance

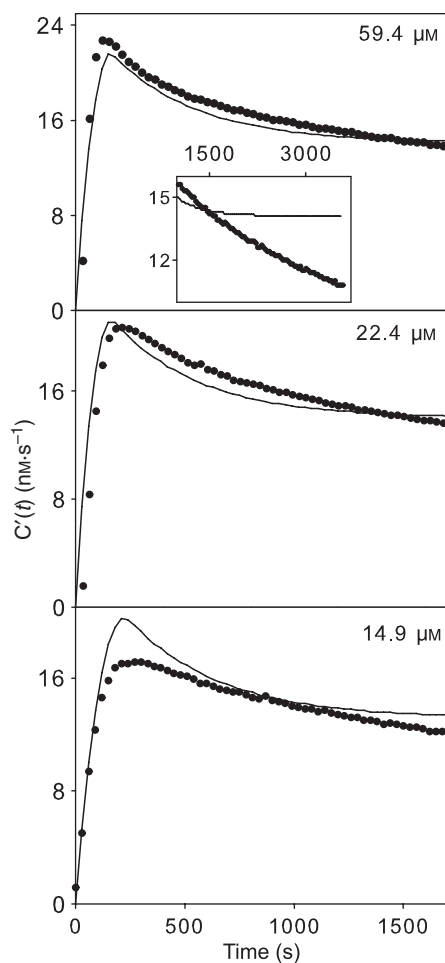


Fig. 6. Experimental data (symbols) and model results (lines) based on Eqn (3). In this case, the substrate was treated as a mixture with different obstacle-free path lengths. Specifically, S_0 was divided into five subsets with $n = 40, 70, 100, 130$ and 160 . The nonlinear regression was based on the data for the first 1700 s. The inset shows an enlarged picture of the course after 1700 s and illustrates that, for the simple model [Eqn (3)], the experimental values fall below the model beyond the time frame considered in the regression.

between theory and experiment. To illustrate this, we considered a substrate distribution with five subsets (each 20% of S_0) with $n = 40, 70, 100, 130$ and 160 , respectively. We analyzed the initial 1700 s of all trials in Fig. 3 using Eqn (5) and the nonlinear regression routine in Mathematica 7.0. It was found that, above $S_0 \sim 15 \mu\text{M}$, the parameters derived from each calorimetric experiment were essentially equal, and we conclude that one set of parameters can describe the results in this concentration range. The parameters were $k_2 = 1.0 \pm 0.2 \text{ s}^{-1}$, $k_3 = 0.0015 \pm 0.0003 \text{ s}^{-1}$ and $k_1 S_0 = 0.0052 \pm 0.001 \text{ s}^{-1}$, and some examples of the results are shown in Fig. 6. Parameter interdependence was evaluated partly by the confidence levels given by Mathematica and partly by ‘grid searches’, which provide an unambiguous measure of parameter dependence [28,29] and hence reveal possible overparameterization. In the latter procedure, the standard deviation of the fit was determined in sequential regressions, where two of the rate constants were allowed to change, whilst the third was inserted as a constant with values slightly above or below the maximum likelihood parameter [28,29]. These analyses showed moderate parameter dependence with 95% confidence intervals of about $\pm 10\%$ (slightly asymmetric with larger margins upwards). This limited parameter interdependence is also illustrated in the correlation matrix in Data S1, which shows that all correlation coefficients are below 0.7, and we conclude that it is realistic to extract three rate constants from the experimental data. The parameters from this regression analysis may be compared with recent work [30], which used an extensive analysis of reducing ends in both soluble and insoluble fractions to estimate apparent first-order rate constants for processive hydrolysis and enzyme–substrate disassociation, respectively. Values for the system investigated in Fig. 6 (i.e. *T. reesei* Cel7A and amorphous cellulose) were $1.8 \pm 0.5 \text{ s}^{-1}$ (hydrolysis) and $0.0032 \pm 0.0006 \text{ s}^{-1}$ (dissociation) at 30 °C [30]. The concordance of these values, which were derived by a completely different approach, and k_2 and k_3 from Fig. 6 provides strong support of the molecular picture in Eqn (3). With respect to the ‘on rate’, it is interesting to note that a constant value of k_1 provided very poor concordance between theory and experiment (not shown), whereas constant $k_1 S_0$ gave satisfactory agreement (Fig. 6). This suggests that the initiation of hydrolysis (adsorption to the insoluble substrate and ‘threading’ of the cellulase) exhibits apparent first-order kinetics. This may reflect the reduced dimensionality or fractal kinetics, which has previously been proposed for cellulase activity on insoluble substrates [31,32], and it appears

that the current approach holds some potential for systematic investigations of this phenomenon.

The model could not account for the measurements at the lowest S_0 , and this may reflect the fact that the assumption $S_0 \gg E_0$, used in the derivation of the expression for $C'(t)$, becomes unacceptable. Thus, the concentration of reducing ends $S_0 : E_0$ ranges from 30 to 2200 in this work (for $S_0 = 15 \mu\text{M}$, it is 300). If, however, we use instead the accessible area of amorphous cellulose, which is about $42 \text{ m}^2 \cdot \text{g}^{-1}$ [33], and a footprint of 24 nm^2 for Cel7A [34], we find an $S_0 : E_0$ area ratio (total available substrate area divided by monolayer coverage area of the whole enzyme population) which is an order of magnitude smaller (3–240). These latter numbers are rough approximations as the average area of randomly adsorbed enzymes will be larger than the footprint, and only a certain fraction of the enzyme will be adsorbed in the initial stages. Nevertheless, the analysis suggests that not all reducing ends are available in amorphous cellulose, and hence the deficiencies of the model at substrate concentrations below $15 \mu\text{M}$ could reflect the fact that the premise $S_0 \gg E_0$ becomes increasingly unrealistic.

The results in Fig. 6 are for the fixed average and distribution of n mentioned above. We also tried wider or narrower distributions with five subsets, distributions with 10 subsets and distributions with a predominance of n values close to the average (e.g. 5%, 20%, 50%, 20%, 5%, instead of equal amounts of the five subsets). The regression analysis with these different interpretations of n polydispersity gave comparable fits and parameters. In addition, average n values of 100 ± 50 were found to account reasonably for the measurements, and we conclude that detailed information on the obstacle-free path n will require a broader experimental material, particularly investigations of different types of substrate.

We consistently found that the experimental $C'(t)$ fell below the model towards the end of the 1-h experiments (see inset in Fig. 6). For a series of 4-h experiments (not shown), this tendency was even more pronounced. This was interpreted as protein inactivation, as discussed in the Theory section. Numeric analysis with respect to Eqn (7) showed that the inclusion of inactivation and the same polydispersity as in Fig. 6 enabled the model to fit the data reasonably over the studied time frame for S_0 above approximately $15 \mu\text{M}$. Some examples of this for different S_0 are shown in Fig. 7.

The parameters from the analysis in Fig. 7 were $k_1 S_0 = (5.2 \pm 1.6) \times 10^{-3} \text{ s}^{-1}$, $k_2 = 1 \pm 0.3 \text{ s}^{-1}$, $k_3 = k_{-1} = (1.2 \pm 0.6) \times 10^{-3} \text{ s}^{-1}$ and $k_4 = (2 \pm 0.7) \times 10^{-4} \text{ s}^{-1}$. The parameter dependence of these fits is illustrated in the correlation matrix in Data S1. It appears

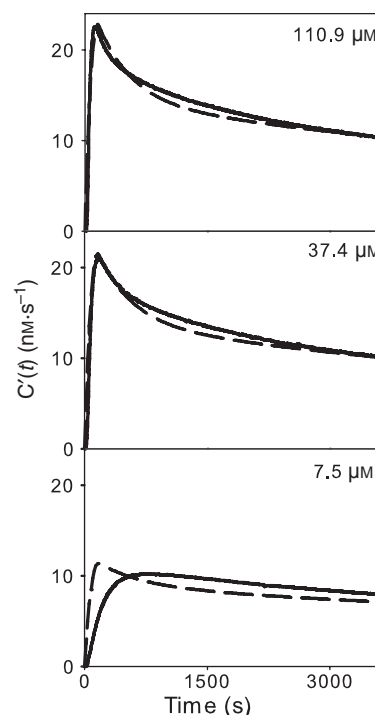


Fig. 7. Experimental data (full lines) and results from the model in Eqn (7) (broken lines) at different substrate concentrations. The concentration of Cel7A was 50 nM . The parameters were $k_1 S_0 = 5.2 \times 10^{-3} \text{ s}^{-1}$, $k_2 = 1 \text{ s}^{-1}$, $k_3 = k_{-1} = 1.2 \times 10^{-3} \text{ s}^{-1}$ and $k_4 = 2 \times 10^{-4} \text{ s}^{-1}$. The obstacle-free path lengths were 40, 70, 100, 130 and 160, respectively, for the five substrate subsets so that the average n was 100. It appears that inclusion of the inactivation rate constant k_4 enables the model to account for 1-h trials.

that k_3 and k_4 show some interdependence, with an average correlation coefficient of 0.88, whereas other correlation coefficients are low or very low. This result supports the validity of extracting four parameters from the analysis in Fig. 7. The parameters for $k_1 S_0$, k_2 and k_3 are essentially equal to those from the simpler analysis in Fig. 6, and the inactivation constant k_4 is about an order of magnitude lower than k_3 . The rates in Fig. 7 were integrated to give the concentration $C(t)$, and two examples are shown in Fig. 8. In this presentation, the accordance between model and experiment appears to be better, and this underscores the fact that the rate function $C'(t)$ provides a more discriminatory parameter for modeling than does the concentration $C(t)$. Figure 8 also shows that the percentage of cellulose converted during the experiment (right-hand ordinate) ranges from a fraction of a percent for the higher to a few percent for the lower S_0 values.

The qualitative interpretation of Fig. 7 is that Cel7A produces a burst in hydrolysis when enzymes make their initial 'rush' down a cellulose strand towards the first encounter with a 'check block', and then enters a

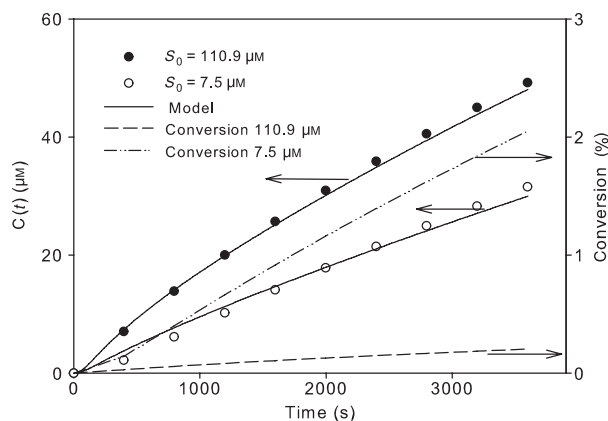


Fig. 8. Concentration of cellobiose produced by 50 nM Cel7A at 25 °C plotted as a function of time. These results for $S_0 = 110.9 \mu\text{M}$ (filled symbols) and $7.5 \mu\text{M}$ (open symbols) and for the model in Eqn (7) (lines) were obtained by integration of the data in Fig. 7. The broken and chain lines show the conversion in percent of the initial amount of cellulose.

second phase with a slow, single-exponential decrease in $C'(t)$ as the enzymes gradually become inactivated. In this latter stage, all enzymes have encountered a 'check block' and, in this sense, it corresponds to the constant rate regime in Fig. 2. Unlike in Fig. 2, however, $C'(t)$ is not constant, but decreasing, as dictated by the rate constant of the inactivation process k_4 . In this interpretation, the extent of inactivation scales with enzyme activity (number of catalytic steps) and not with time. Hence, for any enzyme-substrate complex EC_{n-i} , the probability of experiencing inactivation when it moves one step to the right in Eqn (7) is $k_4/(k_2 + k_3 + k_4)$. For the parameters in Fig. 7, this translates to about one inactivation for every 5000 hydrolytic steps, which is consistent with the frequency of inactivation (1 : 6000) suggested for a cellobiohydrolase working on soluble cello-oligosaccharides [35]. As the final $C(t)$ is about 40 μM in Fig. 8, and we used $E_0 = 50 \text{ nM}$, each enzyme has performed about 800 hydrolytic steps in these experiments. With a probability of 2×10^{-4} , some inactivation can be observed within the experimental time frame used here, and this is further illustrated in Fig. 11. It is also interesting to note that the probability of hydrolysis of an EC_{n-i} complex (k_2) is about 800 times larger than the probability of disassociation (k_3), and hence a processivity of that magnitude would be expected for an ideal, 'obstacle-free' cellulose strand.

The notion of two partially overlapping phases of the slowdown is interesting in the light of the experimental observations of a 'double exponential decay' reported for the rate of cellulolysis [6,36–38]. In these studies, hydrolysis rates for quite different systems

were successfully fitted to empirical expressions of the type $C'(t) = Ae^{-\alpha t} + Be^{-\beta t}$. This behavior has been associated with two-phase substrates (high and low reactivity) [37], but, in the current interpretation, it relies on the properties of the enzyme. The first (rapid) time constant α reflects the gradual termination of the burst as the enzymes encounter their first 'check block', and the second (slower) constant β represents inactivation and is related to k_4 in Eqn (7). As the extent of the first phase will scale with the amount of protein, this interpretation is congruent with the proportional growth of $\pi_{\text{processive}}$ with E_0 shown in Fig. 5. This enzyme-based interpretation of the double exponential decay predicts that a second injection of enzyme to a reacting sample would generate a second burst (whereas a second burst in $C'(t)$ would not be expected if the slowdown relied on the depletion of good substrate). Figure 9 shows that a second dosage of Cel7A after 1 h indeed gives a second burst, which is similar to the first, and this further supports the current explanation of the double exponential slowdown.

In the last section, we show two examples of how the analysis of the kinetic parameters may elucidate certain aspects of the activity of Cel7A. First, we consider changes in the ratio $k_1 S_0/k_3$. This reflects the ratio of the 'on rate' and 'off rate'. At a fixed k_2 , a change in this ratio may be interpreted as a change in the affinity of the enzyme for the substrate. Hence, we can assess relationships of this 'affinity parameter' and the hydrolysis rate $C'(t)$. The results of such an analysis using $S_0 = 25 \mu\text{M}$ and the simple model [Eqn (3)] are illustrated in Fig. 10. The black curve, which is the same in all three panels, represents the cellobiose production rate $C'(t)$, calculated using the parameters from Fig. 3. Figure 10A illustrates the effects of increased 'affinity', inasmuch as k_1/k_3 is enlarged by factors of two, three and five for the red, green and blue curves, respectively. This was performed by both multiplying the original k_1 and dividing the original k_3 by $\sqrt{2}$, $\sqrt{3}$ and $\sqrt{5}$, respectively. It appears that these changes strongly promote the initial burst, but also decrease the rate later in the process (the curves cross over around $t = 300 \text{ s}$). This decrease in $C'(t)$ is mainly a consequence of smaller k_3 values ('off rates'), which make the release of enzymes stuck in front of a 'check block' the rate-limiting step [the population of inactive EC_x in Eqn (3) increases]. Figure 10B shows the results when the k_1/k_3 ratio is decreased in an analogous fashion. This reduces $C'(t)$ over the whole time course, and this is mainly because the population of unbound (aqueous) enzyme becomes large when k_1 (the 'on rate') is diminished. The blue curves in Fig. 10B, C also illustrate how a moderate increase in

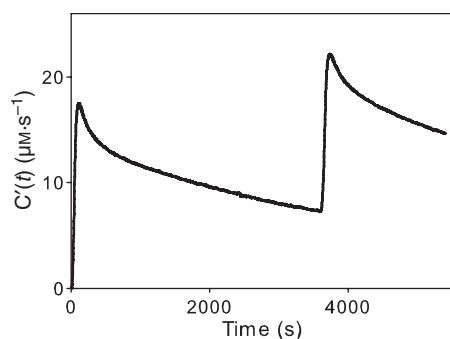


Fig. 9. Rate of cellobiose production $C'(t)$ as a function of time for $S_0 = 70 \mu\text{M}$. One aliquot of 50 nM Cel7A was added at $t = 0$ and a second dose (bringing the total enzyme concentration to 100 nM) was added at $t = 3600$ s.

k_3 tends to abolish the burst (maximum) in $C'(t)$ altogether. This is because the inhibitory effect of the 'check block', as defined by the broken line in Fig. 2, becomes unimportant when the release rate is increased. Multiplying both k_1 and k_3 by $\sqrt{2}$, $\sqrt{3}$ and $\sqrt{5}$, respectively, will obviously not change the ratio (or 'affinity'), but will speed up both adsorption and desorption, and hence increase the rate of hydrolysis (Fig. 10C).

For the model in Eqn (7), the enzyme is distributed between four states: aqueous (E), catalytically active (EC_{n-i}), stuck at 'check block' (EC_x) or inactivated (IC_{n-i}). These enzyme concentrations can be numerically derived from the parameters found in Fig. 7. Figure 11 shows an example of such an analysis for $E_0 = 50$ nM and $S_0 = 37.4 \mu\text{M}$ (i.e. corresponding to the middle panel in Fig. 6). It appears that the concentration of free enzyme (E) decreases for about 10 min and then reaches a near-constant (slowly decreasing) level which is about 20% of E_0 . This calculated course of $E(t)$ is in line with earlier experimental results on different types of substrate [39–43]. In addition, an 80% reduction in free enzyme after about 10 min

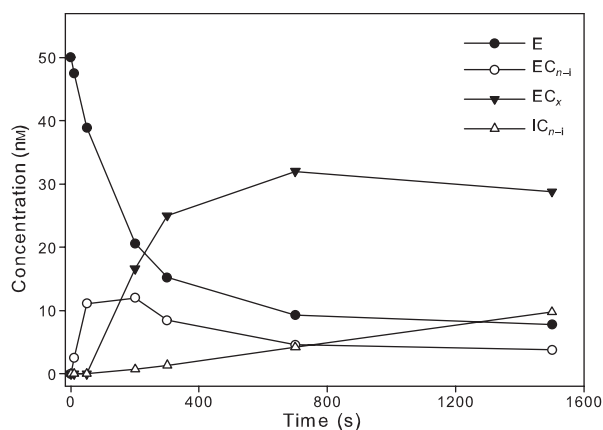


Fig. 11. Time-dependent distribution of enzyme between the four states defined in Eqn (7). The values were calculated at different time points using the kinetic parameters listed in Fig. 7. The total enzyme concentration (E_0) was 50 nM and S_0 was $37.4 \mu\text{M}$ (hence corresponding to the middle panel of Fig. 7).

matches our own adsorption measurements for a mixture of *T. reesei* cellulases on amorphous cellulose (L. Murphy, unpublished data). The population of catalytically active enzyme is highest (and about 25% of E_0) after a few minutes, but decreases at later stages, as a growing fraction of the enzyme becomes stuck in front of a 'check block'. After about 12 min, this population is well over half of E_0 and this transition from active EC_{n-i} to stuck EC_x is the origin of the burst in cellobiose production. As the inactivation of enzyme in Eqn (7) is modeled as an irreversible transition, the concentration of this species grows monotonically. This behavior also appears from Fig. 11, but further analysis of IC_{n-i} is postponed until calorimetric trials over extended time frames (and hence more precise values of k_4) become available.

In summary, we have proposed an explicit model that describes the initial burst and subsequent slow-down in the rate of cellobiose production for processive enzymes such as Cel7A. The focus is on the initial

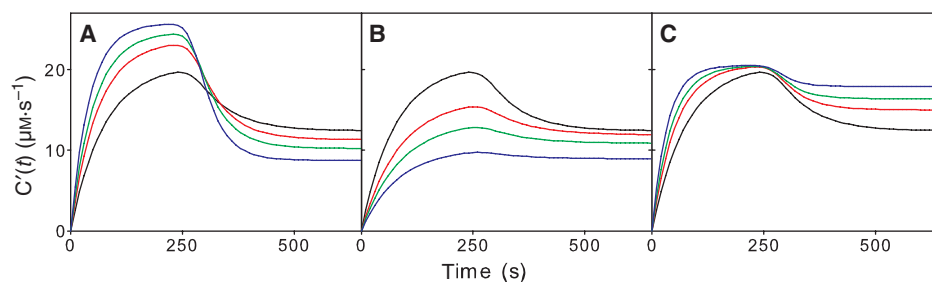


Fig. 10. Parameter dependence of the rate $C'(t)$ calculated from the simple model [Eqn (3)] using $S_0 = 25 \mu\text{M}$. The black curves are identical in the three panels and were calculated from the parameters listed in Fig. 3. The other curves represent $C'(t)$ when the ratio k_1/k_3 is increased (A) or decreased (B) by a factor of two (red), three (green) or five (blue), respectively. (C) Ratio k_1/k_3 is constant, but the values of both k_1 and k_3 are multiplied by $\sqrt{2}$, $\sqrt{3}$ and $\sqrt{5}$, respectively.

phase of the process, where inhibition from accumulated product and/or the depletion of good attack points on the substrate are of minor importance. We found that a burst and slowdown may indeed occur as a consequence of obstacles to processive movement, on the one hand, and the relative size of rate constants for adsorption, processive hydrolysis and desorption, on the other. This interpretation is analogous to that conventionally used for the description of burst phases in systems with soluble substrates and nonprocessive enzymes. The theory was tested against calorimetric measurements of the hydrolysis of amorphous cellulose by *T. reesei* Cel7A. No other enzymes or substrates were investigated, and the conclusions thus only pertain directly to this system. We note, however, that, if the origin of the slowdown is linked to low dissociation rates (low k_3), as suggested here, an analogous burst behavior should be expected on other substrates, and it appears relevant to conduct such measurements. We found that some experimental hallmarks were reproduced in a simple burst model, where the only cause of the slowdown was a protracted release of enzyme that had reached the obstacle on the cellulose chain. However, to account more precisely for the experimental data, it was necessary to consider enzyme inactivation as well as some heterogeneity in the obstacle-free path length. We implemented the former as an irreversible inactivation step that competed with the production of cellobiose in each hydrolytic cycle. The result was a more complex model which could explain the 'double exponential decay' in the rate of cellobiose production which has been reported in several earlier studies. Thus, in this interpretation, the fast component in the double exponential decay reflects the first sweep of each cellulase down a cellulose strand, whereas the slow component is ascribed to random inactivation which is unrelated to the stage of the process. It has recently been stated that 'processivity is more about disassociation than about the rate of hydrolysis' [44], and a pronounced improvement in activity has indeed been observed in an enzyme variant with diminished processivity [45]. We suggest that the models presented here may be useful in attempts to elucidate and rationalize such interrelationships of activity and processivity.

Materials and methods

All mathematical analysis and numerical fitting were performed using the software package Mathematica 7.0 (Wolfram Research, Inc. Champaign, IL, USA).

The substrate in the calorimetric measurements was reconstituted amorphous cellulose (RAC) prepared essen-

tially as described by Zhang *et al.* [46] Briefly, 0.4 g cellulose (Sigmacell 20) was suspended in 0.6 mL MilliQ-water and placed on ice before adding 8 mL cold 85% phosphoric acid with vigorous stirring. After a few minutes, an additional 2-mL aliquot of phosphoric acid was added. This mixture was incubated for 40 min on ice with continuous stirring. Then, 40 mL of MilliQ-water was slowly added with vigorous stirring. The suspension was transferred to a 50-mL centrifuge tube and centrifuged at 2500 g for 15 min. The cellulose was washed in water and spun down three times, and then resuspended in 50 mL of 0.05 M Na₂CO₃ to neutralize traces of acid. The carbonate was removed by four washes in water and four in buffer (50 mM sodium acetate, pH 5.00 + 2 mM CaCl₂), and the final product was then suspended in 50 mL of acetate buffer. RAC was blended for 5 min in a coaxial mixer.

The number of reducing ends (i.e. attack points for Cel7A) in the produced RAC was determined by the BCA method [47]. The BCA stock reagents A (1.942 g·L⁻¹ disodium-2,2'-bichinchoniate + 54.28 g·L⁻¹ Na₂CO₃ + 24.2 g·L⁻¹ NaHCO₃) and B (1.248 g·L⁻¹ CuSO₄·5H₂O + 1.262 g·L⁻¹ L-serine) were mixed 1 : 1. RAC was diluted 20 times before mixing 0.75 mL RAC and 0.75 mL BCA (working solution) in a 2-mL Eppendorf tube. After 30 min at 75 °C in a thermomixer, the cellulose was centrifuged down at 9000 g for 5 min, and the absorbance at 560 nm was measured (Shimadzu UV1700, Kyoto, Japan) and quantified against a 0–50-μM cellobiose standard curve.

Trichoderma reesei Cel7A was purified by column chromatography. Desalted concentrated culture broth from a *T. reesei* strain with deletion of the Cel7A gene was applied in 20 mM Tris, pH 8.5, to a Q-Sepharose Fast Flow column (GE Healthcare Lifesciences, Little Chalfont, UK) and eluted in the same buffer with a gradient to 1 M NaCl. Fractions containing purified Cel7A were identified by SDS/PAGE and pooled. The fraction with Cel7A was mixed with ammonium sulfate to 1 M, and applied to Phenyl Sepharose (GE Healthcare Lifesciences), and eluted in a gradient from 1 to 0 M ammonium sulfate in 20 mM Tris, pH 7.5. Fractions containing purified Cel7A were identified by SDS/PAGE, pooled, concentrated and buffer exchanged to 20 mM Tris, ~150 mM NaCl, pH 7.5.

The enzymatic activity was measured by the calorimetric method recently described in detail by Murphy *et al.* [48]. RAC at different concentrations was loaded into the cell of the isothermal titration calorimeter (VP-ITC, Microcal, Piscataway, NJ, USA) at 25 °C and titrated with Cel7A from the syringe. All samples were dissolved in 50 mM sodium acetate with 2 mM calcium chloride, pH 5.00. In addition to the substrate, the calorimetric cell also contained 0.3 mg·mL⁻¹ β-glucosidase, 25 GODU·mL⁻¹ glucose oxidase and 25 CIU·mL⁻¹ catalase [48]. As a result, the cellobiose produced by the hydrolysis of RAC is first cleaved into two glucose molecules, and then oxidized to two D-glucono-δ-lactone molecules. This strongly amplifies the

heat signal and hence allows measurements at low enzyme dosages such as those used here. The advantages and limitations of the coupled calorimetric assay are discussed elsewhere [48]. The raw result from the calorimetric measurements is the heat flow in $\text{J}\cdot\text{s}^{-1}$ (W), and this is readily converted to the rate of cellobiose production (in $\text{M}\cdot\text{s}^{-1}$) by division with the molar enthalpy change of the coupled reaction ($-360 \text{ kJ}\cdot\text{mol}^{-1}$) [48] and the volume of the calorimetric cell (1.42 mL). The response time of the calorimeter is about 15 s and no correction for this was introduced in the analysis.

Acknowledgements

This work was supported by The Danish Council for Strategic Research (grants 09-063210 and 2104-07-0028). Expert experimental assistance from David Osborne and Erik L. Rasmussen is gratefully acknowledged.

References

- Nidetzky B & Steiner W (1993) A new approach for modeling cellulase–cellulose adsorption and the kinetics of the enzymatic-hydrolysis of microcrystalline cellulose. *Biotechnol Bioeng* **42**, 469–479.
- Zhang S, Wolfgang DE & Wilson DB (1999) Substrate heterogeneity causes the nonlinear kinetics of insoluble cellulose hydrolysis. *Biotechnol Bioeng* **66**, 35–41.
- Yang B, Willies DM & Wyman CE (2006) Changes in the enzymatic hydrolysis rate of avicel cellulose with conversion. *Biotechnol Bioeng* **94**, 1122–1128.
- Eriksson T, Karlsson J & Tjerneld F (2002) A model explaining declining rate in hydrolysis of lignocellulose substrates with cellobiohydrolase I (Cel7A) and endoglucanase I (Cel7B) of *Trichoderma reesei*. *Appl Biochem Biotechnol* **101**, 41–60.
- Igarashi K, Wada M, Hori R & Samejima M (2006) Surface density of cellobiohydrolase on crystalline celluloses – a critical parameter to evaluate enzymatic kinetics at a solid–liquid interface. *FEBS J* **273**, 2869–2878.
- Valjamae P, Sild V, Pettersson G & Johansson G (1998) The initial kinetics of hydrolysis by cellobiohydrolases I and II is consistent with a cellulose surface-erosion model. *Eur J Biochem* **253**, 469–475.
- Berlin A, Maximenko V, Bura R, Kang KY, Gilkes N & Saddler J (2006) A rapid microassay to evaluate enzymatic hydrolysis of lignocellulosic substrates. *Biotechnol Bioeng* **93**, 880–886.
- Eriksson T, Borjesson J & Tjerneld F (2002) Mechanism of surfactant effect in enzymatic hydrolysis of lignocellulose. *Enzyme Microb Technol* **31**, 353–364.
- Meunier-Goddik L & Penner MH (1999) Enzyme-catalyzed saccharification of model celluloses in the presence of lignocellulosic residues. *J Agric Food Chem* **47**, 346–351.
- Bansal P, Hall M, Realff MJ, Lee JH & Bommarius AS (2009) Modeling cellulase kinetics on lignocellulosic substrates. *Biotechnol Adv* **27**, 833–848.
- Lynd LR, Weimer PJ, van Zyl WH & Pretorius IS (2002) Microbial cellulose utilization: fundamentals and biotechnology. *Microbiol Mol Biol Rev* **66**, 506–577.
- Segel IH (1975) *Enzyme Kinetics: Behavior and Analysis of Rapid Equilibrium and Steady-State Enzyme Systems*. John Wiley & Sons Inc., New York.
- Kipper K, Valjamae P & Johansson G (2005) Processive action of cellobiohydrolase Cel7A from *Trichoderma reesei* is revealed as ‘burst’ kinetics on fluorescent polymeric model substrates. *Biochem J* **385**, 527–535.
- Jalak J & Valjamae P (2010) Mechanism of initial rapid rate retardation in cellobiohydrolase catalyzed cellulose hydrolysis. *Biotechnol Bioeng* **106**, 871–883.
- Gutfreund H & Sturtevant JM (1956) Mechanism of the reaction of chymotrypsin with para-nitrophenyl acetate. *Biochem J* **63**, 656–661.
- Hartley BS & Kilby BA (1954) The reaction of para-nitrophenyl esters with chymotrypsin and insulin. *Biochem J* **56**, 288–297.
- Cornish-Bowden A (2004) *Fundamentals of Enzyme Kinetics*, 3rd edn. Portland Press, London, UK.
- Fersht A (1977) *Enzyme Structure and Mechanism*, 2nd edn. W.H. Freeman and Company, New York.
- Gutfreund H & Sturtevant JM (1956) The mechanism of chymotrypsin-catalyzed reactions. *Proc Natl Acad Sci USA* **42**, 719–728.
- Knight CG (1995) Active-site titration of peptidases. In *Proteolytic Enzymes: Aspartic and Metallo Peptidases* (Barrett AJ eds), pp 85–101. Methods in Enzymology **248**, Academic Press, San Diego, USA.
- Gan Q, Allen SJ & Taylor G (2003) Kinetic dynamics in heterogeneous enzymatic hydrolysis of cellulose: an overview, an experimental study and mathematical modelling. *Process Biochem* **38**, 1003–1018.
- Abramowitz M & Stegun IA (1972) *Handbook of Mathematical Functions with Formulas, Graphs, and Mathematical Tables*, 9th edn. Dover Publication Inc., New York.
- Zhang YHP, Himmel ME & Mielenz JR (2006) Outlook for cellulase improvement: screening and selection strategies. *Biotechnol Adv* **24**, 452–481.
- Ma AZ, Hu Q, Qu YB, Bai ZH, Liu WF & Zhuang GQ (2008) The enzymatic hydrolysis rate of cellulose decreases with irreversible adsorption of cellobiohydrolase I. *Enzyme Microb Technol* **42**, 543–547.
- Beldman G, Voragen AGJ, Rombouts FM, Searle van Leeuwen MF & Pilnik W (1987) Adsorption and kinetic-behavior of purified endoglucanases and exoglucanases from *Trichoderma viride*. *Biotechnol Bioeng* **30**, 251–257.
- Converse AO, Matsuno R, Tanaka M & Taniguchi M (1988) A model of enzyme adsorption and hydrolysis of

- microcrystalline cellulose with slow deactivation of the adsorbed enzyme. *Biotechnol Bioeng* **32**, 38–45.
- 27 Xu F, Ding HS, Osborn D, Tejirian A, Brown K, Albano W, Sheehy N & Langston J (2008) Partition of enzymes between the solvent and insoluble substrate during the hydrolysis of lignocellulose by cellulases. *J Mol Catal B-Enzym* **51**, 42–48.
 - 28 Johnson ML (1992) Why, when, and how biochemists should use least-squares. *Anal Biochem* **206**, 215–225.
 - 29 Johnson ML & Frasier SG (1985) Nonlinear least-squares analysis. *Methods Enzymol* **117**, 301–342.
 - 30 Kurasin M & Valjämäe P (2011) Processivity of cellobiohydrolases is limited by the substrate. *J Biol Chem* **286**, 169–177.
 - 31 Valjamae P, Kipper K, Pettersson G & Johansson G (2003) Synergistic cellulose hydrolysis can be described in terms of fractal-like kinetics. *Biotechnol Bioeng* **84**, 254–257.
 - 32 Xu F & Ding HS (2007) A new kinetic model for heterogeneous (or spatially confined) enzymatic catalysis: contributions from the fractal and jamming (overcrowding) effects. *Appl Catal A-Gen* **317**, 70–81.
 - 33 Hong J, Ye XH & Zhang YHP (2007) Quantitative determination of cellulose accessibility to cellulase based on adsorption of a nonhydrolytic fusion protein containing CBM and GFP with its applications. *Langmuir* **23**, 12535–12540.
 - 34 Stahlberg J, Johansson G & Pettersson G (1991) A new model for enzymatic-hydrolysis of cellulose based on the 2-domain structure of cellobiohydrolase-I. *Bio-Technology* **9**, 286–290.
 - 35 Harjunpää V, Teleman A, Koivula A, Ruohonen L, Teeri TT, Teleman O & Drakenberg T (1996) Cellobiohydrolase II from *Trichoderma reesei* – association and rate constants derived from an analysis of progress curves. *Eur J Biochem* **240**, 584–591.
 - 36 Murphy L, Borch K, McFarland KC, Bohlin C & Westh P (2010) A calorimetric assay for enzymatic saccharification of biomass. *Enzyme Microb Technol* **46**, 141–146.
 - 37 Sattler W, Esterbauer H, Glatter O & Steiner W (1989) The effect of enzyme concentration on the rate of the hydrolysis of cellulose. *Biotechnol Bioeng* **33**, 1221–1234.
 - 38 Olsen SN, Lumby E, McFarland KC, Borch K & Westh P (2010) Kinetics of enzymatic high-solid hydrolysis of ligno-cellulosic biomass studied by calorimetry. *Appl. Biochem. Biotech.* **163**, 626–635.
 - 39 Medve J, Karlsson J, Lee D & Tjerneld F (1998) Hydrolysis of microcrystalline cellulose by cellobiohydrolase I and endoglucanase II from *Trichoderma reesei*: adsorption, sugar production pattern, and synergism of the enzymes. *Biotechnol Bioeng* **59**, 621–634.
 - 40 Medve J, Stahlberg J & Tjerneld F (1994) Adsorption and synergism of cellobiohydrolase-I and cellobiohydrolase-II of *Trichoderma reesei* during hydrolysis of microcrystalline cellulose. *Biotechnol Bioeng* **44**, 1064–1073.
 - 41 Nidetzky B, Steiner W & Claeysens M (1994) Cellulose hydrolysis by the cellulases from *Trichoderma reesei* – adsorptions of 2 cellobiohydrolases, 2 endocellulases and their core proteins on filter-paper and their relation to hydrolysis. *Biochem J* **303**, 817–823.
 - 42 Palonen H, Tenkanen M & Linder M (1999) Dynamic interaction of *Trichoderma reesei* cellobiohydrolases Cel6A and Cel7A and cellulose at equilibrium and during hydrolysis. *Appl Environ Microbiol* **65**, 5229–5233.
 - 43 Tomme P, Heriban V & Claeysens M (1990) Adsorption of 2 cellobiohydrolases from *Trichoderma reesei* to Avicel – evidence for exo–exo synergism and possible loose complex-formation. *Biotechnol Lett* **12**, 525–530.
 - 44 Vuong TV & Wilson DB (2009) Processivity, synergism, and substrate specificity of *Thermobifida fusca* Cel6B. *Appl Environ Microbiol* **75**, 6655–6661.
 - 45 Horn SJ, Sikorski P, Cederkvist JB, Vaaje-Kolstad G, Sorlie M, Synstad B, Vriend G, Varum KM & Eijsink VGH (2006) Costs and benefits of processivity in enzymatic degradation of recalcitrant polysaccharides. *Proc Natl Acad Sci USA* **103**, 18089–18094.
 - 46 Zhang YHP, Cui JB, Lynd LR & Kuang LR (2006) A transition from cellulose swelling to cellulose dissolution by o-phosphoric acid: evidence from enzymatic hydrolysis and supramolecular structure. *Biomacromolecules* **7**, 644–648.
 - 47 Zhang YHP & Lynd LR (2005) Determination of the number-average degree of polymerization of cellooligosaccharides and cellulose with application to enzymatic hydrolysis. *Biomacromolecules* **6**, 1510–1515.
 - 48 Murphy L, Baumann MJ, Borch K, Sweeney M & Westh P (2010) An enzymatic signal amplification system for calorimetric studies of cellobiohydrolases. *Anal Biochem* **404**, 140–148.

Supporting information

The following supplementary material is available:
Data S1. Derivations of the expressions for $P_1(t)$, $P_2(t)$, $P_1'(t)$ and $P_2'(t)$ used in Fig. 1 and derivations of Eqns (2) and (4)–(6).

This supplementary material can be found in the online version of this article.

Please note: As a service to our authors and readers, this journal provides supporting information supplied by the authors. Such materials are peer-reviewed and may be re-organized for online delivery, but are not copy-edited or typeset. Technical support issues arising from supporting information (other than missing files) should be addressed to the authors.

Contribution to Article 6: Advantages of isothermal titration calorimetry for xylanase kinetics in comparison to chemical-reducing-end assays.

Martin J. Baumann, **Leigh Murphy**, Nina Lei, Kristian B.R.M. Krogh, Kim Borch, Peter Westh.



Advantages of isothermal titration calorimetry for xylanase kinetics in comparison to chemical-reducing-end assays

Martin J. Baumann^{a,b}, Leigh Murphy^{a,b}, Nina Lei^{a,b}, Kristian B.R.M. Krogh^b, Kim Borch^b, Peter Westh^{a,*}

^a Department of Science, Systems, and Models (NSM), Biomaterials, Roskilde University, DK-4000 Roskilde, Denmark

^b Novozymes A/S, DK-2880 Bagsværd, Denmark

ARTICLE INFO

Article history:

Received 22 June 2010

Received in revised form 28 October 2010

Accepted 3 November 2010

Available online 11 November 2010

Keywords:

Isothermal titration calorimetry

Xylanase assay

CBM

Reducing end

Enzyme kinetic

ABSTRACT

In lignocellulosic raw materials for biomass conversion, hemicelluloses constitute a substantial fraction, with xylan being the primary part. Although many pretreatments reduce the amount or change the distribution of xylan, it is important to degrade residual xylan so as to improve the overall yield. Typically, xylanase reaction rates are measured in stopped assays by chemical quantification of the reducing ends. With isothermal titration calorimetry (ITC), the heat flow of the hydrolysis can be measured in continuous fashion, with the reaction rate being directly proportional to the heat flow. Reaction enthalpies for carbohydrate hydrolysis are typically below 5 kJ/mol, which is the limiting factor for straight forward calorimetric quantification of enzymatic reaction rates using current ITC technology. To increase the apparent reaction enthalpy, we employed a subsequent oxidation of hydrolysis products by carbohydrate oxidase and catalase. Here we show that the coupled assay with carbohydrate oxidase and catalase can be used to measure enzyme kinetics of a GH10 xylanase from *Aspergillus aculeatus* on birch xylan and wheat arabinoxylan. Results are discussed in the light of a critical analysis of the sensitivity of four chemical-reducing-end quantification methods using well-characterized substrates.

© 2010 Elsevier Inc. All rights reserved.

Xylan is a heterogeneous class of hemicelluloses found in plants from unicellular green algae $\beta(1 \rightarrow 3)$ homoxylylans to higher plants with the typical $\beta(1 \rightarrow 4)$ xylose backbone, which may be substituted with arabinose, glucuronic acid, or *O*-acetyl groups [1,2]. The xylan content in typical biomasses used for energy production such as corn stover, corn cobs, and wheat straw can be in the range of 30% of the dry matter [3].

Xylan is degraded by a broad class of enzymes generally referred to as xylanases. The enzymes hydrolyzing the $\beta(1 \rightarrow 4)$ backbone (EC 3.2.1.8) or $\beta(1 \rightarrow 3)$ backbone (EC 3.2.1.32) are categorized into at least five glycoside hydrolase (GH)¹ families [4] of the Carbohydrate Active Enzymes database (<http://www.cazy.org>) [5], with the majority of xylan-active GH families employing the retaining mechanism [6]. Because all known xylanases (*endo*-

1,4- β -D-xylan xylanhydrolase, EC 3.2.1.8) apply an *endo* mode of action, “xylanase” is often used as synonym for *endo*-xylanase [7]. Xylanases are used in large-scale industrial processes such as biobleaching in the pulp and paper industry [8], feed treatment [9], baking [10], and the production of second-generation bioethanol [7].

Xylanase activity is traditionally measured by chemical-reducing-end quantification of the reaction products. Xylanase action on a polymer produces a broad distribution of different chain-lengths, an accurate quantification of the number of reducing ends in solution requires a method that detects chain ends independently of the degree of polymerization and is highly specific for the reducing end.

Chemical-reducing-end assays are stopped assays that integrate (low) reaction rates over reaction time. Often it is preferable to monitor reaction rates continuously, or at least in small time intervals, because this enables straightforward measurement of reaction. This can be realized when a biophysical approach is taken because reaction rates can be derived directly from the heat of reaction measured by isothermal titration calorimetry (ITC) [11]. This method has been applied successfully by our group for a cellobiohydrolase [12] and industrial cellulase mixtures [13]. The low enthalpy of the hydrolysis of the carbohydrate bond can limit applicability to high-reaction velocities [13]. This was overcome by using a coupled assay where the enthalpically silent hydrolysis of a glycosidic bond ($\Delta H < \pm 5$ kJ/mol) is coupled to a secondary enthalpically stronger reaction such as an oxidation [12]. Here

* Corresponding author. Fax: +45 4674 3011.

E-mail address: pwesth@ruc.dk (P. Westh).

¹ Abbreviations used: GH, glycoside hydrolase; ITC, isothermal titration calorimetry; DNS, dinitrosalicylic acid; PAHBAH, *para*-hydroxybenzoic acid hydrazine; MBTH, 3-methyl-2-benzothiazoline hydrozone; BCA, 2,2'-bichinchoninate; Aac-Xyn, xylanase from *Aspergillus aculeatus*; SDS-PAGE, sodium dodecyl sulfate-polyacrylamide gel electrophoresis; Aac-Xyn^{CD}, Aac-Xyn without the carbohydrate binding domain; CBM, carbohydrate binding domain; Aac-Xyn^{CBM}, catalytic domain with CBM; HPAEC-PAD, high-performance anion exchange chromatography with pulsed amperometric detection; MALDI-TOF, matrix-assisted laser desorption/ionization time-of-flight; HPLC, high-performance liquid chromatography; AZCL-xylan, azurine-crosslinked arabinoxylan from wheat; LOXU, lactose oxidase units; XOS, Xyl₃-Xyl₁₀.

we show how the combination of carbohydrate oxidase [14] and catalase can be used to measure xylanase kinetics in a multiple injection assay by ITC.

In this study, calorimetric kinetic data are compared with chemical-reducing-end assays such as dinitrosalicylic acid (DNS) [15], Nelson–Somogyi [16,17], *para*-hydroxybenzoic acid hydrazine (PAHBAH) [18], 3-methyl-2-benzothiazoline hydrozone (MBTH) [19], and 2,2'-bicinchoninate (BCA) [20]. Chemical-reducing assays are performed with pure *mono*-disperse xylan oligosaccharides as well as typical degradation products after xylan hydrolysis.

Materials and methods

Ferulic acid methyl ester (4-hydroxy-3-methoxycinnamic acid methyl ester, CAS 2309-07-01) was purchased from Apin Chemicals (Oxon, UK). Unless otherwise stated, all chemicals were supplied by Sigma–Aldrich (St. Louis, MO, USA). All assays were performed in 50 mM sodium acetate buffer (pH 5.0).

Enzymes

Xylanase from *Aspergillus aculeatus* (*Aac*-Xyn) was produced in *Aspergillus oryzae* and purified in a two-step procedure. Cell-free culture supernatant was diluted and loaded on an anion exchange column, and *Aac*-Xyn was eluted in one peak during a linear gradient. Fractions were pooled based on sodium dodecyl sulfate–polyacrylamide gel electrophoresis (SDS–PAGE). The pool was then further purified by hydrophobic interaction chromatography. Two peaks were eluted and pooled. The first peak was identified as *Aac*-Xyn^{CD}, that is, *Aac*-Xyn without the carbohydrate binding domain (CBM). The second peak was identified as the catalytic domain with CBM (*Aac*-Xyn^{CBM}). Pools were analyzed by SDS–PAGE, and no additional bands were detected after Coomassie staining. The peaks were then analyzed for amino acid composition for an accurate concentration measurement.

Carbohydrate oxidase from *Microdochium nivale* was obtained as a test product from Novozymes (Bagsværd, Denmark). Enzyme production and enzyme properties have been described elsewhere [14,21].

Catalase (EC 1.11.1.6) Terminox 50L was obtained as a commercial product supplied from Novozymes. The activity was declared to be 50 kCIU/g, where CIU is the amount of enzyme that degrades 1 μ mol of H₂O₂ per minute at pH 7.0 and 25 °C.

Substrates

Birch xylan (Sigma–Aldrich, X0502) or medium-viscosity wheat xylan (24 cStokes, Megazyme, Wicklow, Ireland) powder (2 g) was added under vigorous stirring to 100 ml of 50 mM sodium acetate buffer (pH 5.0). Suspensions were heated to boiling temperature in a microwave oven and stirred at room temperature overnight. Volumes were readjusted to 100 ml, and insoluble matter was removed by centrifugation. Birch xylan and wheat xylan solutions were found to contain 16.7 and 21.7 g/L dry matter, respectively, after freeze-drying.

Mixed xylan oligosaccharides were produced by enzymatic hydrolysis. Here 1 mg of *Aac*-Xyn (40 μ l) was added to 2 ml of birch or wheat xylan solution. After incubation for 30 min at 22 °C, the solution was heated to 95 °C for 20 min. Xylan oligosaccharides were analyzed by high-performance anion exchange chromatography with pulsed amperometric detection (HPAEC–PAD).

For oligosaccharide purification, birch xylan oligosaccharides (17 g) in 0.5 L of buffer were produced as described above, and

the volume was reduced under vacuum to 0.2 L. Then 40 ml of this was fractionated by size exclusion purification as described by Zhang and Lynd [22]. Fractions were analyzed by HPAEC–PAD as described below. Pure xylan oligosaccharides were analyzed by matrix-assisted laser desorption/ionization time-of-flight (MALDI–TOF). Pure oligosaccharides from xylobiose to xylooctaose were produced.

Analytical methods

HPAEC–PAD

Xylooligosaccharides were analyzed on a Dionex high-performance liquid chromatography (HPLC) system (Sunnyvale, CA, USA) with a GP40 gradient pump and an ED40 electrochemical detector with a gold working electrode (standard carbohydrate settings). Oligosaccharides were separated on a CarboPac PA10 column (4 mm \times 25 cm, Dionex) with the following gradient program at a flow rate of 1 ml/min: 0–4 min isocratic 50 mM sodium hydroxide, 4–28 min linear gradient to 100 mM sodium acetate, 28–29 min isocratic elution with 600 mM sodium acetate in 150 mM sodium hydroxide, and 29–35 min reequilibration with initial conditions. Lower degrees of polymerization (1–5) were identified by comparison with a series of standards from xylose to xylopentaose (Megazyme).

Product analysis of xylanase ITC assays

The products of xylanase hydrolysis were analyzed after the first injection (3.33 mg/L birch xylan or 4.33 mg/L wheat xylan). The ITC assay was scaled up to a volume of 50 ml. Buffer (5 mM sodium acetate, pH 5.0) with 1.5 nM *Aac*-Xyn^{CBM} or 1.7 nM *Aac*-Xyn^{CD} was incubated in a water bath for 4 min at 30 °C with 100 μ l of birch or wheat xylan solution. Enzymes were inactivated by heating of the sample to 95 °C for 20 min. Samples were freeze-dried and dissolved in 1 ml of water. After centrifugation, 100 μ l of sample was analyzed by HPAEC–PAD as described above.

Reducing-end assays

All assays were prepared on a scale of 0.2–0.5 ml and incubated at 80 °C in a heating block (Eppendorf, Hamburg, Germany) for color development for 15 min with 800-rpm mixing. All samples were analyzed in a plate reader (SpectraMax 190, Molecular Devices, Sunnyvale, CA, USA) in a 96-well plate with a 100- μ l sample aliquot. After initial setup, all assays (including standards) were performed in triplicate. The development temperature was kept constant for all detection methods to simplify the experimental setup. A xylose standard curve was prepared with 100 μ l of 0.5, 1, 1.5, 2, 2.5, 3, 3.5, and 4 mM xylose solution in 50 mM sodium acetate buffer (pH 5.0).

The DNS assay was performed according to Miller [15] using the modification with phenol and sodium potassium tartrate solution.

The reducing-end assay after Nelson [16] was performed using the arsenic molybdate color reagent from Somogyi [17] with the modification that 100 μ l of sample was mixed with 100 μ l of the copper sulfate reagent. After heat incubation, 100 μ l of the arsenic molybdate solution was added and the sample was allowed to cool.

The PAHBAH assay [18] was performed by adding 500 μ l of the freshly mixed PAHBAH reagent to 100 μ l of carbohydrate sample, followed by heat incubation.

The MBTH assay was carried out according to Anthon and Barrett [19].

The BCA assay was performed according to Waffenschmidt and Jaenicke [23]. Xylose standard solutions for the BCA assay had concentrations of 0.2, 0.4, 0.6, 0.8, and 1 mM xylose, and 100 μ l of carbohydrate sample was mixed with 400 μ l of the BCA reagent.

As an independent alternative method to measure xylanase activity, we used azurine-crosslinked arabinoxylan from wheat

(AZCL-xylan, Megazyme, I-AZWAX). Assays were performed according to the manufacturer's recommendations. Aac-Xyn was used in a concentration of 25 µg/ml.

ITC methods

All experiments were carried out on an ITC200 (MicroCal, Northampton, CA, USA) with a 200-µl sample cell equipped with a 40-µl automatic pipette. The reference power was set to approximately 21 µJ/s (5 µCal/s). All assays were run at 30 °C with a stirring rate of 1000 rpm. Calibration and controls were performed as described in Ref. [12].

Pretreatment of xylan solutions was carried out because birch xylan and wheat xylan contain reducing ends. Typically, 1 ml of xylan solution was preoxidized for 30 min at 22 °C in a 15-ml tube containing 0.12 LOXU (lactose oxidase units) carbohydrate oxidase and 5.4 CIU Terminox.

Molar enthalpies

Pure xylan oligosaccharides (xylotriose to xylohexose generated from birch xylan as described above) were titrated to buffer or the carbohydrate/catalase mixture. After initial baseline equilibration for 2000 s, 2 µl of a 0.2-mM oligosaccharide solution was injected. This was repeated seven times separated by 500 s. All apparent enthalpies of carbohydrate oxidase and catalase reaction were corrected for the dilution enthalpies.

Xylanase kinetics measured by ITC

Because oxygen is consumed during the reaction, solutions were not vacuum degassed prior to use. In typical multiple injection enzyme kinetic experiments, xylanase (1.49 nM of the full-length xylanase Aac-XynCBM or 1.69 nM of the catalytic domain Aac-XynCD), carbohydrate oxidase (0.12 LOXU), and catalase (50 CIU) in sodium acetate buffer were loaded into the cell (200 µl), and xylan solutions (16.7 g/L birch xylan and 21.7 g/L wheat arabinoxylan) were added from the pipette in 30 injections of 0.2 µl. To ensure that the heat flow after an injection was independent of the preceding injection, heat flows were also measured in single-injection experiments. Xylanase concentrations were adjusted to a level where its injection generated an essentially constant heat flow (pseudo steady state) for approximately 8 min. In the final assay, we used a 4-min separation period. The pH of the assay solution after a multiple injection assay was found to be the same (pH 5.0) as before the assay. Collected data were analyzed by a customized python script (<http://www.python.org>). Heat flows during steady state were averaged in a window of 30 s before a new injection, and the difference, ΔHF , between this value and the initial baseline was calculated. This difference in heat flow is a direct measure of the rate, r , of the hydrolysis reaction

$$r = \frac{\Delta HF}{V_{\text{cell}} \Delta H_{\text{app}}} \quad (1)$$

where ΔH_{app} is the apparent molar enthalpy change for the coupled reactions and V_{cell} is the volume of the calorimetric cell. Standard deviations and slopes were calculated for control purposes. All curve fitting and analysis were performed using the standard Michaelis–Menten equation in Origin 7 (OriginLab, Northampton, MA, USA).

Results

First we present results from the purification of xylanase, then conditions for the ITC assay were optimized with mixed xylan oligosaccharides, and finally Aac-Xyn activities were measured on xylan. Furthermore, kinetic data obtained by ITC were compared

with kinetic data generated by chemical-reducing-end assays. In addition, chemical-reducing-end assays were tested with pure and mixed xylan oligosaccharides.

Optimization of the enthalpy amplification system and xylanase concentration

In a series of preliminary experiments where the heat flow from xylan hydrolysis was measured without coupled reactions, the observed changes in heat flow were well within the baseline noise. Even an increased birch xylan concentration (5 g/L) and an Aac-Xyn^{CBM} enzyme concentration of 1 g/L left the change in heat flow undetectable. We concluded that the heat flow associated with xylan hydrolysis could not be determined with a good and reproducible signal-to-noise ratio. This observation was confirmed by the reported enthalpy of 0.12 ± 0.26 kJ/mol for hydrolysis of the $\beta(1 \rightarrow 4)$ xylobiose bond [24].

As an alternative, the enthalpic signal can be increased by coupling hydrolysis to a secondary reaction that has a high enthalpy change. Murphy and coworkers [12] demonstrated how the notoriously low reaction rates of a cellobiohydrolase can be monitored by ITC by using a glucose oxidase reaction. Similar to Murphy and coworkers, we attempted to use glucose-*l*-oxidase and catalase as a signal amplification system, but the oxidation activity of glucose-*l*-oxidase on mixed xylan oligosaccharides (degree of polymerization 2–10, analyzed by HPAEC–PAD) or xylose was too low. Glucose-*l*-oxidase was then replaced by carbohydrate oxidase, which has a broad substrate spectrum for oligosaccharides [14]. In depletion experiments on mixed xylan oligosaccharides (degree of polymerization 2–10, analyzed by HPAEC–PAD), carbohydrate oxidase was tested successfully.

To test the amplification system, we conducted a number of initial experiments without xylanase in the ITC cell. Mixed xylan oligosaccharides were injected into a mix of carbohydrate oxidase and catalase. In depletion experiments, the peak area was dose dependent, as expected, for quantitative conversion. In a second series, the amount of mixed xylan oligosaccharides was kept constant and the dosage of carbohydrate oxidase was decreased until the concentration of carbohydrate oxidase became rate limiting. For all further experiments, the concentration of carbohydrate oxidase was increased over the minimal required dosage by a factor of 10. Carbohydrate oxidase performs a reaction analogous to glucose-*l*-oxidase; that is, it uses molecular oxygen as an electron acceptor and produces hydrogen peroxide (Fig. 1). Because dissolved oxygen may be limiting (water equilibrated with atmospheric air contains ~ 0.25 mM O₂ [12]) in the essentially closed calorimeter cell, solutions were not degassed. This is against common calorimetric practice, but we did not see exaggerated noise levels at 30 °C. The addition of catalase increased the heat signal by a factor of 1.7 as hydrogen peroxide is split into water and oxygen and, as an additional benefit, reduced the consumption of dissolved molecular oxygen by a factor of 2.

To test the stability of the carbohydrate oxidase catalase system, we injected mixed xylan oligosaccharides in increasing dosages (Fig. 2). We consistently found a heat production of 153 µJ/µl xylan oligosaccharide solution (22 mg/ml) and saw no sign of exhaustion or inhibition of the oxidation system. After six injections, the total heat released was equivalent to the heat released during a typical kinetic experiment (cf. Fig. 4). Catalase was dosed as in Ref. [12] and was not found to be rate limiting (data not shown). We concluded that the xylanase was rate limiting for the reaction series in Fig. 1 and, therefore, that the heat output gives a true measure of xylanase activity.

The Aac-Xyn activity might be influenced by the presence of carbohydrate oxidase or catalase or by their reaction products. To test this, we performed measurements with an alternative

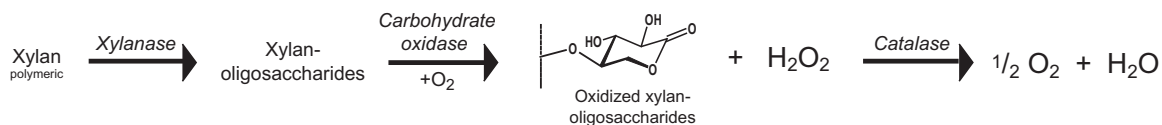


Fig. 1. Reaction scheme for carbohydrate oxidase-coupled assay. A xylanase generates reducing ends, which are oxidized by carbohydrate oxidase, which catalyzes a reaction similar to glucose-1-oxidase. The reducing end of a xylan oligosaccharide is oxidized to the lactone, and one molecule of hydrogen peroxide (H_2O_2) is produced. H_2O_2 is broken down to molecular oxygen and water.

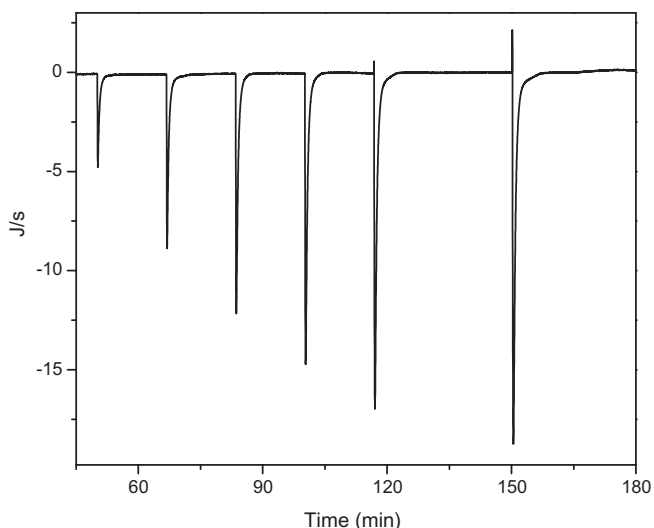


Fig. 2. Injection of 1, 2, 3, 4, 5, and 6 μl of mixed birch xylan oligosaccharides (22 mg/L) into carbohydrate oxidase and catalase in 50 mM sodium acetate buffer (pH 5.0). Peak areas are constant $153 \pm 7 \mu\text{J}/\mu\text{l}$ injectant ($n = 3$). Total heat released ($\sim 3 \text{ J}$) is equivalent to the heat released during a typical xylanase kinetic experiment.

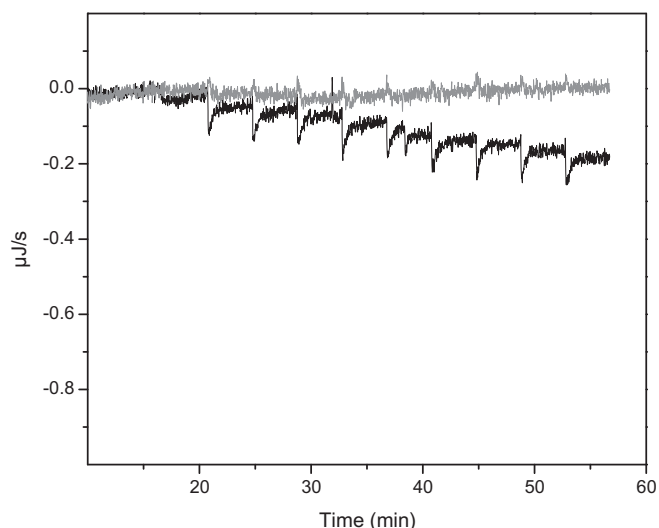


Fig. 3. Injection of xylan into carbohydrate oxidase and catalase in the ITC cell. Birch xylan (black curve) results in a deflection of the baseline for each injection. Injection of birch xylan pretreated with carbohydrate oxidase and catalase (gray curve) does not show the same changes in heat flow. Preoxidation of the reducing ends of the polymer reduces the observed signals from injection.

noncalorimetric assay that is not dependent on the presence of reducing ends. We chose to use the AZCL-xylan method as suggested by Megazyme. In these assays, *Aac-Xyn* showed the same activity when carbohydrate oxidase and catalase, 0.9 g/L preoxidized xylan oligosaccharides, or 0.9 g/L xylan oligosaccharides was present. Although the calorimetric and colorimetric assays are not fully comparable, the results from the AZCL assay indicate that *Aac-Xyn* activity is independent from its reaction products over a broad concentration range. Furthermore, the oxidized reaction products are not influencing the hydrolytic activity.

Initial xylan hydrolysis products were analyzed after the first injection to facilitate HPAEC-PAD analysis, and carbohydrate oxidase and catalase were not added. No xylan-derived oligosaccharides smaller than xylotetraose were detected. Concentrations less than 10 nM (measured as 500 \times concentrate) of oligosaccharides from xylotetraose and larger were detected, indicating that the major amount of xylan still had a higher degree of polymerization. Reaction products of carbohydrate oxidase with mixed xylan oligosaccharides as substrate were also analyzed by HPAEC-PAD. Typical products of mixed xylan oligosaccharides were separated into 20 or more peaks, where the higher molecular weights most likely elute at higher elution volumes. In comparison with the substrate, no peaks were observed during gradient elution after incubation with carbohydrate oxidase, indicating that all xylan oligosaccharides were oxidized independently of the molecular mass.

Molar enthalpy of the enzymatic oxidation pure xylan oligosaccharides

The apparent enthalpy change ΔH for the oxidation by carbohydrate oxidase and catalase of pure birch xylan oligosaccharides

(xylotriose to xylohexaose) was calculated from peak areas of six injections of pure xylan oligosaccharides into the carbohydrate oxidase and catalase mixture (Table 1). The measured ΔH values for the tested xylan oligosaccharides were not, as initially hoped, completely independent of the chain length. Within the tested chain length of XOS (Xyl_3 – Xyl_{10}), no constant was observed. Product analysis by HPAEC-PAD of a typical xylan hydrolysis experiment showed that no chain length below xylotetraose was produced. Lacking other approaches to measure the apparent enthalpy change ΔH , we decided to average the observed ΔH values for the oxidation of xylotetraose to xylopentaose.

Determination of kinetic parameters of hydrolysis of xylan by ITC

Enzyme kinetic parameters were determined using soluble xy-lans from birch xylan and wheat xylan. The birch glucuronoxylan solution is of brownish color, which may be caused by traces of lignin in the concentration used (stock concentration 16 g/L). Wheat xylan is of the arabinoxylan type [2] and is further modified with ferulic acid esters.

Control experiments where xylan was injected into a mixture of carbohydrate oxidase and catalase without xylanase showed a small but measurable deflection from the baseline after each injection (Fig. 3). Preoxidation of the polymeric xylan removed the deflection, indicating that the signal is most likely derived from the oxidation of the reducing ends of the polymer chains (Fig. 3). All subsequent ITC experiments were performed with preoxidized xy-lans.

Data from a typical ITC experiment are shown in Fig. 4A. The initial concentrations of *Aac-Xyn*^{CD} and *Aac-Xyn*^{CBM} in the

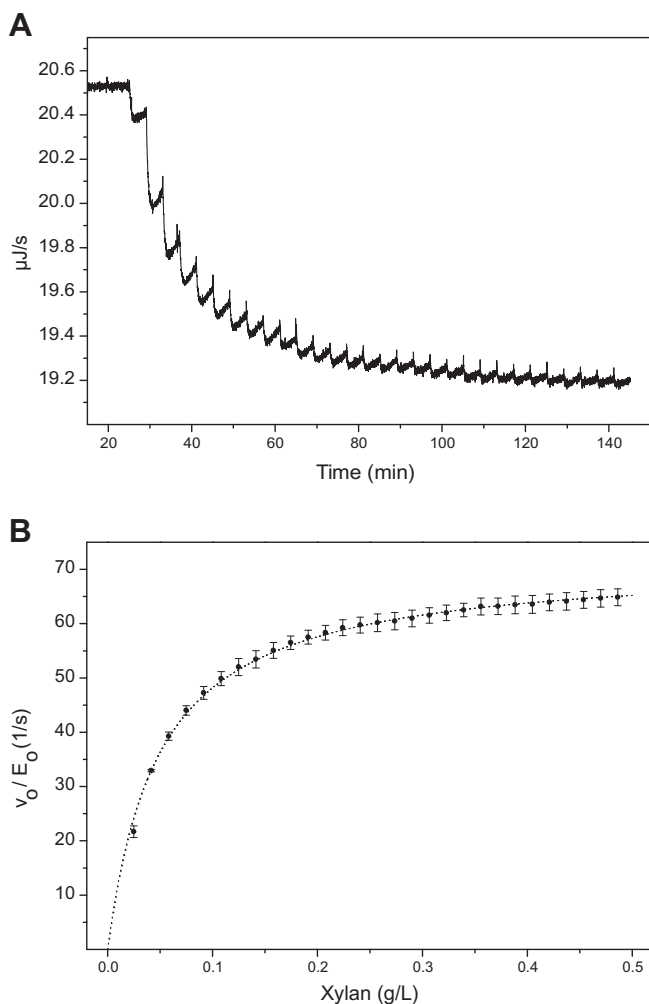


Fig. 4. (A) Raw ITC data catalytic domain only with birch xylan as substrate. Initial baseline equilibration (33 min) was followed by 30 injections of 0.2 μl birch xylan (16.7 g/L) every 4 min, and steady states were calculated from the last 30 s before each injection. (B) Heat flows converted to specific enzyme activities (with standard deviations from three replicates). Data are fitted to the standard Michaelis–Menten equation (dotted line). Data show the activity of GH10 xylanase with birch xylan as substrate.

calorimetric cell were 27 and 24 μM , respectively. These values decrease slightly in the “overflow” calorimetric cell on the addition of substrate, and this was taken into account in the data treatment. The measured enthalpies were converted to reaction rates using Eq. (1) and the apparent enthalpies, calculated from the depletion experiments, shown in Table 1. Fig. 4B shows an average of three independent experiments. A summary of the kinetic parameters for $Aac\text{-Xyn}^{\text{CD}}$ and $Aac\text{-Xyn}^{\text{CBM}}$ is shown in Table 2.

The k_{cat} values for the hydrolysis of birch xylan are in the range of 70 s^{-1} , whereas they are somewhat lower on wheat xylan. Interestingly, the presence of a CBM does increase k_{cat} for 5% with birch

xylan or 25% for wheat xylan. The K_{m} values are very similar and do not show an apparent dependence of the CBM.

Xylanase kinetics measured by the MBTH assay

It was attempted to generate data for full enzyme kinetics for birch xylan and wheat xylan with the $Aac\text{-Xyn}^{\text{CD}}$ and $Aac\text{-Xyn}^{\text{CBM}}$. However, the detection limit of the MBTH assay did not allow substrate and enzyme concentrations as low as the ITC assay. The used substrate concentrations (birch xylan 1–2 g/L, wheat xylan 1.5–2.5 g/L) are at least a factor of 10 higher than the K_{m} value measured by ITC (Table 2); therefore, the measured rates reflect apparent k_{cat} values ($s \gg K_{\text{m}} \rightarrow V \approx V_{\text{max}}$). The employed MBTH assay is practically as sensitive as the BCA assay (Table 3) and has a larger dynamic range (0.2–3 mM xylose), the sensitivity is not sufficient for a full kinetic characterization, which would require for the low concentrations a 20-fold reduction in enzyme activity to ensure that only up to 10% of the available bond are hydrolyzed in the assays.

Evaluation of chemical-reducing-end quantifications with xylan oligosaccharides

To establish a direct proportionality between the heat flow observed by ITC and the number of hydrolytic cycles, it was attempted to quantify the number of newly generated xylan chain ends (reducing ends) with different chemical-reducing-end quantification assays (Table 3).

Pure xylan oligosaccharides in chemical-reducing-end assays

Under the conditions used here, the sensitivity of the DNS and Nelson–Somogyi assays is not high enough. As indicated by Coward-Kelly and coworkers [25], the DNS assay would require longer heat incubation times. Three assays (PAHBAH, MBTH, and BCA) can be compared in detail. PAHBAH and BCA underestimate pure xylan oligosaccharides (XOS); for both assays, the colorimetric response increases with elongation of the chain from xylotriose to xylohexose. MBTH is the only method that overestimated xylopentaose

Table 2

Kinetic parameters of the $Aac\text{-Xyn}^{\text{CD}}$ and $Aac\text{-Xyn}^{\text{CBM}}$ obtained by nonlinear curve fitting to the Michaelis–Menten equation.

Substrate	Enzyme	ITC data ^a	MBTH assay	
		K_{m} (mg L ⁻¹)	k_{cat} ^b (s ⁻¹)	$k_{\text{cat app}}$ ^c (s ⁻¹)
Birch xylan	Xyn^{CBM}	80	68 ± 6	26 ± 1
	Xyn^{CD}	50	71 ± 3	28 ± 1
Wheat xylan	Xyn^{CBM}	110	37 ± 4	63 ± 3
	Xyn^{CD}	90	49 ± 5	58 ± 3

Note: Enzyme activities with birch and wheat arabinoxylan were measured by ITC and MBTH assays.

^a Data are calculated with the ΔH_{app} values for the carbohydrate oxidation and hydrogen peroxide oxidation (Table 1).

^b Errors are given from the curve fitting algorithm based on ΔH of -64 kJ/mol .

^c Errors are the standard deviations.

Table 1

Apparent enthalpy for the oxidation of xylan oligosaccharides by the coupled reaction of carbohydrate oxidase and catalase.

	Xylotriose (X ₃) (kJ/mol)	Xyloetraose (X ₄) (kJ/mol)	Xylopentaose (X ₅) (kJ/mol)	Xylohexaose (X ₆) (kJ/mol)	Xylonanoase/Xylodecaose ^a (X _{9/10}) (kJ/mol)
ΔH_{app}	-36 ± 3	-52 ± 3	-57 ± 2	-68 ± 1	-78 ± 3
$\Delta H_{\text{app}} (X_4\text{-}X_{9/10})$				-64 ± 10	

Note: Errors given are the standard deviations.

^a Mix of two xylan oligosaccharides with a 1:1 ratio (controlled by HPAEC–PAD).

Table 3
Quantification of pure XOS (xylotriose to xylohexaose), mixed xylan oligosaccharides, glucose, ferulic acid, and ferulic acid methyl ester with five reducing-end assays.

Xylose standard curve	Xyl ₃ 1 mM	Xyl ₄ 1 mM	Xyl ₅ 1 mM	Xyl ₆ 1 mM	Glucose 1 mM	Birch XOS (1 g/L)	Wheat XOS (1 g/L)	Ferulic acid 1 mM	Ferulic acid methyl ester 1 mM
	Xylose equivalents (mM)								
DNS	n.d.	n.d.	n.d.	n.d.	n.d.	n.d.	n.d.	n.d.	n.d.
NS	n.d.	n.d.	n.d.	0.34 ^a	1.13	0.15 ^a	n.d.	0.89	0.83
PAHBAH	0.26 ^a	0.60	0.68	0.87	1.43	0.24 ^a	1.25	0.25 ^a	0.25 ^a
MBTH	1.272	0.89	1.06	1.35	1.37	0.42	1.18	1.09	1.06
BCA	1.822	0.50	0.55	0.69	1.00	0.59	0.40	0.80	0.68

Note. All measured concentrations are expressed as xylose equivalents based on linear xylose standard curves. The standard deviation of triplicates was not larger than ± 0.02 mM xylose equivalents. n.d., absorbancies measured were below 0.01 absorbance units; NS, Nelson–Somogyi.

^a Concentration calculated as below lowest xylose standard.

and xylohexaose with respect to xylose. This might indicate that the reaction causes depolymerization of XOS.

Reaction of chemical-reducing-end assays with ferulic acid

Ferulic acid is present in wheat arabinoxylan in low concentrations. The Nelson–Somogyi, PAHBAH, MBTH, and BCA assays did show a color reaction under the condition used with ferulic acid and ferulic acid methyl ester. The BCA reagent reacts spontaneously with ferulic acid and, to a lesser extent, with the ferulic acid ester at room temperature (22 °C).

Quantification of a polydisperse mixture of XOS by chemical-reducing-end assays

The composition of the mixed birch XOS and mixed wheat XOS was analyzed by HPAEC–PAD and found to contain chain-length equivalents from xylobiose to oligosaccharides estimated to be longer than 10 xylose units. Mixed birch XOS shows the highest reading with BCA and mixed wheat shows the highest readings with XOS with PAHBAH, whereas the MBTH readings are slightly lower in both cases. This indicates that the reactivities of mixed birch XOS and mixed wheat XOS are, similar to their chemical compositions, slightly different. The results for the mixed xylan oligosaccharides differ by a factor of 3, clearly demonstrating that the tested methods do not allow an accurate quantification of reducing ends on the material used here.

Discussion

Xylanase is an important enzyme class for industrial applications. Xylanases are used as bleaching agents in the pulp and paper industry and in the baking industry, and they have gained attention in the biomass industry.

Like other *endo*-acting enzyme classes such as glucanases and xyloglucanase, xylanase activity toward polymeric substrates is measured by chemical-reducing-end assays. There are few alternatives when the complex natural carbohydrate is used as substrate. It was demonstrated in a multilaboratory study by Bailey and coworkers [26] that it is difficult to quantify xylanase activity in a comparable way, although substrate (birch xylan) and assay method (DNS) were kept constant. In the light of our results (Table 3), this may be explained by analytical problems associated with the varying degrees of polymerization of the hydrolysis products. Our data suggest that a chemical-reducing-end assay such as Nelson–Somogyi, PAHBAH, or BCA will underestimate xylan oligosaccharides with low degrees of polymerization when the assay is calibrated against xylose. Sengupta and coworkers [27] stated that the differences in reactivity of maltooligosaccharides in the DNS assay become constant above a degree of polymerization of 5. Even though our data are not obtained with the DNS method, the data in Table 3 suggest that this is not a general rule for xylan oligosaccharides. Regarding enzyme kinetic characterization, this is especially problematic because the degree of polymerization will vary with the substrate concentration.

Calorimeters measure the heat flow associated with a reaction. To convert the heat flow to the number of catalytic events, the molar enthalpy of the oxidation of xylan oligosaccharides by the coupled reaction of carbohydrate oxidase and catalase is needed (Eq. (1)). Our results show that the apparent molar enthalpy is 64 ± 10 kJ/mol for the oligosaccharides xylotetraose, xylopentaose, and xylohexaose, whereas the oxidation of xylotriose shows 50% lower oxidation enthalpy (Table 1). For this study, it was chosen to use an average of the tested xylan oligosaccharides larger than xylotriose because these degrees of polymerization reflect the more probable hydrolysis products (tested by HPAEC–PAD). We suggest that the apparent molar enthalpy for oxidation by

carbohydrate oxidase and catalase for all xylan hydrolysis products above a degree of polymerization of 3 is constant within measurement accuracy.

A limitation of the method appears to be a small deviation of the steady-state rate (<8% of the total signal). This is readily illustrated in the slope between the injections in Fig. 4, where a true steady state would give a horizontal line. We suggest that this behavior is not related to any analytic flaws but indeed is a reflection of declining xylanase activity with time. We would also note that rate retardation is generally found for all GHs working on polymeric substrates, which may be related to substrate heterogeneity. Subtle changes in the reaction rate will be particularly clear in a calorimetric measurement because it directly detects the rate and not the cumulated concentration of product, and this makes the new method attractive for such time studies.

Xylans are natural substrates and, as such, are not perfectly uniform in molecular mass, side chain distribution, and acetylation. This is generally referred to as substrate heterogeneity. Side chain distribution most likely has a very important influence on the actually accessible hydrolysis points. This may even vary from enzyme to enzyme and can be mechanistically explained by the ability of the active site to accommodate side chains. In initial rate kinetics, substrate heterogeneity most likely plays a minor role because a surplus of hydrolysis sites is available polymeric substrate. The actual influence of substrate heterogeneity is difficult to address in the absence of homogeneous polymeric or oligomeric model substrates.

To confirm our kinetic ITC data, we chose the MBTH assay for xylanase kinetics because Horn and Eijssink [28] suggested that the color reaction is independent of the degree of polymerization of chitooligosaccharides. Unfortunately, this behavior was not confirmed by our measurements on xylan oligosaccharides (Table 3). Regarding enzyme kinetics, it was not possible to generate full kinetic curves over the complete concentration range. The measured specific activities at the highest tested concentrations ($s \gg K_m \rightarrow V \approx V_{max}$) were interpreted as apparent k_{cat} values. Interestingly, the observed values by MBTH with birch xylan were identical for Aac -Xyn^{CD} and Aac -Xyn^{CBM} (26 and 28 s⁻¹, respectively) (Table 2). Similarly, the k_{cat} values on wheat xylan were also essentially same (63 and 58 s⁻¹ for Aac -Xyn^{CD} and Aac -Xyn^{CBM}, respectively). For both tested xylans, the presence of a CBM did not have a significant influence on the apparent k_{cat} values. The differences between the two xylans are approximately equivalent to a factor of 2. Even though the MBTH assay is most likely overestimating longer chain xylan oligosaccharides with respect to xylose, it remains unknown whether this can explain the higher activity with wheat xylan.

The difference of the specific activities with birch xylan and wheat xylan is not reflected to the same extent by the ITC measurements. The apparent difference is difficult to explain, but the MBTH assay may be sensitive to the different chemical compositions of birch xylan and wheat xylan (ferulic acids and other side chains). It was clearly demonstrated that the presence of a CBM has no apparent effect on k_{cat} on soluble xylans.

The most important parameter in the calculations of the ITC data is the ΔH_{app} value (Table 1) given that k_{cat} scales directly with ΔH_{app} . Considering the error margin of ΔH of 15%, the k_{cat} values are in mutual agreement. In accord with the data from the MBTH assay, the presence of a CBM has no significant influence on the k_{cat} values measured by ITC. The ΔH_{app} values were measured with xylan oligosaccharides generated from birch xylan, and these values might not be directly applicable for the oxidation of wheat xylan. Purification of wheat xylan oligosaccharides was not attempted because the oligosaccharide mixtures are expected to be far more complex than those for birch xylan due to the extensive presence of side chains.

The K_m values in the range between 50 and 110 mg/L xylan are rather similar. These substrate concentrations are already reached with the second injection during a multiple-injection assay, and a new series of experiments would be needed to measure K_m values with higher accuracy. Considering the detection limits of chemical-reducing-end assays, the use of polymeric substrates in the range of 50–100 mg/L is not feasible; therefore, the K_m values can be measured only by the ITC method.

Conclusions

Quantitative kinetic analysis of *endo*-acting GHs is inherently complicated. In fact, the available assay technologies are both labor-intensive and prone to a number of systematic errors. In the current work, we have presented a biophysical approach to this and compared it with several established methods using the same materials. We found that the described calorimetric method offers a number of advantages. Once the enzyme and substrate have been loaded into the calorimeter, an entire kinetic curve with 20–30 connected values of rate and substrate concentration can be produced in an automated protocol in approximately 2 h. In contrast, we were unable to attain a full kinetic curve by any of the tested reducing-end methods. The sensitivity of the calorimetric method is high, with a detection level of approximately 2 pmol of reducing end produced per second. This very sensitive method offers at least two advantages. First, the material requirements are small; a full kinetic curve can be generated from approximately 15 ng of xylanase, and this level of material consumption makes the method applicable to work on noncloned wild-type enzymes as well as engineered material such as mutant libraries. Second, the ITC method allows analysis of highly dilute systems and, thus, the ability to measure low K_m values such as the ones found for the GH10 xylanase in this work. The major limitation of the new method is the uncertainty of ΔH_{app} . This problem, which affects k_{cat} but not K_m in kinetic studies, may result from low activity of carbohydrate oxidase on very small xylan oligosaccharides [21]. It can be alleviated by HPAEC–PAD profiling of the products and the appropriate control measurements for the oxidation of purified xylan oligosaccharides in the ITC, as shown in this work. In many applications, and certainly in comparative trials, this will not be necessary, and reasonable estimates of the kinetic parameters may be derived using the ΔH_{app} reported here or a value from a control experiment with a mixed XOS solution with a known average degree of polymerization.

We tested chemical-reducing-end quantification methods in detail and reached the conclusion that all tested assays are problematic because they do not reflect the true concentration of reducing ends by the color change. Chemical-reducing-end assays are not able to quantify the number of hydrolytic events catalyzed by an *endo*-xylanase. Because chemical-reducing-end assays are fixed-time assays, they can be used to integrate a very small number of catalytic events over time. This can be advantageous when very small activities need to be compared relative to each other, but subtle changes of enzyme activities most likely will be missed.

Acknowledgments

We thank Herje Schagerlöf for the MALDI analysis of the xylan oligosaccharides. This work was supported by the Danish Agency for Science, Technology, and Innovation (Grant 2104-07-0028).

References

- [1] A. Ebringerova, T. Heinze, Xylan and xylan derivatives—biopolymers with valuable properties: 1. Naturally occurring xylans structures, procedures, and properties, *Macromol. Rapid. Commun.* 21 (2000) 542–556.
- [2] M.S. Izydorczyk, C.G. Biliaderis, Cereal arabinoxylans: advances in structure and physicochemical properties, *Carbohydr. Polym.* 28 (1995) 33–48.

- [3] C.R. Brown, *Biorenewable Resources: Engineering New Products from Agriculture*, Wiley-Blackwell, Hoboken, NJ, 2003.
- [4] T. Collins, C. Gerday, G. Feller, Xylanases, xylanase families, and extremophilic xylanases, *FEMS Microbiol. Rev.* 29 (2005) 3–23.
- [5] B.L. Cantarel, P.M. Coutinho, C. Rancurel, T. Bernard, V. Lombard, B. Henrissat, The Carbohydrate-Active Enzymes database (CAZy): an expert resource for glycogenomics, *Nucleic Acids Res.* 37 (2009) D233–D238.
- [6] M.L. Sinnott, Catalytic mechanisms of enzymatic glycosyl transfer, *Chem. Rev.* 90 (1990) 1171–1202.
- [7] C.J. Yeoman, Y. Han, D. Dodd, C.M. Schroeder, R.I. Mackie, I.K. Cann, Thermostable enzymes as biocatalysts in the biofuel industry, *Adv. Appl. Microbiol.* 70 (2010) 1–55.
- [8] L. Viikari, A. Kantelinen, J. Sundquist, M. Linko, Xylanases in bleaching: from an idea to the industry, *FEMS Microbiol. Rev.* 13 (1994) 335–350.
- [9] N. Mathlouthi, S. Mallet, L. Saulnier, B. Quemener, M. Larbier, Effects of xylanase and α -glucanase addition on performance, nutrient digestibility, and physico-chemical conditions in the small intestine contents and caecal microflora of broiler chickens fed a wheat and barley-based diet, *Anim. Res.* 51 (2002) 395–406.
- [10] C.M. Courtin, J.A. Delcour, Arabinoxylans and endoxylanases in wheat flour bread-making, *J. Cereal Sci.* 35 (2002) 225–243.
- [11] M.J. Todd, J. Gomez, Enzyme kinetics determined using calorimetry: a general assay for enzyme activity?, *Anal. Biochem.* 296 (2001) 179–187.
- [12] L. Murphy, M.J. Baumann, K. Borch, M. Sweeney, P. Westh, An enzymatic signal amplification system for calorimetric studies of cellobiohydrolases, *Anal. Biochem.* 404 (2010) 140–148.
- [13] L. Murphy, K. Borch, K.C. McFarland, C. Bohlin, P. Westh, A calorimetric assay for enzymatic saccharification of biomass, *Enzyme Microb. Technol.* 46 (2010) 141–146.
- [14] F. Xu, E.J. Golightly, C.C. Fuglsang, P. Schneider, K.R. Duke, L. Lam, S. Christensen, K.M. Brown, C.T. Jørgensen, S.H. Brown, A novel carbohydrate:acceptor oxidoreductase from *Microdochium nivale*, *Eur. J. Biochem.* 268 (2001) 1136–1142.
- [15] G.L. Miller, Use of dinitrosalicylic acid reagent for determination of reducing sugar, *Anal. Chem.* 31 (1959) 426–428.
- [16] N. Nelson, A photometric adaptation of the Somogyi method for the determination of glucose, *J. Biol. Chem.* 153 (1944) 375–380.
- [17] M. Somogyi, Notes on sugar determination, *J. Biol. Chem.* 195 (1952) 19–23.
- [18] M. Lever, New reaction for colorimetric determination of carbohydrates, *Anal. Biochem.* 47 (1972) 273–279.
- [19] G.E. Anthon, D.M. Barrett, Determination of reducing sugars with 3-methyl-2-benzothiazolinonehydrazone, *Anal. Biochem.* 305 (2002) 287–289.
- [20] L.W. Doner, P.L. Irwin, Assay of reducing end-groups in oligosaccharide homologs with 2, 2'-bichoninone, *Anal. Biochem.* 202 (1992) 50–53.
- [21] J. Kulys, L. Tetianec, P. Schneider, Specificity and kinetic parameters of recombinant *Microdochium nivale* carbohydrate oxidase, *J. Mol. Catal. B* 13 (2001) 95–101.
- [22] Y.H.P. Zhang, L.R. Lynd, Cellodextrin preparation by mixed-acid hydrolysis and chromatographic separation, *Anal. Biochem.* 322 (2003) 225–232.
- [23] S. Waffenschmidt, L. Jaenicke, Assay of reducing sugars in the nanomole range with 2, 2'-bichoninone, *Anal. Biochem.* 165 (1987) 337–340.
- [24] Y.B. Tewari, B.E. Lang, S.R. Decker, R.N. Goldberg, Thermodynamics of the hydrolysis reactions of 1, 4-D-xylobiose, 1, 4-D-xylotriose, D-cellobiose, and D-maltose, *J. Chem. Thermodyn.* 40 (2008) 1517–1526.
- [25] G. Coward-Kelly, C. Aiello-Mazzari, S. Kim, C. Granda, M. Holtzapfel, Suggested improvements to the standard filter paper assay used to measure cellulase activity, *Biotechnol. Bioeng.* 82 (2003) 745–749.
- [26] M.J. Bailey, P. Biely, K. Poutanen, Interlaboratory testing of methods for assay of xylanase activity, *J. Biotechnol.* 23 (1992) 257–270.
- [27] S. Sengupta, M.L. Jana, D. Sengupta, A.K. Naskar, A note on the estimation of microbial glycosidase activities by dinitrosalicylic acid reagent, *Appl. Microbiol. Biotechnol.* 53 (2000) 732–735.
- [28] S.J. Horn, V.G.H. Eijssink, A reliable reducing end assay for chito-oligosaccharides, *Carbohydr. Polym.* 56 (2004) 35–39.

Appendix 1: Quenching and reducing ends assays for the EG work.

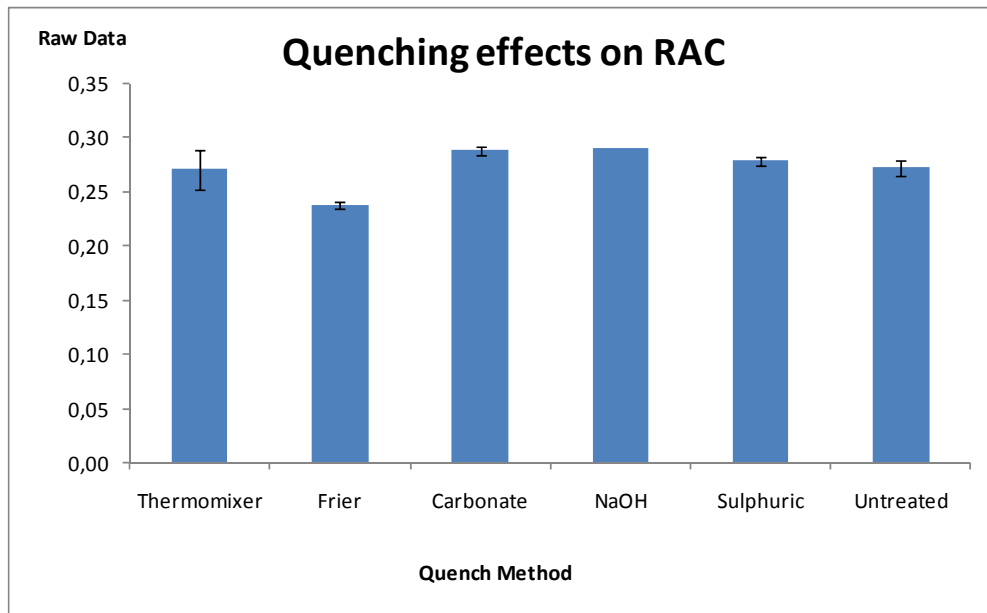
In order to determine the fastest most effective method in which to quench samples the following trials were conducted. This was performed as the ΔH for EG I and EG II were different and one possibility was that the two enzymes are not quenched equally well, leading to the production of more reducing ends.

The PAHBAH test was used to determine the reducing ends. 200 μL of sample + 1 mL of PAHBAH reagent¹ are placed in a 10 mL test tube. This is covered with an eppendorf 1.5 mL tube and the test tubes heated in vigorously boiling water for 6 min. The reducing ends are quantified based on a glucose or cellotetraose calibration curve (these are identical) reading the OD_{410} .

¹**Reagent A** *p*-Hydroxy benzoic acid hydrazide (PAHBAH) (10 grams) is added to 60 ml of water and slurried. To this 10 ml of concentrated HCl is added and the volume is made up to 200 ml. **Reagent B** Dissolve trisodium citrate (24.9 g) in 500 ml of water, Add calcium chloride (2.20 g) and dissolve, Add sodium hydroxide (40.0 g) and dissolve. Adjust the volume to 2 liters. **A is mixed with B in a 1:10 ratio for the PAHBAH reagent.**

Method	Comments	Issues	Result
2 M Na_2CO_3 dose: 50 $\mu\text{L}/\text{mL}$	Weak base	Carbonate has an effect on the Novo HPLC method.	pH increase to over 10.5
200 mM NaOH dose 1:1	Strong base, store samples at 4 °C, for Novo HPLC	Previously seen to cause hydrolysis of RAC in other conc. ranges.	pH increase to over 10.5
20 % H_2SO_4 30 $\mu\text{L}/\text{mL}$	For RU HPLC	All other methods to determine ends or HPLC are basic	pH decrease to approximately 1.0
Heat - thermomixer	Eppendorfs, Slow (?)	Plastic slowly warms up	1 min 09 s to reach 80 °C 93.9 °C after 4 min 50 s.
Heat – deep fat fryer (boiling water)	10 mL test tubes, Faster (?)	Seen to cause hydrolysis of RAC	33 s to reach 80 °C, 98.1°C after 1 min 55 s.

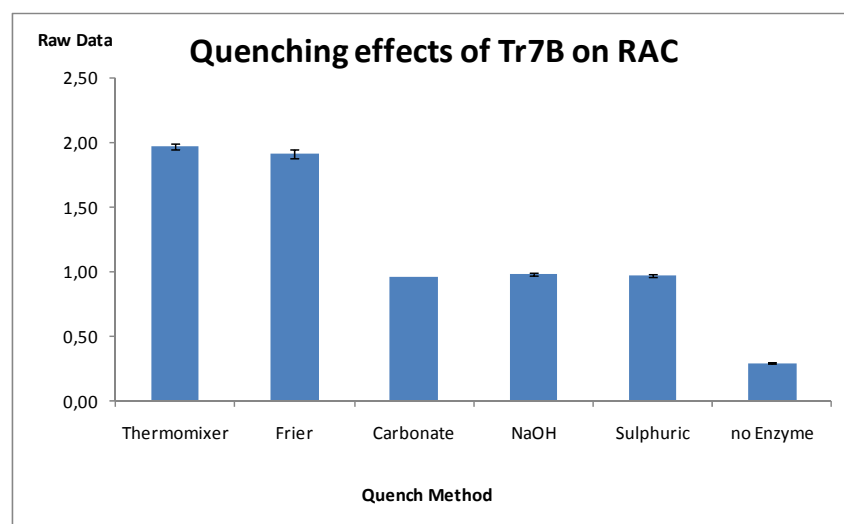
Conditions: The RAC was used at 8 g/L to provide ample substrate for the EG in the ITC.



RAC was subjected to the above treatments and the reducing ends measured, there were no significant variation in any of the samples, RAC is therefore not hydrolyzed by any of the tested methods. Presented is the raw data OD₄₁₀ for comparison only.

Ap 1.1 Enzyme quenching

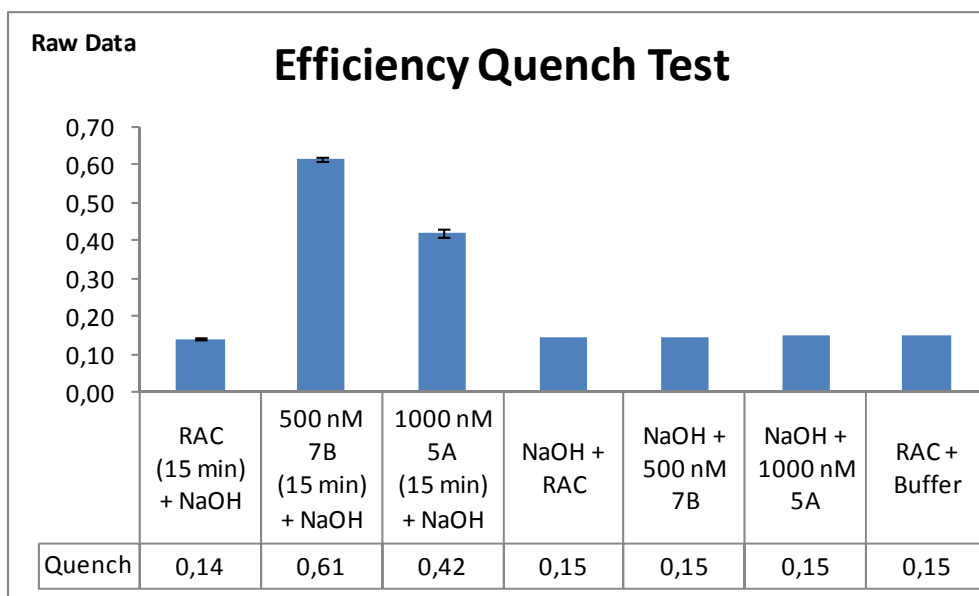
TrCel7B was added to RAC at approximately 300 nM and allowed to hydrolyze for 15 min at 50 °C. After this all samples were treated as above.



- Heat inactivation is ineffective for RAC 8 g/L and does not stop the reaction before allowing for almost double the hydrolysis to continue.

- Given all chemical methods are identical; it is assumed all are equally as good in stopping the reaction immediately.
- There was very little variation in sample triplicates (see error bars).
- Other enzymes may have different sensitivities to these methods.

Ap 1.2 Efficiency test on TrEG's.



Key

Sample	Treatment
RAC (15 min) + NaOH	RAC + Bfr, incubated 15 min 30 °C, then 1:1 200 mM NaOH added
500 nM 7B (15 min) + NaOH	RAC + 7B, incubated 15 min 30 °C, then 1:1 200 mM NaOH added
1000 nM 5A (15 min) + NaOH	RAC + 5A, incubated 15 min 30 °C, then 1:1 200 mM NaOH added
NaOH + RAC	1:1 200 mM NaOH added, then Bfr, incubated 15 min 30 °C
NaOH + 500 nM 7B	1:1 200 mM NaOH added, then 7B, incubated 15 min 30 °C
NaOH + 1000 nM 5A	1:1 200 mM NaOH added, then 5A, incubated 15 min 30 °C
RAC + Buffer	RAC + Bfr, incubated 15 min 30 °C, then 1:1 Bfr added

Bfr = 50 mM sodium acetate + 2 mM calcium chloride, pH 5.00 with 0.01 % triton X-100.

Ap 1.3 Conclusion, quenching.

The chemical methods are recommended in the future.

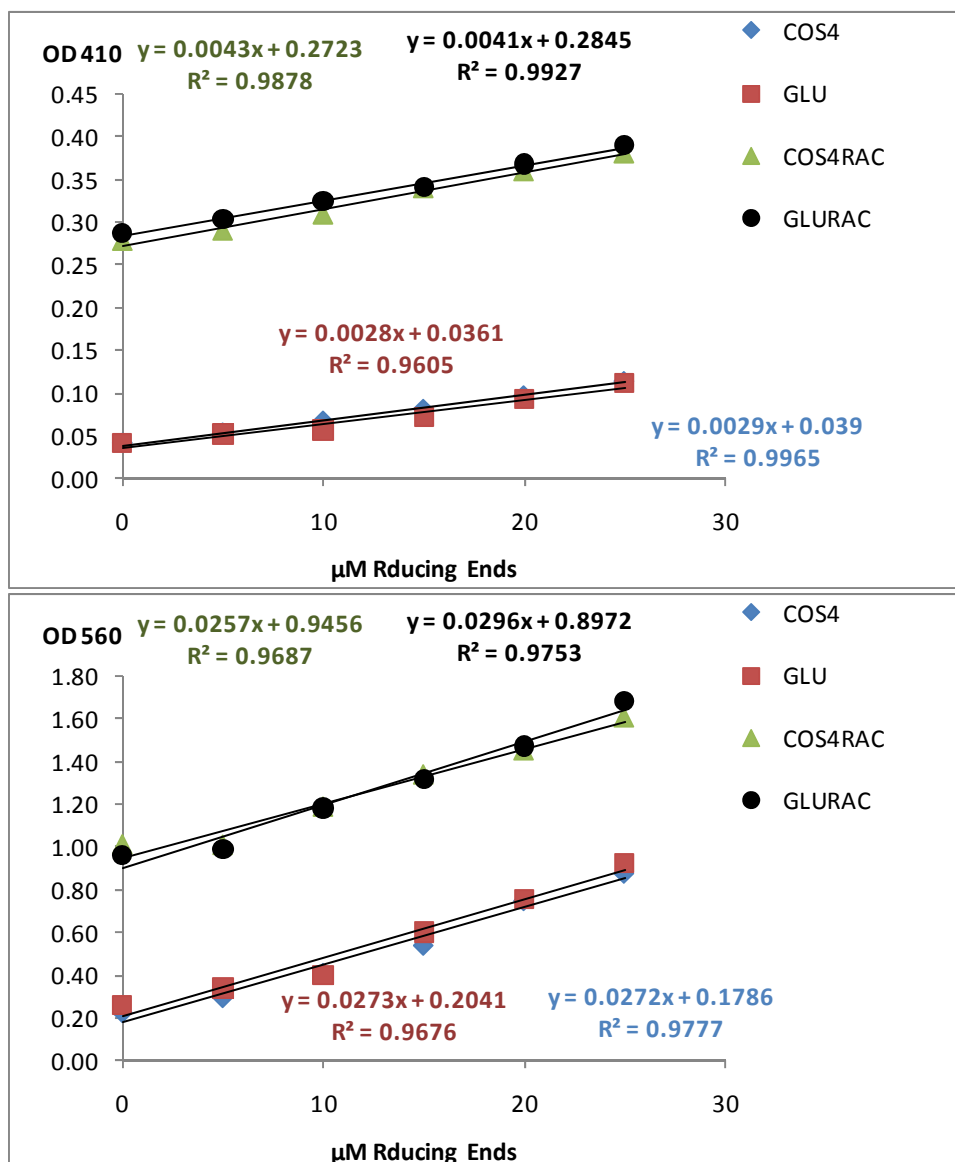
- For Novozymes HPLC (10 – 300 μ M, COS 1 to 6) use NaOH.
- For RUC HPLC (ca. 0.2 mM lower limit, only glucose, cellobiose) use sulfuric acid.
- *TrEG*'s are stopped immediately using NaOH.

Ap 1.4 Reducing ends assays

Given this could not explain the difference in the reducing ends produced and thus the ΔH difference, the PAHBAH assay was further investigated and the BCA assay introduced as well.

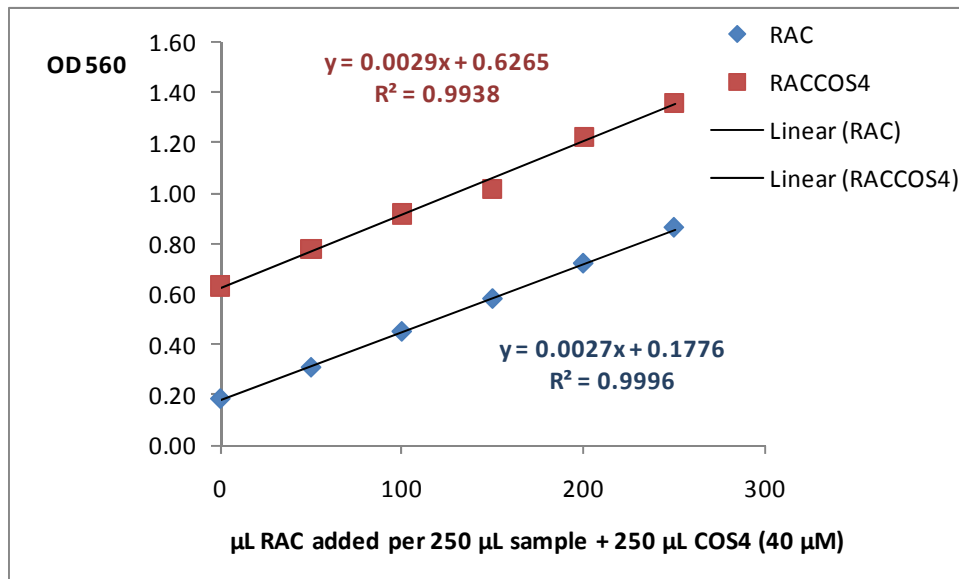
TrCel7B and *TrCel5A* produce a different product profile. The *TrCel7B* produces mainly glucose and cellobiose, both measured by HPLC and confirmed in the literature (213) whereas *TrCel5A* produces a distribution of longer COS's. The following investigations were carried out to determine the effects of a distribution of longer COS's on the PAHBAH and BCA assays.

1. Both Assays were calibrated with glucose and COS4 in the absence and presence of a 1.6 g/L RAC background, typical for assay conditions.



The BCA assay was carried out as outlined in (79) with 0.5 mL of sample incubated with 0.5 mL of freshly made BCA reagent and heated to 80 °C in eppendorfs in the thermomixer at 1400 rpm for 30 min. As may be seen from the slopes, the PAHBAH assay appears to overestimate the amount of reducing ends by a factor of 1.5 in the presence of RAC. One explanation of this could be the hydrolysis of RAC due to the boiling of the samples in the alkali pH leading to an overestimation of reducing ends present in samples. All further assays were carried out with the BCA method.

2. After determining the RAC at a constant level had no adverse effect on the BCA assay, it was investigated whether or not different amount of the insoluble substrate would have an effect on the response of the BCA assay.



The 500 µL samples were 250 µL of COS4 at 40 µM, with varied amounts of 1.6 g/L RAC (8 g/L × 1/5) added from 50 to 250 µL.

As may be seen from the figure there is a slight difference in the slopes, approximately 6 %. The COS4 concentration was determined from the average in the differences of the samples and was 38.2 ± 2.02 µM compared to the 40 µM dosed.

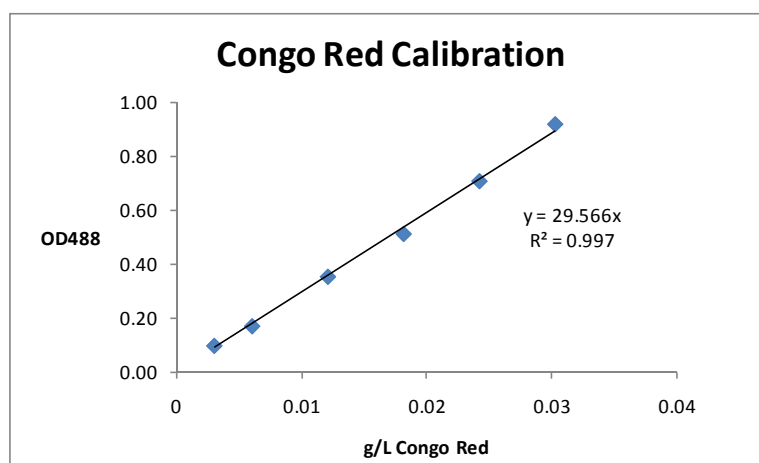
It is therefore concluded the BCA assay is not affected by a RAC background nor is it affected by a varied ratio of soluble and insoluble oligomers.

Appendix 2: Congo red ASA materials and methods

Ap 2.1 Material and Methods

Stock Solutions

1.0 g/L PASC, 10 g/L Avicel, 0.6 g/L Congo Red and 0.5 g/L NaCl, all prepared individually in phosphate buffer pH 7.00.



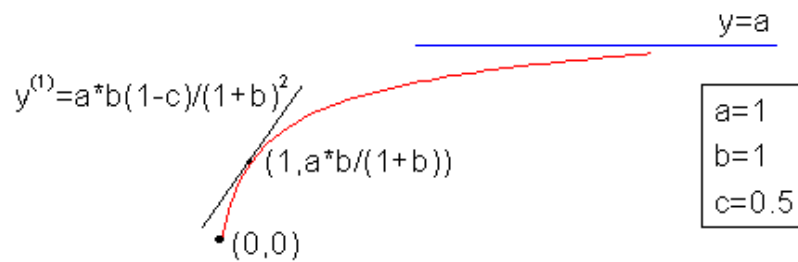
The calibration curve for one experiment with Congo Red.

A typical Set-Up. The amount of each stock solution is presented here in mL added to an 1.5 mL eppendorf tube.

Avicel	Congo Red	NaCl
0.40	0.05	0.55
0.40	0.10	0.50
0.40	0.15	0.45
0.40	0.20	0.40
0.40	0.25	0.35
0.40	0.30	0.30
0.40	0.35	0.25
0.40	0.40	0.20
0.40	0.45	0.15
0.40	0.50	0.10
0.40	0.55	0.05
0.40	0.60	0.00
0.40	0.05	0.55

After mixing, these eppendorfs were incubated overnight at 60 °C, 1400 rpm in a thermomixer. Then the suspensions were centrifuged at 14,000 rpm and the supernatant measured for residual Congo Red concentration was quantified using the above calibration curve.

A plot of bound Congo red g/g substrate (ordinate) and Free Congo Red g/L (abscissa) was prepared and fit to the Langmuir adsorption Isotherm using Origin Pro V 8.0.



$$y = \frac{abx^{1-c}}{1 + bx^{1-c}}$$

The Langmuir fit used to predict the maximum adsorption, a.

References

1. Lin, Y., and Tanaka, S. (2006) *Applied Microbiology and Biotechnology* **69**, 627-642
2. Oil Prices **12- Feb 2011**
<http://www.oil-price.net/>
3. Wyman, C. E. (2007) *Trends Biotechnol.* **25**, 153-157
4. Innovation and technological development in energy **12-Feb 2011**
http://ec.europa.eu/energy/res/legislation/electricity_en.html
5. An energy policy for Europe: Commission steps up to the energy challenges of the 21st Century **12- Feb 2011**
<http://europa.eu/rapid/pressReleasesAction.do?reference=MEMO/07/7&format=HTML&aged=0&language=EN&guiLanguage=en>
6. An overview on the EU biofuels policy **12- Feb 2011**
<http://www.blb.bmlfuw.gv.at/projekte/BLT_072713/Biofuels_in_the_EU/index.htm>
7. SETIS Statement **12- Feb 2011**
<http://setis.ec.europa.eu/newsroom-items-folder/eu-member-states-collectively-forecast-to-exceed-20-target-for-renewable-energy-sources>
8. Solomon, B. D., Barnes, J. R., and Halvorsen, K. E. (2007) *Biomass Bioenerg.* **31**, 416-425
9. Ragauskas, A. J., Williams, C. K., Davison, B. H., Britovsek, G., Cairney, J., Eckert, C. A., Frederick, W. J., Hallett, J. P., Leak, D. J., Liotta, C. L., Mielenz, J. R., Murphy, R., Templer, R., and Tschaplinski, T. (2006) *Science* **311**, 484-489
10. Sun, Y., and Cheng, J. Y. (2002) *Bioresour. Technol.* **83**, 1-11
11. Mosier, N., Wyman, C., Dale, B., Elander, R., Lee, Y. Y., Holtzapple, M., and Ladisch, M. (2005) *Bioresour. Technol.* **96**, 673-686
12. Stephanopoulos, G. (2007) *Science* **315**, 801-804
13. Zaldivar, J., Nielsen, J., and Olsson, L. (2001) *Applied Microbiology and Biotechnology* **56**, 17-34
14. Wayman, M. (1991) *Biotechnology of Biomass Conversion: Fuels and Chemicals from Renewable Resources*. in Wood, John Wiley and Sons. pp 42-72
15. Kamm, B., Kamm, M., Schmidt, M., Hirth, T., Schulze, M. (2006) *Lignocellulose based chemical products and product family trees*. in *Biorefineries - Industrial Processes and Products* (Birgit Kamm, P. G., Michael Kamm. ed.), Wiley-VCH, Weinheim. pp 97 - 139
16. Rubin, E. M. (2008) *Nature* **454**, 841-845
17. Beg, Q. K., Kapoor, M., Mahajan, L., and Hoondal, G. S. (2001) *Appl. Microbiol. Biotechnol.* **56**, 326-338
18. Collins, T., Gerday, C., and Feller, G. (2005) *FEMS Microbiol. Rev.* **29**, 3-23
19. Kulkarni, N., Shendye, A., and Rao, M. (1999) *FEMS Microbiol. Rev.* **23**, 411-456
20. Rabinovich, M. L., Melnik, M. S., and Boloboba, A. V. (2002) *Appl. Biochem. Microbiol.* **38**, 305-321
21. Beguin, P., and Aubert, J. P. (1994) *FEMS Microbiol. Rev.* **13**, 25-58
22. Walker, L. P., and Wilson, D. B. (1991) *Bioresour. Technol.* **36**, 3-14
23. Lynd, L. R., Weimer, P. J., van Zyl, W. H., and Pretorius, I. S. (2002) *Microbiol. Mol. Biol. Rev.* **66**, 506-577
24. Zhang, Y. H. P., Himmel, M. E., and Mielenz, J. R. (2006) *Biotechnol. Adv.* **24**, 452-481
25. Zhang, Y. H. P., and Lynd, L. R. (2004) *Biotechnol. Bioeng.* **88**, 797-824
26. Cantarel, B. L., Coutinho, P. M., Rancurel, C., Bernard, T., Lombard, V., and Henrissat, B. (2009) *Nucleic Acids Res.* **37**, D233-D238
27. Arantes, V., and Saddler, J. N. (2010) *Biotechnol. Biofuels* **3**, 11
28. Henrissat, B. (1991) *Biochem. J.* **280**, 309-316
29. Barr, B. K., Hsieh, Y. L., Ganem, B., and Wilson, D. B. (1996) *Biochemistry* **35**, 586-592
30. Cao, Y., and Tan, H. (2002) *Carbohydr. Res.* **337**, 1291-1296
31. Bhat, M. K., and Bhat, S. (1997) *Biotechnol. Adv.* **15**, 583-620
32. Bayer, E. A., Chanzy, H., Lamed, R., and Shoham, Y. (1998) *Curr. Opin. Struct. Biol.* **8**, 548-557
33. *T. reesei* **12- Feb 2011**
<http://www.thecropsite.com/news/617/the-discovery-of-trichoderma-reesei>
34. Mandels, M., and Reese, E. T. (1957) *J. Bacteriol.* **73**, 269-278
35. Reese, E. T. (1957) *Ind. Eng. Chem.* **49**, 89-93
36. Reese, E. T. (1956) *Appl. Microbiol.* **4**, 39-45
37. Reese, E. T., Siu, R. G. H., and Levinson, H. S. (1950) *J. Bacteriol.* **59**, 485-497
38. Himmel, M. E., Ding, S. Y., Johnson, D. K., Adney, W. S., Nimlos, M. R., Brady, J. W., and Foust, T. D. (2007) *Science* **315**, 804-807
39. Divne, C., Sinning, I., Stahlberg, J., Pettersson, G., Bailey, M., Siikaaho, M., Margollesclark, E., Teeri, T., and Jones, T. A. (1993) *J. Mol. Biol.* **234**, 905-907
40. Rouvinen, J., Bergfors, T., Teeri, T., Knowles, J. K. C., and Jones, T. A. (1990) *Science* **249**, 380-386
41. Withers, S. G. (2001) *Carbohydr. Polym.* **44**, 325-337
42. Sinnott, M. L. (1990) *Chem. Rev.* **90**, 1171-1202

43. Vantilbeurgh, H., Tomme, P., Claeysens, M., Bhikhabhai, R., and Pettersson, G. (1986) *FEBS Lett.* **204**, 223-227
44. Tomme, P., Vantilbeurgh, H., Pettersson, G., Vandamme, J., Vandekerckhove, J., Knowles, J., Teeri, T., and Claeysens, M. (1988) *Eur. J. Biochem.* **170**, 575-581
45. Penttila, M., Lehtovaara, P., Nevalainen, H., Bhikhabhai, R., and Knowles, J. (1986) *Gene* **45**, 253-263
46. Teeri, T. T., Lehtovaara, P., Kauppinen, S., Salovuori, I., and Knowles, J. (1987) *Gene* **51**, 43-52
47. Saloheimo, M., Lehtovaara, P., Penttila, M., Teeri, T. T., Stahlberg, J., Johansson, G., Pettersson, G., Claeysens, M., Tomme, P., and Knowles, J. K. C. (1988) *Gene* **63**, 11-21
48. Sandgren, M., Shaw, A., Ropp, T. H., Bott, S. W. R., Cameron, A. D., Stahlberg, J., Mitchinson, C., and Jones, T. A. (2001) *J. Mol. Biol.* **308**, 295-310
49. Kipper, K., Valjamae, P., and Johansson, G. (2005) *Biochem. J.* **385**, 527-535
50. KlemanLeyer, K. M., SiikaAho, M., Teeri, T. T., and Kirk, T. K. (1996) *Appl. Environ. Microbiol.* **62**, 2883-2887
51. Bailey, M. J., Siikaaho, M., Valkeajarvi, A., and Penttila, M. E. (1993) *Biotechnol. Appl. Biochem.* **17**, 65-76
52. Kurasin, M., and Valjamae, P. (2010) *J. Biol. Chem.* **286**, 169-177
53. Breyer, W. A., and Matthews, B. W. (2001) *Protein Sci.* **10**, 1699-1711
54. Rabinovich, M. L., Melnick, M. S., and Bolobova, A. V. (2002) *Biochemistry-Moscow* **67**, 850-871
55. Teeri, T. T. (1997) *Trends Biotechnol.* **15**, 160-167
56. Henrissat, B. (1994) *Cellulose* **1**, 169-196
57. Joos, P., Sierens, W., and Ruysen, R. (1969) *J. Pharm. Pharmacol.* **21**, 848-&
58. Divne, C., Stahlberg, J., Teeri, T. T., and Jones, T. A. (1998) *J. Mol. Biol.* **275**, 309-325
59. Koivula, A., Reinikainen, T., Ruohonen, L., Valkeajarvi, A., Claeysens, M., Teleman, O., Kleywegt, G. J., Szardenings, M., Rouvinen, J., Jones, T. A., and Teeri, T. T. (1996) *Protein Eng.* **9**, 691-699
60. Kleywegt, G. J., Zou, J. Y., Divne, C., Davies, G. J., Sinning, I., Stahlberg, J., Reinikainen, T., Srisodsuk, M., Teeri, T. T., and Jones, T. A. (1997) *J. Mol. Biol.* **272**, 383-397
61. Macarron, R., Acebal, C., Castillon, M. P., Dominguez, J. M., Delamata, I., Pettersson, G., Tomme, P., and Claeysens, M. (1993) *Biochem. J.* **289**, 867-873
62. Sharrock, K. R. (1988) *J. Biochem. Biophys. Methods* **17**, 81-105
63. Eveleigh, D. E., Mandels, M., Andreotti, R., and Roche, C. (2009) *Biotechnol. Biofuels* **2**, 8
64. Mullings, R. (1985) *Enzyme. Microb. Technol.* **7**, 586-591
65. Dashtban, M., Maki, M., Leung, K. T., Mao, C. Q., and Qin, W. S. (2010) *Crit. Rev. Biotechnol.* **30**, 302-309
66. Ghose, T. K. (1987) *Pure Appl. Chem.* **59**, 257-268
67. Dubois, M., Gilles, K. A., Hamilton, J. K., Rebers, P. A., and Smith, F. (1956) *Anal. Chem.* **28**, 350-356
68. Bourbonnais, R., Leech, D., and Paice, M. G. (1998) *Biochim. Biophys. Acta-Gen. Subj.* **1379**, 381-390
69. Gruno, M., Valjamae, P., Pettersson, G., and Johansson, G. (2004) *Biotechnol. Bioeng.* **86**, 503-511
70. Bohlin, C., Olsen, S. N., Morant, M. D., Patkar, S., Borch, K., and Westh, P. (2010) *Biotechnol. Bioeng.* **107**, 943-952
71. Miller, G. L. (1959) *Anal. Chem.* **31**, 426-428
72. Lever, M. (1972) *Anal. Biochem.* **47**, 273-&
73. Lever, M. (1973) *Biochem. Med.* **7**, 274-281
74. Nelson, N. (1944) *J. Biol. Chem.* **153**, 375-380
75. Somogyi, M. (1952) *J. Biol. Chem.* **195**, 19-23
76. Anthon, G. E., and Barrett, D. M. (2002) *Anal. Biochem.* **305**, 287-289
77. Doner, L. W., and Irwin, P. L. (1992) *Anal. Biochem.* **202**, 50-53
78. Medve, J., Karlsson, J., Lee, D., and Tjerneld, F. (1998) *Biotechnol. Bioeng.* **59**, 621-634
79. Zhang, Y. H. P., and Lynd, L. R. (2005) *Biomacromolecules* **6**, 1510-1515
80. Coward-Kelly, G., Aiello-Mazzari, C., Kim, S., Granda, C., and Holtzapple, M. (2003) *Biotechnol. Bioeng.* **82**, 745-749
81. Sengupta, S., Jana, M. L., Sengupta, D., and Naskar, A. K. (2000) *Appl. Microbiol. Biotechnol.* **53**, 732-735
82. Kongruang, S., Han, M. J., Breton, C. I. G., and Penner, M. H. (2003) Quantitative analysis of cellulose-reducing ends. in *25th Symposium on Biotechnology for Fuels and Chemicals*, Breckenridge, CO
83. Ohmine, K., Ooshima, H., and Harano, Y. (1983) *Biotechnol. Bioeng.* **25**, 2041-2053
84. Garcia, E., Johnston, D., Whitaker, J. R., and Shoemaker, S. P. (1993) *J. Food Biochem.* **17**, 135-145
85. Adney, B., and Baker, J. (2008) "Measurement of Cellulase Activities".
86. Xiao, Z. Z., Zhang, X., Gregg, D. J., and Saddler, J. N. (2004) *Appl. Biochem. Biotechnol.*, 1115-1126
87. Andric, P., Meyer, A. S., Jensen, P. A., and Dam-Johansen, K. (2010) *Appl. Biochem. Biotechnol.* **160**, 280-297
88. Miller, G. L., Blum, R., Glennon, W. E., and Burton, A. L. (1960) *Anal. Biochem.* **1**, 127-132
89. Lee, J. M., Heitmann, J. A., and Pawlak, J. J. (2007) *BioResources* **2**, 20-33
90. Shoemaker, S. P., and Brown, R. D. (1978) *Biochim. Biophys. Acta* **523**, 147-161
91. Child, J. J., Eveleigh, D. E., and Sieben, A. S. (1973) *Can. J. Biochem.* **51**, 39-43
92. *Megazyme* **12- Feb 2011**
<http://secure.megazyme.com/Homepage.aspx/>
93. Vantilbeurgh, H., and Claeysens, M. (1985) *FEBS Lett.* **187**, 283-288
94. Deshpande, M. V., Eriksson, K. E., and Pettersson, L. G. (1984) *Anal. Biochem.* **138**, 481-487
95. Holtzapple, M., Cognata, M., Shu, Y., and Hendrickson, C. (1990) *Biotechnol. Bioeng.* **36**, 275-287

96. Decker, C. H., Visser, J., and Schreier, P. (2000) *J. Agric. Food Chem.* **48**, 4929-4936
97. Decker, C. H., Visser, J., and Schreier, P. (2001) *Appl. Microbiol. Biotechnol.* **55**, 157-163
98. Lange, N. A., and Speight, J. G. (2005) *Lange's handbook of chemistry*, 16th ed., McGraw Hill
99. Kyriacou, A., Mackenzie, C. R., and Neufeld, R. J. (1987) *Enzyme. Microb. Technol.* **9**, 25-32
100. Nidetzky, B., Steiner, W., and Claeysens, M. (1994) *Biochem. J.* **303**, 817-823
101. Todd, M. J., and Gomez, J. (2001) *Anal. Biochem.* **296**, 179-187
102. Olsen, S. N. (2006) *Thermochim. Acta* **448**, 12-18
103. Murphy, L., Borch, K., McFarland, K. C., Bohlin, C., and Westh, P. (2010) *Enzyme. Microb. Technol.* **46**, 141-146
104. Okhrimenko, O., and Jelesarov, M. (2008) *J. Mol. Recognit.* **21**, 1-19
105. Bjelic, S., and Jelesarov, I. (2008) *J. Mol. Recognit.* **21**, 289-311
106. Jeoh, T., Baker, J. O., Ali, M. K., Himmel, M. E., and Adney, W. S. (2005) *Anal. Biochem.* **347**, 244-253
107. Karim, N., Okada, H., and Kidokoro, S. (2005) *Thermochim. Acta* **431**, 9-20
108. Karim, N., and Kidokoro, S. (2004) *Thermochim. Acta* **412**, 91-96
109. Krokeide, I. M., Eijsink, V. G. H., and Sorlie, M. (2007) *Thermochim. Acta* **454**, 144-146
110. Bohlin, C., Olsen, S. N., Morant, M. D., Patkar, S., Borch, K., and Westh, P. (2010) *Biotechnol. Bioeng.* **n/a**
111. Murphy, L., Baumann, M. J., Borch, K., Sweeney, M., and Westh, P. (2010) *Anal. Biochem.* **404**, 140-148
112. Ladbury, J. E., and Chowdhry, B. Z. (1996) *Chem. Biol.* **3**, 791-801
113. Goldberg, R. N., Bell, D., Tewari, Y. B., and McLaughlin, M. A. (1991) *Biophys. Chem.* **40**, 69-76
114. Goldberg, R. N., Tewari, Y. B., and Bhat, T. N. (2004) *Bioinformatics* **20**, 2874-2877
115. Tewari, Y. B., Lang, B. E., Decker, S. R., and Goldberg, R. N. (2008) *J. Chem. Thermodyn.* **40**, 1517-1526
116. Baumann, M. J., Murphy, L., Lei, N. N., Krogh, K., Borch, K., and Westh, P. (2011) *Anal. Biochem.* **410**, 19-26
117. Wood, T. M. (1988) *Methods Enzymol.* **160**, 19-25
118. Zhang, Y. H. P., Cui, J. B., Lynd, L. R., and Kuang, L. R. (2006) *Biomacromolecules* **7**, 644-648
119. Shen, T. Y., and Gnanakaran, S. (2009) *Biophys. J.* **96**, 3032-3040
120. Yang, B., Willies, D. M., and Wyman, C. E. (2006) *Biotechnol. Bioeng.* **94**, 1122-1128
121. Park, S., Baker, J. O., Himmel, M. E., Parilla, P. A., and Johnson, D. K. (2010) *Biotechnol. Biofuels* **3**, 10
122. Vanderhart, D. L., and Atalla, R. H. (1984) *Macromolecules* **17**, 1465-1472
123. Atalla, R. H., and VanderHart, D. L. (1999) *Solid State Nucl. Magn. Reson.* **15**, 1-19
124. Fan, L. T., Lee, Y. H., and Beardmore, D. H. (1980) *Biotechnol. Bioeng.* **22**, 177-199
125. Lee, S. B., Shin, H. S., Ryu, D. D. Y., and Mandels, M. (1982) *Biotechnol. Bioeng.* **24**, 2137-2153
126. Fan, L. T., and Lee, Y. H. (1983) *Biotechnol. Bioeng.* **25**, 2707-2733
127. Lee, Y. H., and Fan, L. T. (1983) *Biotechnol. Bioeng.* **25**, 939-966
128. Mansfield, S. D., deJong, E., and Saddler, J. N. (1997) *Appl. Environ. Microbiol.* **63**, 3804-3809
129. Puri, V. P. (1984) *Biotechnol. Bioeng.* **26**, 1219-1222
130. Hall, M., Bansal, P., Lee, J. H., Realff, M. J., and Bommarius, A. S. (2010) *FEBS J.* **277**, 1571-1582
131. Olsen, S. N., Lumby, E., McFarland, K., Borch, K., and Westh, P. (2010) *Appl. Biochem. Biotechnol.* **163**, 626-635
132. Asenjo, J. A. (1983) *Biotechnol. Bioeng.* **25**, 3185-3190
133. Holtzapple, M. T., Caram, H. S., and Humphrey, A. E. (1984) *Biotechnol. Bioeng.* **26**, 753-757
134. Gusakov, A. V., and Sinityn, A. P. (1992) *Biotechnol. Bioeng.* **40**, 663-671
135. Praestgaard, E., Elmerdahl, J., Murphy, L., Nymand, S., McFarland, K. C., Borch, K., and Westh, P. (2011) *FEBS J., Accepted manuscript*
136. Bradford, M. M. (1976) *Anal. Biochem.* **72**, 248-254
137. Inglesby, M. K., and Zeronian, S. H. (2002) *Cellulose* **9**, 19-29
138. Inglesby, M. K., and Zeronian, S. H. (1996) *Cellulose* **3**, 165-181
139. Galante, Y. A., and Formantici, C. (2003) *Curr. Org. Chem.* **7**, 1399-1422
140. Nagy, T., Simpson, P., Williamson, M. P., Hazlewood, G. P., Gilbert, H. J., and Orosz, L. (1998) *FEBS Lett.* **429**, 312-316
141. Reinikainen, T., Ruohonen, L., Nevanen, T., Laaksonen, L., Kraulis, P., Jones, T. A., Knowles, J. K. C., and Teeri, T. T. (1992) *Proteins-Structure Function and Genetics* **14**, 475-482
142. Teeri, T. T., Koivula, A., Linder, M., Wohlfahrt, G., Divne, C., and Jones, T. A. (1998) *Biochem. Soc. Trans.* **26**, 173-178
143. Stahlberg, J., Divne, C., Koivula, A., Piens, K., Claeysens, M., Teeri, T. T., and Jones, T. A. (1996) *J. Mol. Biol.* **264**, 337-349
144. Divne, C., Stahlberg, J., Reinikainen, T., Ruohonen, L., Pettersson, G., Knowles, J. K. C., Teeri, T. T., and Jones, T. A. (1994) *Science* **265**, 524-528
145. Irwin, D. C., Spezio, M., Walker, L. P., and Wilson, D. B. (1993) *Biotechnol. Bioeng.* **42**, 1002-1013
146. Zou, J. Y., Kleywegt, G. J., Stahlberg, J., Driguez, H., Nerinckx, W., Claeysens, M., Koivula, A., Teeri, T. T., and Jones, T. A. (1999) *Struct. Fold. Des.* **7**, 1035-1045
147. Koivula, A., Ruohonen, L., Wohlfahrt, G., Reinikainen, T., Teeri, T. T., Piens, K., Claeysens, M., Weber, M., Vasella, A., Becker, D., Sinnott, M. L., Zou, J. Y., Kleywegt, G. J., Szardenings, M., Stahlberg, J., and Jones, T. A. (2002) *J. Am. Chem. Soc.* **124**, 10015-10024
148. Wang, L. S., Zhang, Y. Z., and Gao, P. J. (2008) *Sci. China Ser. C-Life Sci.* **51**, 620-629
149. Linder, M., Lindeberg, G., Reinikainen, T., Teeri, T. T., and Pettersson, G. (1995) *FEBS Lett.* **372**, 96-98

150. Bommarius, A. S., Katona, A., Cheben, S. E., Patel, A. S., Ragauskas, A. J., Knudson, K., and Pu, Y. (2008) *Metab. Eng.* **10**, 370-381
151. Bansal, P., Hall, M., Realff, M. J., Lee, J. H., and Bommarius, A. S. (2009) *Biotechnol. Adv.* **27**, 833-848
152. Gan, Q., Allen, S. J., and Taylor, G. (2003) *Process Biochem.* **38**, 1003-1018
153. Nidetzky, B., and Steiner, W. (1993) *Biotechnol. Bioeng.* **42**, 469-479
154. Valjamae, P., Kipper, K., Pettersson, G., and Johansson, G. (2003) *Biotechnol. Bioeng.* **84**, 254-257
155. Creagh, A. L., Ong, E., Jervis, E., Kilburn, D. G., and Haynes, C. A. (1996) *Proc. Natl. Acad. Sci. U. S. A.* **93**, 12229-12234
156. Linder, M., and Teeri, T. T. (1996) *Proc. Natl. Acad. Sci. U. S. A.* **93**, 12251-12255
157. Ooshima, H., Sakata, M., and Harano, Y. (1983) *Biotechnol. Bioeng.* **25**, 3103-3114
158. Zhang, S., Wolfgang, D. E., and Wilson, D. B. (1999) *Biotechnol. Bioeng.* **66**, 35-41
159. Eriksson, T., Karlsson, J., and Tjerneld, F. (2002) *Appl. Biochem. Biotechnol.* **101**, 41-60
160. Igarashi, K., Wada, M., Hori, R., and Samejima, M. (2006) *FEBS J.* **273**, 2869-2878
161. Valjamae, P., Sild, V., Pettersson, G., and Johansson, G. (1998) *Eur. J. Biochem.* **253**, 469-475
162. Praestgaard, E., Elmerdahl, J., Murphy, L., Nymand, S., McFarland, K. C., Borch, K., and Westh, P. (2011) *FEBS J.* **278**, 1547-1560
163. Cornish-Bowden, A. (2004) *Fundamentals of Enzyme Kinetics*, 3rd Ed. ed., Portland Press
164. Hartley, B. S., and Kilby, B. A. (1954) *Biochem. J.* **56**, 288-297
165. Jalak, J., and Valjamae, P. (2010) *Biotechnol. Bioeng.* **106**, 871-883
166. Wadso, L., and Li, X. (2008) *J. Chem. Educ.* **85**, 112-116
167. Sattler, W., Esterbauer, H., Glatter, O., and Steiner, W. (1989) *Biotechnol. Bioeng.* **33**, 1221-1234
168. Shoemaker, S., Watt, K., Tsitovsky, G., and Cox, R. (1983) *Bio-Technology* **1**, 687-690
169. Beldman, G., Searle van Leeuwen, M. F., Rombouts, F. M., and Voragen, F. G. J. (1985) *Eur. J. Biochem.* **146**, 301-308
170. Igarashi, K., Koivula, A., Wada, M., Kimura, S., Penttila, M., and Samejima, M. (2009) *J. Biol. Chem.* **284**, 36186-36190
171. Nidetzky, B., Steiner, W., and Claeysens, M. (1994) *Biochem. J.* **303**, 817-823
172. Vantilbeurgh, H., Bhikhabhai, R., Pettersson, L. G., and Claeysens, M. (1984) *FEBS Lett.* **169**, 215-218
173. Harjunpaa, V., Teleman, A., Koivula, A., Ruohonen, L., Teeri, T. T., Teleman, O., and Drakenberg, T. (1996) *Eur. J. Biochem.* **240**, 584-591
174. Hong, J., Ye, X. H., and Zhang, Y. H. P. (2007) *Langmuir* **23**, 12535-12540
175. Mulakala, C., and Reilly, P. J. (2005) *Proteins-Structure Function and Bioinformatics* **60**, 598-605
176. Pan, X. J. (2008) *Journal of Biobased Materials and Bioenergy* **2**, 25-32
177. Berlin, A., Gilkes, N., Kurabi, A., Bura, R., Tu, M. B., Kilburn, D., and Saddler, J. (2005) *Appl. Biochem. Biotechnol.* **121**, 163-170
178. Berlin, A., Balakshin, M., Gilkes, N., Kadla, J., Maximenko, V., Kubo, S., and Saddler, J. (2006) *J. Biotechnol.* **125**, 198-209
179. Baumann, M. J., Borch, K., and Westh, P. (2011) *Submitted*
180. Langsford, M. L., Gilkes, N. R., Singh, B., Moser, B., Miller, R. C., Warren, R. A. J., and Kilburn, D. G. (1987) *FEBS Lett.* **225**, 163-167
181. Gilkes, N. R., Warren, R. A. J., Miller, R. C., and Kilburn, D. G. (1988) *J. Biol. Chem.* **263**, 10401-10407
182. Lemos, M. A., Teixeira, J. A., Mota, M., and Gama, F. M. (2000) *Biotechnol. Lett.* **22**, 703-707
183. Boraston, A. B., Bolam, D. N., Gilbert, H. J., and Davies, G. J. (2004) *Biochem. J.* **382**, 769-781
184. Tormo, J., Lamed, R., Chirino, A. J., Morag, E., Bayer, E. A., Shoham, Y., and Steitz, T. A. (1996) *EMBO J.* **15**, 5739-5751
185. Lehtio, J., Sugiyama, J., Gustavsson, M., Fransson, L., Linder, M., and Teeri, T. T. (2003) *Proc. Natl. Acad. Sci. U. S. A.* **100**, 484-489
186. Linder, M., and Teeri, T. T. (1997) *J. Biotechnol.* **57**, 15-28
187. Kraulis, P. J., Clore, G. M., Nilges, M., Jones, T. A., Pettersson, G., Knowles, J., and Gronenborn, A. M. (1989) *Biochemistry* **28**, 7241-7257
188. Kyte, J., and Doolittle, R. F. (1982) *J. Mol. Biol.* **157**, 105-132
189. Esteghlalian, A. R., Srivastava, V., Gilkes, N. R., Kilburn, D. G., Warren, R. A. J., and Saddler, J. N. (2001) Do cellulose binding domains increase substrate accessibility? , Humana Press Inc
190. Shen, H., Schmuck, M., Pilz, I., Gilkes, N. R., Kilburn, D. G., Miller, R. C., and Warren, R. A. J. (1991) *J. Biol. Chem.* **266**, 11335-11340
191. Carrard, G., Koivula, A., Soderlund, H., and Beguin, P. (2000) *Proc. Natl. Acad. Sci. U. S. A.* **97**, 10342-10347
192. Hall, M., Bansal, P., Lee, J. H., Realff, M. J., and Bommarius, A. S. (2011) *Bioresour. Technol.* **102**, 2910-2915
193. Gao, P. J., Chen, G. J., Wang, T. H., Zhang, Y. S., and Liu, J. (2001) *Acta Biochim. Biophys. Sin.* **33**, 13-18
194. Ciolacu, D., Kovac, J., and Kokol, V. (2009) *Carbohydr. Res.* **345**, 621-630
195. Lodish, Berk, Kaiser, Krieger, Scott, Bretscher, Pyle, and Matsudaira. (2007) *Molecular Cell Biology*, 6th Ed. ed.,
196. Voutilainen, S. P., Puranen, T., Siika-Aho, M., Lappalainen, A., Alapuranen, M., Kallio, J., Hooman, S., Viikri, L., Vehmaanpera, J., and Koivula, A. (2008) *Biotechnol. Bioeng.* **101**, 515-528
197. Srisodsuk, M., Reinikainen, T., Penttila, M., and Teeri, T. T. (1993) *J. Biol. Chem.* **268**, 20756-20761
198. Xiao, Z. Z., Gao, P. J., Qu, Y. B., and Wang, T. H. (2001) *Biotechnol. Lett.* **23**, 711-715
199. Sinnott, M. L. (1998) The cellobiohydrolases of *Trichoderma reesei*: a review of indirect and direct evidence that their function is not just glycosidic bond hydrolysis. Portland Press

200. Srisodsuk, M., Lehtio, J., Linder, M., MargollesClark, E., Reinikainen, T., and Teeri, T. T. (1997) *J. Biotechnol.* **57**, 49-57
201. Linder, M., Mattinen, M. L., Kontteli, M., Lindeberg, G., Stahlberg, J., Drakenberg, T., Reinikainen, T., Pettersson, G., and Annala, A. (1995) *Protein Sci.* **4**, 1056-1064
202. Mattinen, M. L., Kontteli, M., Kerovuo, J., Linder, M., Annala, A., Lindeberg, G., Reinikainen, T., and Drakenberg, T. (1997) *Protein Sci.* **6**, 294-303
203. Lee, I., Evans, B. R., and Woodward, J. (2000) *Ultramicroscopy* **82**, 213-221
204. Bailey, G. D., Roberts, B. D., Buess, C. M., and Carper, W. R. (1979) *Arch. Biochem. Biophys.* **192**, 482-488
205. Wong, C. M., Wong, K. H., and Chen, X. D. (2008) *Appl. Microbiol. Biotechnol.* **78**, 927-938
206. Shimizu, S., Kataoka, M., Shimizu, K., Hirakata, M., Sakamoto, K., and Yamada, H. (1992) *Eur. J. Biochem.* **209**, 383-390
207. Shinagawa, E., Ano, Y., Yakushi, T., Adachi, O., and Matsushita, K. (2009) *Biosci. Biotechnol. Biochem.* **73**, 241-244
208. Roberts, B. D., Bailey, G. D., Buess, C. M., and Carper, W. R. (1978) *Biochem. Biophys. Res. Commun.* **84**, 322-327
209. Pocker, Y., and Green, E. (1973) *J. Am. Chem. Soc.* **95**, 113-119
210. Hestrin, S. (1949) *J. Biol. Chem.* **180**, 249-261
211. Hucho, F., and Wallenfels, K. (1972) *Biochimica et Biophysica Acta (BBA) - Enzymology* **276**, 176-179
212. Nidetzky, B., Furlinger, M., Gollhofer, D., Haug, I., Haltrich, D., and Kulbe, K. D. (1997) *Appl. Biochem. Biotechnol.* **63-5**, 173-188
213. Karlsson, J., Siika-aho, M., Tenkanen, M., and Tjerneld, F. (2002) *J. Biotechnol.* **99**, 63-78

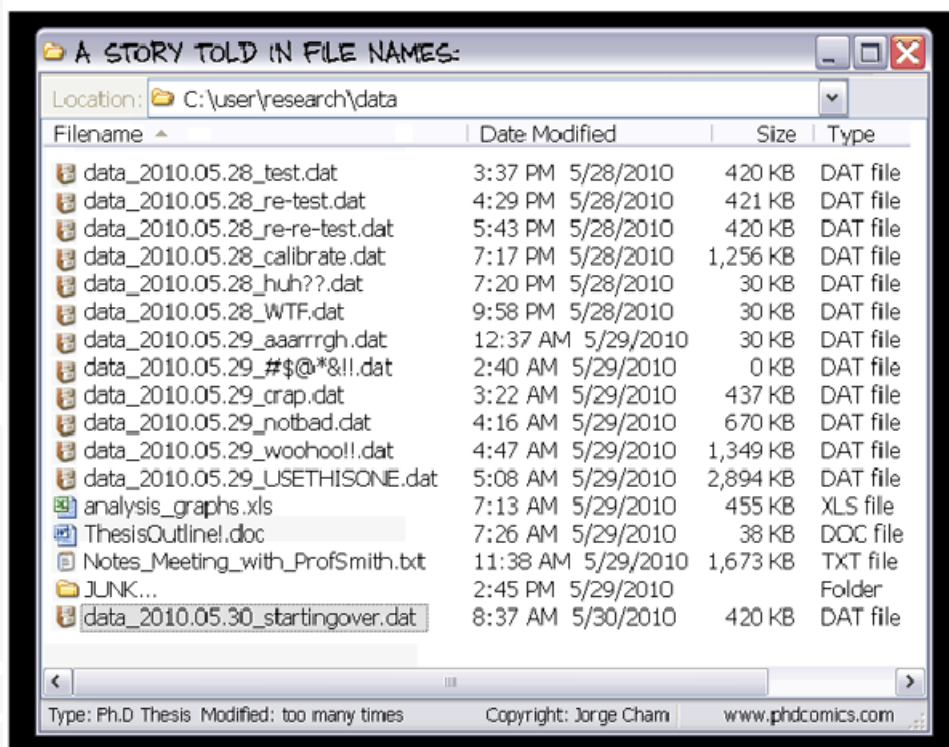
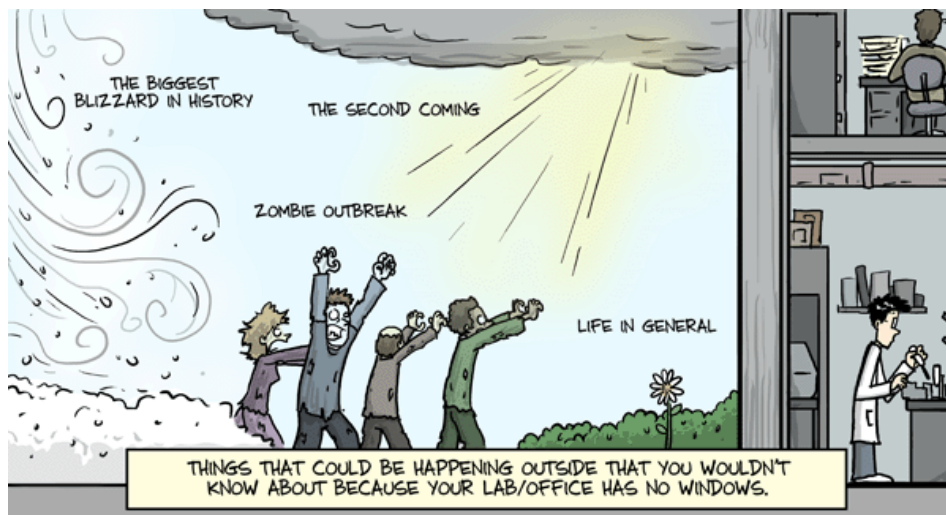


Figure 39. Just for fun.